UNIVERSITY OF COPENHAGEN
FACULTY OF SCIENCE

Western Greenland ice sheet margin (on the way to EGRIP camp, 21 June 2017)

PhD Thesis

Diana Vladimirova

High-resolution methane record of the RECAP ice core (Eastern Greenland) over the last climatic cycle

Supervisor: Prof. Thomas Blunier
Co-supervisor: Dr. Alexey Ekaykin

Submitted on: 08 October 2018

Name of department: Niels Bohr Institute, Centre for Ice and Climate

Author(s): Diana Vladimirova

Title and subtitle: High-resolution methane record of the RECAP ice core (Eastern Greenland) over the last climatic cycle

Topic description: Methane (CH_4) is among the three most important greenhouse gases. Its concentration varied in the past and the only way to extract the information is to measure the past atmosphere samples trapped in the ice cores. We present the REnland ice CAP (RECAP) CH_4 record covering the last glacial cycle (120 000 years).

The modern interglacial (Holocene) section (the last 11 700 years) represents the first continuous high-resolution methane record of the Northern Hemisphere and exhibits the centennial-scale variability. A possible explanation for this observation could be in the global teleconnection of the intertropical convergence zone and its influence on the monsoon activity, which in turn has an effect on the CH_4 emissions for the tropical wetlands - the dominant source of methane.

During a part of the Last Glacial, we reveal that approximately 78 000 - 83 000 years ago an additional source of methane was active in the Northern Hemisphere. The environmental reconstructions suggest that it could be the boreal wetlands, exposed after the retreat of the ice sheet and the following drainage of ice-dammed lakes in the area.

As side projects, we also work on the improvement of the continuous flow analysis (CFA) technique for the gas applications - the technique used for the RECAP ice core measurements, and on the on-site CH_4 measurements at the Eastern GReenland Ice core Project (EGRIP). We identify a diurnal variability of the CH_4 concentration in the surface air an upper firn column, which was earlier considered as convectively mixed.

Supervisor: Prof. Thomas Blunier
Niels Bohr Institute, Centre for Ice and Climate, Copenhagen, Denmark

Co-supervisor: Dr. Alexey Ekaykin
(1) Arctic and Antarctic Research Institute; (2) St Petersburg State University, St Petersburg, Russia

Submitted on: 08 October 2018

Grade:

Number of study units:

☐ 2 ☐ 3

Number of characters:

Table of contents

Abstract

Methane (CH_4) is among the three most powerful greenhouse gases. Since the beginning of the atmospheric monitoring, its concentration has risen abruptly for both natural and anthropogenic reasons. Such abrupt variations may also have occurred in the past, before the start of atmospheric monitoring. The only known direct measure of prehistoric gas content is to recover the air composition trapped within the ice sheets. The current study is focused on the CH_4 concentration variability mainly over three timespans: Last Glacial period, modern interglacial Holocene and at present days.

Here we present a high-resolution CH_4 record, drilled in 2015 through the Renland Ice Cap (RECAP) in eastern Greenland – 71.3N 26.6W 2300 m a.s.l. , a record that covers the last climatic cycle (120 000 years). This record represents the first continuous high-resolution Holocene CH_4 record of the Northern Hemisphere. The pattern of the centennial scale variability is coherent with earlier published Southern Hemisphere ice core CH_4 records, on the long- and midterm variability (600-700, 200-500 yr periodicity) as well as a short-term (down to 70 yr) in the Late Holocene. A possible explanation for this observation could be in the global teleconnection of the intertropical convergence zone and its influence on the monsoon activity, and consequently the CH_4 emission from tropical wetlands.

CH_4 concentrations exhibit variable amplitudes during the succession of the stadial-interstadial (GS/GI) transitions of the Last Glacial. These amplitudes differ from the corresponding temperature variabilities. A comparison between CH_4 concentrations in the two hemispheres, and a paleoclimatic reconstruction at the transitions GS/GI-19-21 (67-87 000 years ago), reveals a presence of an additional CH_4 source in Northern Eurasia, active in 78 000 – 83 000 years ago. The identified elevated relative interpolar difference in the CH_4 concentration possibly occurred due to exposed wetlands, after the retreat of the sheet and the following drainage of ice-dammed lakes in the area.

A CH_4 signal was also measured on site in the ice surface air layer and the upper firn column in the vicinity of the East Greenland Ice-core Project (EGRIP), 75.6268N 35.9915W, during the summer season 2017. The presence of the diurnal variability is exhibited, it is persistent during days with low wind speed (3-5 knots) and without surface melting; the upper firn signal matches the amplitude and the average value of the atmospheric signal. The presence of the diurnal cycle in the convective firn zone demonstrates an earlier unrevealed feature of the atmospheric gas signal propagation.

Abstrakt på dansk and резюме на русском языке

Metan (CH_4) er blandt de tre mest kraftfulde drivhusgasser og koncentration har steget brat af både naturlige og menneskeskabte årsager siden påbegyndelsen vores overvågning af atmosfæren. Sådanne pludselige variationer kan også have fundet sted tidligere, før den atmosfæriske overvågning. Den eneste kendte direkte måling af gasindholdet afledt fra den forhistorisk atmosfære, er ved at genvinde gasen fanget inde i iskernerboringer. Her præsenterer vi et CH_4-datasæt, på baggrund af målinger fra Renland Ice Cap (RECAP) i Østgrønland - 71,3N 26,6W 2300 m a.s.l. indsamlet i 2015.

Dette datasæt repræsenterer det første kontinuerlige CH_4-datasæt fra den nordlige halvkugle, med høj temporalopløsning fra den holocæne epoke. Mønsteret for århundredeskalaændringen er sammenlignelig med tidligere offentliggjorte CH_4-optegnelser med iskerneboringer fra den sydlige halvkugle, på lang- og midtvejsvariabilitet (600-700, 200-500 års periodicitet), såvel som kortfristet (ned til 70 år) i den sene holocæn. En mulig forklaring på denne observation, kunne skyldes den globale telekonnection af den intertropiske konvergenszone og dens indflydelse på monsunaktiviteten og CH_4-udledningen fra tropiske vådområder.

CH_4-koncentrationer udviser variable amplituder under de stadiale-interstadiale (GS/GI) overgange af sidste istid. Disse amplituder adskiller sig fra de tilsvarende temperaturvariationer i perioden. En sammenligning mellem de to halvkuglers CH_4-koncentrationer og en paløoklimatisk rekonstruktion ved overgangene GS/GI-19-21, afslører en tilstedeværelse af en yderligere CH_4-kilde i det nordlige Eurasien, der var aktiv i 78-83 ka BP. Denne observation skyldes muligvis blotlagte vådområder efter tilbagetrækningen af iskarpen og en efterfølgende dræning af is inddæmmede søer i området.

CH_4-signalet blev målt on-line i isoverfladens luftlag og den øvre kolonne i umiddelbar nærhed til det East Greenland Ice-core Project (EGRIP), 75,6268N 35,9915W, i sommeren 2017. Den daglige variabilitet er tydlige i målingerne. Den er vedvarende i rolige perioder uden overfladesmeltning og målingerne svarer præcist til amplituderne og gennemsnitsværdien fra de sideløbende atmosfæriske målinger. Tilstedeværelsen af den daglige cyklus i den konvektive firnzone viser et tidligere ureflekteret træk ved atmosfærisk gassignaludbredelse i firn.

Метан (CH_4) является одним из парниковых газов наиболее значимых по потенциалу воздействия на тепловой баланс. С начала непрерывных атмосферных наблюдений его концентрация существенно возросла и продолжает расти по причине природных факторов

и антропогенного воздействия. Похожие быстрые изменения концентрации могли происходить в прошлом. Единственным способом напрямую извлечь информацию о газовом составе атмосферы в прошлом является измерения газа, захваченного в образцах ледяных кернов. В работе впервые публикуется ряд концентрации метана в атмосфере северного полушария, измеренный методом непрерывного анализа с высоким разрешением, по данным ледяного керна RECAP с полуострова Ренланд, Восточная Гренландия, 71,3˚с.ш. 26,6˚в.д. 2300 м над у.м. (пробурен в 2015 г.)

Ряд метана является первым голоценовым рядом, измеренным с высоким разрешением в северном полушарии. Вековые колебания в ряду концентрации метана находятся в фазе и совпадают по амплитуде с таковыми по данным антарктических рядов. Выявлены колебания с общим периодом 600-700 и 200-500 лет, а в позднем голоцене могут быть более высокочастотные колебания с периодом около 70 лет. Предполагается, что наличие вековых колебаний обусловлено связью внутритропической зоны конвергенции и муссонной активности, которая в свою очередь через влияние влажности регулирует количество выбросов метана из болот тропических широт.

Концентрация CH_4 менялась с различной амплитудой в течение переходов от стадиалов к интерстадиалам (GS/GI) в ходе последнего оледенения (11.7-120 тыс. л.н.). Относительные амплитуды отличались от таковых в изменчивости температуры. В исследовании рассмотрены концентрация метана в северном и южном полушарии, включая ряд, полученный с высоким разрешением по ледяному керну RECAP, а также палеоклиматические реконструкции во время переходов GS/GI-19-21 (67-87 тыс. л.н.). Выявлено наличие дополнительного источника метана в северо-евразийском регионе, потенциально обширных болотных территорий, сформировавшихся на месте отступившего ледника и спущенных приледниковых озер. Дополнительный источник метана был активным 78-83 тыс. л.н.

Помимо образцов ледяных кернов, измерения концентрации метана проводились также непрерывно в приземном слое воздуха и в верхнем горизонте фирна. Мониторинг осуществлялся на базе проекта бурения ледяного керна East Greenland Ice-core Project (EGRIP) в северо-восточной Гренландии в летнем сезоне 2017. Обнаружен дневной цикл в изменении концентрации метана как в воздухе, так и в фирне, который сохраняется в дни штиля без поверхностного таяния. Наличие дневного цикла в конвективной зоне фирна, традиционно считавшейся зоной перемешивания атмосферного газового сигнала, показано впервые.

Introduction

Ice cores represents a valuable geological archive of the Erath climate change record in the past. Gas bubbles trapped in the ice are the direct samples of the past atmosphere allowing to measure concentration and the isotopic composition of the gases in the past (Barnola et al. 1983, Stauffer et al. 1985).

The ice core data allowed tracing the direct link of the temperature variation and the concentration of the greenhouse gases (GHG) in the atmosphere over the past at least 800 kyr (thousand years). The study was based on the deep Antarctic ice cores (Petit et al. 1999, Loulergue et al. 2008, Jouzel et al. 2007). The atmospheric monitoring revealed that the modern concertation of the second and the third most important greenhouse gases – carbon dioxide (CO_2) and methane (CH_4) – has sufficiently increased in comparison with the observed in the ice cores over the past 8 glacial-interglacial cycles. The average global interglacial CO_2 concentration is 280 ppm (parts per million) whilst in June 2018 it reached 410.79 ppm (https://www.esrl.noaa.gov/gmd/ccgg/trends/) preserving the mean annual growth tendency. The corresponding values for CH_4 are 700 ppb (parts per billion) and 1858 ppb in April 2018 (https://www.esrl.noaa.gov/gmd/ccgg/trends_ch4/#global_growth).

Methane atmospheric concentration in the past is amongst the most appropriate paleoclimate proxies as its residence time in the atmosphere is 9.1 ± 0.9 yr (Prather, Holmes and Hsu 2012), which makes this gas fast reacting to the climate change.

Understanding of the role greenhouse gases played in the past climate change is crucial for predicting the reaction of the climate system to the current elevated greenhouse gases content in the atmosphere. The study focuses on the rapid variations in the methane content in the atmosphere and its relation to the general climatic state. The relevance of the study is due to the modern abrupt increase in the greenhouse gases content concentration in the atmosphere that has not been followed yet by the whole climatic system reaction.

The episodes of the CH_4 concentration increase in the atmosphere repeated along with the temperature rise over the climatic transitions. However, the link of the two is likely not direct and is due to the complex interaction of the climate system components. The relative amplitudes differed between the transitions, which points out on a potentially different mechanisms dominating at different transitions.

The recently obtained REnland ice CAP (RECAP – https://recap.nbi.ku.dk/) ice core aided to calculate the relative interpolar methane difference based on the multiple cores comparison. A

compilation of the paleoclimate proxies (stable water isotopic composition as a proxy for air temperature, carbon isotopic composition as an indicator of the methane source, palynology and peat studies as a proxy for the vegetation formation, paleoglaciological reconstruction of the past ice sheets extent) serves the purpose of the different climatic mechanisms identification.
Moreover, RECAP record provides first high-resolution Holocene CH_4 record in the Northern Hemisphere. Short-term variability traced in the cleaned and calibrated record is mirrored in the Southern Hemisphere (based on the Antarctic Holocene CH_4 record), which reveals a new feature of the methane concentration dynamic in the atmosphere under the stable warm climatic conditions. The centennial scale variability was traced earlier during the stable period of glacials and interglacials over the Last Glacial Period (Rhodes et al. 2017).
This study aimed to obtain the high-resolution methane record of the Northern Hemisphere based on the RECAP ice core and analyze the possible climatic short-term characteristics of its variability over the past climatic cycle, i.e. Late Eemian, Last Glacial and Holocene. In order to conduct the study we had to:

1) Improve the experimental CFA set up for the methane measurements
2) Measure and obtain the calibrated and dated RECAP CH_4 record
3) Analyze the high-resolution Holocene record and distinguish between the short-term variability of climatic origin, the melt layers tracers and the measurement artifacts
4) Identify if the short-term variability is also present in Holocene Southern Hemisphere and what are its natural reasons
5) Select a period over the Last Glacial where the relative amplitude of CH4 and temperature increase would differ and reconstruct the natural mechanisms
6) Scan through the part of Eemian record captured in RECAP ice core and compare it with the modern interglacial, i.e. Holocene record
7) Finally, in order to contribute to the studies of the gas signal formation in firn, we perform the CH_4 concentration in the atmosphere and upper firn air in Greenland and evaluate if its features any diurnal or seasonal dynamics in the relation to the meteorological factors.

Chapter 1 provides an overview of the climate change over the known climatic history and the role of the greenhouse gases in it; contains an information about the atmospheric methane, its source and sinks in its past content. The chapter also covers the general theoretical background on the gas trapping in the ice.

Chapter 2 contains a detailed history of the development and implementation of continuous flow analysis (CFA) method along with the technical background and particular developments at CIC. Chapter 3 of the thesis describes the Renland ice cap drilling site and the project, particular features of the RECAP ice core. The CH_4 series was measured using the CFA method at the Centre for Ice and Climate (CIC), University of Copenhagen, Denmark.

Chapter 4 provides a climatic interpretation of the Holocene, Last Glacial and Eemian records resolve in the RECAP ice core. The study led on to the two main points and potential publications:

1) the presence of the centennial-scale variability in the Holocene significantly coherent and in phase with the CH_4 variability in Antarctic ice core record;

2) noted earlier difference in the relative amplitude of the CH_4 and temperature increase at the stadial-interstadial transitions led to a study of the interpolar difference. RECAP CH4 record was compiled with the other published Greenland and Antarctica CH_4 records and we identified an additional biogenic methane source that was active 83-78 ka BP (thousand years before present) in the Northern Hemisphere biasing the relative interpolar difference.

Chapter 5 shows the data of the CH_4 concentration measurements in the atmosphere and the upper firn performed continuously in 2017 Greenland field season at EGRIP site (The East Greenland Ice-core Project – https://eastgrip.org/), which led to the third thesis point:

3) a diurnal cycle is present in the atmospheric methane on 2 m height from the surface over the central part of Greenland ice sheet. It is propagated to the upper firn column (at least to 1-2 m depth) during the calm days, smoothed out by the wind pumping and interrupted by the surface melting forming the isolating crust and dissolving atmospheric methane from the gas pores.

Chapter 1. Overview of the CH_4 signal formation in ice cores

1.1. Greenhouse gases and the climate change over the know Earth climate history

The two factors responsible for the Earth temperature regulation are the exogenous (solar radiation) and the endogenous (radioactive decomposition energy in the Earth mantle). Since 4.5 Byr (billion years ago) and until 500 Myr (million years ago) the endogenous heat dominated as the atmosphere was thick and opaque for the solar radiance. As the atmosphere thinned and the Earth core cooled down the solar radiance began to play a more significant role in the climate regulation. This period is called Phanerozoic Eon, it began 541 ± 1 Myr and lasts until present (Cohen et al. 2013). As the Sun radiated the Earth under a certain angle, which changes due to the orbital and axis rotation, the diurnal cycle and the seasonality appeared. These were not the characteristic of the temperature regime regulated by the internal heat. Interannual variability of the Earth climate became also dependent on the incoming solar radiation and orbital parameters of the Earth (precession, nutation, the elliptical shape). Warm and cold periods became distinguished as well as ice ages. Figures 1 and 2 show the temperature variations reconstructed over the past 500 Myr.

The ice ages have a periodicity of about 150 million yr. They are characterized by the sustain ice sheets and mountain glaciers extent. The Current Ice Age began 35 Myr with Antarctic ice sheet formation (Zachos et al. 2001). Its latest still progressing stage – Quaternary Glaciation (or Pleistocene Glaciation) – began 2.6 Myr and is characterized by the glaciation extent beyond Antarctica and ice sheets formation in the Northern Hemisphere. Within one ice age some more severe climatic conditions during the glacial periods (or glacials, glaciations) take over some more temperate climate during the interglacials. We live in the interglacial called Holocene, which began 11.7 kyr BP (thousand years before present, i.e. 1950 AD). The beginning is marked by the Laurentide and Scandinavian ice sheets degradation (in Northern America and in Europe correspondingly).

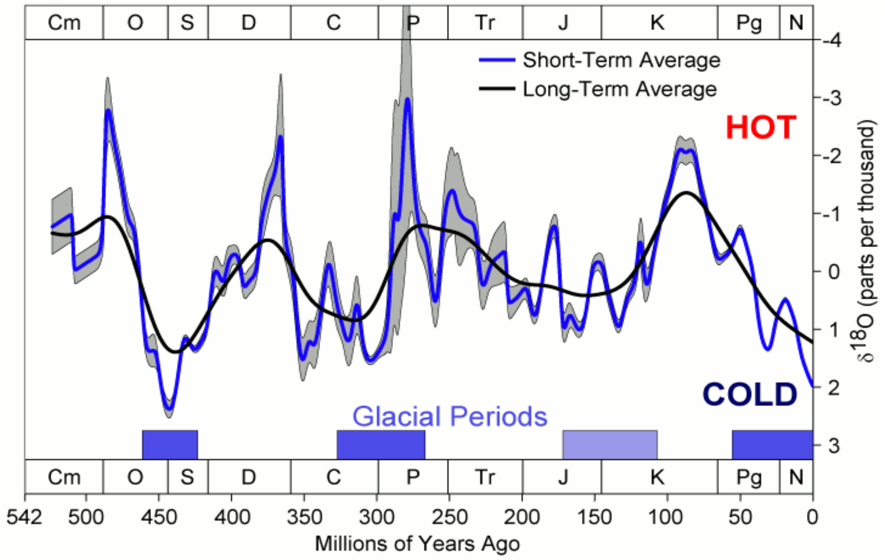

Figure 1: *Phanerozoic climate change (figure is extracted from https://en.wikipedia.org/wiki/Geologic_temperature_record#/media/File:Phanerozoic_Climate_Change.png (Veizer et al. 1999)).*

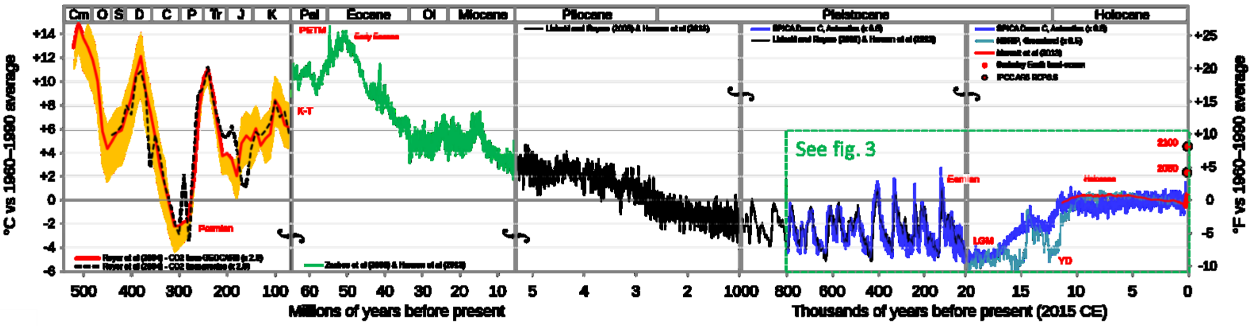

Figure 2: *Temperature of Planet Earth (the figure is taken from https://en.wikipedia.org/wiki/File:All_palaeotemps.png#Summary based on the data by (Royer et al. 2004, Zachos, Dickens and Zeebe 2008, Hansen et al. 2013, Lisiecki and Raymo 2005, Marcott et al. 2013, Jouzel et al. 2007, Andersen et al. 2004, IPCC 2013), http://berkeleyearth.org/land-and-ocean-data/).*

The past 800 kyr were studied in details based on the ice core data (Jouzel et al. 2007). Eight glacial-interglacial cycles occurred during this time. Glacials' duration was about 70-100 kyr and interglacials lasted 10-30 kyr (see fig. 3, upper panel). There is, however, a suggestion that the current interglacial will last 50 kyr more due to the human induced global climate change (Berger and Loutre 2002).

The glacial periods are divided into stadials and interstadials – colder and warmer stages of the glacier advance and retreat correspondingly. During the Last Glacial Period (119-11.7 kyr BP) 25 stadial-interstadial transitions were identified based on the Greenland ice core data (Rasmussen et al. 2014) (see fig .3 – lower panel). The interstadials generally onset with an abrupt warming lasting 20-30 yr, which followed by a warm climate of interglacials and gradually cooled to the stadial climatic conditions, which lasted a few thousand years. The abrupt climatic shifts are called Dansgaard-Oeschger (DO) events (Dansgaard et al. 1993).

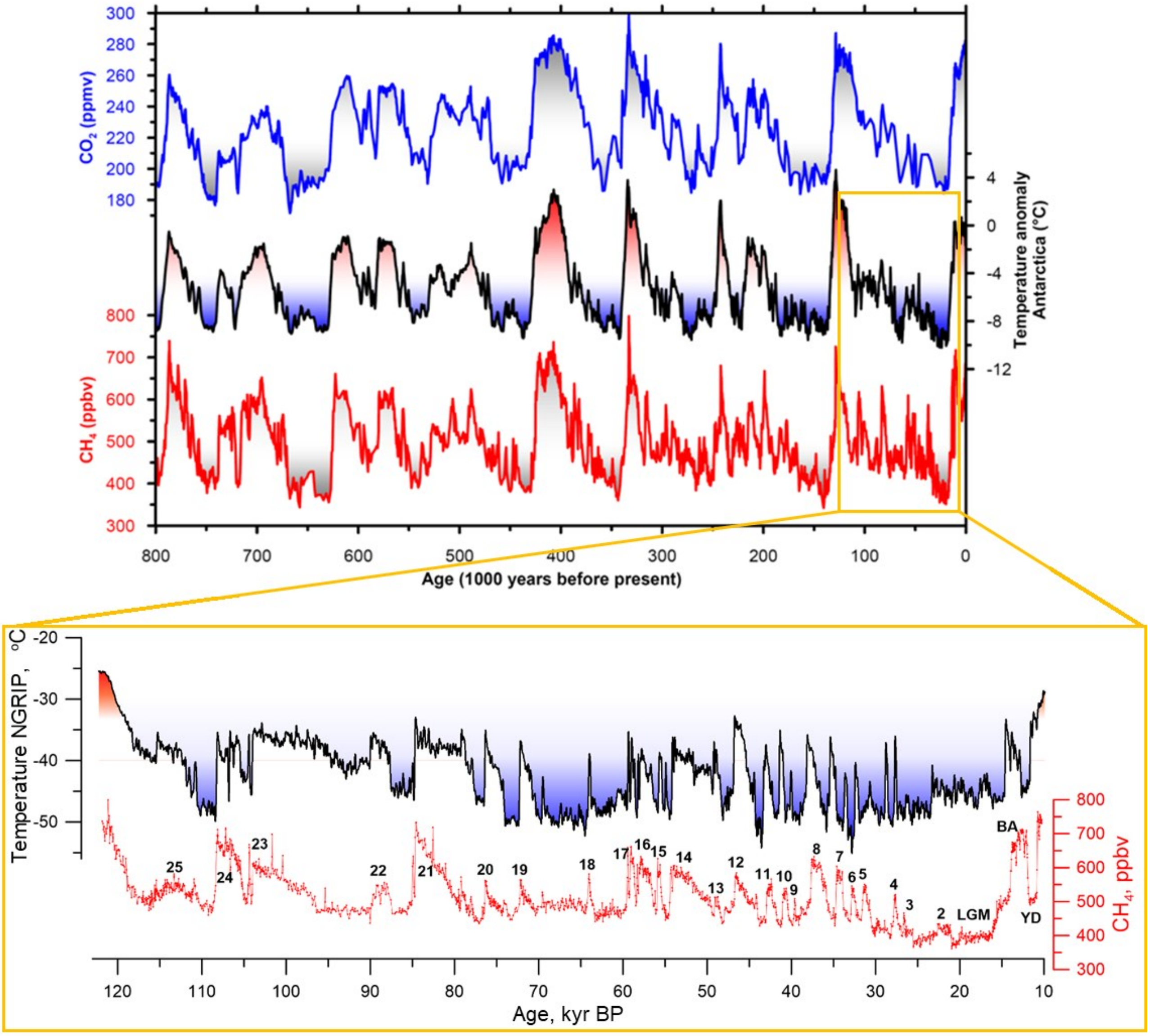

Figure 3: *Upper panel: the surface air temperature (Jouzel et al. 2007) and the greenhouse gas concentration change (CH_4 – (Spahni et al. 2005, Loulergue et al. 2008), CO_2 – (Petit et al. 1999, Monnin et al. 2001, Siegenthaler et al. 2005, Lüthi et al. 2008)) over the past 800 kyr based on EPICA Dome C ice core record (Antarctica), figure is taken from* http://www.iceandclimate.nbi.ku.dk/images/images_research_sep_09/EPICA_without_current.PNG. *Lower panel: temperature and methane concentration change based on NGRIP ice core (Greenland), the figure is adopted from (Baumgartner et al. 2014). The numbers mark the DO events.*

As seen in figures 1-3, the climate changes and glacial/interglacial fluctuations occurred under the natural reasons throughout the known Earth climatic history. The maximum temperature rise during the stadial/interstadial fluctuations approximated the interglacial level but the average temperature was matched to the glacial conditions.

The modern climate change occurs predominantly due to the anthropogenic influence along with the natural forcing – primarily due to the high greenhouse gases emissions. The UN makes an effort to reduce the emissions in order to hold on the temperature rise at +2˚C of the average preindustrial (prior to 1750 AD) temperature level by the end of the XXI century (https://unfccc.int/resource/docs/2015/cop21/eng/l09r01.pdf). The paleoclimatic data suggests (fig. 2) that in this case the modern temperature will approximate Miocene-Pliocene transition – a time when the Greenland ice sheet began to form in favorable climatic conditions. The two states of the system 'air temperature-ice volume' are possible in the given temperature conditions, namely hysteresis (Cuffey and Paterson 2010): 1) if the glaciation did not exist earlier and the temperature decreased continuously, an ice sheet would begin to form; 2) if the glaciation existed but the temperature rose, an ice sheet would progressively degrade. In the second case a temperature decrease to the initial level is not enough, a more sufficient temperature drop is required. This is why Greenland ice sheet is considered as a relict of the last glaciation. The first case might be a general analogue of the Miocene-Pliocene transition and the second case – the modern conditions.

Water vapor, carbon dioxide and methane are the main greenhouse gases in terms of its radiative forcing (Kiehl and Trenberth 1997). The greenhouse effect occurs due to the ability of the gas molecules to adsorb both direct solar irradiation and the radiation of the Earth in the infrared range. The adsorption of the heat prevents the Earth from cooling down by the less emission of the heat to the space.

The past eight glacial/interglacial cycles demonstrated a direct link of the temperature and the greenhouse content in the atmosphere. The modern postindustrial era is an exception: CH_4 and CO_2 already exceeded the observed earlier average interglacial concentrations and the temperature increase did not follow yet by a corresponding relative amplitude (IPCC 2013) (see fig. 4). This leads to the main concern of the modern climate change – how will the temperature and the whole climatic system react to the elevated main greenhouse gases content in the atmosphere. The immediate reduction is impossible due to the varying lifetime of every gas and disrupted balance of the natural sources and sinks (e.g. the ocean almost reached its limit in the CO_2 dissolution and the boreal wetland nowadays emit more CH_4 as a response to the warmer autumns and the reduced sea ice extent in the Arctic (IPCC 2013, Parmentier et al. 2015)).

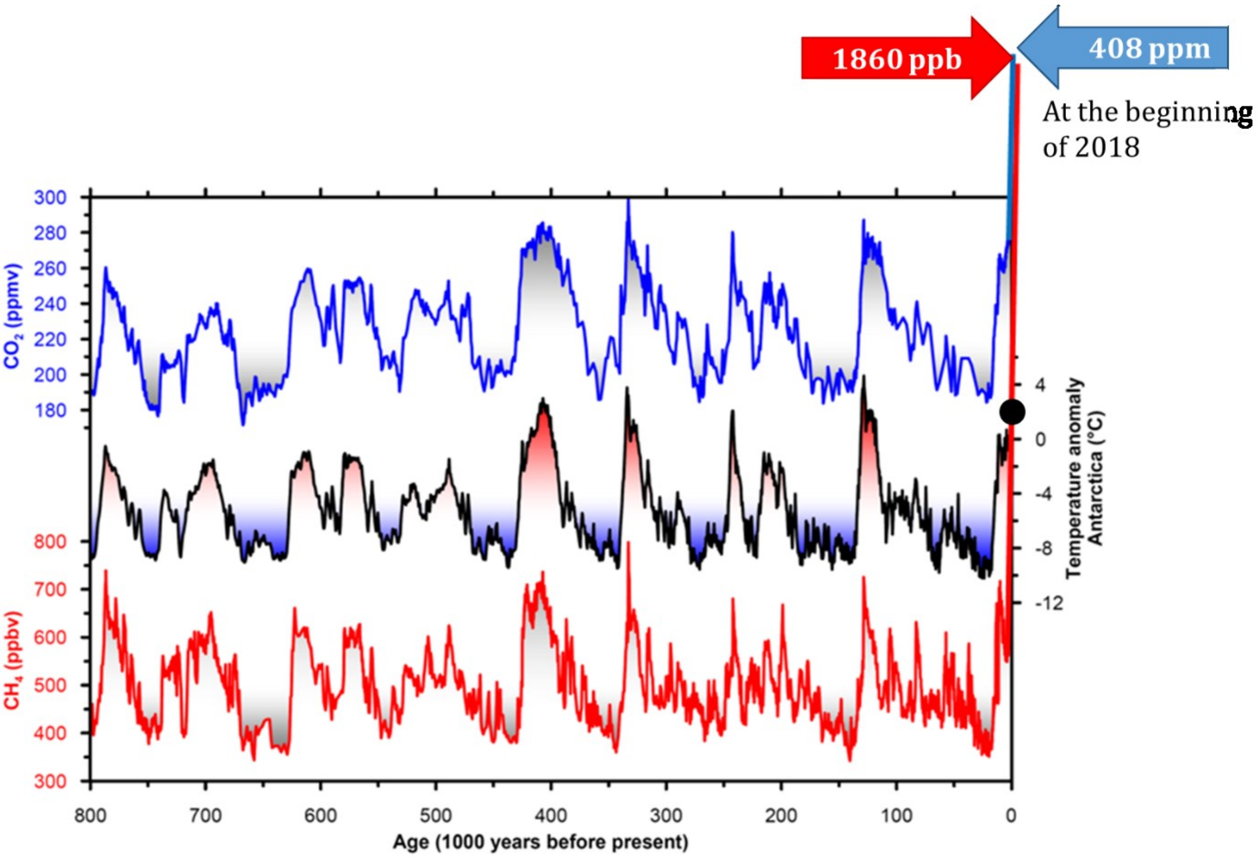

Figure 4: *The same as Fig. 3 with marked modern temperature (black dot, (IPCC 2013)), atmospheric concentration of CO₂ (blue curve and arrow) and CH₄ (red curve and arrow), the data is taken from the Global monitoring division of NOAA https://www.esrl.noaa.gov/gmd/ccgg/trends/. The figure is taken from http://www.iceandclimate.nbi.ku.dk/research/past_atmos/composition_greenhouse/.*

1.2. Methane as one of the most important greenhouse gases

1.2.1. Methane as an atmospheric gas

Methane is a tetrahedron molecule containing of one carbon atom and four hydrogen atoms. It exists in the gaseous phase at a normal conditions, it is flammable at a concentration 5-17% at a normal pressure. Methane molecule turns to a plastic crystal when freezing. The most of the atmospheric methane is concentrated in the troposphere; its global distribution is biased toward the Northern Hemisphere, where the CH_4 concentration is on average 10% higher (https://www.esrl.noaa.gov/gmd/ccgg/carbontracker-ch4/). It occurs mainly because of the larger continental area, i.e. total area of the CH_4 sources. The average exchange time between the hemispheres is 1 yr. The residence time in the atmosphere, i.e. the time between emission by source to the oxidation and decomposition of the methane molecule is on average 9.1 ± 0.9 yr (Prather et al. 2012).

It is not clear how to line a distinctive border between the atmospheres of the Northern and the Southern Hemispheres for methane concentration study. In the scope of the thesis the ch4 concentration of the polar regions was considered based on the Greenland and Antarctic ice core studies. This subdivision is mainly due to the existence of the atmospheric circulation cells, the exchange between which is reduced. Moreover, every hemisphere involves tropical regions and it is not relevant to assess the tropical CH_4 concentration directly based on the polar ice cores studies as tropical wetlands are the dominant source of CH_4 (see e.g. (Chappellaz et al. 1993)). Hereinafter either the Northern or the Southern Hemisphere mentioning in the scope of methane concentration means the atmosphere of the Northern or Southern polar regions.

Atmospheric methane concentration has seasonal and diurnal variability. The diurnal cycle occurs either due to the methane trapping in the near surface inversion layer in the evening (E. Nisbeth, pers. commun., 2018) or due to the variations in the source emissions. The amplitude of the diurnal cycle is gradually damped toward high latitudes due to the decreasing source area and its remoteness. The natural sources emission could be controlled via the diurnal moisture consumption by the plants. The anthropogenic emissions is linked to the diurnal traffic periodicity (Long, Flanagan and Cai 2010).

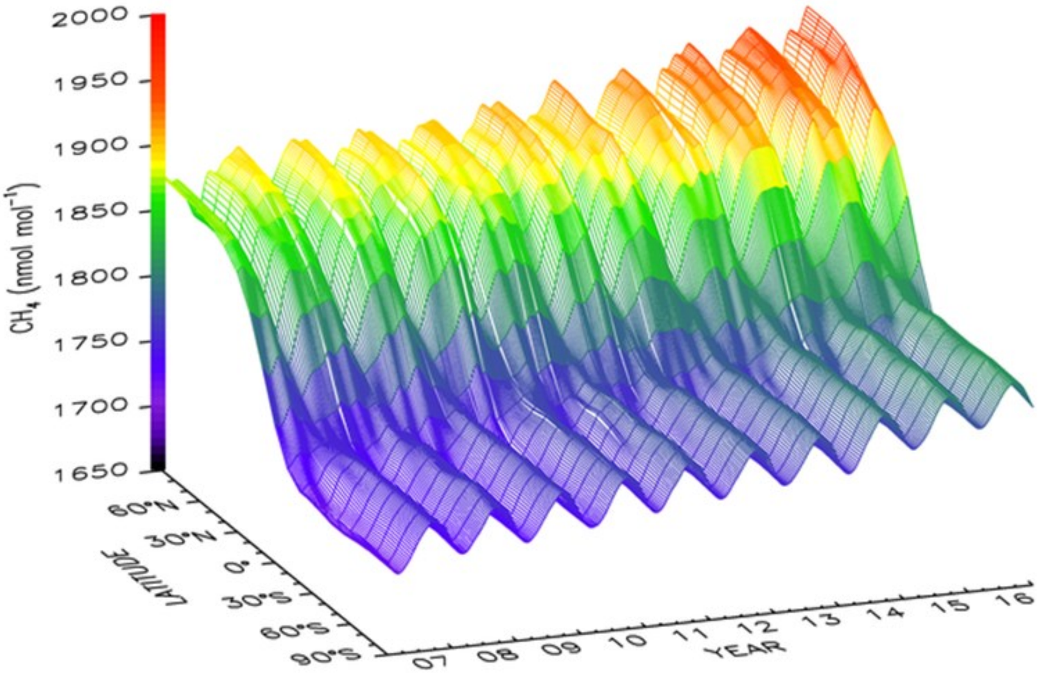

Figure 5: *Global methane distribution over 2007-2016 as observed by NOAA – National oceanographic and atmospheric administration, Earth system research laboratory, Global monitoring division (the figure is taken from https://www.esrl.noaa.gov/gmd/ccgg/gallery/figures/)*

The seasonal variability is due to the annual life cycle of the wetland vegetation and correlates positively with the soil temperature change (Long et al. 2010). The seasonal cycle and the interpolar difference is presented in Fig. 5.

1.2.2. Methane sources and sinks

A few natural sources of methane are known: wetlands, biomes of oceans and lakes, gas hydrates on the sea bed and in permafrost, termites and tundra. Among the anthropogenic sources rice paddies and ruminants emit the most methane followed by coal and peat mining sites, biomass burning, urban areas, sewage outflow, licks at the natural gas mining sites, pits at the biogas mines, concrete production and so on (Khalil 2000). The fluxes of the methane emission contribution from different sources is shown in Fig. 7.

The CH_4 sources can be classified by its origin as biogenic, pyrogenic and thermogenic (Neef, van Weele and van Velthoven 2010) or as natural and anthropogenic. Biogenic sources emit methane as a byproduct of the organic matter decomposition by bacteria in anaerobic conditions (it is relevant for wetlands, ruminants, waste burials, rice paddies, fresh water pools, termites). The thermogenic sources emit methane slowly (i.e. noticeable on the geologic timescale) due to metamorphism of organic matter to fossil fuel (natural gas, coal, oil). The pyrogenic source is characterized by the incomplete biomass burning. The emissions from some sources can imply two mechanisms for instance some geological sources – gas seeping from the sea bed, mud volcanoes or gas hydrates.

Intergovernmental Panel on Climate Change (IPCC) estimated the contribution of the natural sources being 35-50% and the anthropogenic sources as 50-65% over 2000s (IPCC 2013).

The main sink of atmospheric methane is the hydroxyl ion OH^-. It leads to the methane oxidation and decomposition (Fig. 6).

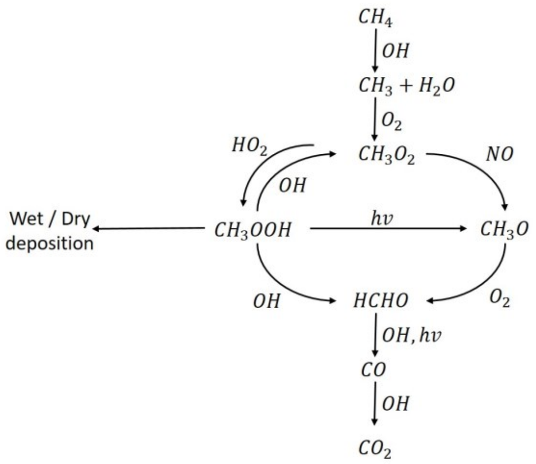

Figure 6: *Atmospheric methane oxidation chain (figure is extracted from (Seinfeld and Pandis 2012)).*

The oxidation occurs predominantly in the troposphere and stratosphere. This process sinks roughly 90% of all atmospheric CH_4 emitted over a year (IPCC 2013). The OH^- radical has very short residence time in the atmosphere, the direct measurements of its concentration is problematic. It is characterized by a small interannual variability equal to 1-3% (1σ) over 2001-2010. The reason lies in high rate of its photochemical reactions in the atmosphere (Voulgarakis et al. 2013, Young et al. 2013).

The secondary methane sinks are: chemical reaction with chlorine in the marine boundary layer (Allan, Struthers and Lowe 2007); a reaction with chlorine adds oxygen ions to the stratosphere (Shallcross, Khalil and Butenhoff 2007, Neef et al. 2010); oxidation by the methanotrophic bacteria in the soil upper layer (Curry 2007, Dutaur and Verchot 2007, Spahni et al. 2011, Ito and Inatomi 2012).

A schematic CH_4 turnover in the frame of the modern carbon cycle is shown in Fig. 7.

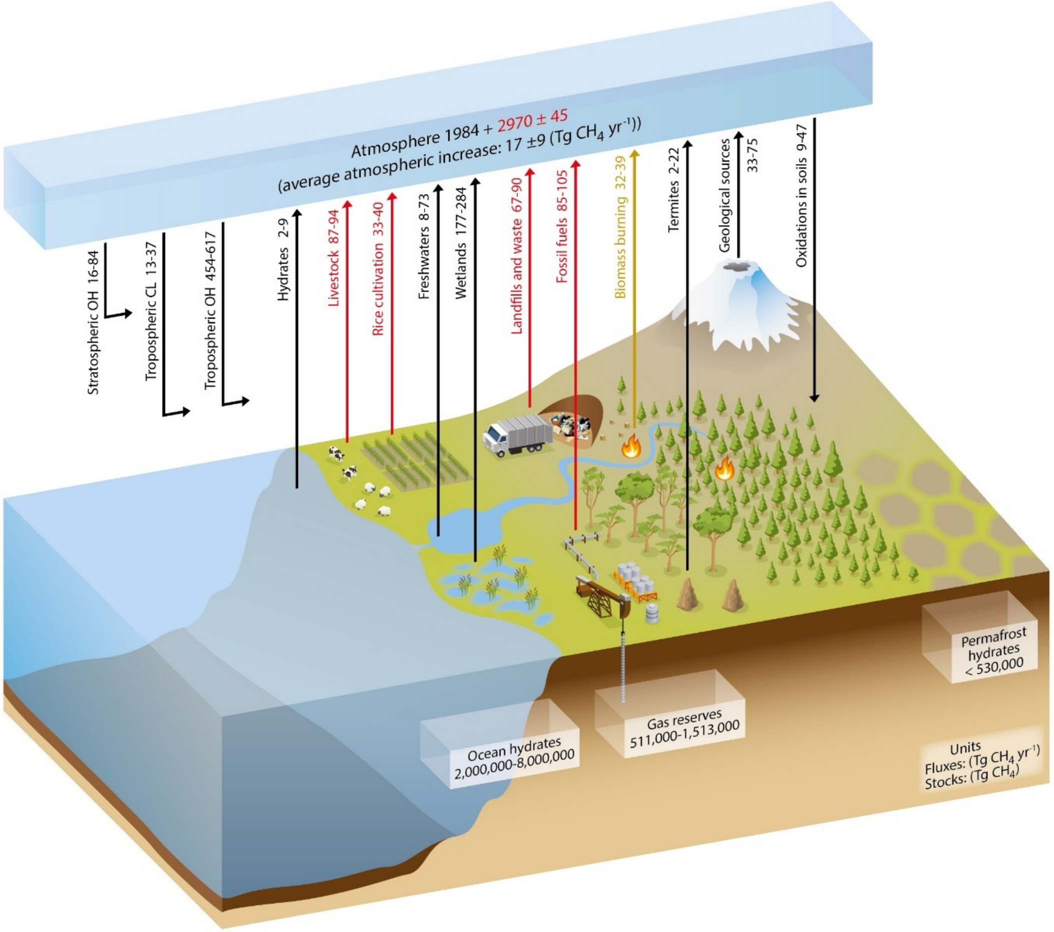

Figure 7: *As scheme of methane cycle (the figure is taken from (IPCC 2013)). Numbers mark the flux in Tg(CH_4) yr^{-1} estimated for 2000-2009 or stocks in Tg(CH_4); the natural sources and sinks are marked as black arrows, the anthropogenic sources – red arrows, the combined source – brown arrow.*

1.2.3. Methane warming potential

Methane is the third main greenhouse gas in the atmosphere following water vapor and carbon dioxide. Its warming potential is 25 times higher than the equivalent volume of CO_2 but due to the fact that its concentration in the atmosphere is lower by a factor of 200, its total warming effect is less.

Prior to the industrial era, i.e. before 1750 AD, CH_4 concentration was estimated as 722 ± 25 ppb (Etheridge et al. 1998, Dlugokencky et al. 2005). It increased more 2.5 times since and reached 1858 ppb in April 2018 (https://www.esrl.noaa.gov/gmd/ccgg/trends_ch4/#global_growth) due to anthropogenic emissions predominantly as suggested by (IPCC 2013). It means that the average rate of the methane concentration increase in the atmosphere is equal to 4.2 ppb yr^{-1} during the industrial and postindustrial era. It matches the range of CH_4 increase over the stadial/interstadial transitions – from 2 to 13 ppb yr^{-1} (calculated based on the data from (Baumgartner et al. 2012)). The only sources emissions are taken into account when calculating the rate of the atmospheric CH_4 concentration change as the abandonee of the dominant sink (OH^-) remains the same at least since the beginning of the direct observations (i.e. since 1979 – (IPCC 2013)).

Likely the wetland methane emissions amplified by the modern climate change are responsible for the high rate of CH_4 increase. Wetlands here is a general term for the ecosystems of wet soils, marshes and swamps, peat bogs in tropical and high latitudes. Such an ecosystems are very sensitive to the climate change especially to increasing summer temperature and precipitations (Dlugokencky et al. 2009). Methane emissions from the thawing permafrost layers in the high latitudes of the Northern Hemisphere will potentially become more abundant within the XXI century due to the modern Arctic warming (Tarnocai et al. 2009, Anthony et al. 2012).

(Myhre et al. 1998) calculated the CH_4 radiative forcing equal to 0.48 ± 0.05 W m^{-2} for 1750-2011 AD, where the uncertainty is mostly due to the errors on the radiate energy transport. Multiplying it by the coefficient 0.8 K m^2 W^{-1} (IPCC 2001) in order to translate the forcing on the radiative balance to the surface air temperature (W m^{-2} to K or ˚C) we obtain the warming equivalent of +0.38 ± 0.4˚C since the beginning of the industrialization forced by the methane emissions only. The total warming over the same period is estimated as +1.83 ˚C (+0.9 – +2.66˚C).

The methane emissions can also have an indirect link to the climate change via the influence to carbon dioxide concentration, to the water vapor content in the stratosphere, to sulfate aerosols and the residence time of the hydrochlorofluorocarbon (HCFC) in the atmosphere (Boucher et al. 2009, Shindell et al. 2009, Collins, Sitch and Boucher 2010).

1.3. Methane in the past atmosphere

1.3.1. Gas trapping during ice formation

Glacier ice is the only direct archive of the past atmospheric content (Stauffer et al. 1985). The ice contains bubbles, which are the actual samples of the past atmsophre (Fig. 8).

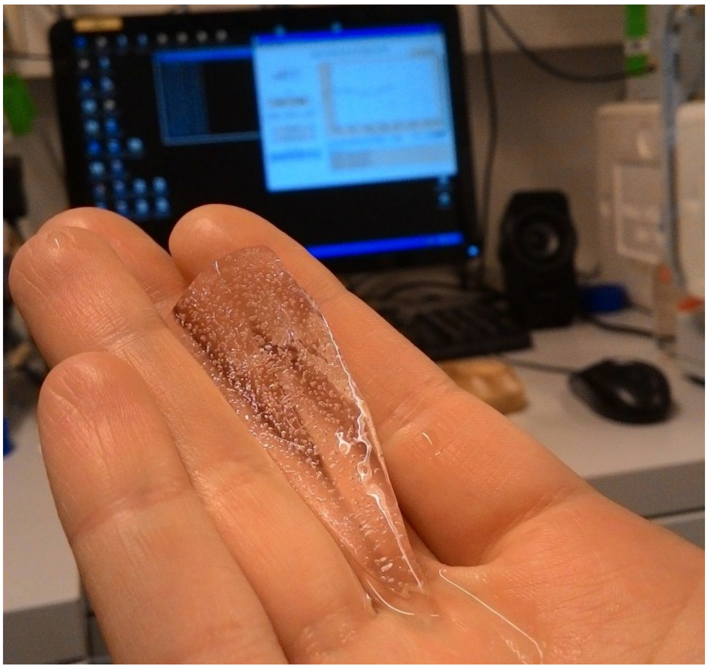

Figure 8: *The appearance of the RECAP ice core sample chop, the approximate depth is 124 m, age 260 yr.*

The dry snow densification is governed by a structural re-arrangement of ice grains by linear-viscous boundary sliding (Anderson and Benson 1993, Alley 1987) until it reaches a relative density (i.e. the density at a certain horizon relative to the density of the pure ice 0.917 g cm^{-3}) equal to 0.6. At this density, the coordination number of the snow grains reaches six, which makes the further sliding impossible. The number of contacts between the grains increases further due to the deformation of grains by power-law creep and the ice sintering (Arzt, Ashby and Verrall 1983, Arnaud et al. 1998), the later occurs because of the water vapor diffusion. At the depth where the relative density is equal to 0.8, the pores take shape of cylinders and ice grains take shape of polyhedrons (Maeno and Ebinuma 1983). When the curvature of the cylinders enhances, they become unstable at some parts, pinch-off and turn to bubbles (Shieh and Evans 1991). Thus the plastic deformation of snow grains, the ice-grain growth, and the disintegration of pores simultaneously control the dynamics of pore closure and air trapping in firn (Arnaud et al. 1998). The atmospheric air trapping occurs at the relative densities range 0.85-0.93. (Stauffer et al. 1985, Kameda and Naruse 1994).

As long as some pores remain open while the firn sinks down, the pore air can be exchanged with the atmosphere at any depth. This age difference, Δage, varies from a few decades (e.g. Law Dome, 66˚44'S, 112˚50'E, East Antarctica, modern conditions) to a few thousands of years (e.g. Vostok, 78˚ 27' 31"S, 106˚ 50' 9"E, East Antarctica, Last Glacial Maximum). The layer settling and the pores close off rate correlate positively with the local surface air temperature and negatively with snow accumulation rate (Salamatin et al. 2009, Bréant et al. 2017).

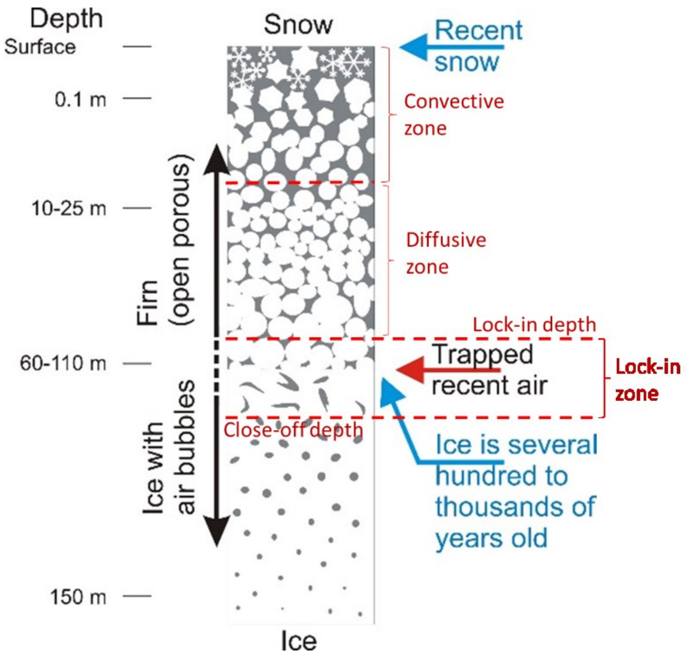

Figure 9: *A sketch of the firn thickness and gradual gas trapping in bubbles (figure is taken from* *http://www.iceandclimate.nbi.ku.dk/research/drill_analysing/cutting_and_analysing_ice_cores/analysing_gasses/firn_zone/* *)*

The whole firn thickness can be subdivided into three zones (Fig. 9) depending on the degree of the pores' closure and the gas signal formation (absolute concentration as well as isotopic composition). The uppermost 2-5 m (up to 23 m in the mega-dunes area in Central Antarctica (Severinghaus et al. 2010)) is a convection zone. Here the snow grains' repacking is in the early stage. All the pores are open and the exchange of the air in pores with modern atmospheric air above the surface occurs unhindered. The atmospheric pressure and the wind regime variability regulates the exchange (Severinghaus et al. 2010).

The following zone, called the diffusive zone, extends down until the first pores close off. The air channel and pores' early formation occurs along the diffusive zone where the gas migration is dominated by molecular diffusion. The diffusive transport leads to gravitational (Craig, Horibe and Sowers 1988, Sowers, Bender and Raynaud 1989, Schwander 1989) and thermal (Severinghaus 1995, Severinghaus et al. 1996) fractionation (or separation) of gases. Heavier gas molecules move downward due to the gravitational settling. There is also migration from the warm to cold fronts (Bender, Sowers and Brook 1997). The latest research suggests that the atmospheric pressure above the snow surface could also play a role in the gas transport causing the molecular gas diffusion (Buizert and Severinghaus 2016). The lower boundary of the diffusive zone, a lock-in depth (LID), corresponds to the point at which the gravitational enrichment stops, and the gas transport by diffusivity becomes low. The lock-in zone (LIZ), where the firn pore closure occurs, is bedded below LID. Its thickness is a few meters, and its bottom corresponds to the close-off depth (COD). Due to the heterogeneity of the firn's properties, in different layers, the pore closure and air trapping may occur at different depths within LIZ. Thus the gas trapped in the ice does not have a unique age at a certain depth horizon but rather

The winter snow is generally characterized by smaller grains thus favoring the faster pores sealing. Moreover, if the moderate summer melting takes place, an ice crust is formed on the surface layer thus sealing (and possibly dissolving) the atmospheric gas, which is contained in the pores. These melt layers are discontinuous, which allows air above and below the crust to exchange. When measuring the gas concentration with high resolution one can clearly trace the increasing noise in the LIZ (Rhodes et al. 2013). It probably occurs due to the alternation of layers with sealed and open pores, which still exchange with the atmosphere. This mechanism of the so-called "layered bubble trapping" is described in (Fourteau et al. 2017, Rhodes et al. 2017). The diffusive lock-in zone dynamic yields to a number of uncertainties in the past atmospheric composition interpretation based on the ice core studies. The first concern is the smoothing of the atmospheric signal in the firn by the gas diffusion, the second is the spikes of non-atmospheric origin, which are either artifacts of trapped gas or the melt layers tracers (Pearman et al. 1986). An example of a noisy gas signal in high-resolution gas record is shown in Fig. 10.

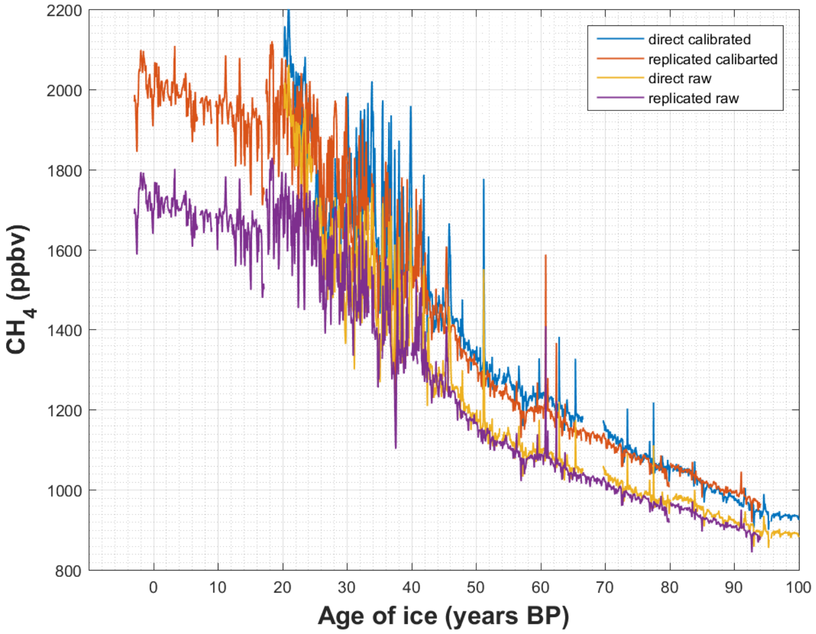

Figure 10: *Methane concentration at the lock-in zone based on the RECAP ice core high-resolution continuous gas measurements. The data is given for the direct and replicated measurements for the raw and calibrated signal in order to show the persistence of the signal with the amplified noose at depth corresponding to ice age 18-42 yr BP (before present, i.e. 2000 AD).*

1.3.2. Modelling of the past atmospheric methane concentration

The methane concentration measured in the ice core samples is a direct indicator of the atmospheric CH_4 in the past. However, the ice core signal does not provide the whole amplitude of an initial atmospheric signal. If a firn gas diffusion time exceed the duration of some atmospheric CH_4 variation, it is likely will not be covered in the resulting ice core signal (or will have smaller amplitude).

For the purpose of the methane flux quantity assessment the various models are used. They include 2-8 atmospheric cells (Northern and Southern Hemisphere subdivided by high, temperate and tropical latitudes) and the parametrization of the methane emissions form different sources (Fischer et al. 2008, Baumgartner et al. 2012, Mitchell et al. 2013). They imply Greenland and Antarctic ice core data as a validation for the modelling output. The results of the methane flux modelling is used as a support for the interpretation of the CH_4 interpolar difference in the past. (Mitchell et al. 2013) used the model of the atmospheric methane transport with eight boxes (every 30˚ of latitude in troposphere and the stratospheric cells of the Northern and Southern Hemispheres), based on the original model written by (Marik 1998). Parametrization of the CH_4 flux between the Hemispheres were copied from the original model. Mitchell’s model allowed calculating the methane flux between the hemispheres during the Late Holocene and evaluating the contribution of the anthropogenic along with the natural sources to the increasing CH_4. The tropical wetland emissions appeared to be the dominant source in Late Holocene. Authors noted some approximations in the model parametrization resulting in the bigger uncertainty on the different source contribution at a certain time: a) the time of the interhemispheric gas exchange is 1.67 yr and is constant throughout the studied period; b) the residence time of methane in the atmosphere is 10 yr and is constant for all latitudinal cells; c) a few scenarios of the different sources contribution are possible; d) the planetary distribution of the methane sources is taken from more complex ecosystem models (Kaplan, Folberth and Hauglustaine 2006, Harder et al. 2007); e) a degree of the gas signal smoothing in the firn is debated.

1.3.2.1. High-frequency methane variability of non-climatic origin

The last issue becomes even more relevant while reconstructing the full amplitude of the atmospheric CH_4 variability in the past. The initial atmospheric signal can be either smoothed out during the gas trapping in firn or the ice core may contain some variability and spikes, which is not characteristic for the initial atmospheric signal (see section 1.3.1 for the details). Such peaks are formed due to the layered bubble trapping (Mitchell et al. 2015, Rhodes et al. 2016, Fourteau et al. 2017). (Fourteau et al. 2017) attempted to model the gas trapping process in the low accumulation rate regions, where they have identified high frequency CH_4 variability up to 50 ppb. These spikes do not appear to be of an actual atmospheric origin, as they would not survive the firn gas smoothing. It was shown that likely the spikes are due to the layered close off process meaning that some bubbles sealed off earlier trapping the older signal while the others were still exchanging with the atmospheric air under the changing CH_4 conditions. This study was conducted using Vostok ice core samples that date back to the Last Glacial Period (60 ka BP). The preceding research was conducted by (Rhodes et al. 2016) based on two Antarctic and four Greenland ice cores samples in the snow accumulation rate range of 6.8-41 cm ice eq. yr^{-1} and mean annual temperature range -24 – -46°C. They showed the appearance of the high-frequency methane spikes, which did not correlate between each other and thus were not relating to the atmospheric signal. (Mitchell et al. 2015) showed the example of the layered bubble trapping performing the CH_4 measurements along the lock-in depth of the WAIS Divide ice core, West Antarctica.

It is important to distinguish the gas trapping artifacts and real atmospheric signal short-term variability when discussing the high frequency CH_4 spikes. For instance, (Rhodes et al. 2017) identified a centennial-scale atmospheric CH_4 variability during the interstadials of the Last Glacial Period. Nonetheless, the CH_4 variability of duration less than the pores close-off time of an individual ice core is hard to interpret unambiguously as an actual atmospheric signal variability.

1.3.3. Methane sources in the past based on the stable methane isotopes analysis

One of the ways to identify the methane sources of the past, besides the modelling, is methane isotopic measurements of gas trapped in the ice cores. A complex isotopic analysis is used for a more precise identification of the CH_4 source, i.e. measurements of carbon stable isotope (carbon 13 – $\delta^{13}C\text{-}CH_4$) and hydrogen (hydrogen 2 or deuterium – $\delta D\text{-}CH_4$). Every methane source has its characteristic isotopic signature (see Fig. 11).

The biogenic sources of methane are characterized by isotopic values -55 to -70‰ for $\delta^{13}C\text{-}CH_4$, thermogenic – by -25 to -45‰, and pyrogenic sources have the $\delta^{13}C\text{-}CH_4$ isotopic signature in the range of -13 – -25‰. The results of the isotopic composition measurements are the boundary conditions at the methane flux models (Bousquet et al. 2006, Neef et al. 2010, Monteil et al. 2011).

However, not in all cases it is possible to identify unambiguously the source using only the isotopic values. E.g. the isotopic measurement results of the gases extracted from ice cores are not always possible to link directly to a certain source. It is necessary to deconvolute the initial atmospheric signal. First, the methane oxidization processes in the atmosphere takes part in the eventual isotopic signal formation making it sufficiently heavier than the source's (Feilberg et al. 2005, Whiticar and Schaefer 2007, Levine et al. 2011). Secondly, the exact contribution of each source to the eventual average isotopic composition of the emitted methane is the subject of modelling (Mitchell et al. 2013). Thirdly, the uncertainty on the exact hemispheric methane concentration is present because often Greenland and Antarctic ice sores samples are measured in different laboratories and setups, which adds an offset to the absolute CH_4 (Sowers 2010, Mitchell et al. 2013). The uncertainty of the hemispheric CH_4 in the past is propagated further throughout the methane flux modelling preventing the exact source contribution evaluation (Fischer et al. 2008, Baumgartner et al. 2012, Mitchell et al. 2013).

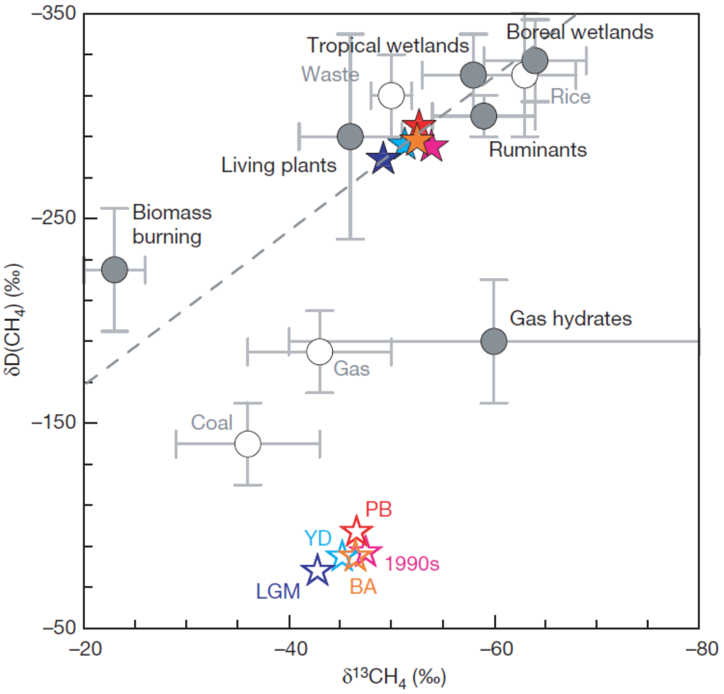

Figure 11: *The stable isotopic signatures of different methane sources. Colored stars identify the mean isotopic values over different periods of the Last Glacial (LGM – the Last Glacial Maximum, YD – Younger Dryas, BA – Bølling-Allerød), Holocene (PB – Preboreal and 1990s AD) – the corresponding colors are marked in the lower part of the plot. Figure is extracted from (Fischer et al. 2008).*

1.3.4. Rapid methane concentration changes during the last glacial cycle

The atmospheric methane residence time is estimated as 9.1 ± 0.9 yr (Prather et al. 2012), which makes this gas a unique indicator of the rapid climatic variations. Greenland and Antarctica ice core studies revealed that the methane concentrations change was closely related to the temperature change not only during the glacial-interglacial cycles (Petit et al. 1999, Delmotte et al. 2004) but also during shorter-term stadial-interstadial variations at least during the Last Glacial Period (Brook, Sowers and Orchardo 1996b, Chappellaz et al. 2013, WAIS community 2013, Baumgartner et al. 2014, Kindler et al. 2014). The rate of the methane concentration increase versus temperature increase varied from 5 to 18 ppb $^{\circ}C^{-1}$ based on Greenland ice core studies. Note that the units do not imply that the temperature is necessarily the driver of the methane variability, but they are rather used for the sake of the data representation convenience. For instance, the rate of change of CH_4 versus temperature over transition to the interstadials 21 and 23 (84.76 and 104.04 ka BP correspondingly (Rasmussen et al. 2014)) was similar to the one of the Last Glacial Termination (Younger Dryas to Preboreal transition 11.7 ka BP) and exceeds the other stadial-interstadial transitions by a factor of two. The statistical analysis of the CH_4 increase rate over individual transitions shows a weak correlation with the temperature rate of change during the corresponding period (Baumgartner et al. 2014). It signifies the relevance of the temperature versus greenhouse gases content studies at a time of rapid climate variations based on the high-resolution ice core data.

The temperature and the methane concentration increases are not linked directly but via a complex regulation of the methane sources productivity by the sea surface temperature variability (Dällenbach et al. 2000, Flückiger et al. 2004). The complexity is expressed e.g. in the fact that the phase shift between the temperature increase and the CH_4 rise is absent during some stadial-interstadial transitions, while during the others this phase shift reaches up to hundred years. (Baumgartner et al. 2014) hypothesized that the longer lag is related to the northward shift of the methane source.

Another type of the rapid methane variations is a centennial-scale variability. Such a variability of 80-500 yr duration was identified in the atmospheric methane signal of both hemispheres over the Last Glacial Period (Rhodes et al. 2017). The existence of such a variability during the Holocene was not found earlier because of the absence of a continuous high-resolution CH_4 series. A recently drilled WAIS Divide ice core CH_4 data (West Antarctic Ice Sheet Divide, 79˚28'S, 112˚05'W, (Rhodes 2015)) demonstrated the presence of the methane concentration centennial-scale variability in the Southern Hemisphere during the Holocene.

The CH_4 ice core signal differ from the initial atmospheric signal due to the firn gas smoothing via the equilibrating diffusion of the methane concentration in the atmosphere and in firn (see section 1.3.1). As discussed above, the firn gas smoothing is a function of the firn temperature and the snow accumulation rate (Spahni et al. 2003, Joos and Spahni 2008, Köhler et al. 2011, Ahn and Brook 2014). (Rhodes et al. 2017) showed a similarity in the atmospheric methane variations amplitude during the Last Glacial and Early Holocene using the deconvoluted signal. (Rosen et al. 2014) applied firn gas smoothing model to WAIS Divide ice core data to reveal the initial CH_4 amplitude. It was acknowledged that the further high-resolution CH_4 measurements of ice cores samples are necessary for more detailed and accurate atmospheric signal amplitude deconvolution. The current research is based on the RECAP ice core data (Eastern Greenland), where the modern mean annual temperature and accumulation rate conditions are similar to those of the WAIS Divide drilling site. It provides an opportunity for the more relevant interhemispheric comparison of the rapid variations in the past atmospheric methane concentration.

The centennial-scale methane variability can be explained via the sources and/or sink changes. Production of the dominant methane sink – OH^- radical – depends on the humidity and the nonvolatile organic compounds content in the atmosphere, which in turn are functions of the surface air temperature (Levine et al. 2011, Levine et al. 2012). The sink variability, however, is considered an unlikely cause of the centennial scale variability. In order to oxidize the amount of methane emissions in the atmosphere, registered in the ice core series, a sufficient amount of the OH^- radical had to be produced. Its emissions is directly linked to the air humidity and the sea surface temperature. Thus the mentioned methane oxidation would require the sea surface temperature increase by 1˚C, which is contradictory to the centennial-scale variability of sea surface temperature in the tropical latitudes (Tierney et al. 2015). Tropical and boreal wetlands as well as biomass burning are considered to be the main sources responsible for the centennial-scale CH_4 variability. The natural variability of the boreal wetlands is linked to the continental ice sheet extent dynamics and the atmospheric circulation variability, which is in turn related to solar radiation change, Atlantic Multidecadal Oscillation, interaction of El-Niño and Pacific Decadal Oscillation (Rhodes et al. 2017).

Chapter 2**. CFA CH_4 measurements at CIC**

2.1. A brief history of CFA measurements

Since the beginning of the studies of gas trapped in the ice cores (in the 1980s – (Barnola et al. 1983)), the measurements were conducted using the discrete samples, i.e. cross-sections of an ice cores cut separately. The gas can be extracted using either melting-refreezing or crushing the sample. Both extraction methods imply the vacuumed cells containing the solid ice core sample, which is connected to the analytical line. Temperature and inner line pressure are controlled. Both methods allow extracting 80% of the gas trapped in the ice. The efficiency of the gas extraction decreases when measuring the samples taken from 600-700 m and deeper. At this depth, the bubbles transit to clathrates meaning that the gas molecules are built into the crystal cage of the ice. An alternative way of the gas extraction is an infrared sublimation (Schmitt, Schneider and Fischer 2011), which was not established as a standard laboratory procedure because of the technical complexity. The advantage of the laser sublimation method is more efficient gas extraction, which improves the precision of the gas measurements at the ice core samples from the horizons deeper 700 m. The research group from Bern University, Switzerland, plans to continue working on the method development.

The methane concentration in the extracted air is analyzed using gas chromatography, mass-spectrometry or the laser absorption techniques. The gas chromatography is essentially separation of the gas mixture in a stream of the carrier gas (argon or helium usually). It occurs at the solid or liquid absorbent chromatograph column. The chromatographic separation is based on the differences between the volatility and solubility (or adsorption) of the gas species. Mass-spectrometry implies the identification of the ions mass-to-charge ratio after the ionization of the analyzed gas mixture. The laser absorption technique is based on the ring-down time of the laser beam emitted from the source and circulating between the mirrors in the cavity. Each gas has its characteristic absorption spectrum and the amount of the gas in the cavity is inversely proportional to the time of the signal ring-down. The total trajectory length can be up to a few kilometers, which allows identifying small gas concentration (in order of ppm or ppb) in a few seconds.

The continuous high-resolution gas measurements is possible to conduct using an ice core analytical technique called the continuous flow analysis (CFA). This method implies a gradual melting of the vertical section of the inner part of an ice core and distribution of the melt stream between the analytical lines including the gas extraction line (for the details see Chapter 2).

The CFA method was developed initially as a sampling method for the high-resolution measurements of the chemical trace elements (Sigg et al. 1994). (Schüpbach et al. 2009) for the first time came up with the idea to reuse the segmented gas flow in the melted sample stream instead of wasting it. They have performed the first continuous flow methane concentration analysis. It became possible by merging the CFA melting line with the gas extraction line and a gas chromatographer. The gas extraction line was set up downstream the debubbler, the dried out gas sample was pumped to a chromatographer. The effective resolution of the measurements was approximately 15 cm.

(Stowasser et al. 2012) modified the CFA CH_4 setup by replacing the analytical part – they changed a gas chromatographer to a laser spectroscopy (wavelength-scanned cavity ring-down spectroscopy – WS-CRDS), the analytical uncertainty of which is 2-5 ppbv.

(Chappellaz et al. 2013) setup two laser analyzers sequentially (WS-CRDS and an optical-feedback cavity-enhanced absorption spectroscopy – OFCEAS) in order to check out the performance of the two technologies given a low sample volume (a few cm^{-3}) and low flow rate (0.8 cc min^{-1}). Moreover, they have assembled the CFA CH_4 setup in the field at the NEEM (North Greenland Eemian ice core project) camp, where they have tested the possibility of the high-resolution gas studies at the drilling site for the quick dating purpose. The first Northern Hemispheric ultra-high resolution CH_4 record covering the Last Glacial period was obtained in the frame of this project.

As the following step (Stowasser et al. 2014) attempted to reduce the effective cavity volume of the laser analyzer in order to decrease the gas smoothing due to the mixing of the sample streams in the cavity.

A typical CFA experimental setup usually consists of the following parts (see fig. 12):

1) vertical ice core frame to sample – small (3.5*3.5 cm) inner section of an ice core, that is not contaminated by the drilling liquid. Each section is 0.55 or 1 m long depending on the ice coring standard.
2) The frame is situated in the freezer at -20°C on the top of the melt head heated up to +20 – +25°C.
3) The melt head has a few radial or concentric slits, through which the outer section of the melted samples flows to waste while the inner section is headed further toward the analytical lines.

4) The peristaltic pumps create a pressure gradient in the lines in order to deliver the sample streams to the analyzer.
5) The air bubbles have to be removed, and the first stage of the gas extraction is a debubbler of pipette or triangular shape. The melted sample stream goes to the debubbler's inlet, the bubbles emerge to the upper outlet of the debubbler due to the buoyancy, while the degassed sample stream is distributed further to the chemical and impurities analytical lines via the lower outlet of the debubbler.

The CFA method has the following advantages:
+ it provides a high resolution paleoclimatic proxies signal
+ it requires a small sample volume, which makes it preferable when distribution the labor- and money consuming ice core samples between the laboratories
+ every melted sample is possible to re-utilize:

a) The gas from the filtered out stream is used for the past greenhouse gases content
b) The termination of the melt stream is discretely sampled for the ion chromatography studies
c) The gas sample can be taken to the sealed flasks in order to perform the isotopic measurements and date the gas sample older 1 Ma, which can be used in the frame of the IPICS Oldest ice challenge, the project Beyond EPICA Oldest Ice – https://www.beyondepica.eu/ (Ritterbuch, pers. communication, 2018);

+ relatively fast measuring speed of the ice core: depending on the measurement campaign schedule (day or round clock shifts) and the melting speed (3-5 cm/min) one can produce the data of 5 to 25 m of an ice core per day. It reduces the time of multi-proxy paleoclimatic series obtaining from years of tedious and time-consuming ice core samples measurements to a few months of an intensive laboratory campaign.

The CFA method is characterized by a few disadvantages:
- the complexity of every CFA experimental set up building and the controversial technical requirements of the different compartments
- gas signal diffusion in the gas extraction line due to the non-segmented flow an low sample flow rate over 2-10 min of the extraction plus measuring time
- asynchrony of the different types of analysis leading to the uncertainty and relative shifts in the depth scale of the proxies.

The CFA is nowadays implemented worldwide at the laboratories conducting ice core analysis because of its minor sample consumption required for a number of simultaneously performed analyses. International CFA measurement campaigns are organized in collaboration with the partner institutions gathering expert in different ice core science fields. There are only 9 CFA setups in the laboratories dealing with the ice cores analysis worldwide: at the British Antarctic Survey – BAS, Cambridge, UK; the Institut des Géosciences de l'Environnement – IGE, Grenoble, France; the Universität Bern, Bern, Switzerland; the Centre for Ice and Climate – CIC, Copenhagen, Denmark, where the current research was conducted; Oregon State University – OSU, Corvallis, USA; the Desert research institute – DRI, Reno, USA; Antarctic research center, Wellington, New Zealand; National Institute of Polar Research – NIPR, Tokyo, Japan. Another CFA s setup is under the construction at the Alfred Wegener Institute – AWI, Bremerhaven, Germany. All setups are of different modifications existing in a single copy and are customer-made. The analytical compartments and supplies come from chemical, geoscience and medical applications. Melt heads and frames are made in the research institutes workshops.

2.2. NEEM and RICE preceding set-ups

Initially the CFA setup existed at the CIC was developed by the research group from the University of Bern for its deployment in the field at the North Greenland Eemian Ice Drilling (NEEM) project (NEEM community 2013) in 2010 (see the modification in Fig. 12). The results of the CH_4 measurements are published in (Chappellaz et al. 2013). Then a slightly modified setup of a reduced size was transported to Queen Victory University, Wellington, New Zealand, where during the two successful measurement campaigns in 2013 and 2014 was deployed to Antarctic ice core measurements in the frame of Roosevelt island climate evolution project (RICE - http://www.rice.aq/drilling-rice-ice.html).

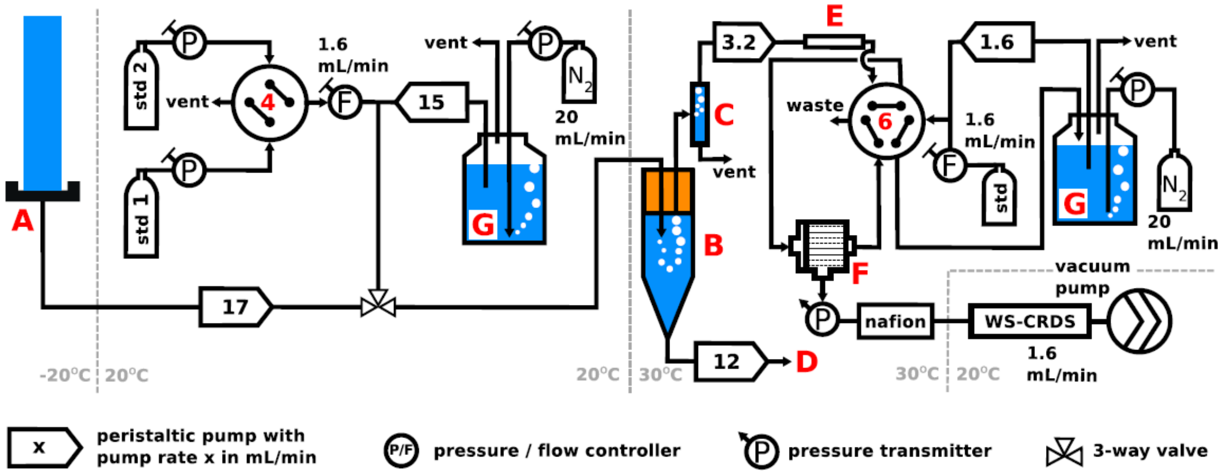

Figure 12: *A sketch of the CFA setup for the methane concentration measurements deployed for the NEEM field measurement campaign (figure is taken from (Stowasser et al. 2012)). A – melthead, B – pipette debubbler, C – open split, D – chemical analysis outlet, E – heated line, F – degassing micromodule, G – MiliQ water used in calibrations; numbers mark the peristaltic pumps' flow rate, cc min*$^{-1}$.

The CH_4 CFA setup operational principle is described based on (Stowasser et al. 2012): an ice core sample of the 3.5*3.5 to 2.6*2.6 cm depending on the melthead modification is placed on top of the heated plate. The standard length of the core is 55 cm and it is placed in the correspondingly long Plexiglas frame. The frame and the melthead are situated in the freezer at -20˚C. The ice core is melted with nearly constant speed 3.2 to 5 cm min^{-1} depending on the analysis requirements. The gas takes 10% of the total volume of the melted sample. The stream is pumped from the freezer to the warm laboratory using a set of the peristaltic pumps (Ismatec REGLO Digital MS-4/12, ISM 597, IDEX Health & Science SA, Switzerland). A debubbler separates the segmented gas flow and the melted sample stream to be distributed to the gas and chemical analysis correspondingly (see (Schüpbach et al. 2009, Kaufmann et al. 2008) for more details). The debubbler has an internal volume of 0.8 cm^3, it is a pipette tip (in the given modification of the setup) with the self-made plug. It has one inlet tube deepened in the debubbler and two outlet tubes – one is on the top for the segmented gas stream outflow and the other is below as a chemical analysis outlet (see fig. 12). The peristaltic pump moves the sample stream for the chemical analysis. An open split is set downstream this outflow to prevent the pressure buildups. The segmented gas flow from the upper outlet, containing approximately 40-50% of gas by volume, is pumped toward the gas extraction line with an average rate of 3.2 cc min^{-1}. The gas is extracted by the hydrophobic membrane micromodule (MicroModule 0.5'' ×1'', G591, Membrana GmbH, Germany). The micromodule has an internal volume of 5.4 ml, the gas extraction occurs due to the pressure gradient created by the laser analyzer's internal pump.

The efficiency of the gas extraction depends on the pressure gradient around the membrane (degassing module). The gas dissolution in water depends inversely on the temperature. Thus, the pressure and temperature conditions are controlled along the gas extraction line. The micromodule is located in the heated box at +30 ± 0,2°C. The pressure is regulated to 700 ± 20 mbar using the inner digital pressure-regulating unit in the analyzer cavity (EPC Proportional Control Valve, EPCA06SSVXAA, Parker Hannifin Corporation). It creates a pressure gradient of 300 mbar, which was enough to extract all visible gas from the segmented flow. A variability of the gas-to-water ratio in the melted sample stream as well as some changes inside the gas extraction line, e.g. a pressure drop in the peristaltic pump lines, cause the extracted gas sample variability in the range of ± 20 mbar. An additional pressure regulator downstream the degassing unit stabilizes the pressure variations.

The extracted gas sample at a flow rate of approximately 1.6 cc min^{-1} is dried in the following unit as it is 100% saturated with the water vapor. It is a custom made dryer where a 1 m long sulfonated tetrafluoroethylene tube (Nafion TT-020, Perma Pure LLC, USA, inner volume 0.3 mm) is cased in 1/8" stainless steel tube. A space between the outer part of Nafion and the inner walls of the casing tube is blown with the dry air mixture or nitrogen at a rate of 20 cc min^{-1} in the direction opposite to the sample flow and exhausts through an open split. The Nafion's drying efficiency depends on the partial water vapor pressure in the space between the Nafion itself and the casing. A humidity of the gas sample in the outlet of the Nafion is 0.03% of volume. This drying of the extracted gas sample is enough to skip the correction of the CH_4 concentration measurements on the water content (Rella 2010). The sample is pumped further into the cavity of the cavity-ringdown spectrometer Picarro G1101-i (Picarro Inc., USA). A built-in diaphragm pump controls the gas flow rate and creates the pressure gradient along the degassing and drying units. Note that the analyzer is capable to recognize only carbon 12 and hydrogen 1 among the CH_4 isotopes, i.e. the heavy stable isotopologues of the CH_4 are not included in the total CH_4 concentration. However, given the negligible natural abundance of the heavy stable isotopologues of the CH_4, the eventual uncertainty on the absolute methane concentration measurements is very small and beyond the detection limit.

The moment of the ice core frames reload requires special care as the ambient air may sneak into the system contaminating the gas extraction line. The ambient air is enriched in methane (see section 1.2.1), which yields the long memory effect (≈ 10 to 30 min) due to the relatively slow gas turnover throughout the line and the analyzer cavity given that the sample flow rate is 1.6 cc min^{-1}. The ambient air penetration into the melthead also causes emptying of the debubbler, which affects the chemical analysis calibration baselines. In order to prevent the sample extraction line contamination by the ambient air, the segmented standard gas flow is launched into the line in the stream of the MiliQ water. The switch from the sample flow, or the external line, to the MiliQ and standard gas stream, i.e. in the internal line, is carried out using the 6-way valve (Cheminert C22Z-3186EH, VICI AG, see fig. 12, mark “6”). This is the way to keep nearly constant pressure in the gas extraction line between the melting runs. The peristaltic pump (marked as 1.6 in the arrow on fig. 12) and a mass flow controller (MFC 5850E, Brooks Instrument, USA, marked as black “F” on fig. 12) control the constant water and gas flow rates, correspondingly.

A modification of the CFA CH_4 setup used later in the NEEM field campaign in 2010 (Chappellaz et al. 2013) had the following modifications: two laser spectroscopes were set sequentially (optical-feedback cavity-enhanced absorption spectroscope – OF-CEAS; SARA instrument, LIPhy, Grenoble, France) and the cavity ring-down spectroscope (WS-CRDS; Picarro Inc., USA); the MiliQ water bottle was outside the thermally regulated box; the segmented standard gas stream was not connected to the gas extraction line downstream the melthead.

In the RICE ice core measurement campaign in 2013 and 2014 (Lee et al., in prep.) the initial version of the CFA CH_4 setup was reduced to fit the size of a thermal insulating box (60*40*30 cm).

Later in 2013 (Stowasser et al. 2014) in collaboration with Picarro Inc. (https://www.picarro.com/) designed a prototype of the low volume laser analyzer (9.6 cm^3) capable to measure the CH_4, CO and H_2O concentration in the sample at a constant pressure 20, 45 or 140 Torr. The corresponding efficient volume of the cavity is 0.25, 0.57 and 1.8 cm^3 at a normal conditions. The usage of laser analyzer Picarro G1301 was also capable to detect the sample at a pressure 140 Torr but the cavity volume was bigger, which yielded the response time 6 times slower than for the modified analyzer. Linearity, precision and stability of the previous generation is preserved in the modified analyzers. The reduction of the inner volume of the cavity was achieved by installing the triangular prism inside the cavity. The modified laser analyzer capable of measuring CH_4, CO и H_2O concentration was connected to the CFA gas extraction line and is used up until now at the CIC for the CFA CH_4 measurements.

2.3. RECAP CFA campaign preparations

In the frame of current research we have conducted a measurement campaign of RECAP ice core (see section 3.1) at the CIC CFA setup (Fig. 13 and 14). This gas extraction setup (circled in green in Fig.13 and shown in more details in Fig. 14) is essentially a modification of the CFA CH_4 setup described above (Stowasser et al. 2012).

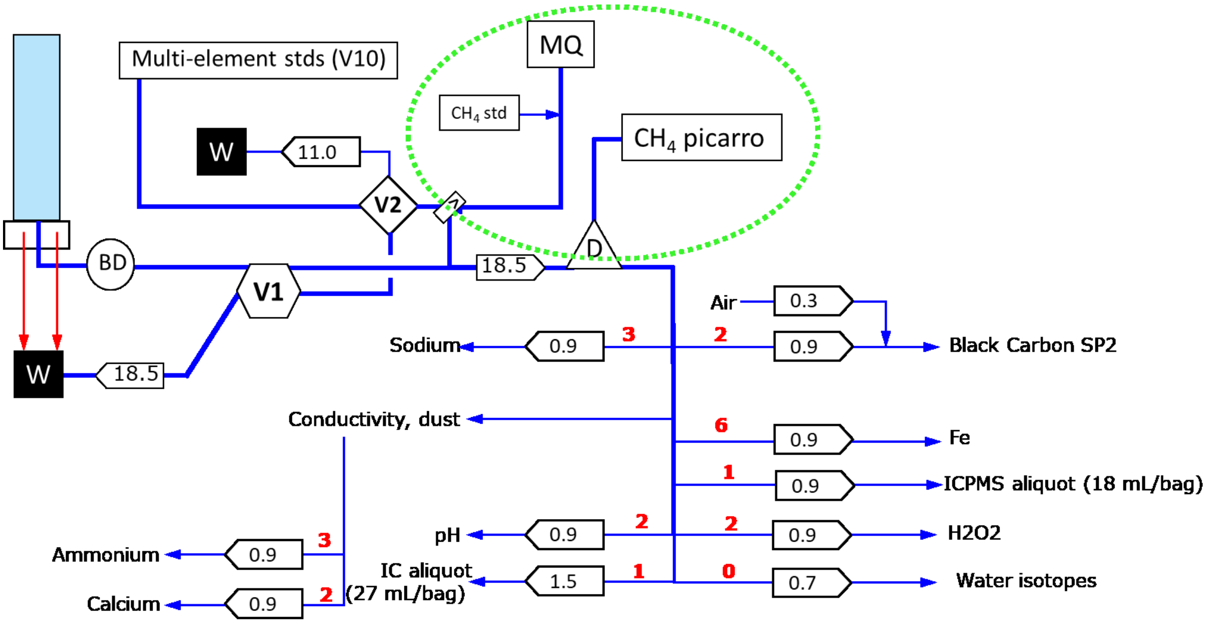

Figure 13: *A sketch of the CIC CFA setup modification deployed for the RECAP ice core measurement campaign (numbers mark sample flow rate in cc min^{-1}).*

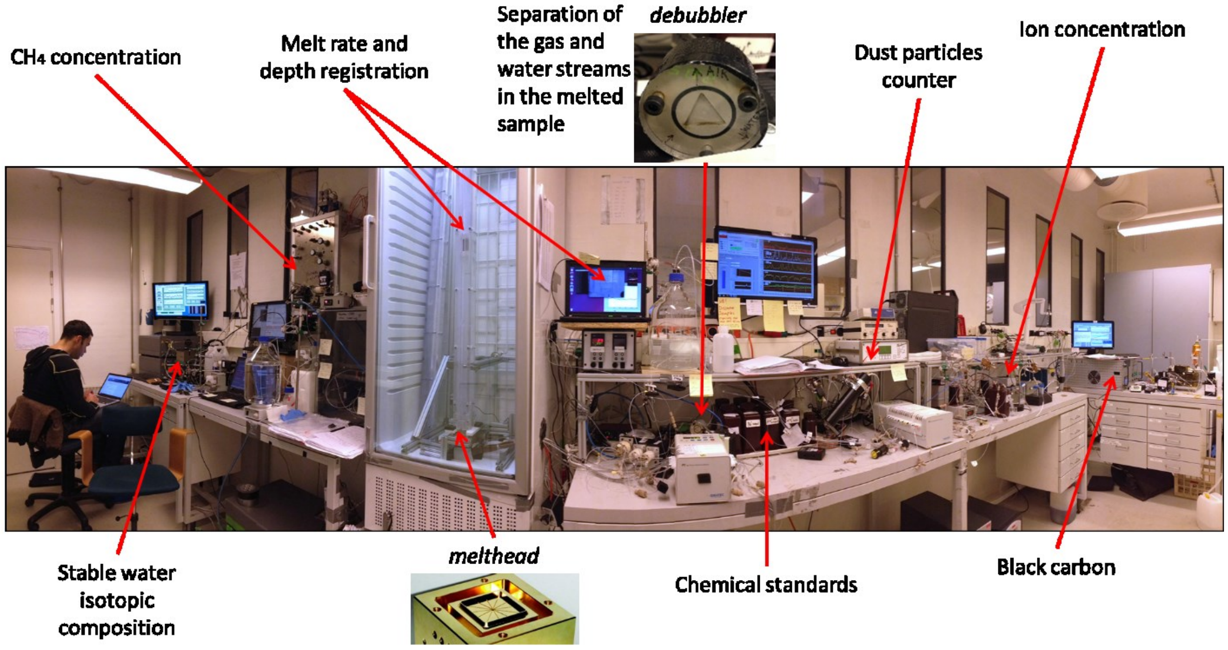

Figure 14: *An appearance of the CIC CFA setup (figure is taken from the poster by P. Vallelonga et al., T09 ID133, 10.03.2016, IPICS OSC, Hobart, Australia).*

The different components of the gas extraction line were tested for their sensitivity in order to find out the more efficient measurement condition by Rachael Rhodes at DRI, USA, by Xavier Faïn at IGE (former LGGE), France and by the author at CIC, Denmark. The most efficient components were used in the RECAP measurement campaign preparations in 2015. We modified the following components of the CFA CH_4 setup (see the corresponding numbers in the Fig. 15):

1 – debubbler: a pipette debubbler was replaced by a triangular prism debubbler, which allowed decreasing the sample volume passing through the debubbler and thus reducing the gas mixing making the gas flow more segmented. The emptying of the pipette debubbler due to the gas pressure build-up interrupted the downstream chemical measurements. The full emptying of the triangular debubbler occurs rarely. Moreover, the water pushed through a narrowed down upper channel helps to segment the gas flow better.

2 – membrane degasser: the membrane micromodule was replaced by transfer line degasser (9000-1549 - Transfer-Line Degasser 1.1 m, IDEX, USA, membrane material Poridex, inner volume is 4 ml), which allowed to reduce the gas diffusion as well due to the smaller inner volume or the extracted gas sample (the micromodule has a volume of 5.4 ml). A typical micromodule degasser is 4*4 cm block containing 600 hydrophobic membrane small tubes installed in parallel while the transfer line degasser has only one membrane tube with a length of 1.1 m, which decreases the resistance of an extracted gas sample pumping. An attempt to set up two parallel membranes twice shorter than the original one in order to decrease the residence time of the gas sample in the extraction line (and thus reducing the gas diffusion) was not successful as the visible segmented gas stream was not extracted and the gas sample got partly lost in the wastewater.

3 – the second thermal insulating heated console: in order to create the stable gas extraction conditions the temperature conditions along the line should be controlled. The second heated box (up to +50˚C) was build inside the first +30˚C box covering the pressure regulator at the membrane degasser outlet and the upstream part of Nafion. The Nafion's drying efficiency can be enhanced by creating the cooling gradient along the sample flow in order to decrease the due point and thus to absorb quantitatively more water vapor from the gas sample stream. The control of heating is technically easier to embody than the cooling, thus we decided to create a gradient form a warmer to a room temperature along the Nafion casing. Nafion itself is a copolymer of tetrafluoroethylene (Teflon®) and perfluoro-3,6-dioxa-4-methyl-7-octenesulfonic

acid. Sulphonyl acids absorb 13 water molecules per every sulfonic acid group in the copolymer and thus Nafion absorbs 22% of the water mass. Nafion is a highly selective semipermeable membrane for the water. It acts as a dryer if the gases inside the tube are more humid then the outer gas stream and as a humidifier in the opposite case. The Nafion^{tm} recommends to cool the downstream part of the tube to 0˚C (the lowest temperature of the dew point without freezing). The efficiency of the water extraction from the humid gas stream depends on the partial pressure of the water vapor in the space between the Nafion and the casing. The absorbed water vapor is carried by the dry gas or nitrogen in that space through the open split.

4 – the space above the melthead: it was decided to stack the ice core samples of a standard length 55 cm in the Plexiglas frame. Five frames were prepared in advance in the cold room (-18˚C) before the beginning of every measurement run (total length of the measured core 5.5 m). Every frame was hung on the holding pins above the melthead right before the top 10 cm of the previous sample were melted. A sample in the new frame was held by the pin, which was taken away using the belay in order to place the new sample on top of the previous one. The belaying pin (a chemically inert plastic spoon) was manipulated through a gap in the frame and the holder above the melthead.

The overall operational principle of the CFA CH_4 setup remains unchanged since the original setup by (Stowasser et al. 2012). We replaced the gas extraction line compartments by more efficient analogues and prevented the ambient air penetration to the system by launching the segmented standard gas flow in the stream of deionized water in the breaks between the melting runs. It prevented the system contamination by the high concentration of CH_4 in the laboratory air, eliminated the memory effect in the beginning of every run and prevented the back flow due to the pressure drop in the system.

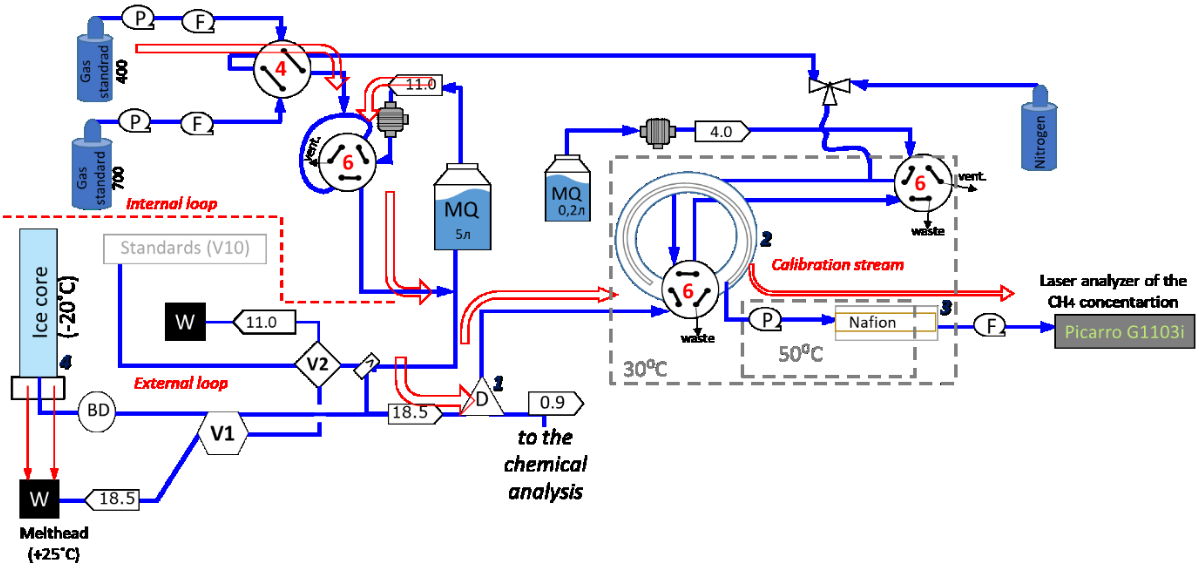

Figure 15: The scheme of the CFA CH₄ setup used in the RECAP measurement campaign.

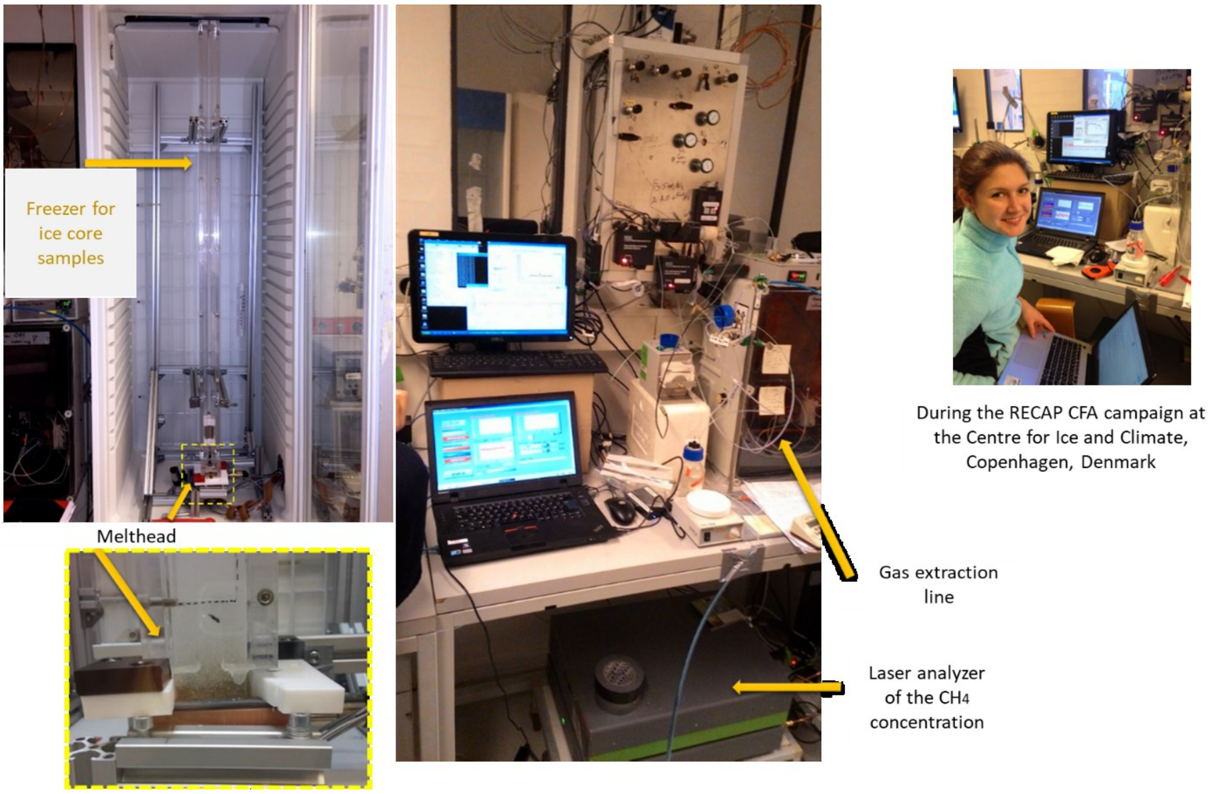

Figure 16: *A view of the CFA CH₄ setup used in the RECAP measurement campaign.*

2.4. Improvements and build-ups, tests and calibrations after the RECAP campaign

The RECAP measurement campaign was one of the stages of the CFA CH4 setup development at the CIC. After the measurement campaign was terminated, there were a few tests carried out to suggest the future improvements.

1. A relative pressure change sensor was plugged between the debubbler and the membrane degasser inlet. A flow rate logger was set into the membrane wastewater line (marked as ”Δp” and “F” in a blue rectangular in Fig. 17). An example of different parameters monitoring during the gas extraction line test is shown on figure 17. Particularly the differential pressure sensor and the flowrate sensor allow following the gas-to water-ratio fluctuations in the measured sample and correct the CH4 concentration on the corresponding gas loss due to the dissolution. The correction slopes are supposed to be obtained in the scope of a calibration in the controlled varying gas-to-water ratio.
2. The efficiency the gas extraction and diffusive gas smoothing were tested using the parallel transfer line degassers. The idea was to shorten the residence time of the gas sample in the degassing line in order to reduce the dissolution and at the same time to preserve the gas signal discretization achieved in the line degasser in comparison with the micromodule. The existing transfer line degasser was manually remade into a twice-shorter two parallel degassing lines preserving the same internal volume. The test showed that 0.5 m transfer line degasser is not sufficient for the visible gas bubbles absorption from the water stream – part of the gas sample was lost through the membrane wastewater outlet.
3. The different melt rate conditions were reproduced using controlled standard gas flow in the deionized water. The aim was to identify the range of the melt rate appropriate for the most efficient CFA gas extraction. For the chemical analysis only a melt rate of 2.5 cm min^{-1} would be preferable while the gas analysis favor a higher melt rate (up to 4 cm min^{-1}). A higher melt rate would reduce the gas dissolution due to the more intense segmented gas flow rate through the extraction line. Moreover, a high melt rate would enhance the membrane extraction and the Nafion drying efficiency due to the built-up pressure gradient. Eventually a higher melt rate would lead to a faster turn over of the gas sample through the analyzer’s cavity, which would lead to a higher effective temporal resolution of the obtained continuous methane record. A precision of measurements does not decrease sufficiently as the instrument readings is averaged over every 2-7 seconds interval, which is shorter than the gas turnover time in the cavity. The instrument response time matters in this case.

The recommendations on the optimal melt rate for the efficient CFA gas extraction were given at the EGRIP (The East Greenland Ice Core Project - https://eastgrip.org/) Steering Committee meeting for processing and measuring of an ice core planned to be drilled in 2015-2020. As a result the decision was made to carry out a separate CFA gas measurement campaign on a separately cut stick of the ice core. It will allow obtaining the highest possible effective temporal resolution of the chemical tracers and gas record in the past.

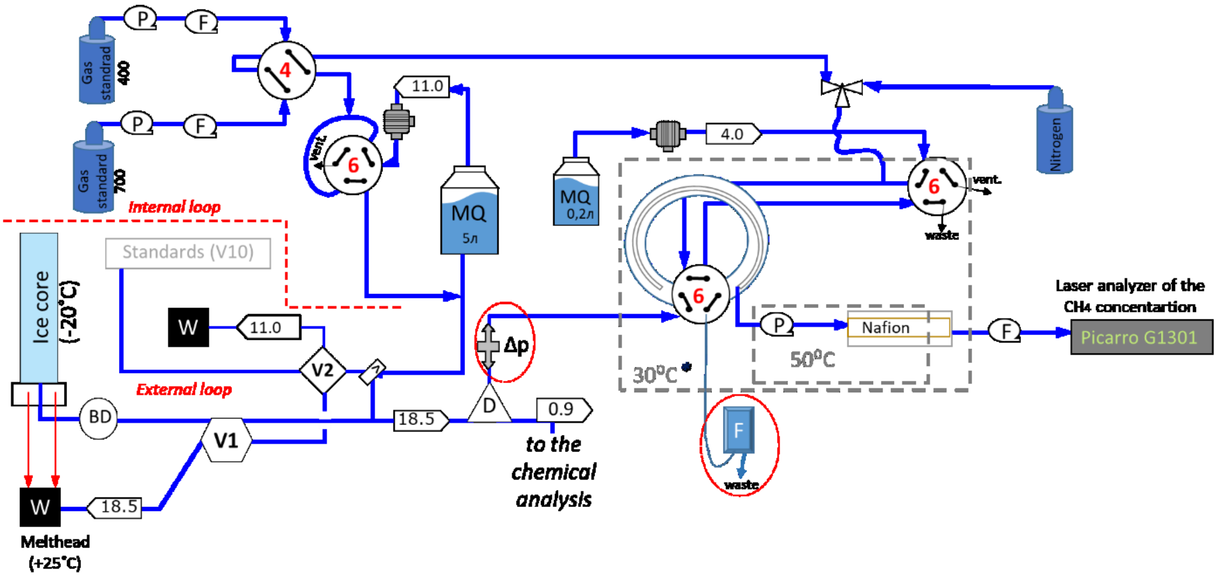

Figure 17: *A scheme of the CFA CH_4 setup modified after the RECAP measurement campaign. The new loggers installed are circled in red.*

We identified the following points to improve in the future CFA CH_4 measurement campaigns at the CIC:

1) the unique depth scale assignment is complicated due to the different length of the transport lines from the melthead toward the analytical lines and due to the different response time of the instruments;
2) floating gas sample pressure, flow rate and gas-to-water ratio.

The issue (1) has to be solved in order to reduce the eventual uncertainty on the gas record time scale. Every gas time scale involves the uncertainty on the ice core dating (in the range n – n*100 yr) and the uncertainty on the gas pores closure age modelling (n*10 – n*100 yr) (see section “Gas trapping during ice formation”). The gas age modelling can be checked by the climatic records match on the ice and gas timescales. An obtained delta depth in this case is put as a constrain to a modelled delta age. An analytical bias of the gas depth scale yield a bigger uncertainty on the delta age and/or the model data mismatch.

This issue is possible to solve by installing the electrical conductivity measurements (ECM) at the sample inlet to every line analytical line. Every ice sample run is normally preceded by the MiliQ bubble-free ice run to clean the melthead and flush the lines. A change from deionized water to the meteoric ice is clearly marked in the ECM signal. This issue is successfully solved in the CFA setups at the National Institute of Polar Research (NIPR), Tokyo, Japan and at the University of Bern, Bern, Switzerland.

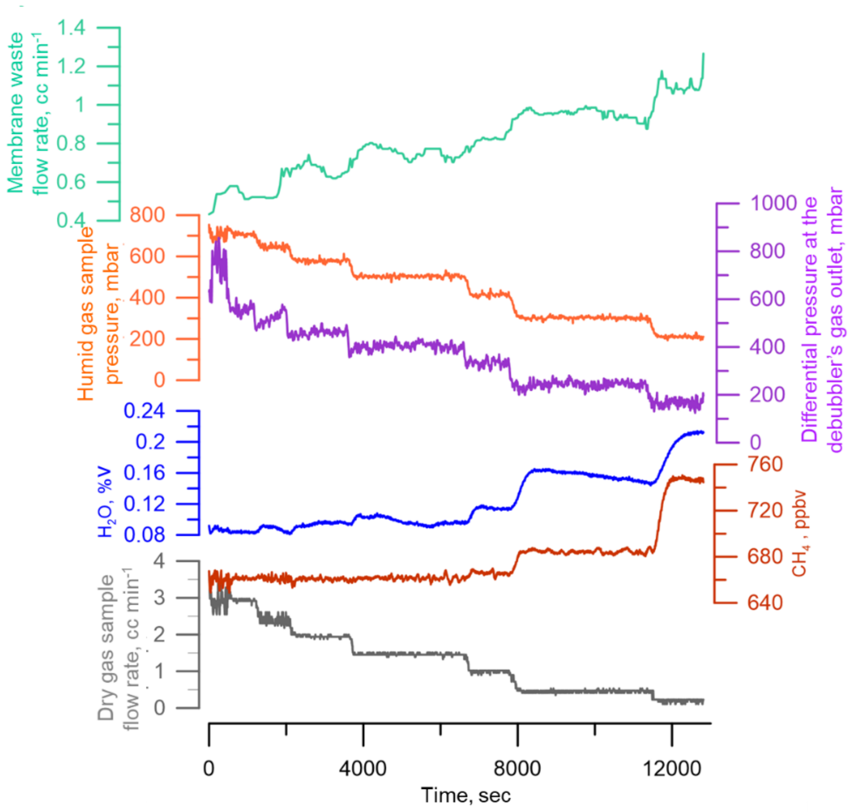

Figure 18: *The parameters of the gas extraction line in the controlled segmented standard gas flow rate.*

The issue (2) is necessary to solve in order to evaluate the gas loss due to the dissolution and the gas signal diffusion in the melted sample stream. The gas loss estimation is used in the deconvolution of the atmospheric signal amplitude (of methane in this case). The gas signal of the rapid climatic variations is smoothed already during the gas trapping in the firn. Additionally, it is diffused when extracted gas sample is mixed with the previous portion in the analytical line or an analyzer cavity. Frist, one has to estimate the analytical smoothing (the effective resolution) and then assume that none of the variations in the atmospheric signal can be resolved better than the effective resolution of the CFA gas measurements.

The second issue is possible to solve by setting up a pressure logger to the melthead and to the debubbler's gas outlet, a flowrate logger of the membrane degasser wastewater and the flowrate logger of the dried gas sample in addition to the existing pressure logger of the humid sample between the membrane gas outlet and the Nafion. Five loggers would allow keeping the record of the gas-to-water ratio fluctuations during the melting run and correct a measured CH_4 concentration for the gas loss. A calibration, where different gas-to-water ratio steps are simulated would help to estimate the calibration slopes. The gas loss percentages is calculated plugging in the known CH_4 concentration of the standard gases used in the CFA setup calibration. An example of the successfully solved problem is the CH_4 CFA setup at NIPR, Tokyo, Japan.

In summary, the CFA method is advantageous in terms of (1) a sufficiently smaller volume of the ice core sample consumed and (2) a much faster data acquisition time. However, the state of the art of the CFA method for the gas applications suggests that the better resolution of the CFA data does not necessarily mean the higher effective resolution of the climatic signal. Moreover, it the CFA gas measurements is a balance between a possible higher time resolution and bigger amount of work to carry on processing the data along with the record cleaning.

Chapter 3. RECAP CFA CH_4 record – dating and evaluating the data

3.1. RECAP drilling project

REnland ice CAP project (RECAP, https://recap.nbi.ku.dk/#) is an ice core drilling project carried out in 2015. It was targeted to retrieve an ice core from a separated ice cap in Eastern Greenland (71.3° N, 26.7° W), see Fig. 19. The summit of the ice cap reaches elevation of 2340 m a.s.l., modern mean annual temperature is -18°C and the snow accumulation rate is 0.5 ice eq. yr^{-1}. The surrounding topography (mountain range surrounding the ice cap) suggests that the ice cap likely did not change its elevation in the past significantly, which gives an advantage in the total air content study and its variability independent on the site elevation change. The obtained ice core, drilled throughout the ice cap, has a length of the 584 m, 532 m of which is the Holocene ice. The lower boundary of the Holocene section is still above the brittle ice zone, which provides a unique opportunity of obtaining high-resolution continuous gas and chemistry records. Another point if scientific interest is the fact that the ice cores drilled in the main Greenland ice sheet earlier (NEEM, NGRIP, GISP2, GRIP) are under the influence of the Western sector, i.e. Canadian Arctic, while it still remains unknown what was the Eastern Greenland response to the abrupt climate change during the Last Glacial. Renland is exposed to Fram strait supporting the study of the sea ice transport and its geochemical signature study based on the RECAP ice core.

The first ice core was drilled at the Renland ice cap in 1988 (Hansson 1994) but the drilling site was selected in a relatively shallow place, thus both Holocene and Last Glacial record had lower depth resolution. The new ice coring sited was selected based in the radar survey in the bedrock valley in order to capture the thickest possible ice with the low amount of the ice flow perturbance yielded by the bedrock conditions.

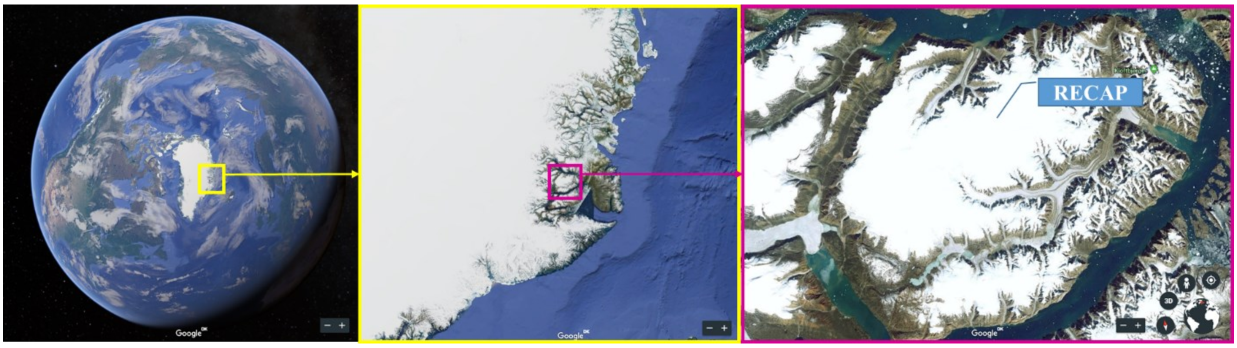

Figure 19: *The satellite image of Greenland (left), zoomed-in east coast, Renland is squared in magenta (middle) and the RECAP drilling site (right). Satellite images are extracted from Google Earth, 71.30° N 26.72° W, 01 September 2018.*

3.2. Measurement campaign

3.2.1. Ice core processing at AWI

The ice core was processed, i.e. cut into sample, at Alfred Wegener Institute (AWI, Bremerhaven, Germany) in August-September 2015. The cutting scheme is shown in Fig. 20. Every ice core bag is a 55 cm long core and 10 cm in the diameter. The core bags were logged for every sample section cut off the main core because of the differences in the length if the core dogs cut during the drilling was not made perpendicular to the core axis.

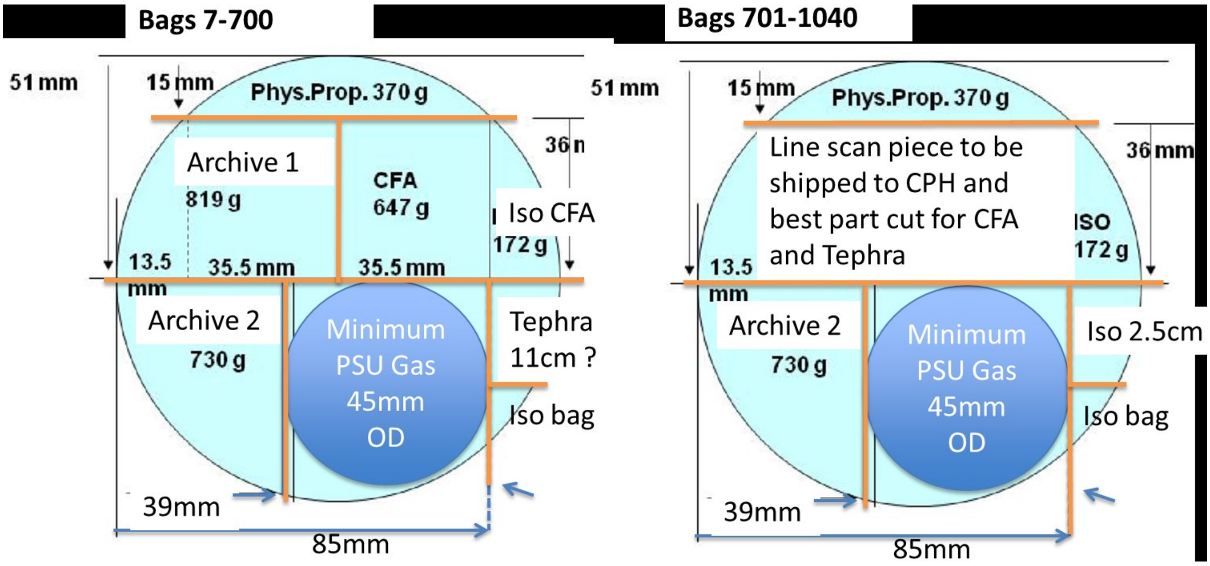

Figure 20: *A cutting plan for the RECAP ice core samples as seen in the cross-section of the core (Sowers, pers. communication, 2015).*

3.2.2. CFA campaign 2015-16 at CIC

The RECAP CFA campaign was conducted in September 2015 – January 2016. The CFA campaign was a collaborative effort of the institutions involved in the Ice2Ice (https://ice2ice.w.uib.no/) and the RECAP (https://recap.nbi.ku.dk/) projects: University of Bergen (Norway), University of Bern (Switzerland), Alfred Wegener Institute (Germany), University of Venice (Italy), Penn State University (USA), Oregon State University (USA), Institute of Arctic and Alpine Research (USA). The preparations, instrument installations and the full CFA setup reconstruction took 3-4 weeks. Measurements were conducted daily Monday to Friday in two shifts every day. The goal was to execute three runs of 5.5 m each measuring 16.5 m a day of 584 m of the total core length. A day began with the gas line calibration followed by the chemistry line calibration and terminated on the opposite order. Chemical tracers' baseline calibrations were also performed between each run. The stable water isotope part of the CFA setup was calibrated one a day. While the morning calibrations took place starting at 7 am, first five ice core frames with the samples were cut, cleaned and loaded in the freezer. During the first run the rest of the ice core samples were processed and stored into the cold room located in front of the CFA laboratory. Every frame was carried from the cold room to the little laboratory freezer casing the melthead. The ice core load in the melthead is described in the section 2.3.

The CFA setup for the methane concentration measurement is the isolated analytical line connected to the melthead uptaking a portion of the melted stream. The line is manipulated via the operational algorithm written in a visual programming environment LabView. All parameters of the gas extraction line are logged in .lvm format, the data is updated on-line on the data plots. Additional loggers can be connected to the data acquisition board (National Instruments Corp., Austin, USA), the data file content can be modified. The operational system also allows to manipulate the digital valves and regulate the mass flow controllers. A valve allowing to switch between the stand by and the main CFA lines (or internal and external) is controlled manually as well as the peristaltic pumps.

The CFA CH_4 line was calibrated twice a day prior to the morning chemistry lines calibration and the melting start and after the daily routine and the evening calibration. The daily CH_4 calibration aimed to identify possible leaks or improperly working components and troubleshoot them before the measurement begin. See the operational manual for the calibration steps in the appendix.

Between the calibration and the melting runs the CFA CH_4 system was kept in the internal loop measuring the segmented stream of the standard gas in the deionized water. It was done in order to hold on the system within an average sample pressure and flow rate. It allows avoiding the backflow and long memory effect due to the pressure jumps in the analyzer's cavity. The standard gas with the CH_4 content lower than the expected sample's content was selected in order to mark the transition from the stand by to measurements mode.

The CFA CH_4 setup needs to be generally calibrated also before and after the whole measurement campaign. The purpose of these calibrations is to monitor the stability of the setup and the instrument by measuring the dry standard gas. Moreover, if any of the compartments need to be replaced, the calibration should be carried out with a spare compartment in order to check the performance of the system in the new conditions. If any systematic shift can be traced and coincides in time with the setup modifications, the new calibration coefficients will be implemented to the measurements after the modification.

The general calibrations are (I) the dry standard-gas measurements in order to identify the laser analyzer shift from the true values of the CH_4 concentration and (II) gas-to-water ratio calibration and its influence on the gas loss.

(I)The dry gas calibration is carried out in the internal CFA line: the dry standard gas (i.e. without a flow of the MiliQ water) is launched through the gas extraction line. The CH_4 concentration is compared to the one measured directly from the gas bottle (bypassing the gas extraction line). Normally, the values of the CH_4 concentration in the first case should roughly equal or slightly lower than the true value of the CH_4 concentration of the standard gas. The loop measurements sometimes give lower value due to the additional humidity in the setup. An enrichment in CH_4 values at the dry gas calibration evidences a leak or an in-situ CH_4 production in the setup.

Any leaks in the CFA CH_4 setup is identified based on the common principle of connecting to the setup the compartments, which might potentially leak, gradually while measuring the standard gas (or any other gas mixture with a known CH_4 concentration below the one in the ambient air). The CH_4 concentration increase points out on the spotted compartment with a leak. The connection should be checked and tightened; the outdated compartments should be replaced by the new ones.

(II)The gas-to-water calibration is carried out in order to estimate the slopes of the gas loss due to the dissolution. In normal melting conditions, the gas sample in a segmented melted water flow reaches the extraction line at a ratio 40:60 to 50:50. But gas-to-water ratio varies on the melted sample stream because the meteoric ice has layers of different density and total gas content. The gas loss changes correspondingly. The whole possible range of the gas-to-water ratios has to be covered at the calibration (i.e. from 10:90 or any other lower limit of the gas content of the CFA CH_4 setup sensitivity to 90% of gas versus only 10% of water in the stream). One should make sure that the dependence of the gas loss on the gas-to-water ratio has a linear slope. This calibration is carried out following a protocol of the daily calibration running the external loop, the transitions between the standard gases are repeated for every increment of the gas-to-water ratio. A standard gas flow rate is regulated via the mass flow controller, the MiliQ flow rate stays the same (i.e. the peristaltic pumps are run at the same speed). The gas pressure in the system is regulated by making the laser analyzer's inlet valve open wider or narrower (a corresponding parameter can be found in the Tools tab, "Sample handling parameters"). At the calibration data processing, the recorded parameters of the gas and water flow rate are recalculated to the gas-to-water ratio. A corresponding gas loss of the measured CH_4 concentration is estimated versus the known CH_4 concentration of the standard gas. This general calibration defines a gas loss as a function of the gas-to-water ratio. Note the gas-to-water ratio is not measured directly but calculated from the experimental setup logged parameters. In this case, we use a ratio of the pressure of the gas sample in the Nafion inlet to membrane wastewater flowrate.

3.3. Depth scale assignment

The depth of the core melted is measured using a string stretched along the core at attached to a hook on a weight placed above the ice core in the frame. The string is under the stress and it rolls back to a winch (the tool is called Encoder) while the ice core is melted, the number of rolls is counted and the lengths of every turnover is translated to the melting depth. The melting depth is recalculated to the ice sheet depth by adding the gaps to a corresponding places where the ice core breaks were observed. An information on the breaks length and the ice loss while cleaning the sides of an ice core sample prior to its loading to a CFA frame at the freezer was noted in the CFA processing log. Marius Simonsen conducted the melting rate to the depth scale processing. In parallel, the melting rate is measured by image correlation method. The ice melting was constantly video recorded from a certain point and images were correlated every second providing an information of the distance shift in a time domain. The corresponding Python script was written by Christian Panton. ∆

The results of the CH_4 concentration measurements are translated to the depth scale by a single run increment, i.e. after melting of every 5.5 m is finished. The melting time is translated to the depth using the Encoder data. A beginning of every gas run is shifted by 140-170 seconds from the beginning of the melting, as this time is needed for the melted sample to reach the gas extraction line after the melthead and the debubbler. An information on the core breaks and gaps as well as the length spared on the edges cleaning (a few mm up to 1 cm) is taken from the ice core processing log an added to a corresponding places at every run. An example of the resulting depth shift after adding the gaps to the depth scale obtained directly from the gas measurement time is shown in Fig. 21.

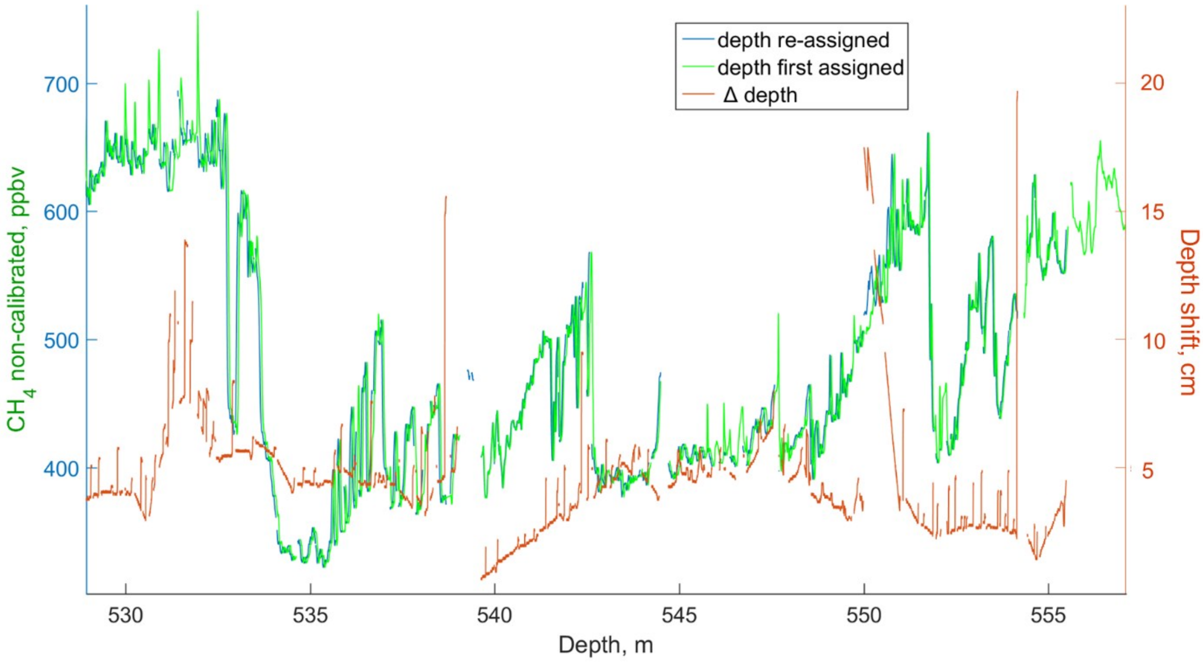

Figure 21: *A section of the RECAP CH_4 record on depth scale assigned first based on the measurement time (green curve) and reassigned adding the ice core breaks as gaps (blue curve). The resulting depth shift, steadily accumulated every melting run, is as a red curve.*

3.4. Calibration of CFA CH_4 absolute values

A calibration of the absolute CH_4 values is carried out as following: a record has to be first corrected for the water level offset as the slopes of the instrumental calibration is normally obtained using the dry gas standards; then the corrections of the absolute values has to be applied taking in account the instrumental shift (i.e. the values logged by the analyzer) of the true values of the CH_4 concentration; as the next step the gas loss due to the dissolution is figured out, the lacking concentration is added to the measured one. After finishing a sequence of the analytical corrections one should consider the difference in the amplitude and smoothness of the ice core gas signal and the initial atmospheric CH_4 concentration.

1. The water level correction

The water level correction is necessary due to the presence of the water vapor molecules in the analyzed gas sample and the corresponding bias of the CH_4 concentration. The H2O molecules are considered as a part of the gas sample mixture relative to which the concertation of the CH_4 is calculated. I.e. if one measures a pure methane of 20% relative humidity, the laser analyzer will identify 80% CH_4 concentration in the gas mixture. Besides the dilution effect, firstly, the varying water vapor presence broadens the methane concertation line and secondly, as the measured water vapor concentration does not vary linear due to the self-scattering of the values (Rella 2010).

In this study, we run the Picarro analyzer G1101-i capable to measure the concentration of CH_4, CO and H_2O simultaneously. The current state of the CFA technology does not allow to dry the gas sample completely. The minimum relative humidity of the gas sample is 0.02% of volume. It is achieved by increasing the concentration of the gas bubbles in the sample stream using the debubbler, extracting the gas using the transfer line degasser and absorbing the water vapor molecules in the Nafion (for the details see section “CFA CH4 measurements at CIC”). If the sample is dried out properly in the Nafion, the correction is minimal.

The results of daily calibrations and the general calibrations of the setup (see the Appendix “the everyday calibration protocol”) are used in the water level correction:

$$[CH_4]_{dry\,gas} = k_{H_2O} \cdot [H_2O]_{measured} + b_{H_2O} = b_{H_2O}, \text{ as } [H_2O]_{measured} = 0$$

$$\Delta[CH_4] = \left(k_{H_2O} \cdot [H_2O]_{measured} + b_{H_2O}\right) - [CH_4]_{dry\,gas}$$

$$\Delta[CH_4] = \left(k_{H_2O} \cdot [H_2O]_{measured} + b_{H_2O}\right) - b_{H_2O} = k_{H_2O} \cdot [H_2O]_{measured}$$

$$[CH_4]_{H_2O\,corrected} = [CH_4]_{measured} - \Delta[CH_4] = [CH_4]_{measured} - k_{H_2O} \cdot [H_2O]_{measured}$$

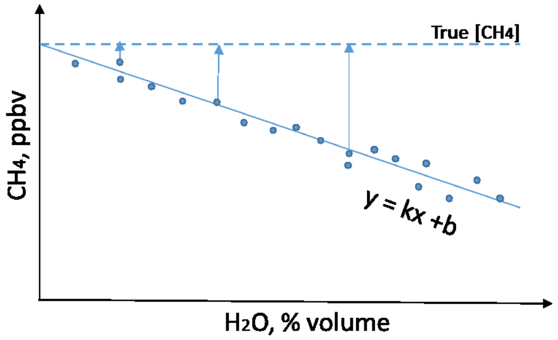

Figure 22: *A schematic representation of correction to the water level.*

The system drift test and every day calibrations revealed that it is preferable to use the median values of all the calibration coefficients. Using of the median value instead of the scattered daily-obtained calibration coefficients decreases the total deviation from the true CH_4 concentration. The difference is shown as a principle sketch in Fig. 23. An implementation of the daily-obtained calibration corrections yields a bigger difference of the true value of the CH_4 concentration (thin blue increments) and the total distance between the mean measured and true CH_4 concentration (shown as blue solid and dashed lines correspondingly). The calibration corrections changed after every single calibration yield some false trends in the data (black thin lines). The true drift of the instrument as well as the whole CFA CH_4 setup is likely deviates from a linear slope captured in between the daily calibrations, thus using the daily-obtained calibration corrections does not bring the understanding of the setup behavior closer. A median value is preferred to the average from the statistics point of view as it depends on the outliers to a minor degree.

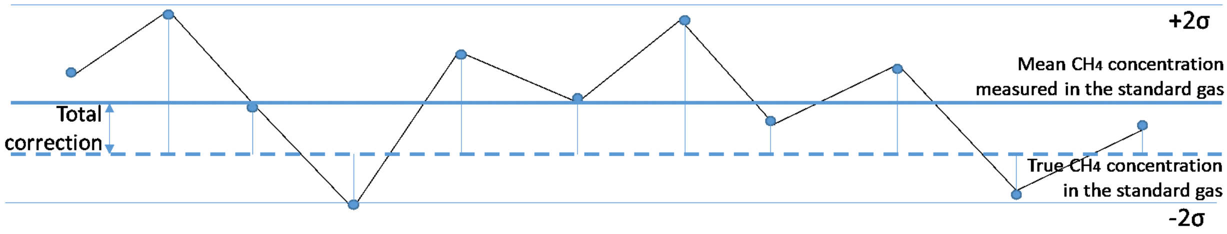

Figure 23: *As schematic representation of the difference between the calibration using the daily obtained coefficients (thin black lines show a false trend in the standard gas measurements) and a total correction preventing the false trend in the measurements (a shift from the solid to dashed blue lines).*

The water level correction is the first step of the calibration of CFA CH_4 absolute values. We need to implement the correction first as the absolute values calibration is made using dry standard gases and is related to the instrumental correction itself. See (Rella 2010) for more details on the water level correction of the laser analyzers. Note that in this work (the only published specific study of the water concentration correction applied to the methane concentration measurements using the laser analyzer) the analysis was made for the Picarro G1301, the correction term was quadratic and the total humidity range was 0.01-6% volume. It was also recommended to conduct the water correction measurements for every brand new instrument suggesting that the correction coefficients deviate from each other. In the case of the CFA measurements, a working range of the sample humidity (0.02-0.08% volume) is relatively narrow, which allows approximating the correction with the linear fit.

2. The absolute CH_4 concentration value correction

The concentration of gas species identified by the laser analyzer has to be adjusted in order to obtain the absolute concentration. Though the laser analyzers produced by Picarro Inc. have the default calibration algorithms, the eventual measurement results of the standard gases do not match the true values used by the laboratories worldwide. The calibration is carried out using the secondary gas standards manufactured by NOAA (National ocean and atmospheric administration, USA – https://www.esrl.noaa.gov/gmd/ccl/). Every laboratory usually has a measurement offset relative to the true values of the gas concentration. In order to unify the uncertainty on the accuracy of the measurements, the laboratories agreed to calibrate the instruments and the setups versus primary and secondary NOAA gas standards (this is the case at least for the ice core laboratories dealing with the gas concentration and isotopic composition measurements).

During the RECAP CFA campaign, we used two secondary standard gas mixtures with the CH_4 concentration 403.1 ppbv and 701.2 ppbv (hereinafter referred as the Glacial and Holocene working standards correspondingly). The CH_4 concentration in these gas mixture was calibrated in 2011 versus the primary NOAA standards with the known CH_4 concentration 344.3, 688.6 and 1646.2 ppbv (Stowasser, 2011). The working standard mixtures were selected by matching the purpose of the measurements to cover the natural variations of the CH_4 concentration in the atmospheric air during the Last Glacial and interglacials – Holocene and possibly Eemian. The natural variations of the CH_4 concentration is in the range 350-720 ppbv (Petit et al. 1999).

The calibration is a linear fit of the measured and water level corrected CH_4 concentration to the true value obtained by measuring the standard gases.

$$[CH_4]_{true} = m \cdot [CH_4]_{H_2O\ true} + l$$

The using of the third standard gas would be preferable as in this case we can possibly check the linearity of the fit. Given a small range of the measured CH_4 concentration, the approximation is likely linear between the two standards. The calibration coefficients were obtained by measuring the dry standard gases launched directly to the analyzer's cavity (bypassing the extraction line) at a controlled flow rate 5 cc min^{-1}. This correction is essentially an instrumental correction and it should not imply any variations of the humidity or the state the CFA setup.

Despite numerous tests, the CFA measurements cannot be calibrated independently with the current state of the setup development. Normally the adjustment to the absolute values of the methane concertation measured by the mass-spectrometry is used. These measurements are conducted using the discrete samples and matching them to the average methane concentration obtained by the CFA method from the corresponding depth range.

The RECAP CFA measurement results were calibrated to the discrete measurements conducted by Todd Sowers at the Penn State University in 2016. For every discrete sample (7 cm long) the raw CFA CH_4 data were selected from the corresponding depth interval. CFA data were averaged over each interval and the fit were made of the CFA raw CH_4 values to the calibrated discrete values (see Fig. 24). A second order polynomial fit was selected due to its highest determination coefficient ($R^2 = 0.93$) and because it match the measurements in the low concentration range, which corresponds to the glacial section. The upper part the record (< 100 m) is poorly covered with the discrete measurements thus is not calibrated to them.

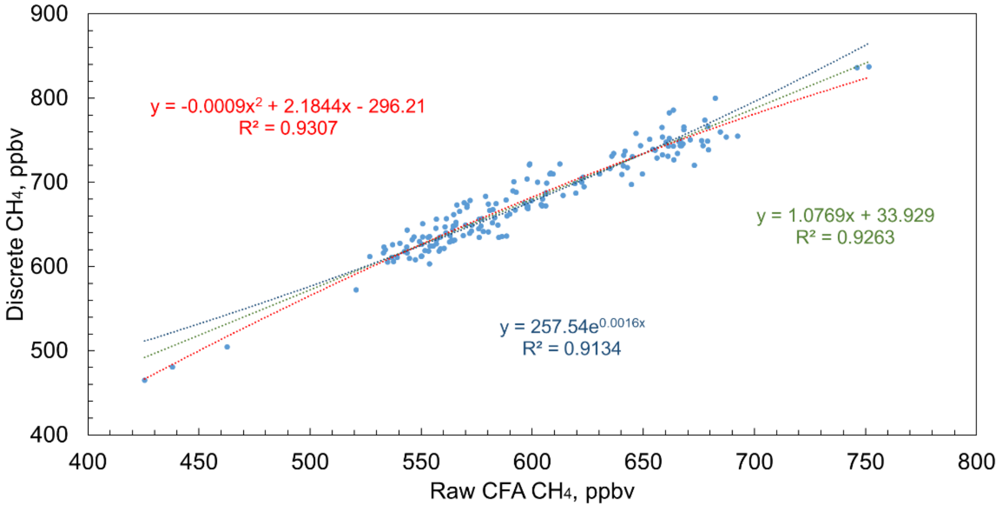

Figure 24: *Calibration fitting curves for the RECAP CFA CH_4 data adjustment to the discrete data.*

The results of the RECAP CFA CH_4 data calibration are presented in Fig. 25.

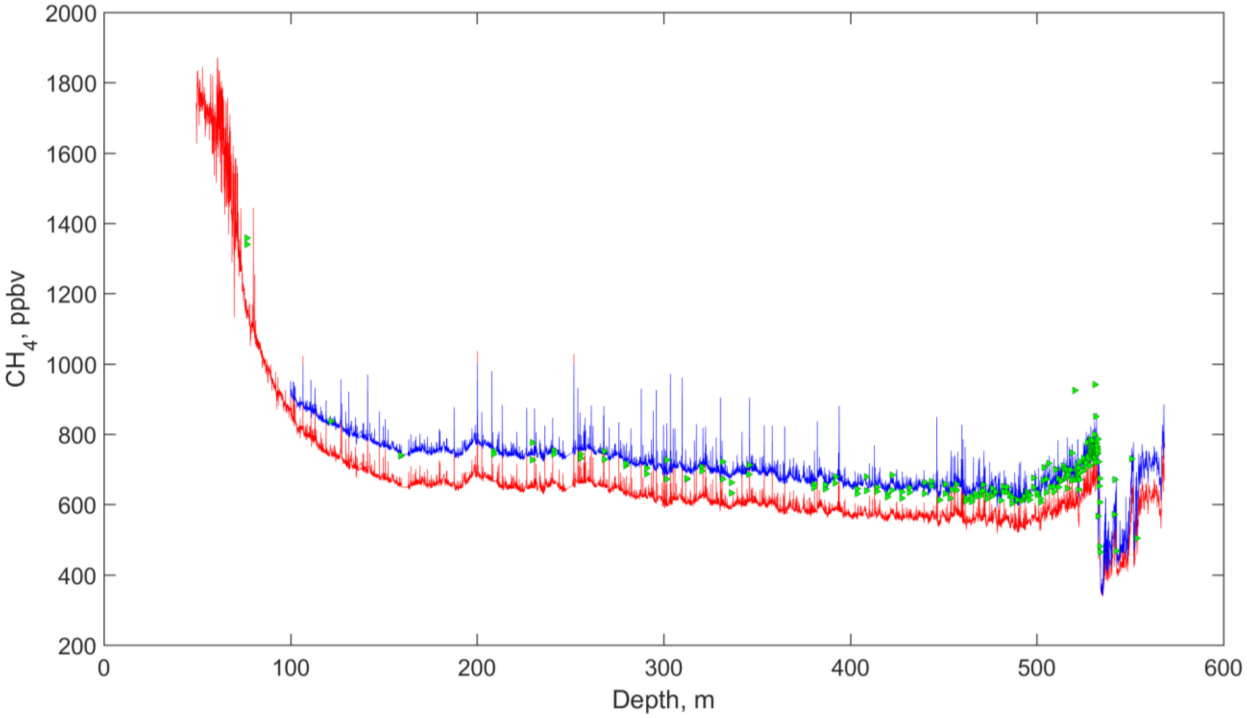

Figure 25: *The results of the CH_4 measurements of the RECAP ice core: raw CFA measurements (red curve), discrete CH_4 measurements (green triangles) and the calibrated CFA results (blue curve).*

3. The gas loss due to the dissolution in the melted stream:

A melted sample flowrate varies during a single measurement run as well as the total gas content of the sample. It occurs due to the diverging density and total air content of the meteoric ice formed in different climatic conditions. The more is the residence time of the melted sample in the gas extraction line (consequently, the lower is the flowrate and the gas pressure), the more is the gas loss due to the dissolution. The gas loss as a function of the different working parameters of the CFA setup is shown on Fig. 26.

We do not discuss the temperature influence as the gas extraction line was placed in the thermally regulated box (see Chapter 2) thus excluding the possibility of the gas loss variance due to the temperature change.

In order to implement the correction of the gas loss to the CFA CH_4 measurement results, one should conduct the calibration of the experimental setup simulating different melt rates and the gas-to-water ratio in the melted stream. The results of one of the relevant tests are shown in Fig. 27. During the test of the different melt rates simulation, the lower melt rate region indicates the saturation in the methane concentration, which identifies either a potential leak or a contamination of the loop. At the normal uninterrupted conditions, the lower melt rate step would reveal a strong gas dissolution and a big gas loss. An example of the gas loss test is presented in Fig. 28, it was conducted on the similar CFA CH_4 setup during the internship at the National Institute of Polar Research (NIPR, Tokyo, Japan).

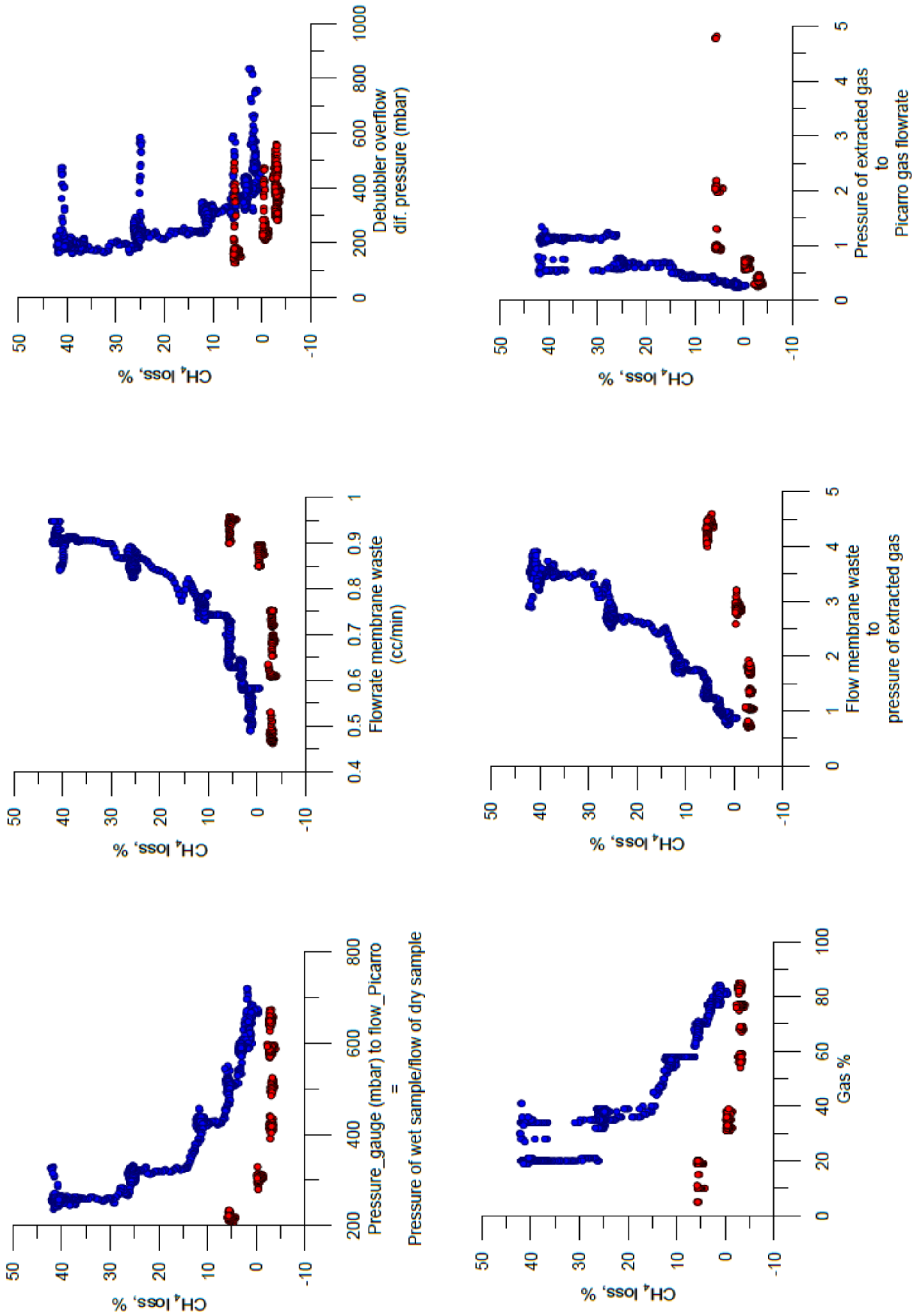

Figure 26: *Gas loss (as referred to the dry standard gases measurements) as a function of different parameters of the CFA CH_4 setup. The results are presented for Glacial (blue dots) and Holocene (red dots) working standards.*

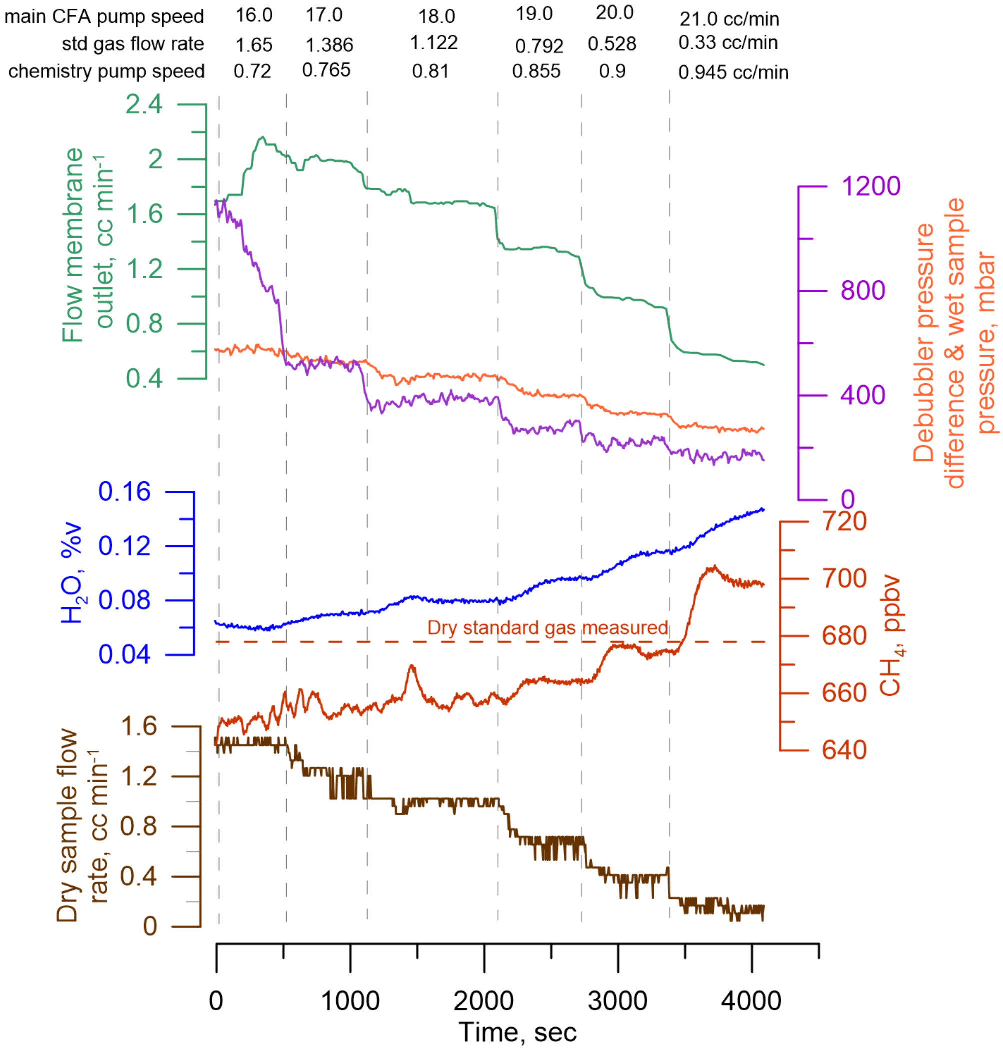

Figure 27: *Variability of the different CFA CH_4 parameters depending on the simulated melt rate variations. The parameters of the standard gas and the MilIQ water flowrate are marked in the upper panel; the dashed lines separate the different steps of the simulated melted rate, see the flowrates in the top panel.*

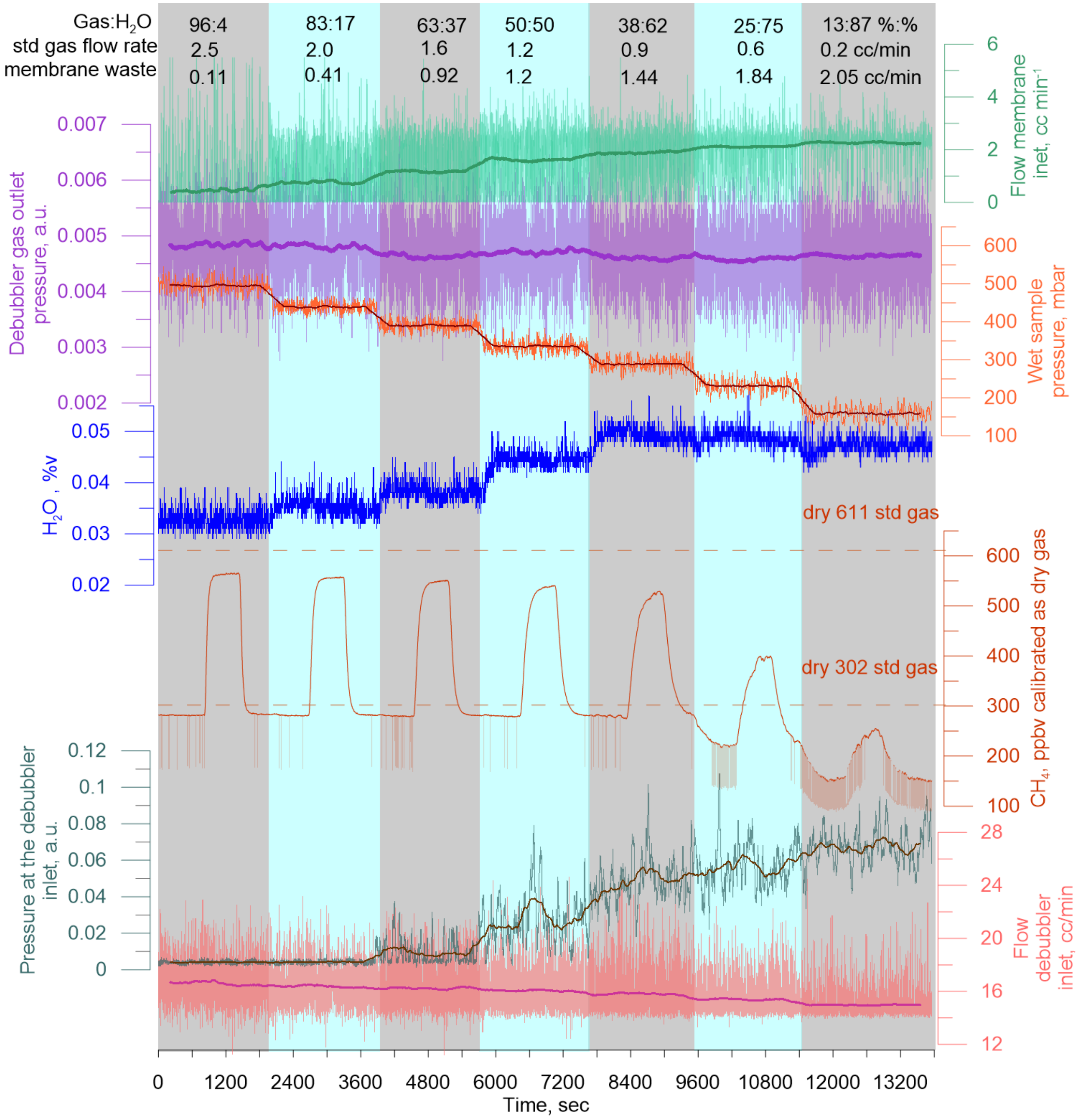

Figure 28: *The same as Fig. 25 for the test conducted on the CFA CH_4 setup during the internship at the National Institute of Polar Research (NIPR, Tokyo, Japan).*

4. Gas signal analytical smoothing

The loss of the gas resolution signal occurs during the analysis due to the gas mixing in the analyzer's cavity. A relatively slow flow rate of the gas sample leads the slowed down exchange of the newer portion of the gas sample and yields the analytical smoothing of the initial ice core gas signal. The bigger is the cavity volume and the slower is the sample flow rate, the slower will be the gas exchange in the cavity – the gas portions mixing will take place and consequently the more ice core signal will be smoothed in depth domain.

In order to calculate the CH_4 gas signal smoothing one uses the response time of the system (Stowasser et al. 2014). The response time indicates how fast the system reacts on the changing CH_4 concentration in the measured gas stream. It is proportional to the gas sample flow rate and inversely proportional to the effective volume of the cavity. A relation of the effective volume (V_{eff}) to the operational pressure (p_{op}) of the laser analyzer and the cavity volume (V) is expressed as:

$$V_{eff} = V \cdot \frac{p_{op}}{p_{std}}$$

where $p_{std} = 760\ Torr$ is a normal ambient pressure. The results of the test measurements are presented on Fig. 28, the time is shifted so that 0 sec would coincide with the time of the maximum rate of the CH_4 concertation change (a peak of the CH_4 concentration derivative). The test measurements are fit by the function (Gkinis et al. 2010):

$$f(t) = K_1 \left[\frac{1}{2} + \frac{1}{2} erf\left(\frac{\ln t - \mu}{\sigma\sqrt{2}}\right)\right] + K_2$$

where K_1, K_2, μ, σ are estimated by the least squares approximation applying a non-linear algorithm to improve the parametrization of the fit. Usually, the response time for the 10 to 90% of the new sample CH_4 concentration level is used. The previous results (Stowasser et al. 2014) indicate the response time of the analyzer is 38 sec until the 90% level of the new sample's CH_4 concertation is reached, and 77 sec – until 99% level (see Fig. 29). The data is for the laser analyzer working at the constant cavity pressure 45 Torr and the sample flow rate 0.9 – 1.2 cc min^{-1} as it was during the RECAP measurement campaign. The calibration measurements conducted after the RECAP indicate in contrast 45-78 sec needed for reaching 90% level and 124-133 sec needed for reaching 99% level of the CH_4 concentration of the new portion of the standard gas launched at the 1.0 cc min^{-1}. This time has to be taken into account when estimating the effective resolution of the CFA CH_4 measurements. 45-78 sec translates to 2.4-4.2 cm of ice core (given the average melt rate 3.2 cm min^{-1}), while 124-133 sec translates to 6.6-7.1 cm of the ice core sample. It means that any oscillations of the CH_4 concentration of the ice core, which take less 3-7 cm, cannot be fully resolved in terms of the CH_4 amplitude due to the experimental setup characteristics.

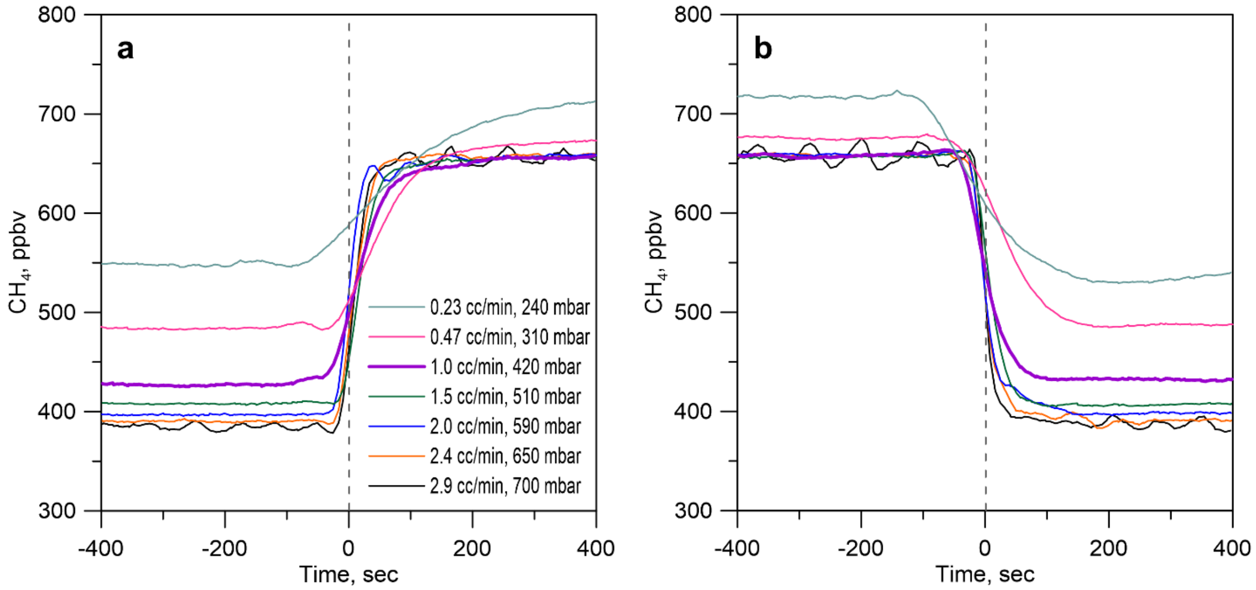

Figure 29: *The response time of the laser analyzer to the transition from measuring the* CH_4 *concentration of one standard gas to another (a – from Glacial to Holocene, b – reversed). The data is shown for the different measurement conditions simulation, particularly over the varying gas-to-water ratio. The legend indicates flowrate of the dried gas sample and the pressure of the humid sample extracted by the membrane. The purple curve (1.0 cc* min^{-1}*, 420 mbar) represents average ice core measuring conditions.*

Variations of the logged parameters in the CFA CH_4 setup while measuring two working gas standards (403.1 and 701.2 ppbv) is shown on Fig. 30. The gas and MiliQ water flow rate parameters were controlled manually, at every settings step gas standards were measured in the order Glacial-Holocene-Glacial. Non-calibrated CH_4 concentration of the dry standard gases bypassing the gas extraction line is marked as dashed lines – the lower one for the Glacial standard and the upper one for the Holocene standard. One can notice an enrichment of the measured CH_4 concentrations of the standards in the lower flow rate and gas pressure region. It contradicts to the expected gas dissolution when the gas-to-water ratio gets lower according to Henry's law:

$$H^{cp} = {}^{c_a}/_{p} \,,$$

where, c_a – concentration of gas species in the aqueous phase (mol m^3), p – is partial pressure of the gas species in the gas phase in the normal conditions (Pa), H^{cp} – mole concentration of the gas in the solution (mol $(m^3 \text{ Pa})^{-1}$).

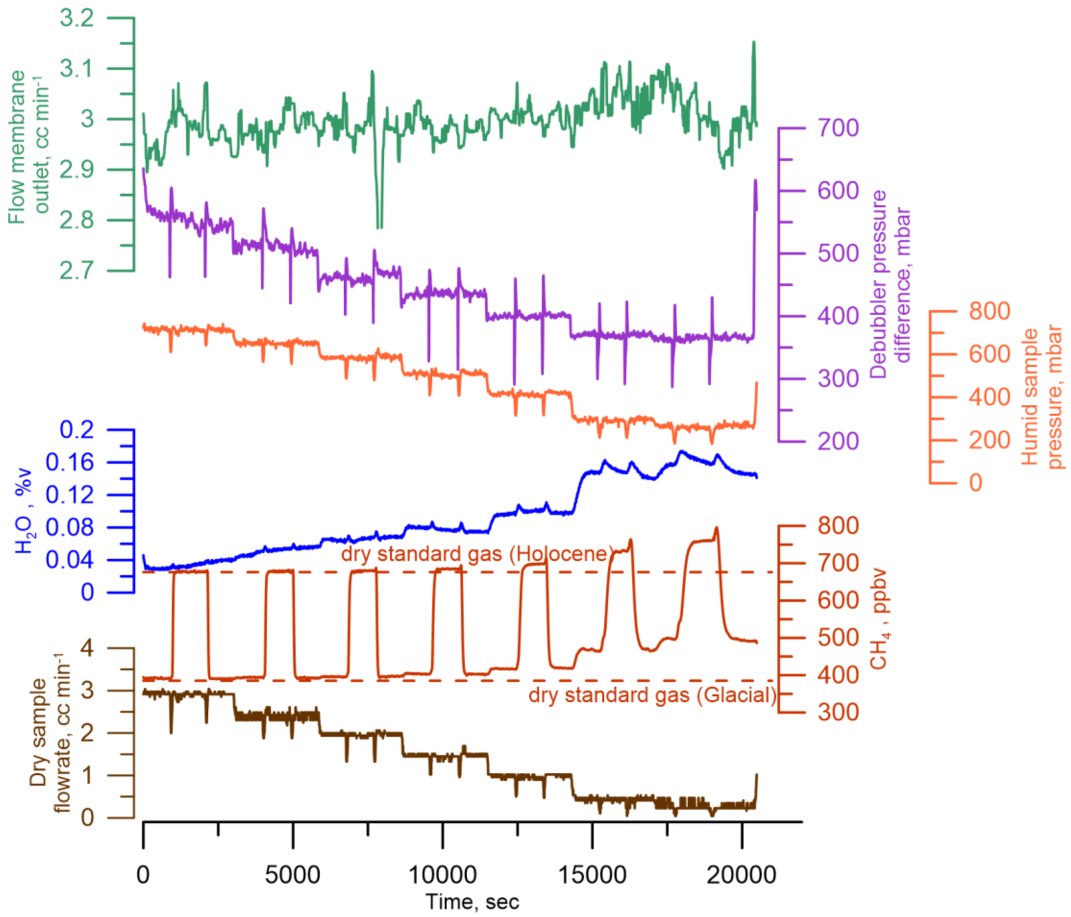

Figure 30: *The parameters of the CFA CH_4 measurements of the two gas standards in the varying flow rate conditions running the internal loop.*

Since there is no dissolution seen in the experimental data (Fig. 30), either leak or lines contamination is suspected. Another possibility for the enrichment is a dissolved CH_4 in the MilQ water. For preventing this effect, the MiliQ bottle was flushed with helium and the stream was degassed using the micromodule.

As the reason for the CH_4 enrichment at the test standard gas measurements yet remains unclear, the usage of the current test results in the gas loss calculation is not reasonable. The current test results were used in calculation the response time of the system. Timing of the new portion of the gas sample reaching the cavity of analyzer was accounted as the middle point in the CH_4 concentration transitions from one standard to another. A middle point is defined as the time of the CH_4 concertation’s maximum rate of change (or the maximum in the derivative). The response time was used in the CH_4 measurement results processing when one needed to synchronize the Encoder data (melting rate) and the gas measurement results by identifying the common starting point.

Ideally, the gas signal obtained by the CFA method should be firstly processed by synchronizing with the melt rate, secondly accounted for the gas loss due the dissolution (depending on the gas-to-water ratio in the stream) and thirdly deconvoluted given the mixing in the analyzer's cavity. The resulting analytical uncertainty of the CFA gas measurements is 10-15 ppbv.

5. Gas smoothing in the firn

The gas signal is affected not only by the analytical smoothing but also by the smoothing in the firn column while trapping the gas bubbles. Molecular effusion (Craig et al. 1988, Sowers et al. 1989) transforms the initial atmospheric gas signal due to the migration of small size gas molecules between the ice crystals. It creates an effect of saturation with nitrogen as nitrogen molecules are bigger than the micro gaps in the ice. The nitrogen stays in the ice while oxygen and argon molecules slip out. It might have an effect on the relative CH_4 concentration change though its abundance in the atmospheric air is a few orders of magnitude lower. It is unclear if enrichment takes place at the pores closer during the ice cores storage time (Bender et al. 1997). The gravitational settling and the thermal fractionation corrections are crucial when measuring the isotopic composition of the species. The barometric molecular diffusion affects the isotopic composition of the noble gases. The molecular effusion is taken account while estimating O_2/N_2 ratio. The CH_4 concertation becomes smaller than the initial atmospheric one due to the gravitational fractionation effect. Overall, the correction is in order 2-3 ppbv (Baumgartner et al. 2012), which is in the span of the CFA analytical uncertainty. Thus, the gravitational correction was not implemented to CFA CH_4 RECAP series.

The diffusive gas smoothing in the firn column is another factor transforming the initial atmospheric signal. One approach to determine the degree of the gas signal smoothing is implemented by (Rhodes et al. 2017). They used Oregon State University firn air model (Rosen et al. 2014) to estimate the gas signal smoothing measured in the West Antarctica Ice Sheet Divide (WAIS Divide) ice core. The modern climatic conditions in that site is similar to the one at RECAP drilling site (mean annual temperature ≈ -18˚C, the snow accumulation rate is 0.5 m ice eq. yr^{-1}. (Rhodes et al. 2017) revealed in the corrected for the firn gas smoothing CFA CH_4 results the 80-500 yr variability during the Last Glacial. It is characterized by an amplitude of 17 ppbv at the colder periods (stadials) and 24 ppbv at the warmer periods (interstadials).

A fraction of the remaining amplitude of the CH_4 signal is depicted as a function of the surface air temperature, snow accumulation rate and the ice-gas age difference on Fig. 30 (as analyzed by (Rhodes et al. 2017). The data was obtained using the Oregon State University firn air model (Rosen et al. 2014), the reconstructed temperature (Buizert et al. 2015) and snow accumulation rate (Cuffey et al. 2016) over the Last Glacial for the WAIS Divide ice core drilling site.

As the climatic parameters at the RECAP and WAIS Divide drilling sites are similar, one can assess the RECAP CH_4 signal damping using the described above (Rhodes et al. 2017) parametrization: the CH_4 record has to be decomposed into 100, 150 and 200-yr periodicity components, the signal of each will be amplified depending on the corresponding delta age accumulation rate and the reconstructed temperature (by applying fitting functions shown as dashed curves on Fig. 31), and summing up the amplified frequency components to obtain a CH_4 signal close to the actual atmospheric signal. This is a simple approximation to deconvolute the ice core CH_4 signal.

Another approach is convolution to assess how much can the ice core gas signal be potentially smoothed. It is typically done using the gas age distribution function of the gas in the firn at the bubbles close-off depth. The mechanism is described in the section ”DO events 19-21 – the Northern Hemisphere wetlands and the ice-dammed lakes drainage” (Discussion I.3).

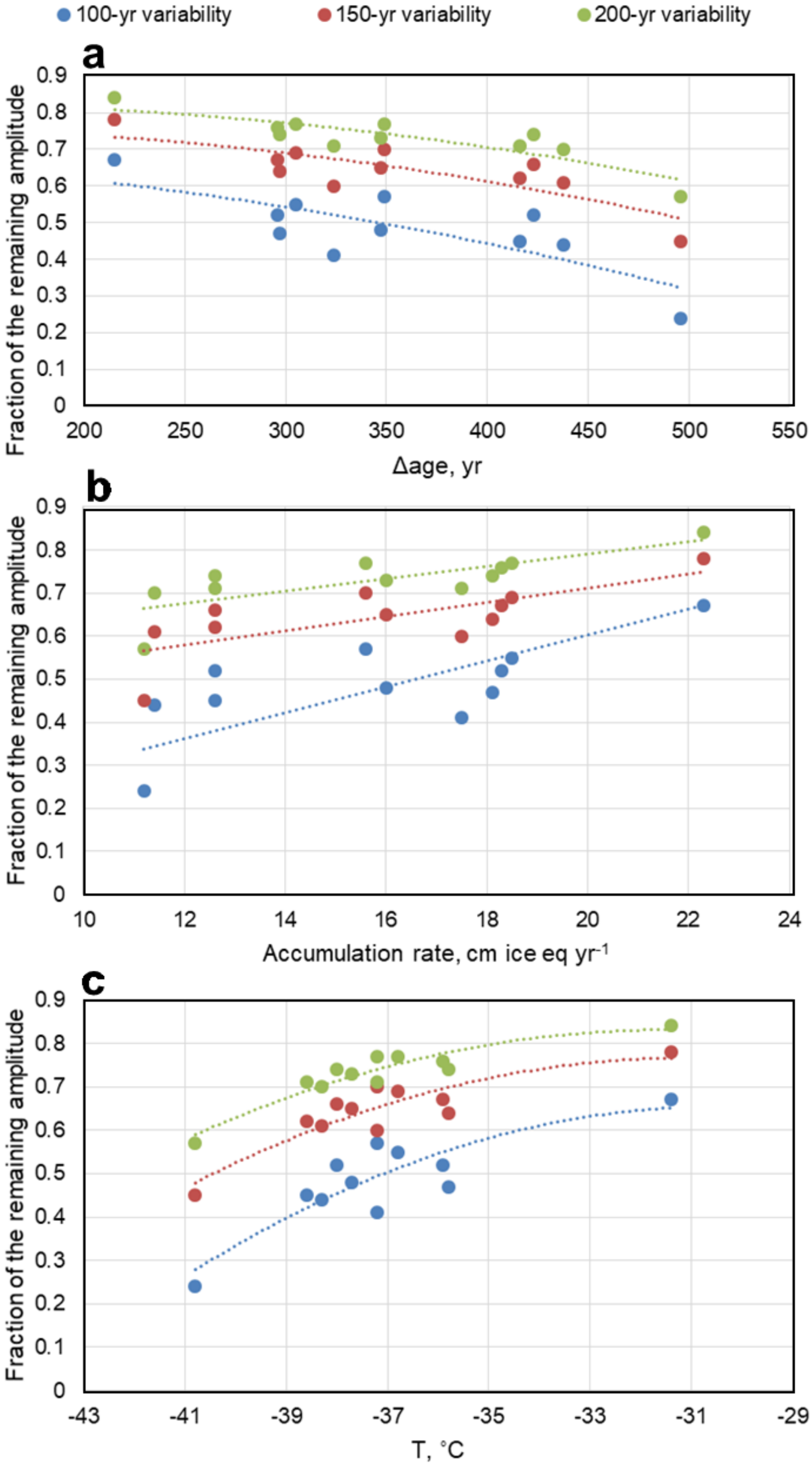

Figure 31: *A fraction of the remaining amplitude of the* CH_4 *signal as a function of the ice-gas age difference (Rhodes et al. 2017), snow accumulation rate (Cuffey et al. 2016) and the surface air temperature (Buizert et al. 2015).*

3.5. Dating of the gas record

A CH_4 record is possible to date using the synchronization with the other well-dated methane records. At this procedure used by (Blunier et al. 1998, Blunier and Brook 2001) the CH_4 peaks are matched consequently and iteratively reaching the highest possible correlation between the records.

An alternative way is to synchronize the CH_4 record with the stable water isotope record on the established timescale of the particular core. This way is appropriate for the Last Glacial period of Greenland ice cores: the climatic shift such as stadial-interstadial transitions are clearly marked in two records, the previous studies (Chappellaz et al. 1993) suggest that methane concentration and Greenland climate changed synchronously at the Last Glacial.

The third possible way is to model the variations of the ice-gas age difference (delta age or Δage) and apply the difference to the distributed ice age in order to figure out the gas age at a corresponding depth.

We applied all three procedures to the RECAP CH_4 record. First, in order to conduct a preliminary gas record dating, the newly obtained CFA CH_4 record was put on the WAIS Divide gas timescale (WD2014) (Buizert et al. 2015, Sigl et al. 2016). The well-known procedure of the gas records synchronization (Blunier et al. 1998, Brook et al. 2000). It allowed dating the Holocene (0-11.7 kyr b2k) record, for which none of the high-resolution Greenland CH_4 ice core records existed. These data cannot be used directly to estimate the Δage, however, as WD2014 is tuned to the Antarctic ice core timescales and the RECAP dating was made linking to the Greenland timescale. Second, the Glacial part of the record was tuned to NGRIP discrete CH_4 record. On the next step – to the RECAP $\delta^{18}O$ record (The Glacial section and the Last Glacial termination). On the later stage, the modelled Δage (Buizert, pers. communication 2017) was compared to the Δage predicted by the $\delta^{18}O_{ice}$-CH_4 date comparison (see Fig. 49). The results are presented on Fig. 30. The resulting age uncertainty is extracted from the WD2104 and RECAP timescales (tuned to GICC05) and is scaling down to 55 yr for the Holocene section and accumulating from 98 to 2600 yr during the Last Glacial.

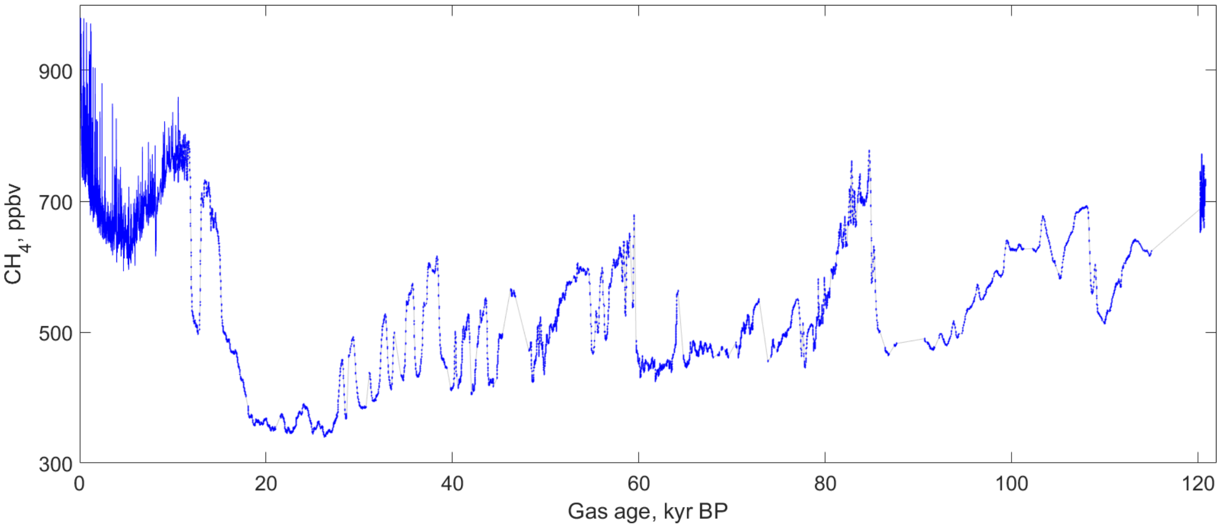

Figure 32: *RECAP CFA CH_4 record.*

Chapter 4. Climatic interpretation of RECAP CFA CH_4 record

4.1. Holocene – first high-resolution CH_4 record for the Northern Hemisphere

The RECAP CFA CH_4 record covers the entire Holocene capturing the atmospheric gas with zero age at the close-off depth and until the very onset of the Holocene. We emphasize the first high-resolution record as this record was obtained using the continuous flow analysis with a resulting average effective resolution 3.5 data points per 100 yr. Previously obtained CH_4 Holocene records (see Fig. 33) include predominantly the discrete data, the continuous datasets are patchy. Greenland records are represented for the early Holocene based on NEEM record (Chappellaz et al. 2013, Rhodes et al. 2013), for the late Holocene section based on recent GISP2 record (Mitchell et al. 2013), and for the whole Holocene based on the GRIP record (Chappellaz et al. 1997, Chappellaz et al. 1993, Blunier et al. 1995)and GISP2 records (Brook, Sowers and Orchardo 1996a). One of the GRIP datasets (Blunier et al. 1995) experienced a laboratory offset 15 ppbv. The RECAP record corresponds well in the millennial-scale patterns with the published records of the discrete CH_4 measurements in Greenland ice core samples, which is more clear in the late Holocene section. The absolute values if the RECAP record are slightly offset from the other Greenland records. The reason for the offset remains debatable, likely the reason is in presence of the surface melting. Multiple CH_4 spikes in the records are discussed below in the section 4.1.3.

4.1.1. Lock-in zone CH_4 variability

The loch-in zone exhibits high-frequency reproducible spikes in the CH_4 record (see Fig. 10 and section 1.3.1). We suppose that the spikes are caused by the layered bubble-trapping process: some pores in the lock-in zone are closed earlier and capture the varying concentration of the CH_4. If the atmospheric concentration is rising abruptly, like it was 80-96 years ago (the ice dating range at the lock-in zone of the RECAP core), the earlier closed bubbles will trap the concentration lower, then the neighboring pores, which will be later enriched in the atmospheric CH_4. A model of the layered bubble trapping and the CH_4 signal formation is described more detailed in (Fourteau et al. 2017). If the melting occurs, the CH_4 will be dissolved in a melt layer, appearing as a higher concentration spike (Pearman et al. 1986). The CH_4 concentration in the firn lock-in zone was measured using the continuous flow analysis technique also in the NEEM core (Rhodes et al. 2013) corroborating a suggestion of the high-frequency spikes origin.

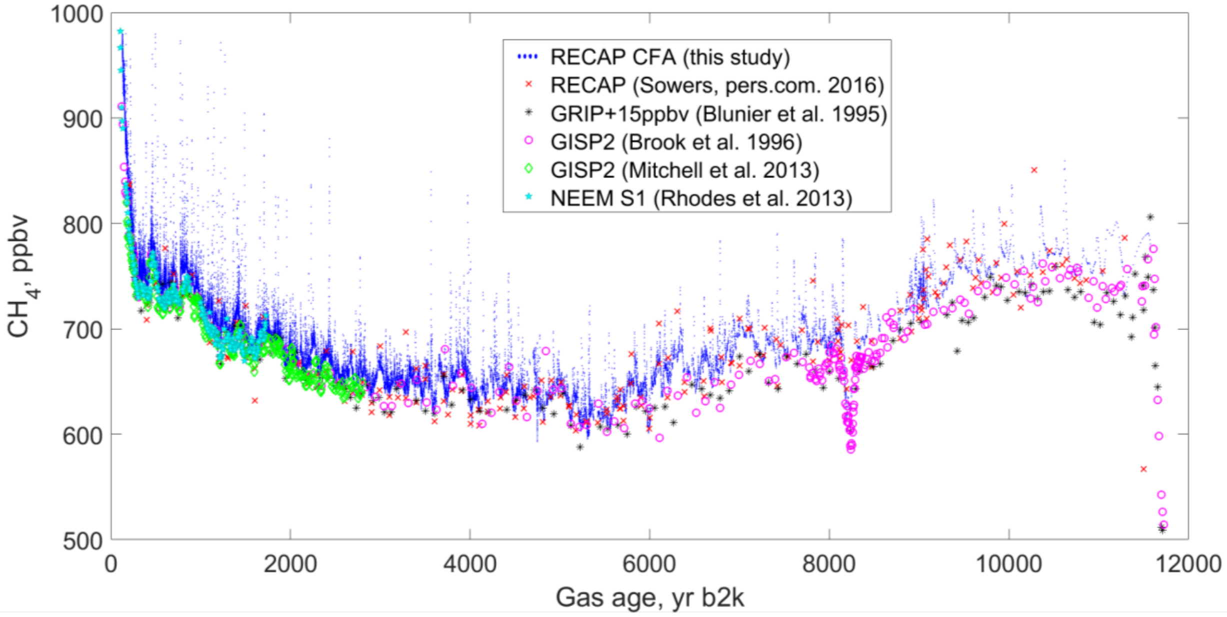

Figure 33: *Holocene CH_4 ice core records on its gas timescales translated to yr b2k (years before 2000 AD). GRIP record was shifted by 15 ppbv.*

4.1.2. Centennial scale variability

As seen in the CFA CH_4 RECAP record (Fig. 33 and 37), the CH_4 variability exhibits a millennial-to-centennial scale variability. We use the wavelet transformation and the wavelet coherence in order to check the evolution of the periodic variability in time and depth domains. The Cross Wavelet and Wavelet Coherence Toolbox was written for MatLab by (Grinsted, Moore and Jevrejeva 2004). The X-axis of such plots (e.g. Fig. 35b) is either depth or timescale. Along the X-axis one can follow how significant is periodic variability at a particular intercept of the dataset. The more powerful parts are denoted as orange and yellow. Black bands circle down statistically significant periodicity. Semitransparent white shaded area in the lower part of the plot is the cone of confidence related to the fact that long-term periodicity cannot be confidently defined at the margins of the data series. The wavelet coherence plots (e.g. Fig. 38b) depict not only the significant variability but also the phase relationship of the periods. The arrows are shown only for the significantly coherent variability of the two analyzed data series. An arrow pointing to the right means that the oscillation is totally in phase. Any phase shift is depicted as the radial angle of the arrow turned counterclockwise from the initial right horizontal position. E.g. an arrow pointing to the left means an antiphase relationship.

As the annual layer thickness decreases sufficiently toward the deeper sections yielding 463 m of the late Holocene record (11 m of ice core per 100 yr), 59 m of mid-Holocene (1.5 m yr^{-1}) and only 10 m (0.4 m yr^{-1}) of the early Holocene section (0.4 m yr^{-1}), it is worth checking the spectral properties of the CH_4 series in depth (Fig. 35) and time (Fig. 37) domains. It helps to figure out if the centennial scale variability is the measurements artefact/the ice core feature or it has a climatic origin. If the average frequency variability has similar spectral power throughout one of the domains, it possibly points on its origin. The climatic origin should presumably exhibit a significant variability throughout the record in centennial-to-millennial periodicity. Indeed, 100-1000 yr period are significant throughout the CH_4 record except 2.5-3.5 kyr BP (see Fig. 37). It probably occurs due to the enhanced high-frequency variability (spikes in the younger part of the record), which decreases the relative spectral power of middle and low frequencies. The climatic origin of the centennial-to-millennial scale variability is corroborated by the periods longer 8-10 m, which are significant only in the late Holocene part of the record (see Fig. 35, upper 400 m).

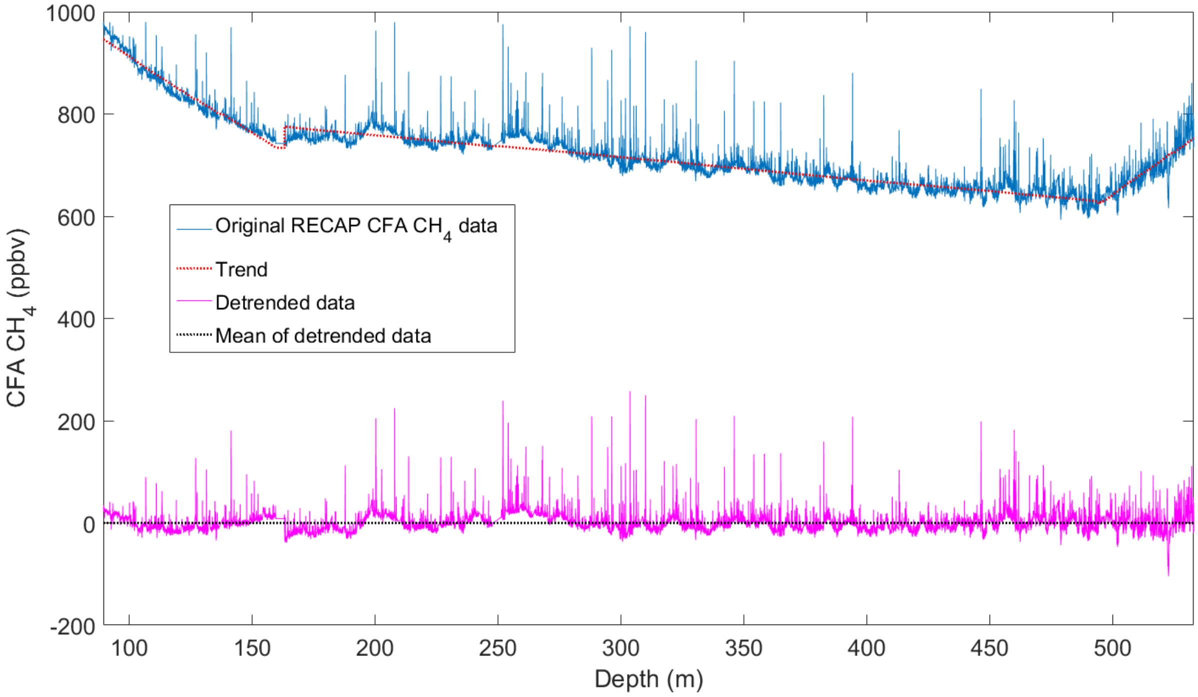

Figure 34: *Original and detrended RECAP CFA CH_4 data versus depth.*

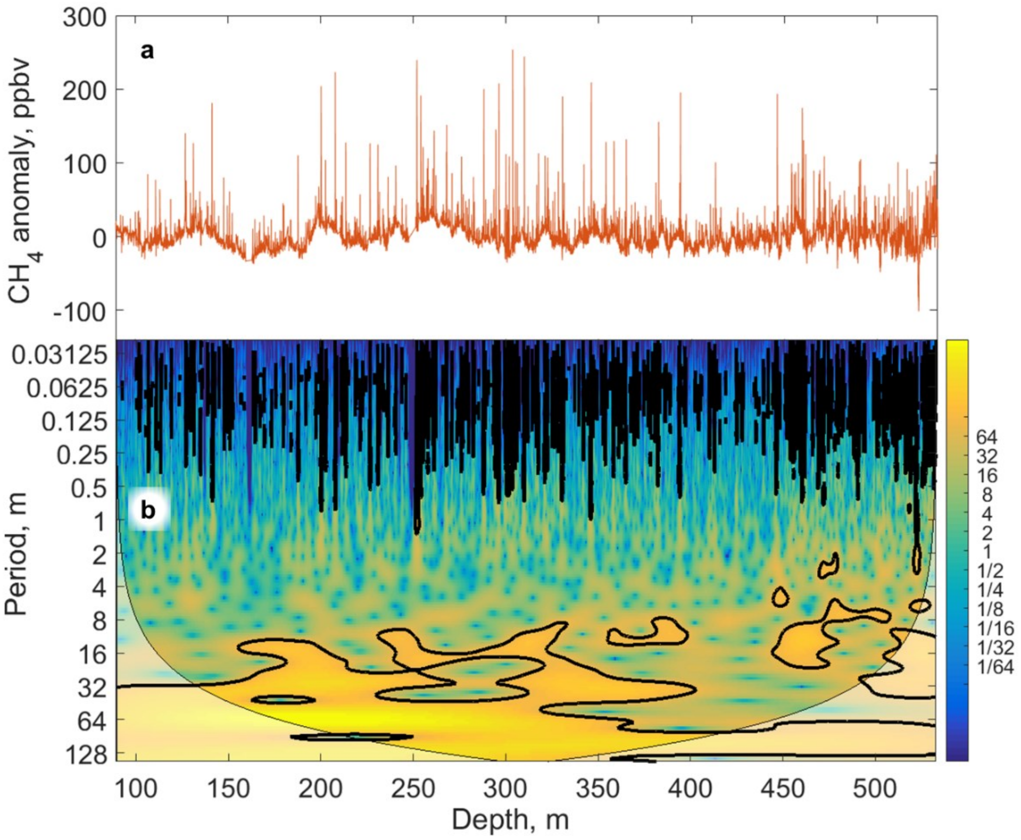

Figure 35: *Spectral properties of the RECAP CH$_4$ record on the depth scale: a – detrended CH$_4$ series, b – wavelet transformation of detrended CH$_4$ series in depth domain.*

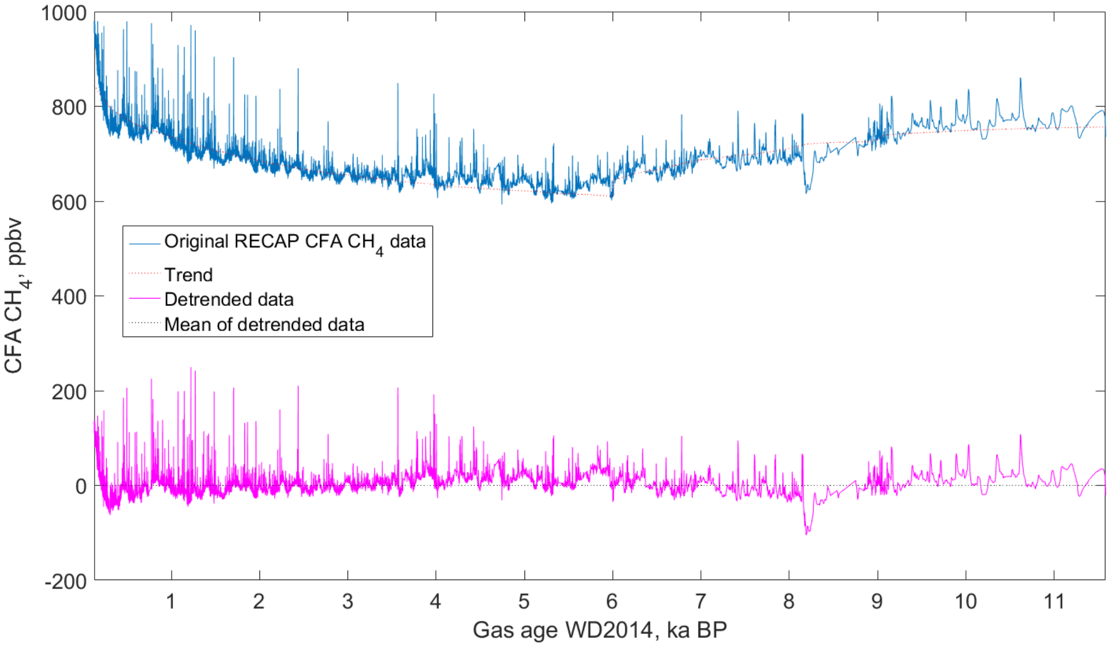

Figure 36: *Original and detrended RECAP CFA CH$_4$ data versus gas age.*

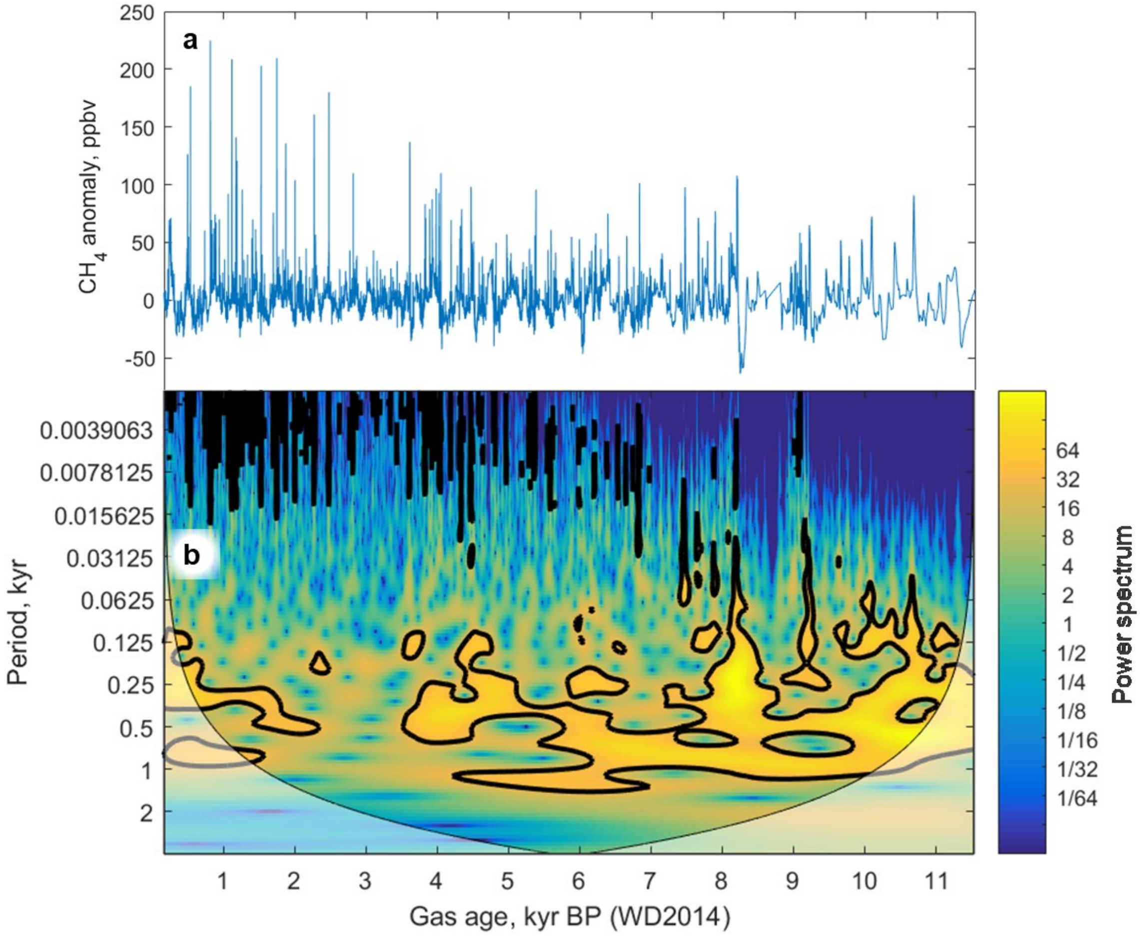

Figure 37: *Spectral properties of the RECAP* CH_4 *record on the WD2014 timescale: a – detrended* CH_4 *series, b – wavelet transformation of detrended* CH_4 *series in time domain.*

Interestingly, the recent high-resolution Antarctic CH_4 record (Members et al. 2013, Sigl et al. 2016, Mitchell et al. 2013) – West Antarctic ice core record (WAIS Divide - http://www.waisdivide.unh.edu/) demonstrates the similar feature – the presence of the centennial scale variability (Fig. 38a). Note that the offset between the records is caused by the interpolar difference of the methane concentration in the atmosphere.

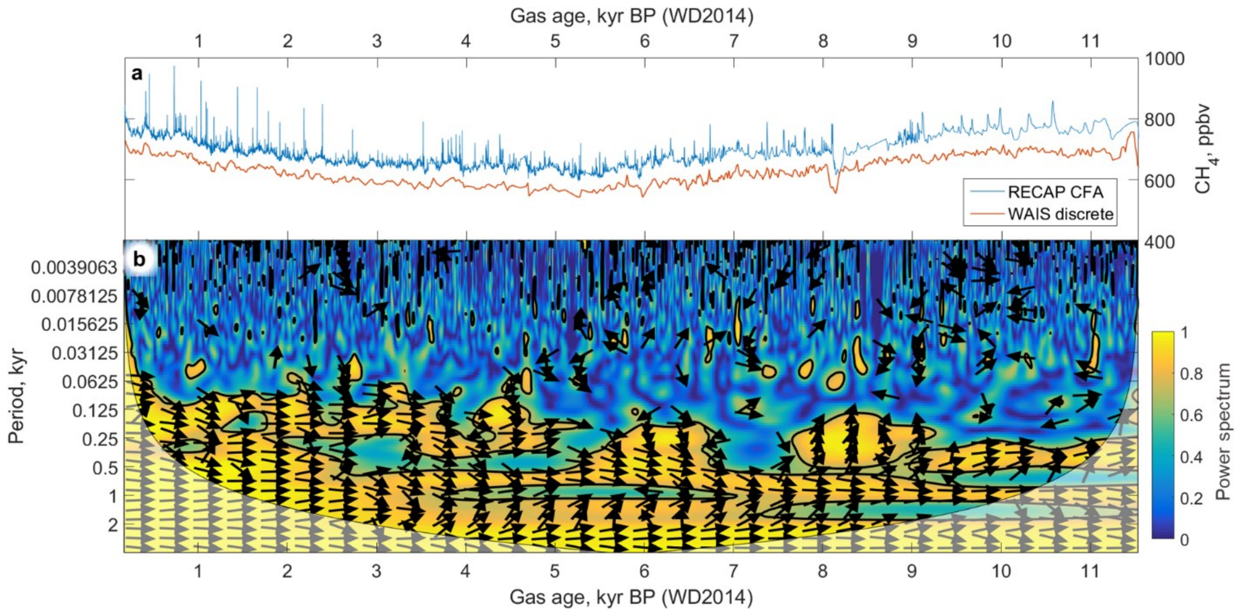

Figure 38: *Wavelet coherence of the RECAP (Greenland) and WAIS (Antarctica) CH$_4$ records: a – RECAP and WAIS CH4 records on WD2014 timescale, b – wavelet coherence of the two methane records.*

It would not be fully credible to compare the RECAP record matched to WAIS Divide timescale in order to identify the common variability. In order to avoid artificially high coherence of the two records yielded by the match, we analyze the coherence of Greenland and Antarctica Holocene CH$_4$ records on the RECAP ice timescale and WAIS Divide gas timescale WD2014 (Buizert et al. 2015, Sigl et al. 2016) – Fig. 39. The delta age is assumed to remain constant throughout the Holocene, thus the phase shift should be constant as well in case the common centennial scale variability is present in the two hemispheric methane records. The RECAP CH$_4$ record on the different timescales, used in this study, is shown in Fig. 39. Any Antarctic timescale is shifted relative to the Greenland timescales (Buizert et al. 2015, Svensson et al. 2013), and as seen in this case the shift is more than estimated delta age for the RECAP record. Thus, we do not discuss further the exact phase shift duration or its absence for the RECAP and WAIS CH4 records and focus only on the presence of the common variability.

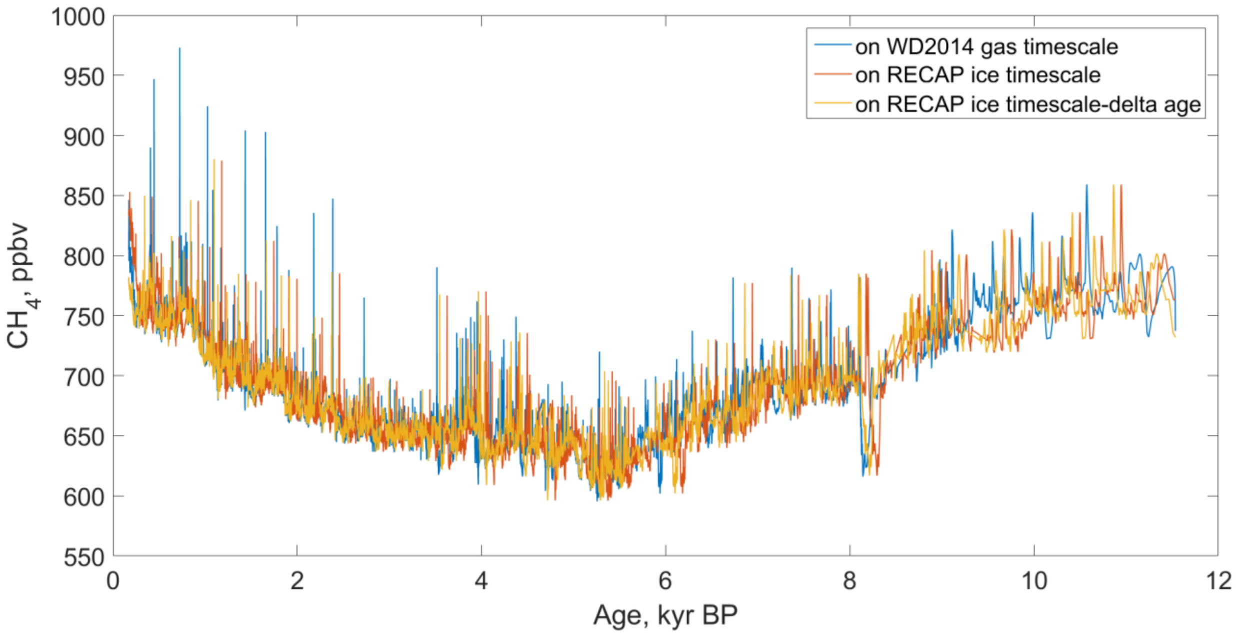

Figure 39: *The RECAP CH$_4$ record on different timescales.*

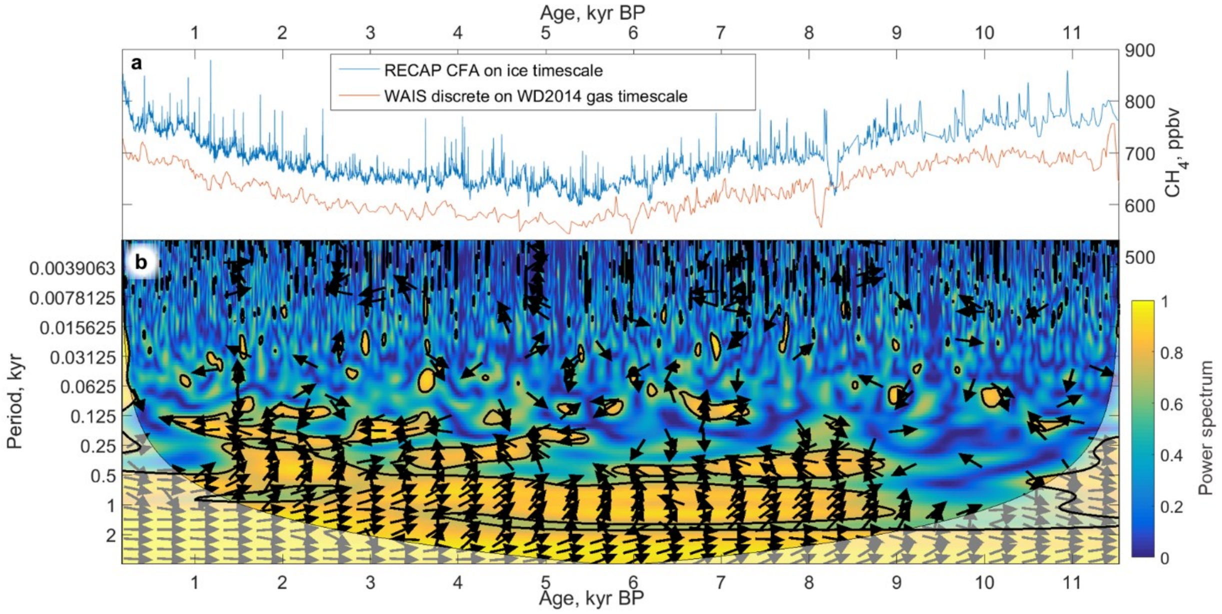

Figure 40: *Wavelet coherence of the RECAP (Greenland) and WAIS (Antarctica) CH$_4$ records: a – RECAP CH$_4$ record on RECAP ice timescale and WAIS CH$_4$ record on WD2014 timescale, b – wavelet coherence of the two methane records.*

The detrended data (Fig. 41) reveals more significant 250-1000 yr periodic variability in the early Holocene due to the enhanced reletive spectrum power and absence of the significant long-term variability.

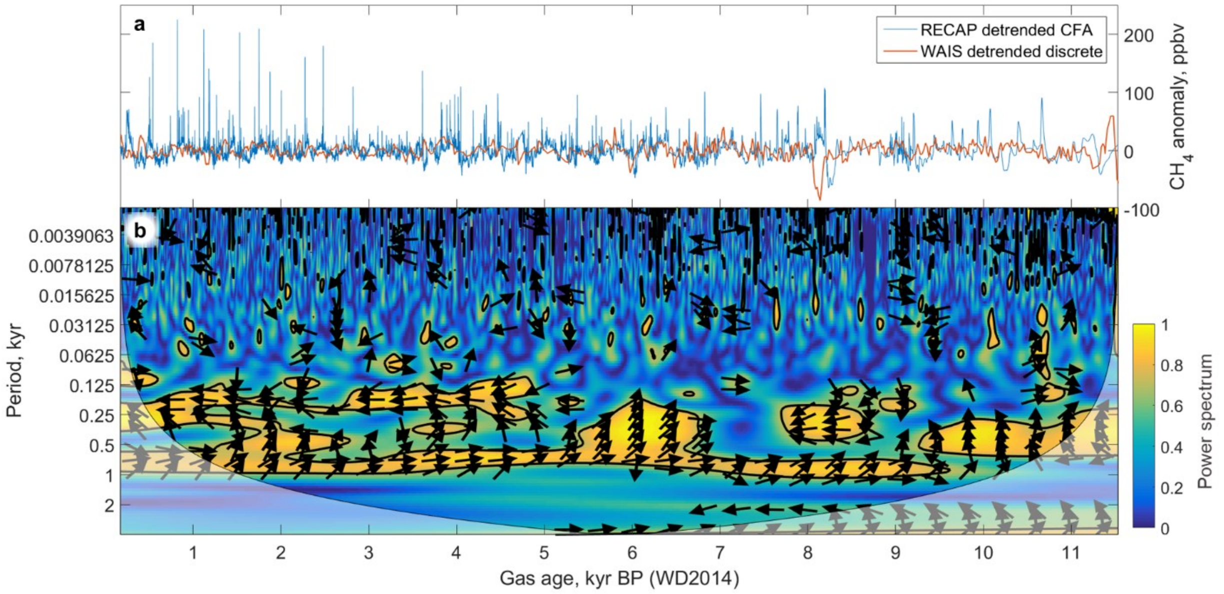

Figure 41: *Wavelet coherence of the detrended RECAP (Greenland) and WAIS (Antarctica) CH_4 records: a – RECAP CH_4 record on RECAP ice timescale and WAIS CH_4 record on WD2014 timescale, b – wavelet coherence of the two methane records.*

Summarizing the wavelet analysis, the pattern of the centennial scale variability seen in the RECAP CH_4 record is coherent with the earlier published Southern Hemisphere record based on the WAIS Divide CH_4 record. The wavelet coherence analysis identifies a high correlation at the long- and midterm variability (600-700, 200-500 yr periodicity); the late Holocene section reveals a common variability down to 70 yr.

4.1.2.1. On the origin of the centennial scale CH4 variability in Holocene

8.2 ka event is foot printed in the CH_4 ice core records both in Greenland and in Antarctica. We omit a discussion of the interpolar difference, as this is the subject of a separate research project. The event – a sudden drop in the temperature proxy a well as the CH_4 concentration and a recurrence 200 yr later suggest that the change occurred in the CH_4 sources and sinks globally and synchronously.

(Rhodes et al. 2017) identified a centennial-scale variability of 80-500 duration in the early Holocene (prior to 9.8 ka) and related the change to the tropical wetlands activity in methane emissions.

The centennial scale variability might be explained through source variations. The underlying mechanism is related to the sea surface temperature change affecting the tropical latitudes and the methane emissions from the wetlands. The tracers are in the sea surface temperature proxies and the ocean circulation indices (Mitchell et al. 2011, Rhodes et al. 2017). (Harder et al. 2007) carried out a model-based study and suggested discussing the variations in the CH_4 interpolar difference change during the Holocene, that not only change in source (wetlands) but also in a sink should be taken into account. The CH_4 sink might be affected by the change in sea surface temperature and in volatile organic compounds concentration. The Antarctic ice sheet discharge caused by small changes in the subsurface ocean temperature can affect global multi-centennial scale climate variability (Bakker et al. 2017). However, the changes in sink, i.e. in OH^- radical capable to oxidize as much CH_4 as yielded a clear centennial variability change, would require an improbable change in average SST (Tierney et al. 2015) and/or in the volatile organic compounds content.

(Sebacher et al. 1986) based on the CH_4 flux measurements from the wetlands, bogs and tundra in Alaska, found a logarithmic dependence of the methane flux from the water level, i.e. the higher is the water level the stronger is the CH_4 emissions from wetlands.

(Smith et al. 2004, Yang et al. 2017) suggested the northern hemispheric source, particularly Siberian peatlands to be the long-term global methane source in the early Holocene (prior to 9.5 ka BP). The development of the peatlands in the Arctic region is confirmed by a number of radiocarbon dates (MacDonald et al. 2006).

(Chappellaz et al. 1997) evaluated the CH_4 interpolar difference evolution throughout the Holocene based on Greenland and Antarctica ice core records. They pointed on the tropical wetlands being the dominant source. However, the extending boreal wetlands and their methane emissions could counterbalance the drying tropical latitudes during the second part of Holocene.

(Yang et al. 2017) observed for local minima roughly every 1000 yr in the period 7.7-11.7 ka BP in the Antarctica CH_4 record (Siple Dome core). These CH_4 minima correspond to cold periods in Greenland and possibly to migration of the intertropical convergence zone (ITCZ) northward reducing the CH_4 production from the southern tropical wetlands.

The increase in the CH_4 concentration since 6 ka BP is likely not explained solely by the Northern Hemisphere wetlands development as most of them evolved from a type, which generates high levels of CH_4 to the less productive (fens to ombotrophic bogs) (MacDonald et al. 2006).

(Wen et al. 2016) revealed a multi-centennial scale (300-600 yr) occurrence of the humid episodes in the desserts in Central China, which were modulated by the Eastern Asian monsoon activity. The analysis was based on paleo-aeolian sands and paleosoils deposited in Early Holocene. (Bird et al. 2016) identified a millennial long pluvial periods in southeastern Tibet during the Late Holocene, which are correspondent to the enhanced Indian summer monsoon, warmer temperatures in Tibet and La-Niña-like state of the tropical Indian Ocean. (Meltzner et al. 2017) traced the relative sea level change in Eastern and Southeastern Asia and figured two fluctuations in mid Holocene. The relative sea level change might indirectly influence the wetland CH_4 emissions by regulating the water level. The Eastern Asian monsoon, in turn, is oppositely related to the Indonesian-Australian monsoon in its weaker and stronger phases on the multi-centennial scale (Eroglu et al. 2016). (Fleitmann et al. 2007) suggested that the Indian and Asian monsoon were characterized by the centennial variability correlated with the Greenland temperature variability.

(Conroy et al. 2008) pointed out that the tropical Pacific and Asian monsoon were interconnected on the centennial timescale.(Bernal et al. 2016) revealed 140 and 80 years statistically significant periodicity in South American monsoon intensity. The analysis was based on the high-resolution ion chromatographic studies of stalagmite samples from southeastern Brazil.

Thus, the centennial scale variability was traced all over the tropical wetland regions during the Holocene and was related to the dynamics of the intertropical convergence zone. We hypothesize that the tropical wetland CH_4 emissions varied accordingly and were regulated via the humidity in the region and the water plane level fluctuating due to the relative sea level change.

4.1.3. Nature of high frequency CH_4 spikes in RECAP Holocene record

High frequency CH_4 concentration variability is expressed as sharp spikes or oscillations of the resolution higher than the effective analytical method resolution. The effective resolution also depends on the average residence time of CH_4 in the atmosphere and the gas age distribution width in the firn. In other words, if we cannot resolve any variability more frequent than 3.5 data points 100 yr^{-1} (as for the late Holocene section of the RECAP ice core, i.e. back to 4.2 ka BP) also the other variations have to be suspected for non-climatic.

There are several possible origins of the high frequency CH_4 variability as noted by (Mitchell et al. 2011, Rhodes et al. 2013):

1. In-situ bacterial production
2. Melt layers
3. Contamination during the measurements
4. Layered bubble trapping artifacts
5. Dust
6. Unknown mechanism

4.1.3.1. In-situ production

(Rhodes et al. 2013) suggested that high amplitude (35-80 ppbv) long period (n·10 cm) CH_4 spikes are related to the in-situ CH_4 production in the layers with the organic content. This organic content originated from the biomass burning end products.

In-situ bacterial CH_4 production can be traced by the high-resolution chemistry preferably measured at the same CFA setup in parallel with the gas measurements. The in-situ CH_4 spikes are also marked in the high black carbon and nitric acid content (HNO_3). The sulfate ions (SO_4^{2-}) are not always well correlated with the CH_4 high amplitude spikes (Rhodes et al. 2013).

The in-situ production might potentially happen in the bottom part of the ice sheet due to the bedrock layers enriched in the organic compounds (e.g. buried peatlands) and mineral material (buried lake sediments, clays). The bottom part of the RECAP ice core (from 10 m above the bedrock and down) is highly enriched in the CH_4 – up to 250 ppm non-calibrated values (the detection limit of the laser analyzer). We hypothesis that it might be due to the in-situ production and/or the gas seeping from the bedrock sediments. The data affected by the CH_4 enrichment was included from the record, the Eemian section presented in this chapter (see Fig. GD) is from the depth above the affected interval. We assume that the presented Eemian signal captures the natural atmospheric variability as the CH_4 concentrations matches the order of magnitude and the range of the interglacial CH_4 variability (600-750 ppbv) based on Greenland and Antarctic ice core records.

(Telling et al. 2015) have measured the molecular hydrogen production of the silicate rocks in the water environment under the controlled laboratory conditions at an ice melting temperature. They suggested that the hydrogen produced due to the rock granulations could serve as a nutrient for the subglacial life. The more fine is the grain size the more hydrogen can be produced. This suggestion may support the presence of bacterial life including methanogenic bacteria near the bedrock. If the deepest part of the Renland Ice Cap is in contact with the subglacial melt flow, then it could potentially create an environment favorable for the in-situ CH_4 production.

The other possibility of the methanogens is an organic carbon decomposition. (Stibal et al. 2012) estimated the CH_4 bacterial production rate in the different subglacial sediments as 10^{-15}-10^{-10} mol g^{-1} day^{-1}.

4.1.3.2. Melt layers

The presence of melt layers is possible to check using either the light scanning data (Fig. 42) or fine resolution total air content (TAC) measurements (Fig. 43). The light scan data reveal dark grey bands at the layers containing frozen percolated water while the total air content data should reveal low to no air content at the melt layers. If a suggestion that the melting causes the CH_4 dissolution and thus a spike in the CH_4 record (Pearman et al. 1986) was valid for the RECAP record, than the quantile regression (Fig. 43) would demonstrate the excess CH4 values at a low TAC range. The light scan data In turn do not indicate any visible melt layers in the ice older than 2 ka BP due to the layers thinning. The total air content measurements in turn require an ice core sample 2 cm long, which decreases the resolution as normally the melt bands are 1-5 mm wide. A comparison of the total air content data and the light scan data with the CFA CH4 measurement results identified that presence of the melt layers can explain less than 50% of the CH_4 spikes.

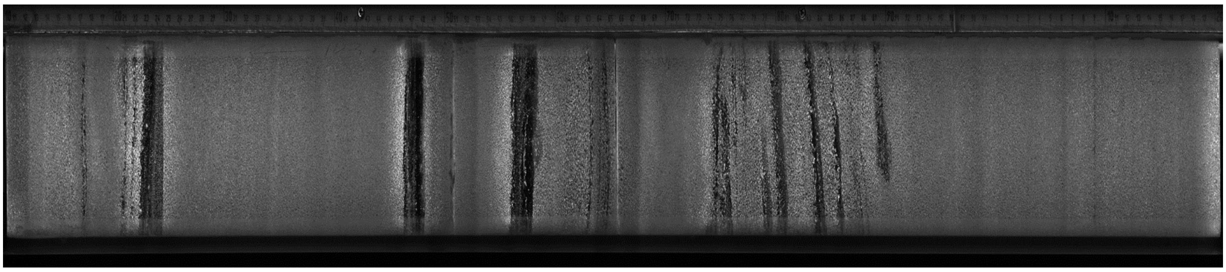

Figure 42: *Light scan image of a section of the RECAP ice core in the depth interval 78.1-79.2 m (Kipfstuhl, pers. communication, 2015). Dark bands are the melt layers.*

Note RECAP data suffered the depth scale assignment offset in the range of 5-20 cm per 5.5 m. It was detected first along the Glacial section while comparing CFA CH_4 data to discrete CH_4 data and $\delta^{15}N$ data measured by Todd Sowers at Penn State University. The CFA CH_4 depth scale was corrected for the entire Glacial section as it was crucial for the dating, while the Holocene section containing 532 m of ice would lead to a shift of a few years. This is smaller than the effective resolution and thus not crucial for the timescale assignment. However, at the end of the work on the thesis the timescale reassignment is planned in order to deliver the best possible quality of the CFA CH_4 data. Afterwards, a more fine comparison of the separate melt layers visible in the light scan data and individual CH_4 spikes will become reliable.

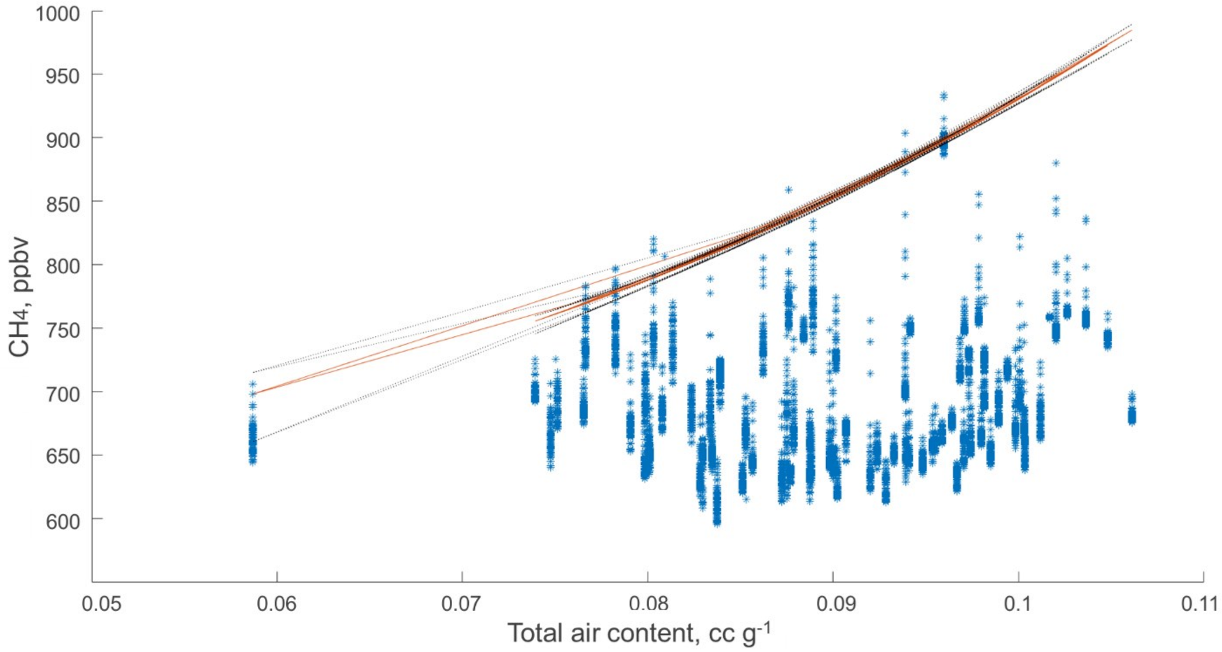

Figure 43: *Quantile regression of the RECAP CH_4 record vs total air content (Vudayagiri, pers. communication, 2017). The blue stars correspond to the data pairs of the CFA CH_4 and TAC data from the same depth interval. The red curve is the second order 99-percentile fit and the dashed black lines are its 95% confidence interval.*

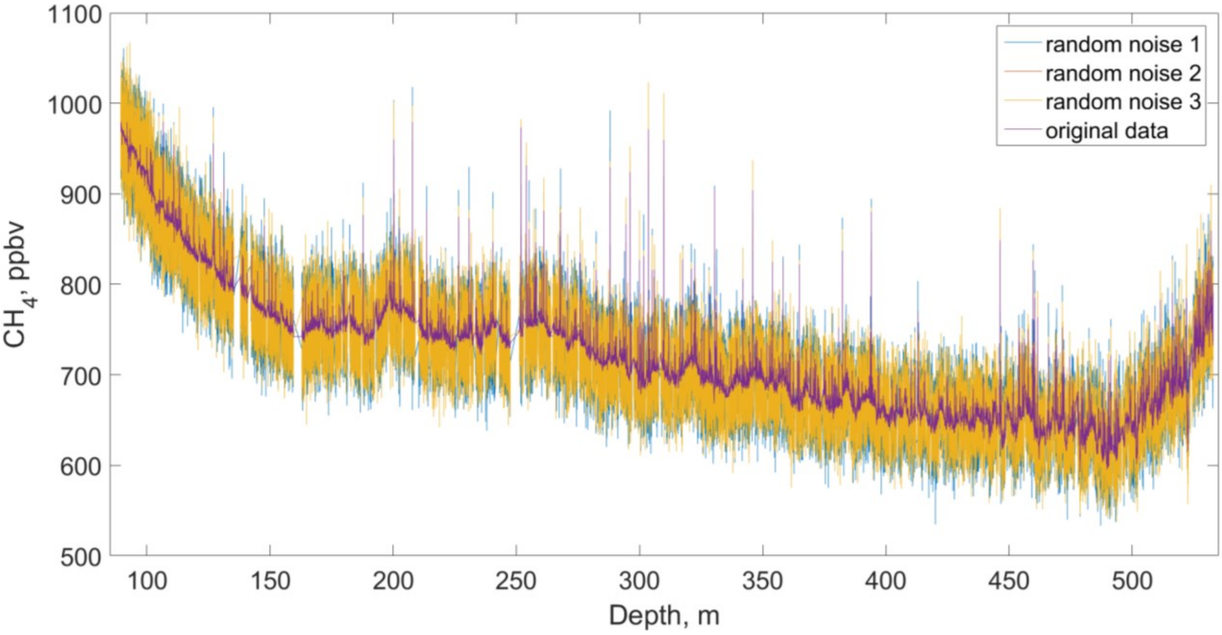

Figure 44: *RECAP CH_4 (original data) and the three test random noises datasets simulated with properties similar to the original series on the depth scale.*

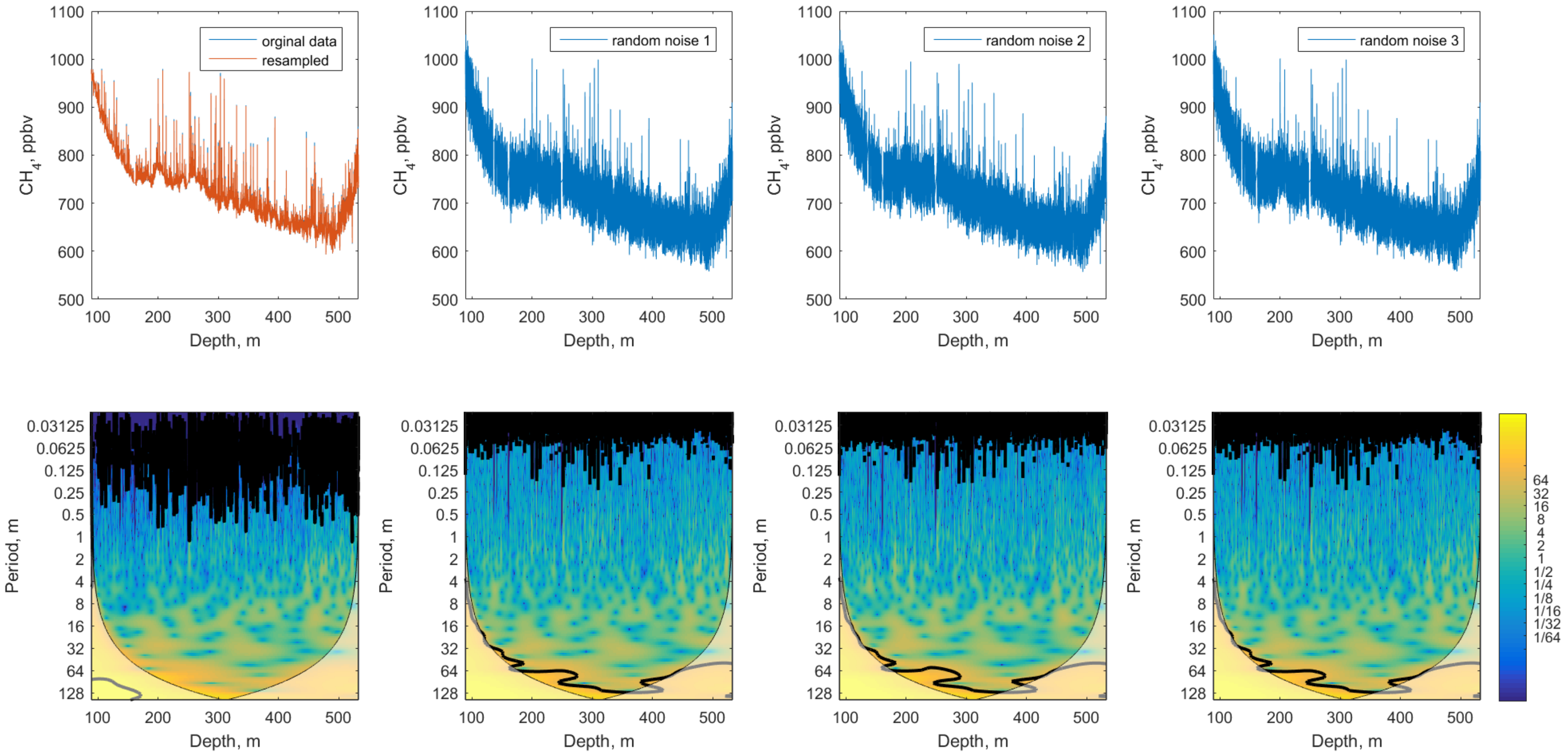

Figure 45: *Upper panels – RECAP CH_4 (original data) and the three test random noises datasets simulated with properties similar to the original series on the depth scale. Lower panels – the corresponding wavelet transformations of the CH_4 and random noise series.*

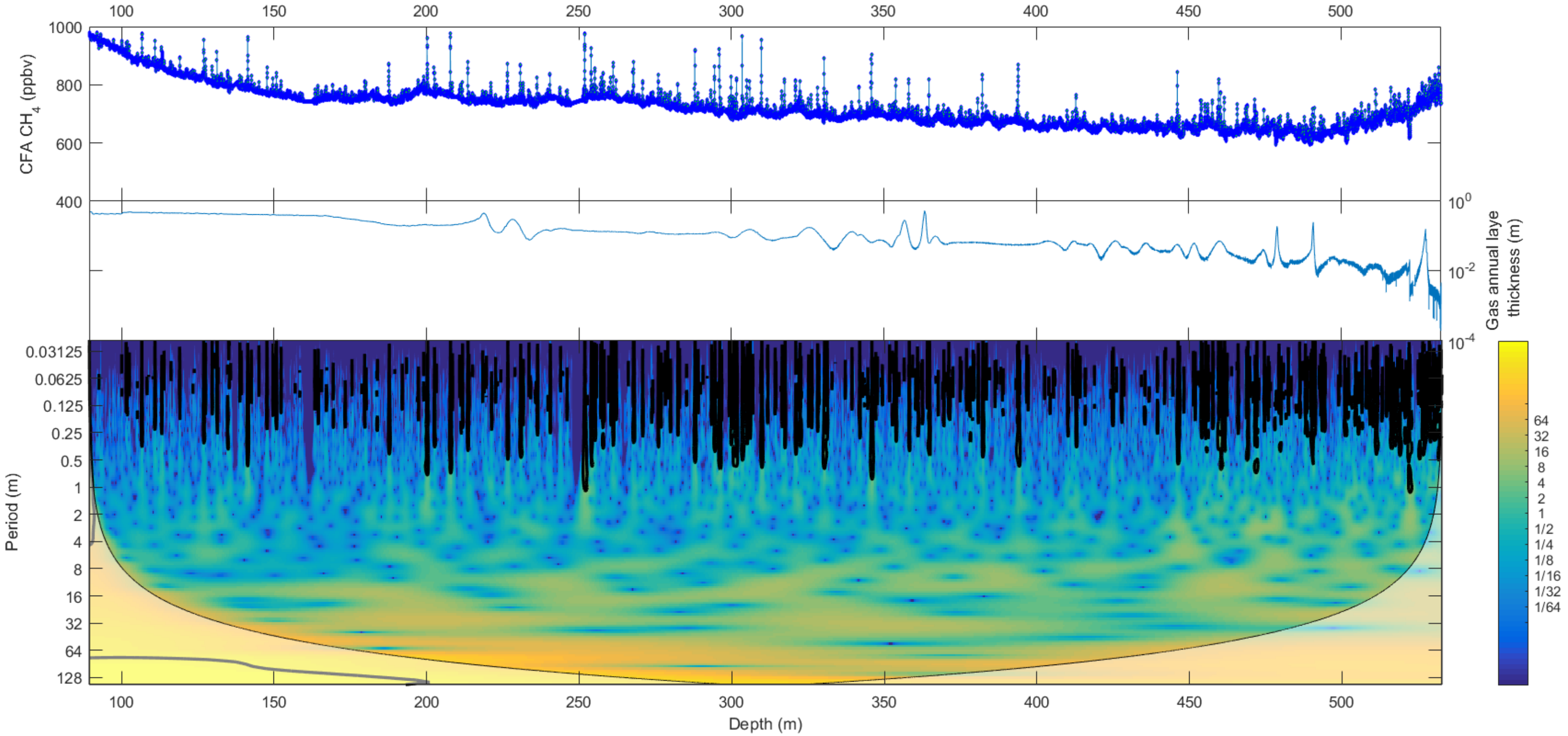

Figure 46: *Upper panel – RECAP CFA CH_4 series, middle panel – annual layer thickness of the gas record, lower panel – wavelet transform of the CH_4 series in depth domain.*

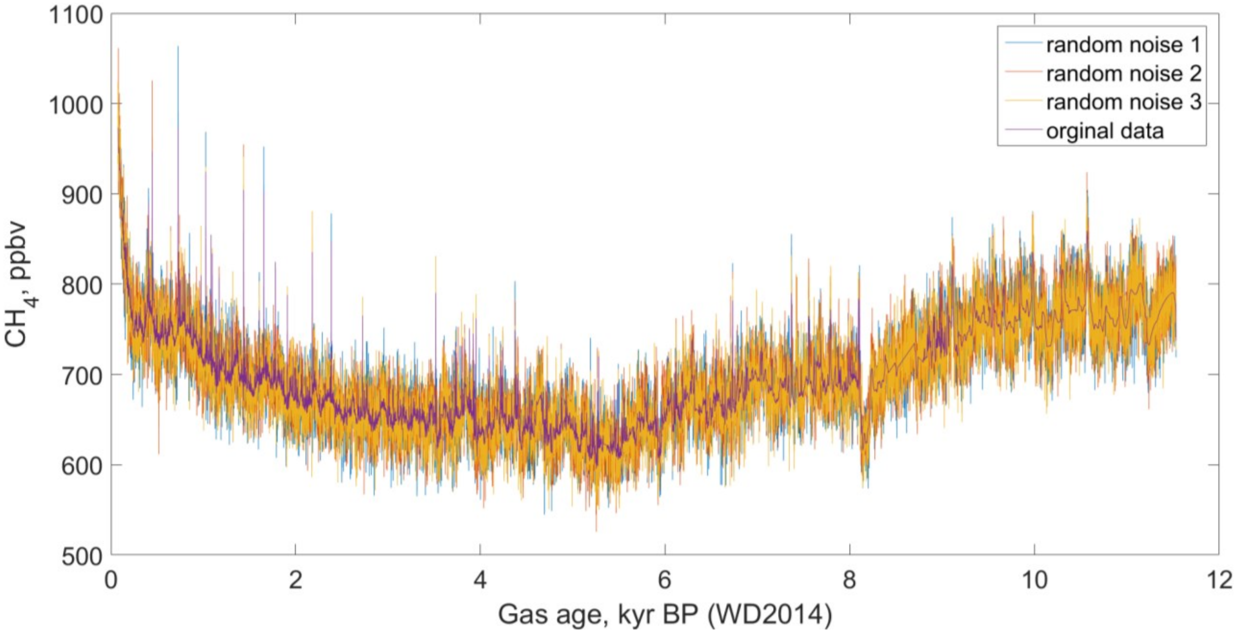

Figure 47: *RECAP CH$_4$ (original data) and the three test random noises datasets simulated with properties similar to the original series on the WD2014 gas timescale.*

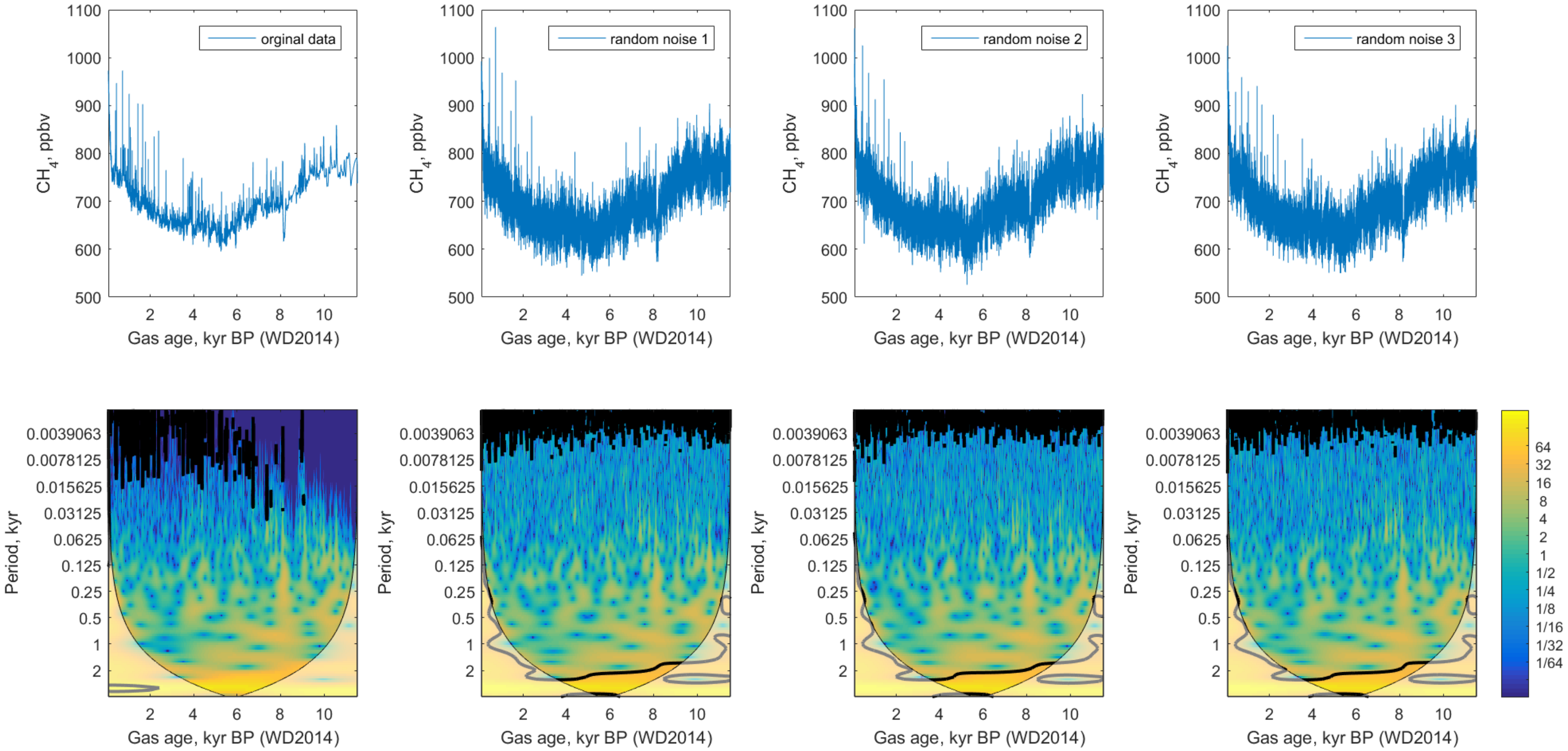

Figure 48: *Upper panels – RECAP CH$_4$ (original data) and the three test random noises datasets simulated with properties similar to the original series on the WD2014 gas timescale. Lower panels – the corresponding wavelet transformations of the CH$_4$ and random noise series*

Three random noise series were generated in depth and time domains matching the characteristics (such as moving average and standard deviation) of the original RECAP CFA CH_4 record. The spectral properties of the CFA CH_4 series in depth and time domains match the spectral properties of the random noise series only in the high frequency region. The medium scale variability with the period 6-60 cm is preserved throughout the Holocene record with the same spectral power (see Fig. 35). While in time domain the variability with the period 3-30 yr, which is of the longer periodicity than the random noise series, are significant in terms of the spectral power only in the mid and late Holocene. It suggests that the short-scale (a few cm) high amplitude (up to 200 ppbv) spikes originate from the measurement and/or storage artefacts, an additional drilling fluid affect is also possible. The annual layer thickness based on the gas record dating is presented in the middle panel of the Fig. 46. It decreases from 8.2 ka BP toward the Holocene onset, which suggests that short-term climatic variability CH_4 signals can not be resolved in the core in the early Holocene section. Thus if the lengths of the spike in the early Holocene section is similar to the length of the spike in the late and mid Holocene sections, than this CH_4 spike was formed after the snow deposition and the atmospheric gas trapping and possibly even after the ice core was drilled.

4.1.3.3. Contamination during the measurements

A contamination during the measurements occurs occasionally when the new sample touches the melthead. It happens due to penetration of an atmospheric air bubble into the gas extraction line. This type of contamination appears as a high amplitude ($n \cdot 100$ ppbv of CH_4, up to atmospheric concentration ≈2000 ppbv). A peak is usually asymmetric and skewed toward the upper depth, which reaches the melthead first. The smaller amplitude contamination spikes can be traced by the wavelet transformation in 55-cm period band (i.e. the standard length of an ice core). Other contamination spikes are not periodic as they occur at the depth of the core breaks. These contamination spikes can be diagnosed by the shape of the spike and by the notes on the breaks in the ice core processing log.

4.1.3.4. Layered bubble trapping

The layered bubble trapping (Rhodes et al. 2016, Fourteau et al. 2017) is an effect yielding the spikes in the CH_4 record. It occurs as a consequence of not gradual pores closure in the firn lock-in zone: some of the pores are closed earlier capturing a variation in the atmospheric gas signal, which will not be propagated to the neighboring layers with the open pores. The effect was described in the sections 1.3.1, 1.3.2.1 and 4.1.1. Layered bubble trapping is suggested as possible mechanism for the high amplitude (up to 100-200 ppbv) CH_4 variability on the sub annual scale. The pores closure process has a stochastic nature, thus the CH_4 signal formed by the layered bubble trapping would not have a significant periodic variability.

4.1.3.5. Dust

(Lee et al., in prep.) suggested that the CH_4 production can be induced in-situ in the dusty layers. A possible mechanism could underlay in the melt-refreeze method: the methane is released either from the dust particles, which absorbed the gas prior to the deposition or due to the bacterial production in the mineral dust environment during the ice core melting. The RECAP CFA CH_4 data does not reveal, however, any tracers of the in-situ dust-influenced CH_4 production (Lee, pers. communication, 2018).

4.2. Last Glacial

4.2.1. Resolving the full amplitude and absolute values of CH_4 concentration during GSs and GIs

The gas signal trapped in the ice cores provides credible but not exact picture of the atmospheric gas concentration at a certain time span. The factors affecting formation of the eventual gas signal measured in the ice core samples are described in the section 1.3. In a brief recap the are the following:

- fast variations in the atmosphere, which are not capable to capture due to the longer firn pores closure time; varying to an uncertain extent gas pores closure time;
- gas diffusion in the firn column;
- gravitational enrichment in the firn column;
- melt layers percolating to the firn and dissolving the gas;
- gas loss due to the dissolution due to the measurements;
- gas diffusion in the analytical gas extraction line and in the analyzers cavity during the measurements.

Due to the bug in the depth assignment algorithm, the depth assigned to the CFA measurements had an offset of 5-22 cm. The depth shift was accumulated stepwise from one melting run to another (5.5 m). The offset occurred due to the ice core breaks and gaps, which were not taken into account when translating the melting depth based on the Encoder data to the depth of the ice

sheet. A comparison of the initially assigned and corrected depth scales is provided in Fig. 21. The credibility of the updated depth scale was independently proved by a better fit of the experimental and modelled delta ice-gas age results (Buizert, pers. communication, 2018).
The analysis if the CFA setup response time to a change of the measured standard gases (see section 3.4) revealed that any fluctuations of the CH_4 signal, which take less an 3-7 cm in terms of the core lengths, do not preserve their full amplitude. Its CH_4 amplitude captured in the ice core is possible to estimate using as simple Gaussian smoothing.

4.2.2. Was the deep convective zone possible during the last glacial?– project members' contribution

The attempts to reconstruct the delta age were made by (Buizert, pers. communication 2018) based on the nitrogen isotope ($\delta^{15}N$) measurements (Sowers, pers. communication 2017), by (Vinther, pers. communication 2018) based on the $\delta^{18}O$ record, reconstructed accumulation rate and RECAP timescale and by the author based on matching RECAP CH_4 record to the $\delta^{18}O$ record using the ice timescale as well as WD2014 assigned gas ages comparison to the RECAP ice timescale. The reconstructed delta ice-gas age difference throughout the Last Glacial reveals a discrepancy (Fig. 49). The Δage values obtained based on the $\delta^{15}N$ modeling and the Δage values obtained based on the stable water isotopic ($\delta^{18}O_{ice}$) and the CH_4 record comparison deviate from each other in the different directions. This discrepancy is not possible to eliminate by tuning the temperature and/or the accumulation rate in the Δage reconstruction based on the $\delta^{15}N$ data.
There are a few possible phenomena causing the discrepancy in different Δage:

1) deep convective zone
2) decoupled temperature and accumulation variations
3) dust content responsible for changing the firm densification properties.

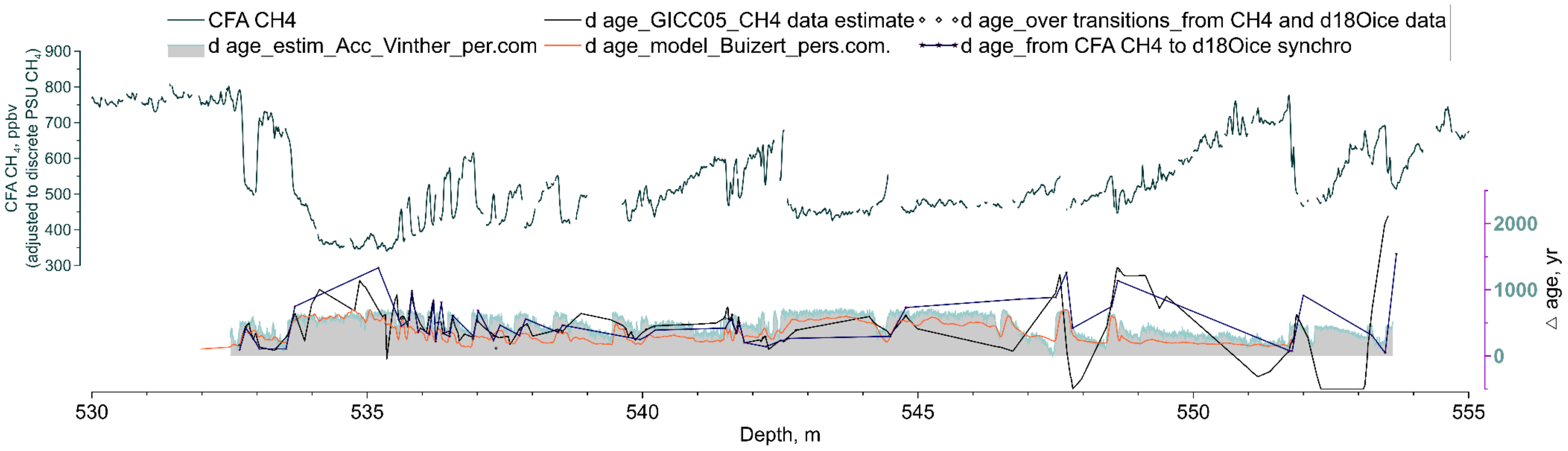

Figure 49: *RECAP CH_4 series and various delta ages estimates.*

1) The deep convective zone, formed in the near zero accumulation sites, causes a thicker layer (up to 20 m instead of 2-5 m) of the near zero δ^{15}N, i.e. a thicker layer of the atmospheric air exchange with the air in the open pores. Following this scenario, the eventual nitrogen 15 isotopic composition at the pores close-off would be heavier than expected from the theoretically predicted gravitational enrichment component should the convective zone have been shallower. A heavy δ^{15}N isotopic composition (without taking into account a deep convective zone) results in the misinterpreted higher temperatures, which makes a predicted pores close-off depth shallower thus Δage – smaller. That matches the picture that we see in the δ^{15}N modelled Δage and Δage obtained based on the CH_4 and the stable water isotopic data – the first one is smaller than the second during the cold phases (see Fig. 49). However, the deep convective zone forms in the nearly zero snow accumulation conditions similar to the modern Central Antarctic megadune areas (Severinghaus et al. 2010). To our knowledge, there is no evidence of the formation of such conditions in the isolated ice cap like Renland ice cap, at the elevation ca. 2 km.

2) Renland ice cap is exposed to the marine storm activity. Thus, the snow accumulation rate, though a relative high accumulation rate – ca. 0.5 m ice eq. yr-1, is a matter of a few snowfall events. In this case, the amount of the accumulated snow is decoupled from the temperature variations. A similar mechanism was described for the Law Dome ice cap in East Antarctica (Van Ommen, Morgan and Curran 2004).

3) Dust as well as other impurities accelerates the firn densification process. The faster (i.e. the shallower) pores close off leads to a smaller Δ age than the one predicted by the δ^{15}N modelling. The argument requires an additional investigation.

4.3. Eemian

The atmospheric methane concentration variability during a part of the Eemian interglacial is covered in the RECAP CH_4 record. The lower boundary of the earliest age from the Eemian section captured in the record is poorly constrained. The record was preliminary cleaned of the contamination caused by the near bedrock layers affected by the elevated CH_4 values.

The bottom part of the RECAP CH_4 record (approximately the lowest 20 m before reaching the bedrock at the depth 584 m) is characterized by the excessively high CH_4 concentration (up to 250 ppm). This part affects the Eemian record, thus the contaminated part, i.e. deviating more than 100 ppbv from the known average Eemian CH_4 concentration (Dahl-Jensen et al. 2013), was deleted from the climatic record. The CH_4 enrichment source is likely an in-situ production (Dieser et al. 2014, Portnov et al. 2016), see section 4.1.3.1 for more details.

4.3.1. Negative $\delta^{15}N$, low total air content, smooth CH_4 – does it suggest cold winters and hot summers with melt?

The $\delta^{15}N$, total air content and O_2/N_2 ratio (Fig. 50) were measured at the Penn State University at the same sample each using the mass-spectrometry technique (Sowers, pers. communication 2016, 2017). The measurements cover the early Holocene, the Last Glacial (not shown) and the Eemian section. The Eemian ice in the RECAP record is characterized by the negative $\delta^{15}N$, low total air content and smooth CH_4 series. Low or negative $\delta^{15}N$ cannot be consistent with a normal firn column at RECAP, as either of the scenarios would suggest interrupted gravitational or thermal fractionation. One can only hypothesize the sharp seasonal contrasts, i.e. cold winters and hot summers with melt in order to produce the observed nitrogen 15 isotopic and $\delta O_2/N_2$ signals. Alternatively, the post depositional changes, i.e. the bottom melt and/or possible ice folds near the bedrock could account for the CH_4 signal smoothing and an effect on the gas ratios and isotopic fractionation.

4.3.2. Can we deconvolute the Eemian atmospheric CH_4 record?

Comparing Holocene and Eemian records (Fig. 50) one can notice a more smoothed Eemian CH_4 signal. Likely, the underlying reason is in the gas signal smoothing in the deeper part of the ice core rather than in different CH_4 atmospheric histories of the two interglacials.

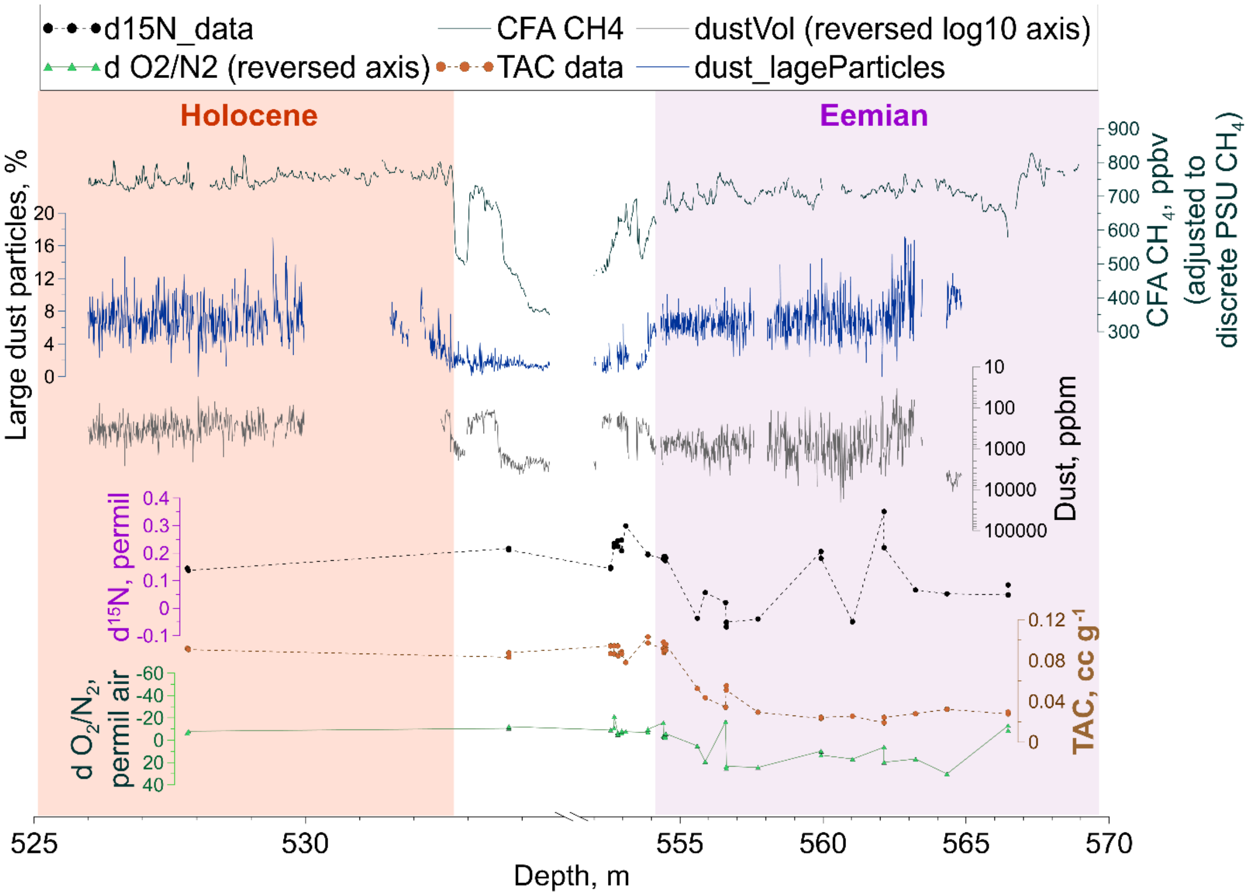

Figure 50: *A comparison of the paleoclimatic proxies during the interglacials captured in RECAP ice core. Dust particles count and volume is from (Simonsen et al. in prep.), $\delta^{15}N$, total air content and $\delta O_2/N_2$ is provided by (Sowers, pers. communication, 2016, 2017).*

A comparison of the CFA gas flow properties along the onset of the Holocene, the Last Glacial and Eemian is shown in Fig. 51. The pressure of the humid gas sample and the flowrate of the dry gas sample drops down when transiting to the Eemian ice. As demonstrated in the section 3.4, the system response time at the flow regime 1.0 - 1.2 cc min^{-1} (as for the Holocene and the Last Glacial sections) and 0.8 cc min^{-1} (as for the Eemian section) does not differ significantly, spikes longer 3-7 cm can be distinguished. However, at the transition from higher to lower CH_4 concentration, the response time of the analytical line is doubled and the lower CH_4 concertation does not reach its true low value. It thus leaves a room for a suggestion that in fact the drops and minima in the Eemian CH_4 record remain unknown rather than how big were the CH_4 increases in the atmosphere.

An alternative possible explanation is in the gas signal transformation in the ice sheet. If the oldest age captured in the Eemian section is possible to identify (Simonsen et al., in prep.), the youngest Eemian age mark is not well defined. The age constraints used to date the RECAP CH_4 Eemian records are (1) the match to NGRIP CH_4 GI25 peak (Baumgartner et al. 2014) and (2) the sharp change in NGRIP $\delta^{18}O_{atm}$ (Capron et al. 2010) record observed approximately 120 ka BP. There is no data, however, to rule out a disturbance in the ice near the bedrock and thus a false $\delta^{18}O_{atm}$ trend as well as there is no consistency with the similar $\delta^{18}O_{atm}$ being younger (the 120 ka $\delta^{18}O_{atm}$ signal is unique in its absolute values). The temporal resolution of the Eemian CH_4 signal remain unclear at the current state of the RECAP ice core record investigation.

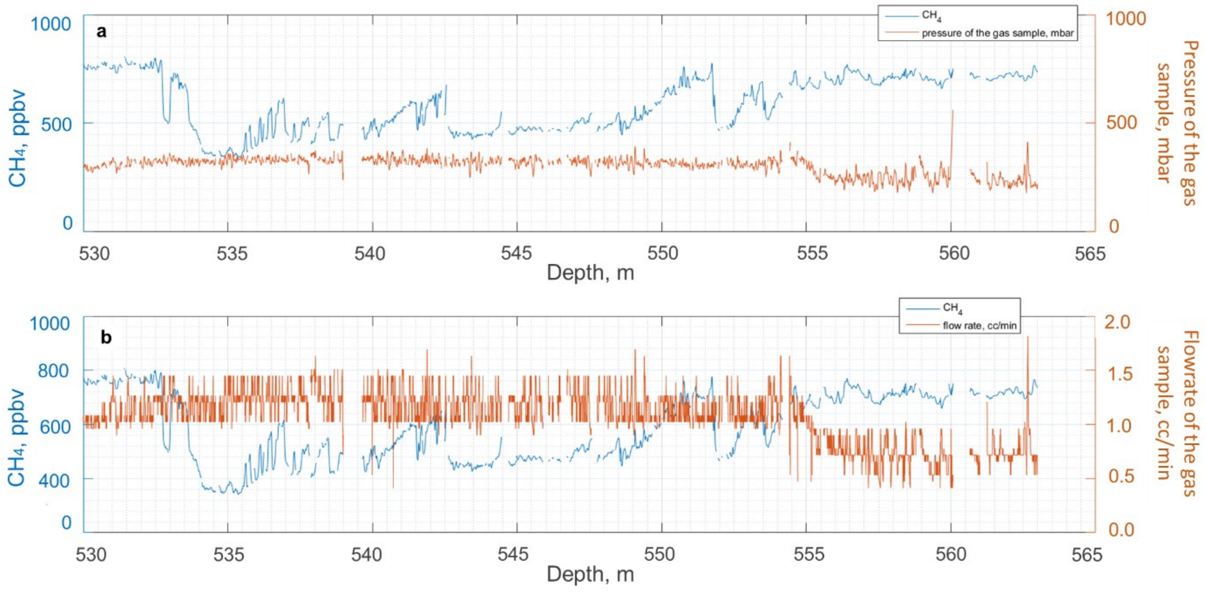

Figure 51: *a – RECAP CH_4 record (blue curve) and pressure of the humid gas sample after extraction (red curve), b – RECAP CH_4 record (blue curve) and flowrate of the dry gas sample after extraction (red curve).*

4.4. CH_4 interpolar difference during the last climatic cycle

4.4.1. DO events 19-21 – NH wetlands and ice-dammed lakes drainage

Here we present a paper draft on the part of the RECAP CH_4 record, which along with the other Greenland records rises an interesting question of the discrepancy in the relative temperature and CH_4 concentration rates of change at some of the stadial-interstadial transitions during the Last Glacial.

An additional biogenic methane source 83-78 ka BP from the Northern Hemisphere

Diana Vladimirova (1), Thomas Blunier (1), Emilie Capron (1,2), Rémi Dallmayr (3,6), Alexey Ekaykin (4,5), Vasileios Gkinis (1), Helle Astrid Kjær (1), Sune Olander Rasmussen (1), Paul Travis Vallelonga (1), Bo Møllesøe Vinther (1)

(1) Centre for Ice and Climate, Niels Bohr Institute, University of Copenhagen, Copenhagen, Denmark (diana.vladimirova@nbi.ku.dk (2) British Antarctic Survey, Cambridge, UK, (3) National Institute of Polar Research, Tokyo, Japan, (4) Climate and Environment Research Laboratory, Arctic and Antarctic Research Institute, St Petersburg, Russia, (5) Earth Sciences Institute, St Petersburg State University, St Petersburg, Russia, (6) now at Alfred Wegener Institute, Bremerhaven, Germany

Abstract

Atmospheric methane (CH_4) concentration closely changed accordingly to Greenland temperature variations during the transitions from Greenland stadials to interstadials (GS/GI) over the Last Glacial period. However, the relative amplitudes of the variations in temperature and CH_4 concentration diverge across the GS/GI transitions. E.g. large differences occurred for the transitions to interstadials 19-21: CH_4 concentration rate of change was 5-8 ppbv/˚C during the transitions 19.2 and 20 in contrast to 16.5 ppbv/˚C during the transition 21.1.

Here we present a part of the recent high-resolution continuous flow analysis CH_4 record of the Renland Ice Cap (RECAP) ice core combined with published Greenland and Antarctic data from 7 ice cores. In order to identify the reasons for the aforementioned difference in the relative CH_4/temperature amplitude we calculate the CH_4 interpolar difference (IPD) changes at a centennial resolution across the time interval 87-67 ka BP. We find that CH_4 IPD values exceeded the previously estimated average interstadial IPD (Dällenbach et al. 2000, Baumgartner et al. 2012) during the GI 21.1 pointing to an enhanced CH_4 production from the Northern Hemisphere. We propose that the Northern Hemisphere wetlands served as an additional biogenic CH_4 source during part of the GI-21.1, while this was not the case for GI-20 and GI-19.2.

Key words

Ice cores, methane, Last Glacial, DO events, Greenland stadials/interstadials, Greenland, Antarctica, methane source, RECAP, CFA, IPD

Introduction

Methane is one of the most important greenhouse gases. Its warming potential is approximately 25 times higher than for equivalent carbon dioxide (CO_2) volume. The residence time of CH_4 in the atmosphere is 9.1±0.9 years (Prather et al. 2012), which makes this greenhouse gas a unique indicator of the rapid climate change. The main source of the atmospheric methane during glacials is considered to be tropical wetlands (Chappellaz et al. 1993, Brook et al. 1996b). Further, decomposing permafrost, gas hydrates, emissions from tundra and biomass burning also contribute to CH_4 emissions (Sowers 2006, Sperlich et al. 2015, Serov et al. 2017).

Ice cores represent a unique archive of the past atmosphere trapped in bubbles in the ice (Stauffer et al. 1985). The gas composition registered in the ice differs from the original atmospheric one due to the firn gas diffusion through the open gas pores and the dynamics of the pores enclosure leading to the gas signal smoothing (e.g. see (Buizert et al. 2012)). The smoothing depends mainly on the accumulation rate and on the surface air temperature at the ice core retrieval site (Spahni et al. 2003, Joos and Spahni 2008, Köhler et al. 2011, Ahn, Brook Edward and Buizert 2013).

The series of Dansgaard-Oeschger events occurring during the last glacial period is characterized in Greenland ice core water isotopic ($\delta^{18}O$) records (a qualitative proxy for local temperature) by the succession of cold Greenland Stadials (GS) and relatively mild Greenland Interstadials (GI) (Rasmussen et al. 2014). Atmospheric methane (CH_4) concentration closely followed Greenland temperature variations during these dramatic climatic shifts (Chappellaz et al. 1993, Kindler et al. 2014, Baumgartner et al. 2014).

The observed rate of CH_4 concertation change relative to the temperature fluctuations varied between the stadial/interstadial transitions from 5 to 18 ppbv $^{\circ}C^{-1}$ in the Northern hemisphere (Baumgartner et al. 2014, Kindler et al. 2014). E.g. large differences occur for the transitions to interstadials 19-21. The CH_4 rate of change 5-8 ppbv/˚C during the transitions 19 and 20 contrasted to 16.5 ppbv/˚C during the transition 21.1. The data is taken from NGRIP ice core: CH_4 record – (Baumgartner et al. 2014), temperature reconstruction – (Kindler et al. 2014). Such a high rate of the CH_4 increase (16.5 ppbv/˚C) is comparable to the one at the last glacial termination (11.7 ka BP) and exceeds the rate at the other stadial-interstadial transitions by a factor of two. The greenhouse gas concentration increase and the temperature rise are not linked directly but through a complex influence of the air and sea surface temperature on the methane sinks and sources (Dällenbach et al. 2000, Flückiger et al. 2004). The complexity manifests itself e.g. in the lags of different duration (0-100 yr) between the initiation of the temperature rise and the CH4 concentration increase during the stadial-interstadial transitions. It is hypothesized that for the longer lag interstadials the CH4 concentration is controlled by the northward source shift (Baumgartner et al. 2012).

Changes in the CH4 atmospheric concentration could also be related to changes in the sinks. The dominant sink of atmospheric CH4 is the OH- radical. It oxidizes and decomposes methane. The process occur predominantly in the troposphere and stratosphere. Production of the OH- radical in the atmosphere is linked to the absolute humidity and the concentration of the nonvolatile organic compounds. Both parameters depend on the sea surface and surface air temperature change (Levine et al. 2012). For sinking a full amount of the emitted CH4, a 1˚C warming of the sea surface temperature would be required. Such warming is not confirmed by the paleoclimatic reconstructions (Tierney et al. 2015).

Yet, the reason for a difference in CH_4 concentration and temperature amplitude occurred between stadial-interstadial transitions 19-21 remains unclear.

We used seven published and one newly obtained dataset to construct the stack CH_4 records of the Northern and Southern Hemisphere 87-67 ka BP. It is generally assumed that the CH_4 records measured in Greenland ice cores represent the CH_4 content of the atmosphere in the Northern Hemisphere and Antarctic records – in the Southern Hemisphere. Hereinafter we follow this assumption keeping in mind that the compiled CH_4 records are representative of the hemispheric temperate and polar latitudes. Tropical regions are not included due to the presence of buffer atmospheric zone in the low latitudes. The aim of the study is to clarify the natural reasons of the diverging CH_4 concentration and temperature increase rates at the stadial-interstadial transitions 21 and 19-20.

Data and methods

Ice core CH_4 records

This work provides a multicore comparison of the past CH_4 atmospheric concentration in order to reduce the uncertainty on the absolute values of the CH_4 concentration. We used the published results from 4 Antarctica cores – EDML (Schilt et al. 2010), EDC3 (Loulergue et al. 2008), Byrd (Ahn and Brook 2008), Vostok (Delmotte et al. 2004) – and 3 Greenland cores: GISP2 (Brook et al. 2000), NGRIP (Baumgartner et al. 2014), NEEM (Chappellaz et al. 2013). The cores were selected based on their time span and the samples resolution. The characteristics of the records are listed in Table 1.

Table 1. Metadata of the ice core CH_4 records

Ice core	Total number of the data points	Depth interval, m	Resolution, data points 1 m^{-1}	Resolution, data points 1 ka^{-1}	Average resolution, yr	CH_4 data reference
NGRIP	363	2483-2722	1.5	<17	61	(Baumgartner et al. 2014)
GISP2	61	2545.17-2691.68	2.4	<3	357	(Brook et al. 2000)
NEEM CFA[1]	69296	1993.102-2107.021	608.3	3150	min 10	(Chappellaz et al. 2013)
RECAP CFA	3175	544.75-552.014	437.1	144	min 10	this study
EDC3	145	998.25-1235.9	1.6	<7	152	(Loulergue et al. 2008)
EDML	141	1805.078-2059.978	0.6	>7	142	(Schilt et al. 2010)
Byrd	59	2077.01-2138.01	≈ 1	<3	339	(Ahn and Brook 2008)
Vostok	16	962.4-1251.5	0.06	<1	1250	(Delmotte et al. 2004)

New data – RECAP

In this work we for the first time present a new high-resolution methane record (Fig. 1a) obtained in the frame of the REnland ice CAP (RECAP) project – an ice core drilling project carried out in 2015. It was targeted to retrieve an ice core from a separated ice cap in Eastern Greenland. A 584 m ice core drilled over one summer field season avoids the brittle ice zone. The surrounding topography suggests that the ice cap likely did not change its elevation in the past significantly. These two circumstances make the site advantageous for the high-resolution past atmospheric greenhouse gas content study.

The CH_4 record is entirely consistent with the previously obtained Greenland records (Baumgartner et al. 2014, Chappellaz et al. 2013). Its change relative to the temperature

---

[1] CFA – continuous flow analysis. See ”CFA measurements and calibration” in Methods for the details.

amplitude at the stadial-interstadial transitions 19-21 (Fig. 1) is in agreement with the previous reconstructions for Greenland (Baumgartner et al. 2014, Kindler et al. 2014).

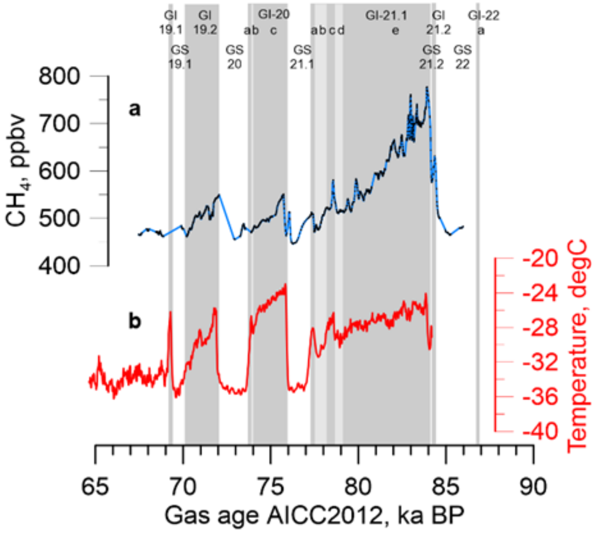

Fig.1. RECAP ice core data: a – continuous CH4 record, b – surface temperature reconstructed based on δ^{18}Oice and δ^{15}N data (Buizert pers. communication, 2018). Greenland stadials and interstadials (Rasmussen et al. 2014) translated to AICC2012 timescale are shown as the gray background shading and indexed on the top of the figure.

<u>CFA measurements and calibration</u>

The RECAP CH4 record was obtained using a continuous flow analysis (CFA) technique (Schüpbach et al. 2009) during the melting campaign in 2015-2016 at the Centre for Ice and Climate, Copenhagen, Denmark at the setup similar to (Stowasser et al. 2012). The average melting rate was about 3.5 cm min-1. The depth scale was assigned based on the Encoder string logger. The set-up was calibrated two times a day using the segmented stream of the secondary NOAA gas standards in the MiliQ water mimicking the segmented gas stream of the sample. The degassing was conducted in two stages: a triangular debubbler and a transfer line degasser, after which the sample was dried passing through Nafion. The measurements were conducted using a cavity ring-down spectrometer Picarro G1101-i with the modified reduced volume cavity (Stowasser et al. 2014).

RECAP CFA CH4 data were calibrated with the absolute values of the discrete CH4 data measured at the Penn State University. A reference to discrete measurements was necessary due to the unresolved gas loss (dissolution) at the CFA system.

Since (a) the gas trapping happens on the same depth at different core locations and (b) the gravitational settling depends is linear to the depth, it has a negligible effect on the resulting CH_4 interpolar difference (< 0.1% (Baumgartner et al. 2012)).

Timescale assignment

In order to avoid any artifacts in the CH_4 interpolar difference related to the discrepancy in the gas timescales we synchronized all CH_4 records using a well-known procedure of the gas records (Blunier et al. 1998, Blunier and Brook 2001). The peaks are matched consequently and iteratively reaching the highest possible correlation between the records. We used the AICC2012 gas timescale distributed for NGRIP, Vostok, EDC, EDML (Members et al. 2013) and matched Byrd, NEEM and RECAP records to these records. Hereinafter all CH_4 and interpolar difference data is shown on AICC2012 gas timescale (fig. 2).

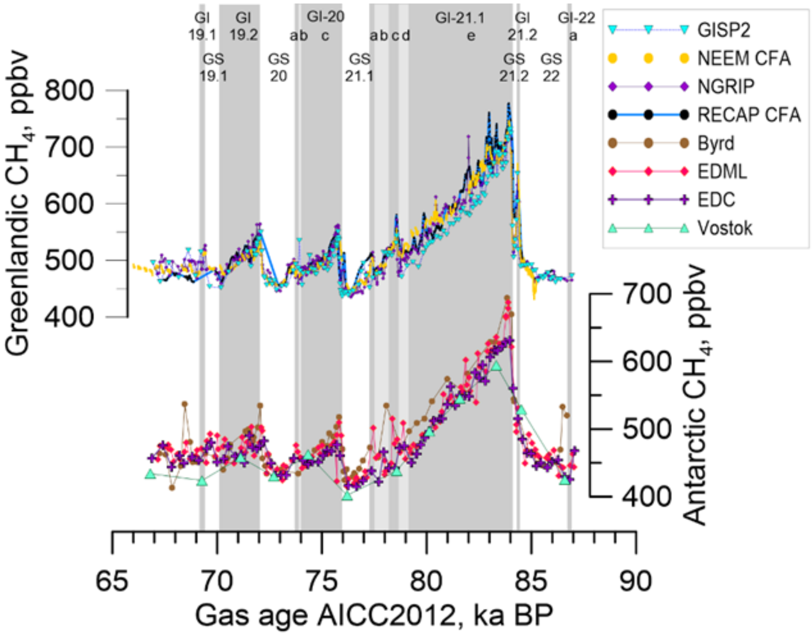

Fig. 2. Greenland and Antarctica methane ice core records on AICC2012 timescale. See Table 1 for the references to the individual CH_4 records.

Note that the gas timescale differs from the ice timescale due to the age difference of the ice at a certain depth and entrapped gas – the delta age. It varies depending on the firn pores close-off time, which is a function of the surface air temperature and the accumulation rate. A gradual gas trapping over diverse time intervals leads to the smoothing of the atmospheric gas signal in the ice cores of a different degree (e.g. (Schwander and Stauffer 1984)). See fig. S1 for the overview of the delta ages of the ice core gas records included in the study.

In addition to the gas smoothing issues the CH_4 interpolar difference values could be also affected by the interlaboratory offsets as discussed in the following sections.

rIPD calculation

The interpolar difference is a useful tool to assess the methane flux between the hemispheres. Along with the stable isotopic composition data and the box atmospheric CH_4 modelling, it is widely used in the paleoclimatic interpretation of the CH_4 sources evolution and location of the dominant source (see e.g. (Baumgartner et al. 2012, Mitchell et al. 2013)).

It is common to use the relative interpolar difference:

$$rIPD = \frac{IPD}{\left[CH_4^{global}\right]} = \frac{[CH_4^{NH}] - [CH_4^{SH}]}{\frac{1}{2}\left([CH_4^{NH}] + [CH_4^{SH}]\right)}$$

The average hemispheric CH4 concentrations (CH_4^{NH} and CH_4^{SH}) were obtained as following: individual CH4 ice core records were resampled in common 100 yr increments (e.g. 1 data point for the time steps 67.0, 67.1, 67.2, … 87.0 kyr BP); the hemispheric CH4 concentration was calculated as the median value of four data points from individual ice cores at every 100 yr time step. The median value was chosen in order to omit possible shifts due to the initially low sample resolution (see e.g. Vostok record on Fig. 2) or the interlaboratory offsets of the absolute values (see e.g. GISP2 record on Fig. 2).

The uncertainties on the hemispheric CH_4 records were estimated as the standard error mean of four data points' individual analytical uncertainties at every time step. The error on the rIPD is propagated given the resulting uncertainty of the median NH and SH values (see section S2).

Results

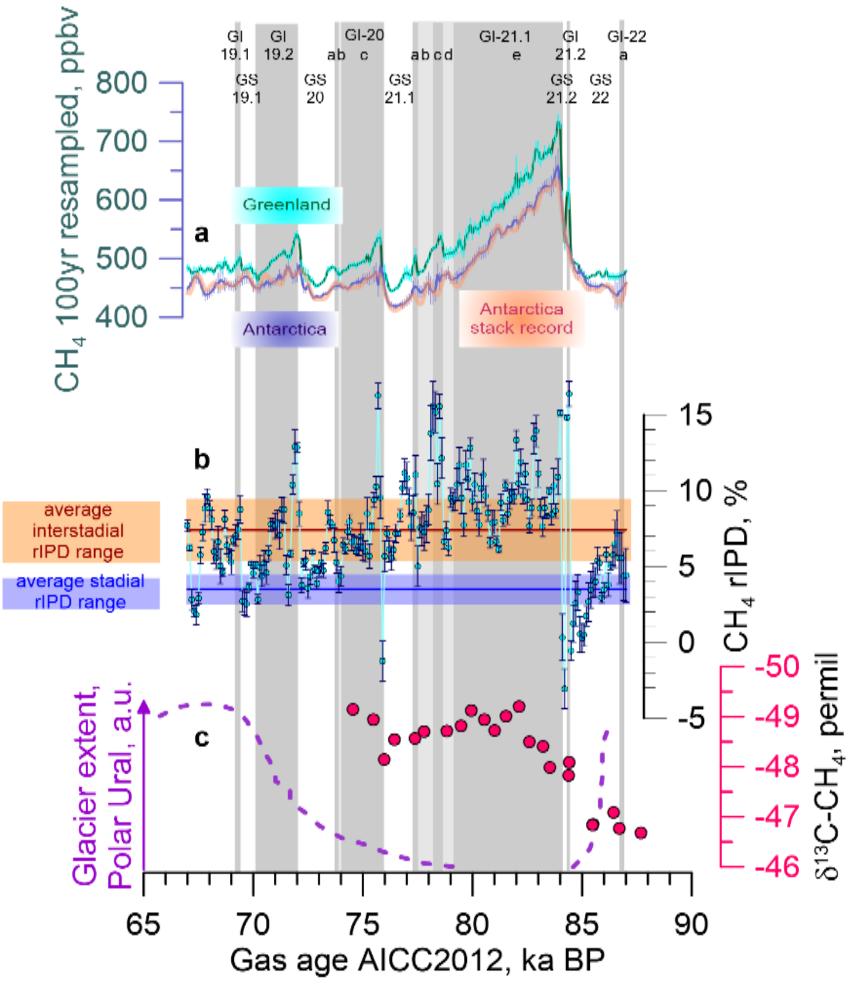

Fig. 3. a – Nothern and Southern Hemisphere CH4 concentration based on the ice core data (this study) and modelling results (Antarctica stack record – (Köhler et al. 2017)).
b – the relalitve interpolar difference of CH4 with 2σ uncertainty bars plotted on top of the average stadial (blue line) and interstadial (brown line) rIPD and its uncertainties span (blue and orange shaded areas correspondingly) (Dällenbach et al. 2000, Baumgartner et al. 2012).
c – carbon isotopic composition (δ^{13}C-CH4) of NGRIP and NEEM gas records (pink dots, [Sperlich, 2013]) and an example of the glaciation extent (dashed purple curve, (Svendsen et al. 2014)).

The calculated median Northern and Southern hemispheric CH4 variability is shown in Fig. 3a. A different set of Antarctic gas records was stacked earlier by (Köhler et al. 2017), the gaps between the data points were filled in with the spline-smoothing algorithm of an individually prescribed cut-off periods (Fig. 3a, orange curve). Our analysis fits well with the analysis obtained by (Köhler et al. 2017) based on the independent Antarctic ice core records; the discrepancy is in the span of median Southern hemispheric record uncertainty.

On average Antarctica records demonstrate less stadial-interstadial amplitude than Greenland's, which is likely related to the firn gas smoothing. The short-term precursor event – Greenland interstadial 21.2 (≈ 85 ka BP) is possibly masked in the Antarctic records due to the stronger firn smoothing and longer time of the gas pores closure (see fig. S1). Even though the precursor event was possibly present in the Southern Hemisphere atmosphere, it might not be trapped in the firn gas because the time of an air exchange in the open pores was longer than the vent duration. The presence of the precursor event in the Greenland record and its absence in Antarctic's yields negative outlier and spike in the rIPD, which we ignore in the current analysis. An artificial spike around 74 ka BP is also excluded from the analysis for a similar reason. The precursor events were masked applying the gas age distribution function to an individual gas record in order to test its effect on the CH_4 rIPD (see Section I.3 in the Discussion).
The resulting rIPD is plotted versus the average stadial and interstadial values (Dällenbach et al. 2000, Baumgartner et al. 2012) of the CH_4 rIPD (Fig. 3b), error bars represent ±2σ. GS-22 and GI/GS-20-19 agrees well with the range of the previously obtained values, while the GI-21.1 r IPD values (83-78 ka BP) demonstrate an excess of the average GI CH_4 rIPD.
The bigger delta age and the wider age distribution in Antarctica cores may potentially lead to the overestimated rIPD and a bias toward the Northern Hemisphere. The reason is the enhanced gas smoothing and smaller amplitude of the signal in Antarctica cores. Moreover, there is a possibility of the in-situ gas production and high frequency gas record artefacts as was discussed recently (see e.g. (Fourteau et al. 2017)). The influence of gas trapping nature on the resulting CH_4 rIPD is considered in the following section.

Discussion

I. Factors that may alter CH_4 record in ice core

1. Melt layers

Melt layers potentially lead to spikes in the CH_4 record (Pearman et al. 1986, Rhodes et al. 2016). Melt layers are only observed in the warm periods, there is no signs of such analytical artifacts during the Last Glacial (Chappellaz et al. 2013). All the possible spikes during the warm climatic stages of an unknown origin resolved by the CFA method were neglected when calculating the median hemispheric CH_4 values with 100 yr increment. The possible ambiguities are taken into account in the uncertainty range.

2. Dusty layers

The CH_4 content of the bubbles trapped in the ice might be potentially compromised by the dust as was shown by [Lee et al., 2018] for the some sections of NGRIP and NEEM cores corresponding to 52-35 ka BP. The mechanism of the in-situ production remains unclear and not well quantified. The saturation happens while melting-refreezing a sample, the artifact depends on the lab procedure and not just on the dust level. The CH_4 stadial concentration may potentially be entirely elevated due to the higher dust content (Buizert C., 2018, pers. communication).

Previous studies cover only air trapped in the clathrates (Lee et al., POLAR 2018; Lee J., 2018, pers. communication). The RECAP samples were essentially the bubbly ice. The CH_4 in-situ production in the dusty layers was not studied earlier for the bubbly ice case.

The melting-refreezing CH_4 gas extraction technique is what possibly yields the in-situ CH_4 production (Lee et al., POLAR 2018). No evidence for the CFA (i.e. solely melting) technique influence on the in-situ CH_4 production was found. The RECAP CFA data (i.e. melted only sample) was calibrated to the discrete CH_4 measurements (melted-refrozen), thus all the potentially shifted values would pop up. This is not the case (as seen of Fig. S3.1), the RECAP methane values are not elevated relative to the reference NGRIP gas record. Alike, Greenland discrete CH_4 values do not seem to exceed CFA CH_4 values over the studied period (Fig. S3.1).

All Greenland dust records are similar and ReCAP is not an exception over the Last Glacial period (Simonsen et al., in prep.). A comparison of Greenland CH_4 records and a single dust proxy (Ca^{2+}) record is credible – see Fig. S3.1. Greenland CH_4 values do not seem to exceed each other along the intervals of the high dust concentration. For the uniformity of the data representation, the dust depth scale was translated to the gas age similar to the CH_4 depth scale. CH_4 rIPD calculated on the basis of the three Greenland and three Antarctic records and NGRIP Ca^{2+} data over the studied period do not obviously correlate (see fig. S3.2) as it was fond for NGRIP-WAIS IPD 52-37 ka BP by (Lee et al., POLAR 2018).

The interval of an elevated CH_4 rIPD values (83-78 ka BP) corresponds to long interstadial with low dust content, thus, a chance of a consistently elevated CH_4 content in Greenland record due to the high dust content is extremely low.

Note that the ReCAP record overall the studied period exhibits only one CH_4 spike obviously coinciding with the dust concentration spike (marked with arrow on Fig. S3.3). The CH_4 content was high in the record over the GI-19.2. We assume it was a contamination – this part of the core was badly fractured, which may affect the CFA measurement. This piece of data interval was excluded from the ReCAP CH_4 record.

Overall, the effect of the dusty layers causing the in-situ CH_4 production is minor. Thus, the dust in the analyzed cores does not affect the rIPD record over the considered time 67-87 ka BP.

3. Smoothing of the atmospheric signal in firn

Ice core gas records differ from the initial atmospheric one due to the firn gas smoothing. A diffusive gas transport in firn dominates the signal smoothing and regulates the width of the gas age distribution at any depth in the firn (Blunier and Schwander 2000). Moreover, the pores close-off process, i.e. the gas bubbles sealing, does not happen immediately but takes place gradually over a few meters of the so-called lock-in zone. The depth of the lock-in zone and the ice-gas age difference (delta age – Δage) depend on the surface conditions – mean annual temperature, snow accumulation rate and surface snow density. Colder sites are generally characterized by wider gas age distribution (GAD) and bigger Δage (see compilation at e.g. (Bréant et al. 2017)).

The delta age of Antarctic records used in the current study is on average bigger than the one of Greenlandic (see Fig. S1). It means a longer time of the pores closure and wider gas age distribution, which more intensively smooths out the initial atmospheric CH_4 signal and thus potentially biases the interpolar difference toward the Northern Hemisphere. We tested out how would the CH_4 records evolve if they experienced similarly intensive firn gas smoothing conditions. We applied a log-normal filter to the CH_4 series and then recalculated rIPD record with the smoothed methane data. The filter is essentially a fit to a GAD function. We used the one provided by (Köhler et al. 2011):

$y = \frac{1}{x\cdot\sigma\cdot\sqrt{2\pi}} \cdot e^{-0.5\left(\frac{\ln(x)-\mu}{\sigma}\right)^2}$, and the parametrization by (Fourteau et al. 2017) for the Vostok vicinity at roughly 60 ka BP (μ = 4.337,σ = 1.561), and for the Dome C area at the time of the Last Glacial Maximum (μ = 5.88 ,σ = 1). The filtering was applied to data series as in a standard convolution procedure:

$$CH_{4\,filtered} = \frac{\sum_{i=1}^{n}(CH_{4\,n} \cdot y(x))}{\sum_{x=0.1}^{m} y\,(x)}$$

At every time step (1 yr) the filter was centered at x_{min}, the CH_4 series were run through the filter in the reversed order, i.e. from the older to the younger data points, mimicking the firn gas age distribution at every time step.

Results are presented in Fig. S4. The initial CH_4 rIPD series (Fig. S4a) is shown in comparison with the rIPD series calculated based on the smoothed CH_4 records. Fig. S4d depicts rIPD obtained using the gas age distribution parameters for the Vostok vicinity at roughly 60 ka BP, while Fig. S4c shows the one using the parametrization of the Dome C area at the time of the Last Glacial Maximum. Finally, the long-term variability of the initial rIPD series was clarified using Gaussian filter to keep the frequencies > 0.23 ka^{-1} (i.e. variability period 4.4 kyr and longer) (Fig. S4d). The results of three tests as well as the initial CH_4 rIPD series demonstrate sustainably high values 78-83 ka BP (timing of warm interstadial 21.1). The CH_4 rIPD at that period exceeded the average value calculated for the interstadial conditions by (Dällenbach et al. 2000, Baumgartner et al. 2012).

In summary, even a very coarse CH_4 records smoothing of unlikely big extent, i.e. implementing much colder surface conditions or longer pores closure time, did not diminish the high CH_4 rIPD 83-78 ka BP. Thus, there is a very low chance that the identified elevated CH_4 rIPD values are of the artificial origin rather than they have natural reasons. It points to the enhanced CH_4 production in the Northern Hemisphere 83-78 ka BP.

II. An overview of paleoclimatic events 87-67 ka PB

1. Methane stable isotopic composition

The carbon isotopic composition of methane ($\delta^{13}C$-CH_4) is used as an indicator of the source footprint. The average planetary carbon 13 isotopic composition of the tropospheric CH_4 ($\delta^{13}C$-CH_4) is -47‰. Generally, lighter carbon isotopic signature suggests either the wetland source (both boreal and tropical) or decomposing gas hydrates source. Heavier carbon 13 isotopic composition points out on the CH_4 production due to the biomass burning (see (Fischer et al. 2008)).

[Sperlich, 2013] measured $\delta^{13}C$-CH_4 in NEEM and NGRIP ice cores samples covering the studied period (see Fig. 3c). The Greenland ice core records demonstrate similar to the average planetary $\delta^{13}C$-CH_4 values over the GS-22 (prior to 85 ka BP in the presented data). Later the $\delta^{13}C$-CH_4 becomes depleted by 2-2.5‰ and stays relatively light since 82 ka BP until 74 ka BP (the data limit). The depletion may be explained by:

(a) declining oxidization rate of methane in the atmosphere and its correspondingly longer residence time, which would bring the $\delta^{13}C$-CH_4 of the atmospheric gas closer to the average planetary source average of -53‰;

(b) a contribution of a source with some isotopically lighter signature – a biogenic source (both boreal and tropical wetlands, living plants or ruminants), the $\delta^{13}C\text{-}CH_4$ of its emissions is -60 ± 5‰ on average (Sapart et al. 2012);
(c) stored biogenic gas – it has similar to the wetlands isotopic signature and could also potentially contribute to the emissions (Sapart, pers. com., 2018);
(d) alternatively, the observed range of $\delta^{13}C\text{-}CH_4$ was hypothesized as the isotopically light hydrates emissions compensated by a heavy isotope enriched pyrogenic methane emissions. However, for the precursor event GS/GI-21.2 (Sperlich et al. 2015) found no evidence of the biomass burning, thus the scenario of the compensating gas hydrates emissions is unsubstantiated.
In short, the depletion of the methane isotopic composition prior to 82 ka BP supports a suggestion of the biogenic source becoming prevailing. Sustainably light carbon 13 isotopic signature over 82-74 ka BP points out on the unchanged balance of the sources' contribution. At the same time (83-78 ka BP) the CH_4 relative interpolar difference stays high indicating an enhanced methane production in the Northern Hemisphere. To clarify the exact boreal biogenic source of methane 83-78 ka BP we look for the further information in the paleogeographic reconstructions.

2. <u>Paleogeographic reconstructions</u>

2.1 Northern Eurasia

Data- and modelling-based reconstructions [Krinner et al., 2004; Astakhov and Nazarov, 2010] suggest a presence of an ice sheet in the northern part of Western Siberian Plain. The ice-sheet dammed Siberian rivers, discharged earlier into the Arctic Ocean, formed ice-dammed lakes. The ice sheet-lake system could be in an equilibrium when a modest warming occurs and the lakes provide a negative feedback cooling down the climate and providing precipitations for the ice sheet positive mass balance. A major warming caused by the insolation increase 90-85 ka BP led to the ice sheet retrieval and the following ice-dammed lakes drainage. We hypothesize, that vast ice and water-free areas were filled shortly with the wetland vegetation. It finds a confirmation in the peat sediments aged 80 ± 11 ka BP in the lower reaches of Ob river [Lakhutin, 2008].
The explanation of the peatland expansion and carbon accumulation could possibly be in response to high summer insolation and strong summer-winter climate seasonality like it was shown for the early Holocene (Greenlandian stage) by (Yu et al. 2010). The general warming and the continental ice sheet retreat were possibly linked to a decreased sea ice extent. Recently

(Parmentier et al. 2015) showed that the reduced sea ice extent in the Northern Hemisphere prompted an increased methane emissions from the wetlands. The underlying reason seems to be caused by the seawater enhanced solar heat absorption inducing higher autumn temperatures.

As for the whole Northern Hemisphere glaciation, (Charbit et al. 2007) compared the numerical reconstructions of the Northern Hemisphere ice sheets extent. They showed a significant decrease in the ice volume and ice covered area in the Northern Hemisphere some 85-83 ka BP with a higher rate of degradation in Eurasia.

(Svendsen et al. 2014) made an OSL-based reconstruction of the glaciation extent in the Polar Ural region over the past 100 ka (see Fig. 3c). The study revealed a similar picture: ice-dammed lakes existed during MIS 5b (87-82 ka BP) and during the next cold stage MIS 4 owing the low summer temperature. Pollen data from the lake El'gygytgyn (Far East Russia) shows a sharp transition from trees and shrubs dominated vegetation to the herbs and spores dominated 75±5 ka BP as a response to the regional climatic conditions change (Lozhkin et al. 2007).

To our knowledge, any data suggesting a decomposition of the permafrost following the warming ≈ 85 ka BP is absent. However, considering the modern conditions as an analogue we hypothesize that if a temperature regime change occurred then some biogenic gas stored in the permafrost could be emitted serving an additional CH_4 source.

Concisely, a number of data- and modelling-based reconstructions suggest a decreasing ice volume 85-83 ka BP, drainage of the ice-dammed lakes and the following tundra and wetland formation of the vast free continental areas in the Northern Eurasia. The reduced ice sheet and neighboring wetland landscapes prevailed over the time of an identified above elevated CH_4 rIPD (83-78 ka BP).

2.2 Northern American continent

The climatic fluctuations over the Northern American continent are in agreement with the Northern Eurasian. During MIS 5a (82-71 ka) the subarctic climate is suggested for the Arctic Canada by the pollen flux data (de Vernal, Miller and Hillaire-Marcel 1991). The interglacial conditions occurred 85 ± 10 ka as indicated by the lacustrine sediments from Baffin Island, Arctic Canada. The area was covered with shrub tundra and the corresponding sector of the Laurentide Ice Sheet retreated at a time (Miller et al. 1999). To our knowledge no evidence of the ice-dammed lakes existence was found. However, tundra landscape generally serves as a biogenic CH_4 source.

2.3 Tropical wetland

MIS 5c (96-87 ka) and 5a (82-71 ka) are shown to be much drier then the glacials based on the speleothem data-model compilation for tropical South America (Baker and Fritz 2015). A dry lakebed core from Northern Chile does not exhibit any major wet period linked to a local summer insolation maximum around 93 ka and reveal a relatively wet period 76-61 ka. Cariaco basin sediment lightness indicates no big difference between the interstadials 19, 20 and 21 (Ann and C. 2014).

Southern African tropics pollen records reveal a continuing drought up until 90 ka and a semi-desert vegetation for the following 18 kyr with the increasing humid evergreen woodland reappearing 75-65 ka (Beuing et al., 2011). Madagascar record shows the development of a wooded grassland under a dry climate 83 ka. This was a warm phase of a local climate following the cold phase 94-88 kyr and preceding another cold phase 75-69 ka (Gasse and Van Campo 2001).

In contrast, Northern African region is characterized by the Saharan pluvial period 98-72 ka BP fingerprinted in the sediments of the Nile margin (Revel et al. 2010). The emissions from the Northern tropical wetland could potentially contribute to the enhanced CH_4 production of the Northern Hemisphere overall the pluvial period.

Compendiously, the tropical wetlands exposure and its corresponding methane emissions activity does not reveal any big difference between the time of elevated CH_4 rIPD 83-78 ka BP and the preceding or following periods. The only humid period was observed in the Northern African region; however, it began prior to the rIPD increase not supporting an idea of the prevailing tropical influence on the enhanced CH_4 production 83-78 ka BP.

III. A suggested scenario

Summing up considered paleoreconstructions and the data analysis, we hypothesize the following sequence of events.

Up until approximately 85 ka BP the ice-dammed lakes were present in the Northern Siberia (Krinner et al. 2004). Some 85 ka BP the summer insolation increase and the general onset of the climate warming forced the Barents-Kara ice sheet to retreat stronger than it could be compensated by the negative feedback (local climate cooling by the lakes).

As a result, the ice-dammed lakes drained (Krinner et al. 2004). We suppose that the ice-dammed lake drainage caused an outburst of the fresh water to the ocean and potentially weakened the thermocline circulation causing a short-term cold reversal GS-21.1 (84.9-84.7 ka

BP). The mechanism is similar to that for “8.2 ka event” reasons (Teller, Leverington, and Mann, 2002; Hillaire-Marcell et al. 2007; Hoffman et al. 2012). (Lachniet et al. 2004, Wiersma and Renssen 2006) pointed out on the teleconnection via the Atlantic thermohaline circulation change of the tropical and extratropical regions. A fresh water outburst might indirectly influence on the monsoon weakening, which in turn may be linked to the wetland contraction and a decrease in CH_4 concentration observed in Greenland ice cores (Thomas et al. 2007) of a duration 150 yr (Kobashi et al. 2007).

Wetlands began to form on the water-free continental areas shortly after the drainage ≈ 85 ka BP, which is confirmed by the peatland sediments data (Lakhutin et al. 2008; Astakhov and Nazarov 2010). A paleoatmospheric circulation modeling (Sánchez Goñi et al. 2008, Sánchez Goñi et al. 2013) revealed a northward shift of the westerlies and an increased humidity over the Western Siberia area favoring the wetlands formation. An additional Northern hemispheric CH_4, as shown by the interpolar difference ice cores-based record, came from the biogenic source actively emitting 83-78 ka BP.

Further general climate cooling and transition to a cold stage MIS-4 caused the glaciation advance (Svendsen et al. 2014), which possibly contracted the Northern hemispheric wetlands and its CH_4 emissions. It favored the CH_4 rIPD during the interstadials 19 and 20 return to an average interstadial level. Insignificant deviations of an average interstadial rIPD level support the hypothesis of the predominant tropical wetland CH_4 production over GI-19 and GI-20 as it was observed for the cooling climate conditions.

Upon completion, the Northern Siberian wetlands, formed because of the ice-dammed lakes drainage, served 83-78 ka BP as an additional CH_4 source to the main background CH_4 source, which is tropical wetlands.

Conclusions and outlook

We combined the newly obtained high-resolution CH_4 record from the RECAP ice core spanning the time 87-67 ka BP with the published 4 Antarctic and 3 Greenland CH_4 ice core records. We aimed to study the difference between the stadial-interstadial transition 21 and 19-20. The first transition is characterized by a considerably higher CH_4 amplitude compared to the other two (>200 ppbv versus 70-90 ppbv – for the Greenland records) while the temperature rise was of a similar amplitude over all three transitions.

We calculated the relative interpolar CH_4 difference and demonstrated that it exceeds the average interstadial values 83-78 ka BP (during a part of Greenland interstadial 21.1). The assessed earlier average stadial and interstadial values of the CH_4 rIPD suggest that the tropical wetlands were the main source of the CH_4 during the Last Glacial Period. However, the elevated rIPD during the period 83-78 ka BP points out on an additional source in the Northern Hemisphere being active at that time.

We discussed a possible influence of the gas signal smoothing in firn on the atmospheric CH_4 records. The applied wider firn gas age distribution filter does not diminish the identified rIPD excess 83-78 ka BP. The other possibility of deviating Greenland CH_4 ice core records from the initial atmospheric one, namely a probable in-situ production of CH_4 in dusty ice layers, is also disproved by comparing the ice core dust and gas records on the corresponding depth scale. However, we were unable to reconstruct the full amplitude of the rIPD and thus to apply it as input data to the box atmospheric CH_4 model in order to quantify the fluxes from the different sources. The methane isotopic composition measurements at the same time suggest a biogenic source of CH_4 throughout the period 83-78 ka BP.

We argue that 85 ka BP the drainage of the Northern Eurasian ice-dammed lakes occurred due to the Barents-Kara ice sheet retreat. It caused an outburst of the fresh waters into the ocean and a short-term cooling – Greenland stadial 21.2 as an analogue to “8.2 ka” cooling event clearly seen in Greenland CH_4 record. The tundra and peatlands formed shortly after on the vast ice- and water-free areas serving as an additional biogenic source of methane in the Northern Hemisphere 83-78 kyr BP. None of the enhanced monsoon activity for tropical wetlands leading to bigger CH_4 emissions were evidenced. The following ice sheet advance (later 78 ka BP) due to the summer insolation decrease and general climate system cooling covered the areas of the peatlands, the additional Northern hemispheric CH_4 source became contracted, the tropical wetlands became prevailing in the CH_4 emissions since 78 ka BP.

In an outlook, CH_4 concentration increase exceeding the corresponding Greenland temperature rise by a relative amplitude occurred repeatedly at the stadial/interstadial transitions over the last glacial (Baumgartner et al. 2014, Kindler et al. 2014). It remains unclear if the reason was the same for every episode. A more detailed study combining a high-resolution rIPD calculation, CH_4 isotopic composition measurements and box modelling of the CH_4 flux in the atmosphere (e.g. eight box model by (Mitchell et al. 2013)) is required throughout the Last Glacial. The ultra-high resolution CFA CH_4 records of the ice cores drilled lately in Greenland (RECAP) and Antarctica (WAIS Divide) bring the solution closer. A possible influence of a Toba eruption 74 ka BP (Svensson et al. 2013) to the climatic shifts could be also considered in a future work.

Acknowledgments

We are grateful to the CIC radar team for selecting a great drilling spot at the Renland ice cap in 2015, to the CIC drillers for obtaining a core of an excellent quality during the summer season 2015, RECAP (https://recap.nbi.ku.dk/about/). The research leading to these results has received funding from the European Research Council under the European Community's Seventh Framework Programme (FP7/2007-2013) / ERC grant agreement 610055 as part of the ice2ice project (https://ice2ice.w.uib.no/). We thank the international collaborators for the help in the ice core processing and the CFA measurement campaign conduction in 2015-2016.

We are thankful to Todd Sowers for provided discrete CH_4 data of the RECAP ice core, which supported the calibration of the CFA gas data.

We deeply appreciate Christo Buizert's contribution to the fruitful discussion on the factors possible influencing the CH_4 signal shifts and his effort to the temperature reconstruction.

D.V. thanks Russian Foundation for the Basic Research for providing a funding via grant 18-35-00582 мол_а "Rapid climatic variations in the modern warm period and during the abrupt warming at the last ice age based on the high-resolution ice core records".

E.C. received funding from the European Union's Seventh Framework Programme for research and innovation under the Marie Skłodowska-Curie grant agreement no 600207.

Supplementary

S1. Delta age span of the individual CH_4 ice core records. The delta age range covers only the studied period 87-67 ka BP. The delta age values were calculated for every CH_4 data point as the ice-gas age difference on an initial timescale of an ice core. See the references for the ice core records in Table 1.

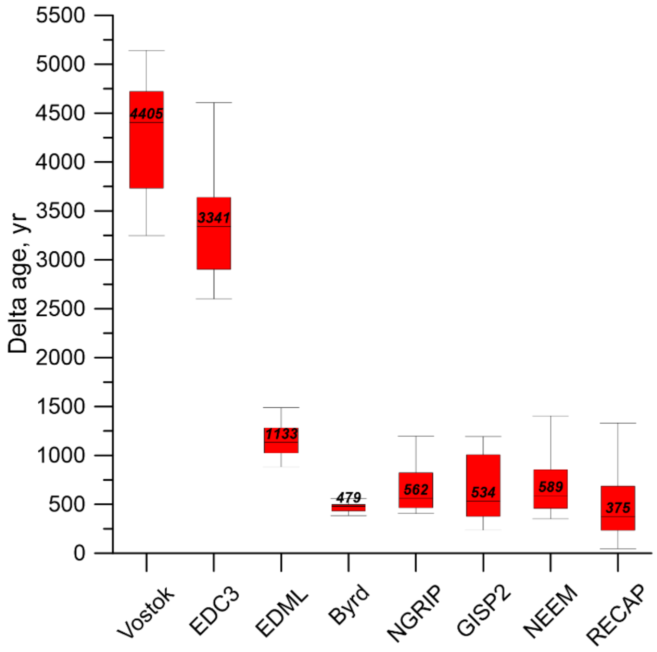

Fig. S1. Ice-gas age difference of the individual ice core records over the studied period 87-67 ka BP. The median value is indicated in the middle in italics, the red bars mark the lower and upper quartiles, and the whiskers identify a whole range of the delta age values.

S2. The error on CH_4 rIPD was propagated using the initial uncertainty of the hemispheric CH_4 records. The interpolar difference (IPD) is calculated as a difference between the Northern (NH) and the Southern (SH) Hemispheric average methane concentration ($[CH_4]$):

$$IPD = [CH_4^{NH}] - [CH_4^{SH}]$$

Relative **interpolar difference (rIPD)** is IPD divided by the average planetary CH_4 content:

$$rIPD = \frac{IPD}{\overline{[CH_4^{global}]}} = \frac{[CH_4^{NH}] - [CH_4^{SH}]}{\frac{1}{2}\left([CH_4^{NH}] + [CH_4^{SH}]\right)}$$

If $[CH_4^{NH}] = A$

$[CH_4^{SH}] = B$

$rIPD = f$

$IPD = C$

$([CH_4^{NH}] + [CH_4^{SH}]) = D$

$$rIPD = f = 2\frac{C}{D}$$

The error on the relative interpolar difference is propagated using the generalization of the error propagation on the variable and a constant multiplication (a), a sum of variables (b) and the product of variables (c):

a) $f = kX,$

$\sigma_f^2 = k^2\sigma_X^2\ , \ \ \sigma_f = |k|\sigma_X$

b) $f = kX + mY$

$\sigma_f^2 = k^2\sigma_X^2 + m^2\sigma_Y^2 + 2km\sigma_{XY}$

c) $f = \frac{X}{Y}$

$\sigma_f^2 \approx f^2\left[\left(\frac{\sigma_x}{X}\right)^2 + \left(\frac{\sigma_y}{Y}\right)^2 - 2\frac{\sigma_{XY}}{XY}\right]$ – dispersion

$\sigma_f \approx |f|\sqrt{\left(\frac{\sigma_x}{X}\right)^2 + \left(\frac{\sigma_y}{Y}\right)^2 - 2\frac{\sigma_{XY}}{XY}}$ – standard deviation, where σ_{XY} is covariation of X and Y:

$\sigma_{XY} = \ r_{XY}\ \sigma_X\ \sigma_Y$, where r_{XY} – correlation coefficient of X и Y.

$$\sigma^2(f) = 4\sigma^2\left(\frac{C}{D}\right) = 4\frac{C^2}{D^2}\left[\left(\frac{\sigma_C}{C}\right)^2 + \left(\frac{\sigma_D}{D}\right)^2 - 2\frac{\sigma_{CD}}{CD}\right]$$

$$\sigma_C^2 = \sigma_{(A-B)}^2 = \sigma_A^2 + \sigma_B^2 - 2\sigma_{AB}$$

$$\sigma_D^2 = \sigma_{(A+B)}^2 = \sigma_A^2 + \sigma_B^2 + 2\sigma_{AB}$$

$$CD = (A - B)(A + B) = A^2 - B^2$$

$$\sigma_f = 2\frac{A - B}{A + B}\sqrt{\left[\frac{\sigma_A^2 + \sigma_B^2 - 2\sigma_{AB}}{(A - B)^2} + \frac{\sigma_A^2 + \sigma_B^2 + 2\sigma_{AB}}{(A + B)^2} - 2\frac{\sigma_{CD}}{A^2 - B^2}\right]}$$

$$\sigma_{CD} = r(C, D)\ \sigma_C\ \sigma_D = r[(A - B), (A + B)]\ \sigma_{(A-B)}\ \sigma_{(A+B)}$$
$$= r\left[IPD, \left[\overline{CH_4^{global}}\right]\right]\ \sigma_{IPD}\sigma_{\left[\overline{CH_4^{global}}\right]}$$

The eventual uncertainty on the rIPD record is expressed as:

$$\sigma_{rIPD} = 2\frac{IPD}{\left[\overline{CH_4^{global}}\right]}\cdot$$

$$\cdot\sqrt{\left[\frac{\sigma^2_{[CH_4^{NH}]}+\sigma^2_{[CH_4^{SH}]}-2\sigma_{[CH_4^{NH}][CH_4^{SH}]}}{(IPD)^2}+\frac{\sigma^2_{[CH_4^{NH}]}+\sigma^2_{[CH_4^{SH}]}+2\sigma_{[CH_4^{NH}][CH_4^{SH}]}}{\left[\overline{CH_4^{global}}\right]^2}-\right.}$$

$$\overline{\left.-2\frac{r\left[IPD,\left[\overline{CH_4^{global}}\right]\right]\sigma_{IPD}\sigma_{\left[\overline{CH_4^{global}}\right]}}{[CH_4^{NH}]^2-[CH_4^{SH}]^2}\right]}$$

S3. This section is related to the discussion of the dusty layers as a factor that may alter CH_4 record in ice cores. Here we compare dust concentration or dust proxy (Ca^{2+}) ice core records with the CH_4 and rIPD records on the common depth scale or gas age scale for the convenience of the data representation. In summary, there is a very little or no influence of the dust on the in-situ CH_4 production over the studied period 67-87 ka BP in Greenland cores. Antarctic ice cores were not considered as they have sufficiently lower dust content.

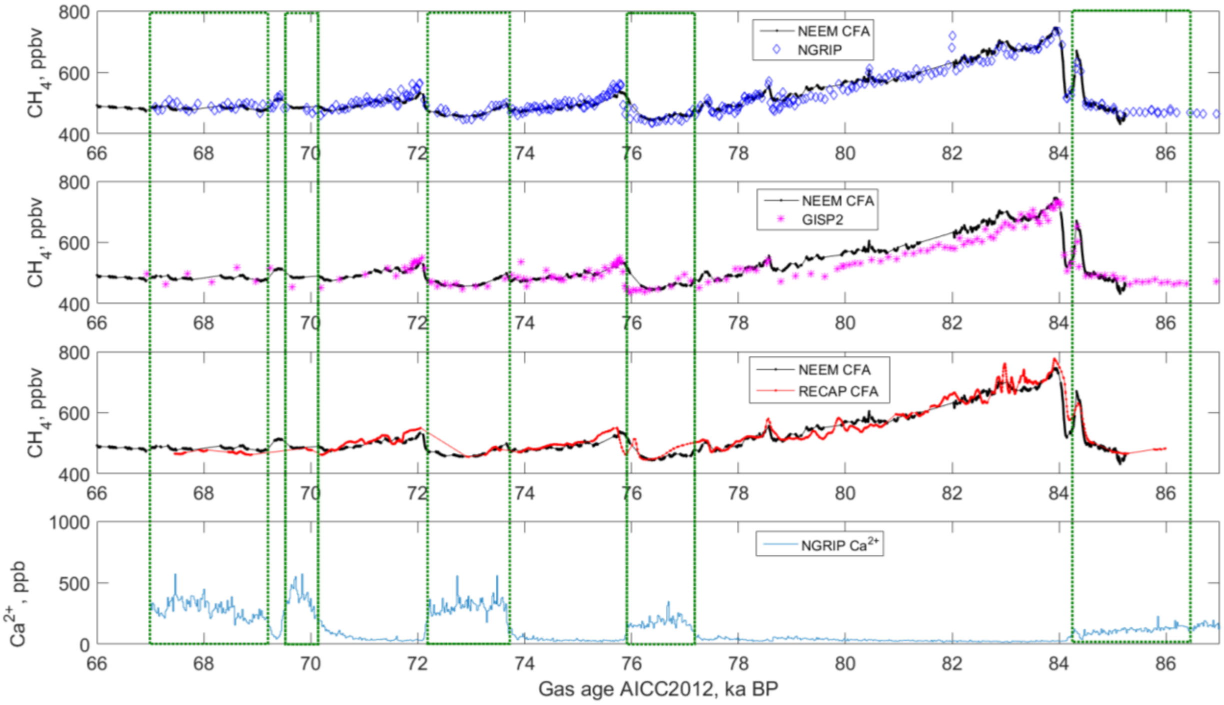

Fig. S3.1. Greenland CH_4 records and NGRIP dust proxy record on the gas age timescale.

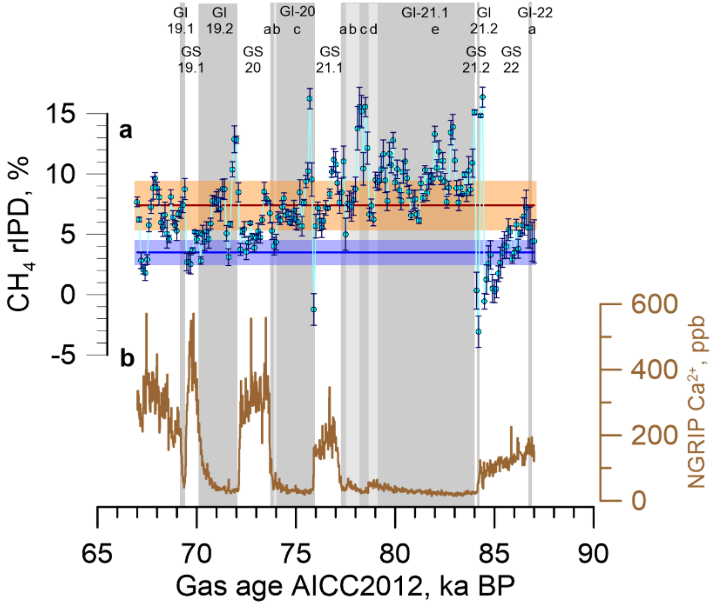

Fig. S3.2. CH4 IPD record and NGRIP dust proxy on the gas age timescale.

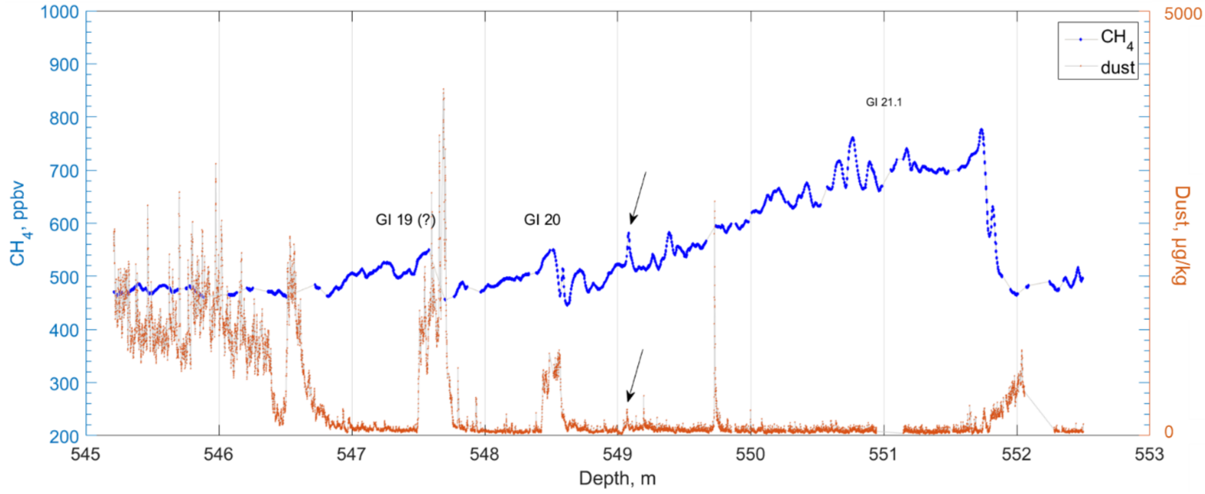

Fig. S3.3. RECAP CH4 and dust concentration on the depth scale.

S4. This section is related to Discussion I.3. Here we present the results of the smoothed gas records tests. We smoothed the ice core CH4 records using a wider gas age distribution than initial and demonstrated that even a more intensive gas signal diffusion did not smooth out the elevated rIPD values 83-78 ka BP.

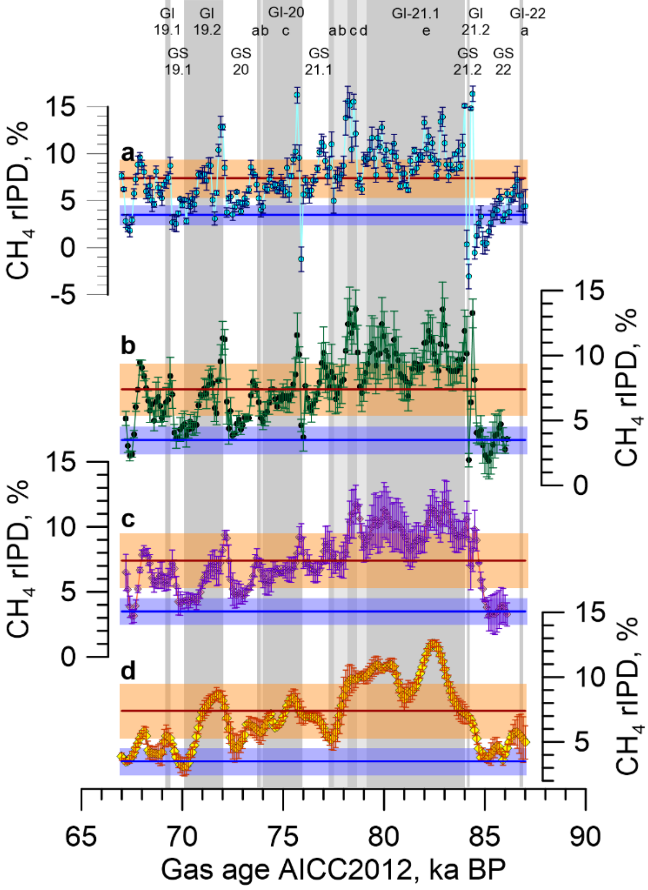

Fig. S4. CH$_4$ rIPD: a – calculated using original CH$_4$ series; b – calculated using GAD-filtered CH$_4$ series with DO 17 Vostok parametrization; c – calculated using GAD-filtered CH$_4$ series with LGM Dome C parametrization; d – calculated using Gaussian filtered series to keep the low frequencies > 0.23 ka^{-1}.

Chapter 5. Diurnal variability of CH_4 in northeaster Greenland

5.1. Introduction

(Buizert and Severinghaus 2016) suggested that the firn gas content and the isotopic composition can be changed on a synoptic scale. A molecular dispersion caused by the barometric variability, affects the isotopic composition of the greenhouse ($\delta^{15}N_2$, $^{14}CO_2$) and noble (^{86}Kr) gases. The effect was named the barometric pumping. If it occurs at the lock-in zone, the dispersed signal might be trapped in the ice cores thus providing a proxy for the past wind activity. The study was conducted based on modelling of the gas molecules dispersion and the discrete firn air measurements. The barometric pumping signal propagation was proposed down to 40-60 m depth.

During the summer field season 2017 we conducted continuous measurements of the CH_4 concentration in the air and in the firn air. Due to the technically challenging penetration down to 40-60 m without interrupting the firn pores structure, the experiment was focused on the convective zone of the firn, i.e. upper few meters. The null hypothesis suggested that no propagation of the atmospheric signal should be seen in the convective zone due to the air mixing. The experiment was targeted to trace the wind pumping effect on the CH_4 concentration in air in the convective zone if any is present.

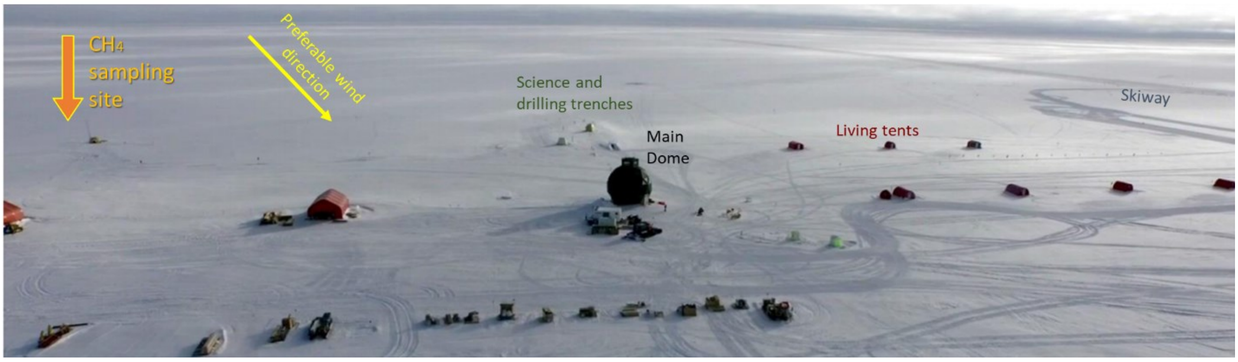

Figure 52: *The EGRIP camp layout (the picture taken by the drone in July 2016, source https://eastgrip.org/documentation/2018/2018-05-09_EGRIP2018FieldPlan.pdf) and the location of the CH_4 sampling site.*

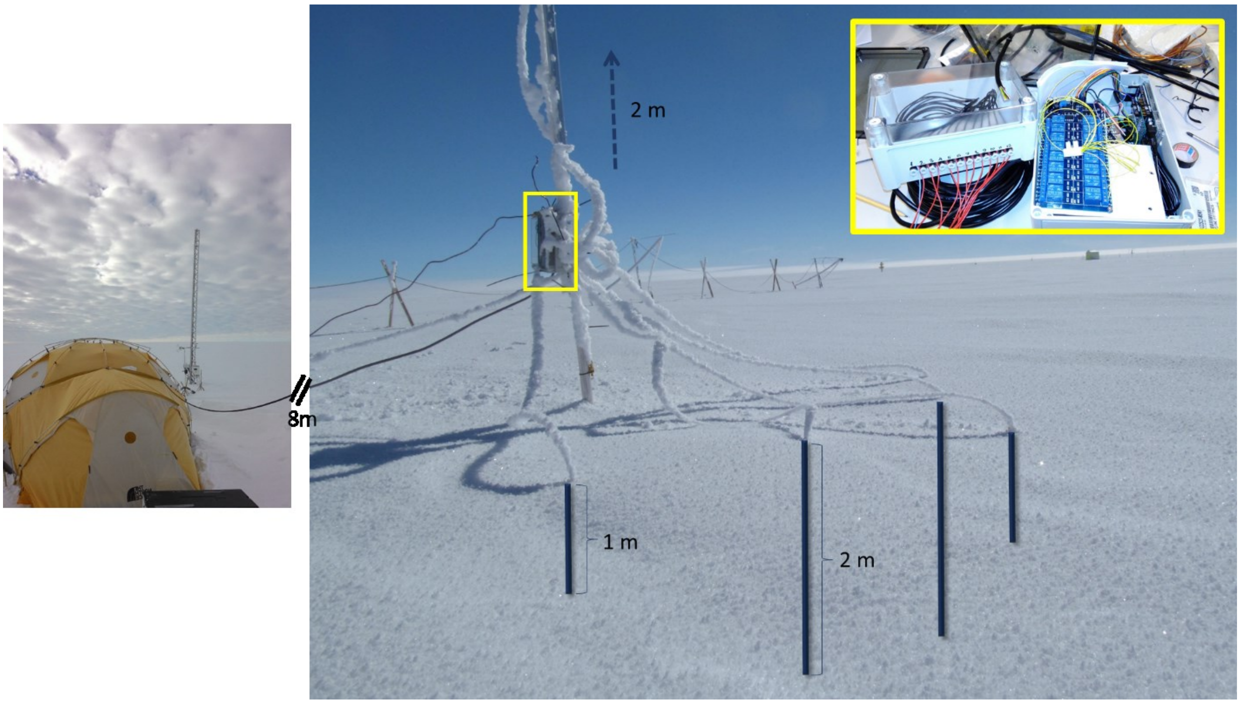

Figure 53: *An experimental setup for the continuous measurements of CH_4 concentration in the air and upper firn column, Greenland, June-August 2017: left – the tent where the laser analyzer and the standard gas bottle were placed; right – appearance of the sampling tubes with the rime for contrasting image, the firn air sampling tubes are shown schematically, the sampling box with different inlets and valves is circled in yellow and showed zoomed-in in the upper right corner.*

5.2. Data and method

5.2.1. Experimental setup

Continuous measurements of the CH_4 concertation in the atmospheric air (2 m above the surface) and in the upper firn column (1 m and 2 m depth) were conducted during the field season 2017 in the vicinity of the East Greenland Ice-core Project camp - EGRIP (https://eastgrip.org/) (75.6268N 35.9915W). The sampling tower was set up in the clean snow area accounting on the preferable wind blowing toward the camp area from the outer clean snow zone (see Fig. 52 and 53). The sampling setup is essentially two parallel tubes deepen vertically to 2 m to the snow, two tubes – to 1 m and one tube as an atmospheric air inlet set 2 m above the ground. The sampling tubes in the snow were made out of stainless steel 1/8" inner diameter, the transferring lines and the atmospheric inlet is TFZL transparent tube 1/8" inner diameter. All tubes were connected using the Swagelok© unions. A distance between the sampling site and an analyzer was 8 m, all inlets were merged through the solenoid valves to one transfer line (TFZL transparent tube 1/8" diameter). The measurements were conducted using the laser analyzer Picarro G-1301 implying cavity ring down technology (similar to the analyzer described in

Chapter 2 but with the option measuring carbon dioxide, CO_2, concentration instead of CO). The operating pressure was set to 140 Torr, the cavity of this analyzer was not modified, i.e. the effective volume was not decreased. However, for the atmospheric monitoring applications such technical specifications are appropriate as the sample flow rate was in the order of 17-20 cc min^{-1}, which provided a sufficient rate of gas sample exchange in the cavity. The setup was calibrated once in two days using the technical air containing roughly the same amount of CH_4 as a modern atmospheric air. The working standard was launched through the parallel line toward the solenoid valve at the sampling site. After the valve was switched to the standard gas' inlet via the analyzer's computer, the standard gas was pumped along the 8 m long transfer line in order to simulate a sample's path. Thus, the standard gas experienced the same humidity variations inside the transfer line as a sample did.

5.2.2. Memory effect

The obtained data were processed initially by merging the daily recorded data files, subsetting them to the following categories: tower inlet (2 m high air inlet), 1 m deep snow inlet (includes two tubes), 2 m deep snow inlet (includes two tubes) and the standard gas. Because all samples and the standard gas were transferred trough an 8-m long line, every measurement experienced the memory effect, i.e. the portion of the previously measured sample or standard mixed into the new portion. The data scan and the transition time (2-10 min) calculation allowed eliminating the memory effect by deleting the affected data.

5.2.3. Calibration

5.2.3.1. Water level adjustment

Note that the data had to be preliminary corrected for the water level as the calibration of the absolute values was carried using the dry gas streams (see the details on the water level correction in section 3.4). The absolute humidity of the sample stream is presented on Fig. 54. After the day 207 (27 July 2017) the water percentage level drops due to the installation of Nafion (an air stream drying unit – see section 2.2).

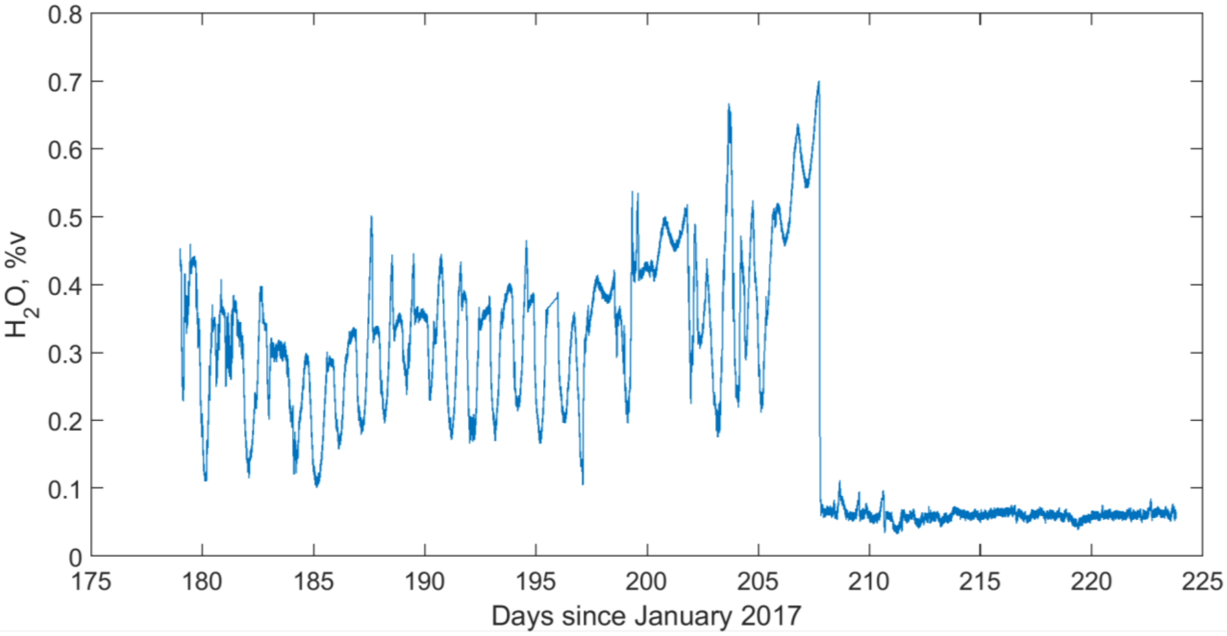

Figure 54: *Absolute humidity (in % per volume) of the surface air measured along with the CH_4 concentration at EGRIP site in 2017.*

In agreement with (Rella 2010) drying of the sample air stream causes much less deviation of the measured CH_4 concertation of the true value (see Fig. 55). For the data processing and calibration purposes, we have divided the CH_4 dataset to the measured prior and after the day 207 since January 2017, i.e. the date of the dryer installation. The data prior to day 2017 (Fig. 55a) was adjusted by applying a linear slope (-25.13) and an insert (1991.3), and after the day 207 (Fig. 55b) – by the linear shift -0.28%.

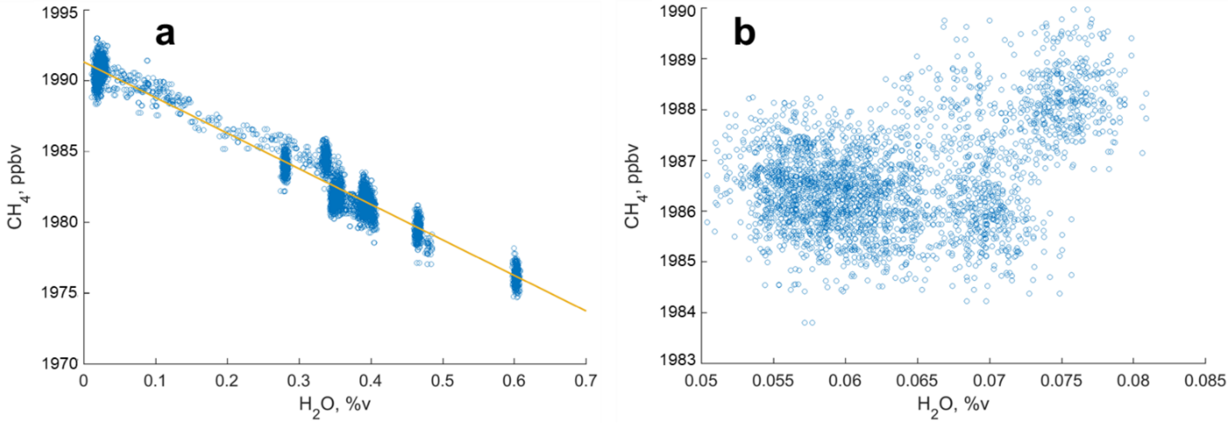

Figure 55: *The CH_4 concentration of working standard gas and the humidity of the gas line measured during the EGRIP field campaign 2017 before the Nafion installation (a) and after (b).*

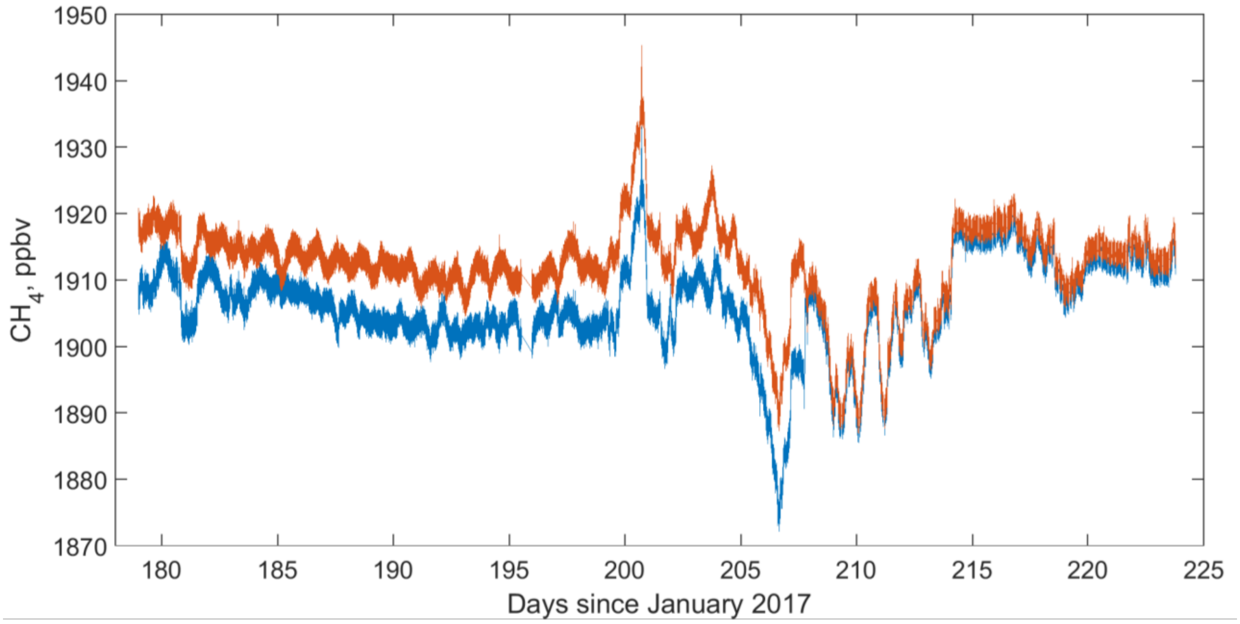

Figure 56: *CH_4 concertation of the air at 2m above the surface before (blue curve) and after the water level correction (red curve).*

After the water correction was implemented, the CH_4 values during the day 207 matched, the discrepancy caused by the dilution and the water-induced shift was corrected (see Fig. 56).

5.2.3.2. Absolute values calibration

The absolute value of the CH_4 concentration was calibrated versus the secondary NOAA gas standards when the gas bottle and the laser analyzer were brought back to the laboratory at CIC. The dry gas was connected to the cavity inlet, the gas flowrate was regulated using a pressure gauge on the bottle and a manual flowrate controller. The standard gases were connected one by one to the same line by the 3-way valve allowing alternating the gas flow from either of the two bottles without opening the gas line to the ambient air (and thus causing a contamination). The calibration of absolute values of dry gases was made in the following order: Glacial standard (G), the dry gas bottle used as the working standard during the field season 2017 (EGRIP), G, Holocene standard (H), EGRIP, H, G, H, NEEM air standard (NEEM), EGRIP. The eventual calibration curve is presented in Fig. 57. It is built based on the true values of the CH_4 concentration of Glacial and NEEM standards, the Holocene standard is put in order to check the linearity. The true value of EGRIP working standard was calculated based on the linear calibration equation:

$$CH_{4\,true} = 1.033 \cdot CH_{4\,measured} - 8.8442$$

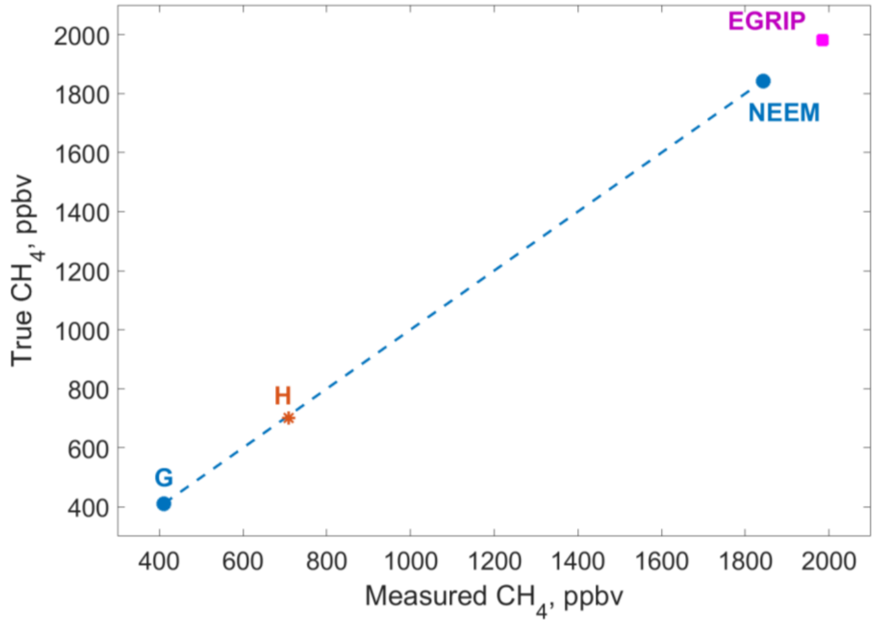

Figure 57: *Secondary NOAA standards (G, H), NEEM air standard and the working EGRIP standard CH_4 concentration measurements, the calibration curve (dashed line).*

The absolute values of the measured CH_4 concentration should be adjusted to the true values using the following intercepts: -9.8 ppbv for the data before the day 207 since January 2017 (the date of the Nafion installation) and -6.4 ppbv after the day 207. The intercepts were introduced instead of a typical linear calibration equation because we used only one working standard in the field.

5.3. Results

The corrected to the water level CH_4 series were calibrated to the absolute values based on the results of the working standard gas calibration. The results are presented in Fig. 58. The average CH4 concentration measured in the air in June-August 2017 is 1904 ppbv, no significant trend is identified. The observation period (29 June – 13 August 2017) is insufficient to justify the presence of seasonal or interannual variability. Methane spike at the day 201 since January 2017 (see Fig. 58) is likely a contamination originating from the camp emissions (which was clearly seen in the high CO_2 concentration measured simultaneously), it is not taken into consideration in the further analysis. The data corresponding to the measuring system tests (prior to the day 179 since January 2017) and opening the transfer line to install the Nafion upstream the cavity inlet (day 207 since January 2017) were excluded from the data set.

The CH_4 concentration measured in the air 2m above the ground (shown in blue on Fig. 58) and the CH_4 concertation measured in the air space in the upper firn column at 1 m and 2 m depth (shown in yellow and red on Fig. 58) reveal diurnal periodic variability of 10 ppbv amplitude. This feature is present at the days 179-197 since January 2017. Later in the observational period, variations in the surface air CH_4 concentrations are characterized by an enhanced amplitude of 30 ppbv and longer period than a daily cycle. The diurnal cycle in the snow air CH_4 is smoothed out since the day 197.

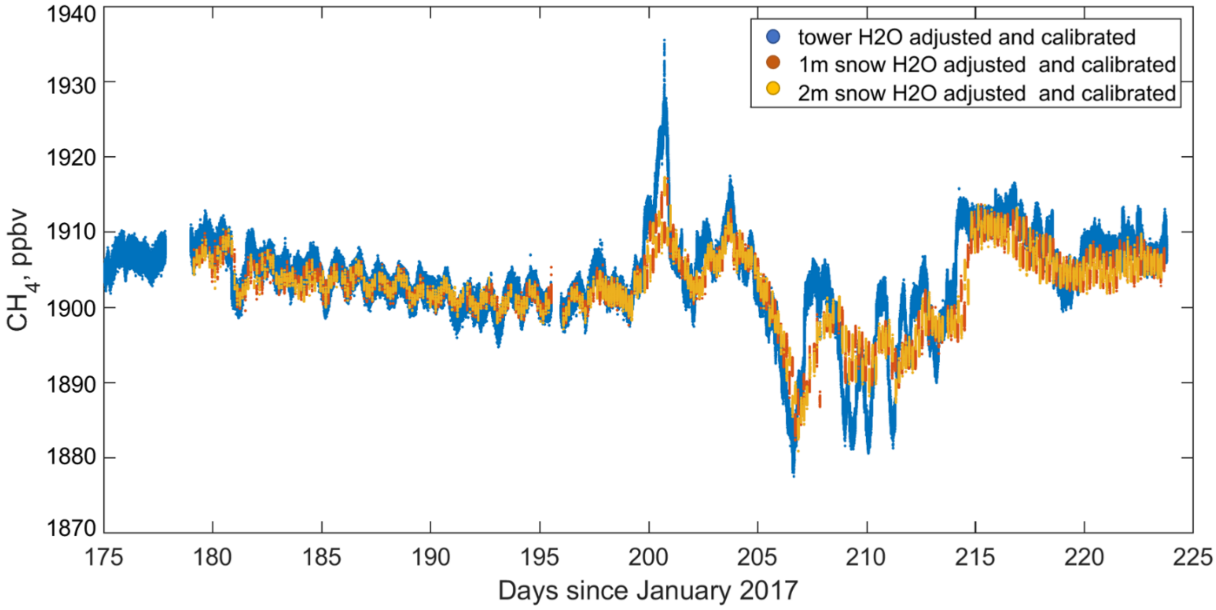

Figure 58: *The results of CH_4 concentration measurements in the air 2m above the surface and in the air of the upper firn column at 1m and 2m depths.*

5.4. Discussion

The monitoring of the CH_4 atmospheric composition (Dlugokencky et al. 2018) is carried out by NOAA (http://www.noaa.gov/) worldwide including Greenland ice sheet, particularly at the Summit station (72.596˚N 38.422˚W). The monthly average data from the air samples, which are collected in the flasks, is available at ftp://aftp.cmdl.noaa.gov/data/trace_gases/ch4/flask/surface/ch4_sum_surface-flask_1_ccgg_month.txt . The average methane concentration in Summit during the summer 2017 corresponds well to the CH_4 concentration measured at EGRIP – see Table 1. As the data from Summit is an averaged over a month value (flask measurements), a comparison of the seasonal and diurnal variability is not possible.

The CH_4 concentration is measured with an hourly resolution only in Barrow, Alaska (ftp://aftp.cmdl.noaa.gov/data/trace_gases/ch4/in-situ/surface/brw/ch4_brw_surface-insitu_1_ccgg_DailyData.txt), and in Mauna Loa (ftp://aftp.cmdl.noaa.gov/data/trace_gases/ch4/in-situ/surface/mlo/ch4_mlo_surface-insitu_1_ccgg_HourlyData.txt), Hawaii. Both observational datasets do not demonstrate any trend over the period 29 June – 13 August 2017 and do not reveal a diurnal cycle. The concentration in Alaska is characterized by an occasional not periodic spikes (seven spikes over 1.5 months) up to 300 ppbv amplitude likely originating from the biogenic source and the habitant area (i.e. pollution source).

Table 1. Average CH_4 concertation (ppbv) measured in thein the air at Summit and EGRIP, Greenland, during the summer field season 2017

	Summit	EGRIP
June	1904.74	1907
July	1902.27	1905
August	1915.82	1908

The CH_4 concentration in the upper firn follows the variability of the CH_4 concentration in the air above the surface with no lag in time during the calm days with no particular variation in the daily mean temperature (Fig. 58, days 180-200). The surface melting occurred at the days 206-208 and was followed by the icy crust formation on the surface, which slowed down the exchange of air between the surface and the upper firn. The change in average concentration of the CH_4 in the upper firn column lagged the CH4 fluctuations in the air above the ground (see Fig. 58). The diurnal cycle was not traceable in the upper firn since that event.

The meteorological parameters such as surface or temperature, the wind speed and wind direction, surface air pressure and the relative humidity were measured at the PROMICE weather station every 10 min at a height 2 m above the ground, see Fig. 59.

The CH_4 concentration was measured in the air alternating with the CH_4 concertation in the upper firn: 170 min of measurements of the concertation in the air with 5 min per each snow inlet. After the Nafion was installed, the time of measurements for every snow inlet was increased up to 25 min due to the increased memory effect. The processed data was then resampled every 10 min, the gaps in measurements during the time when the alternating inlet was connected were filled in by linearly interpolated data from previous and following series of measurements. The difference in the CH_4 concentration between the 2 m high inlet and 1 m and 2 m deep snow inlets taken with 10 min increment approximates zero during the calm days with no sufficient temperature variability (days 180-200 since January 2017) – see black and blue curves on Fig. 60. Surface air and upper firn air CH_4 concentration deviated from each other when the wind speed picked up (days 200-215). The difference of the CH_4 concentration in the air and in the upper firn column (see Fig. 60, black and blue curves) corresponds well to the CH_4 fluctuations above the ground throughout the observational period, besides the days 214-217 since January 2017. On average, the periods of increased atmospheric pressure coincide with the enhanced variability of the CH_4 concentration in the air above the ground and in the snow.

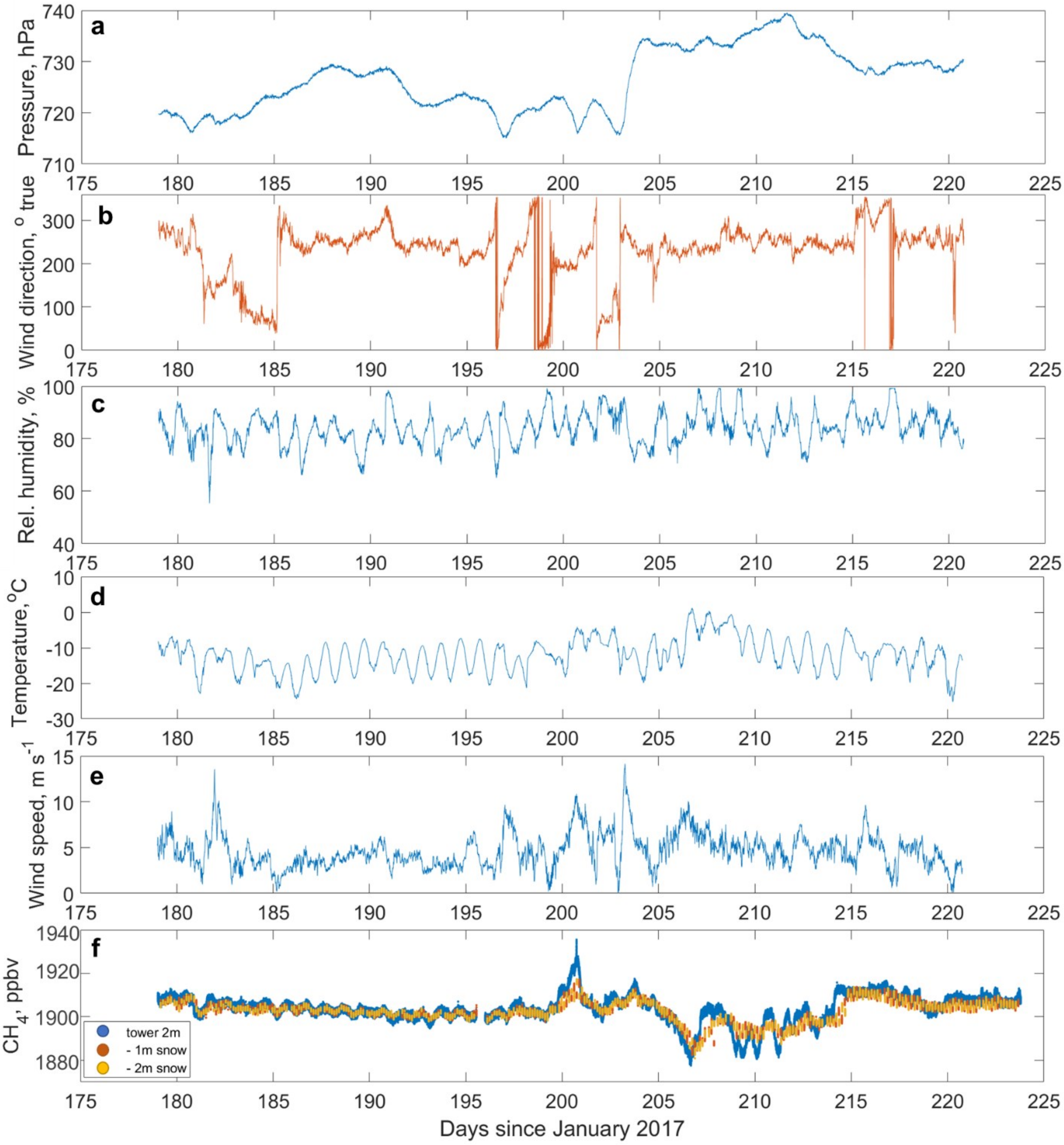

Figure 59: *Meteorological data (extracted from an automated PROMICE weather station, standard measurements 2 m above the ground): a – surface air pressure, b – wind direction expressed as degrees*

from north, c – relative humidity, d – surface air temperature, e – wind speed; f – CH_4 concentration in the air 2 m above the surface and in the air of the upper firn column at 1 m and 2 m depths.

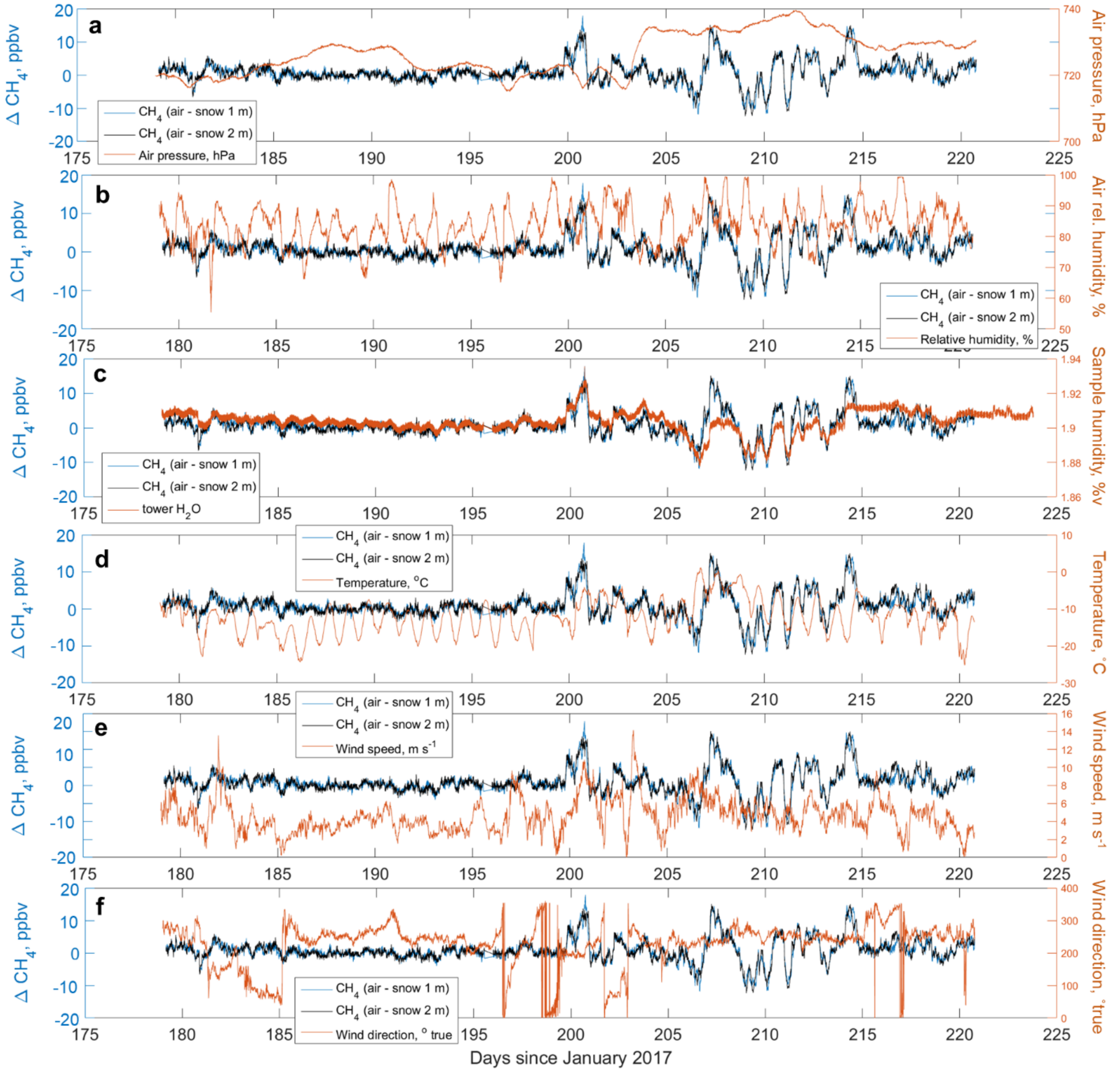

Figure 60: *Meteorological data (red curves): a – surface air pressure, b – relative humidity in the air, c – water content measured by Picarro, d – surface air temperature, e – wind speed, f – wind direction plotted versus the difference between the CH_4 concentration in the air 2 m above the surface and in the air of the upper firn column at 1 m (blue curves) and 2 m depths (black curves).*

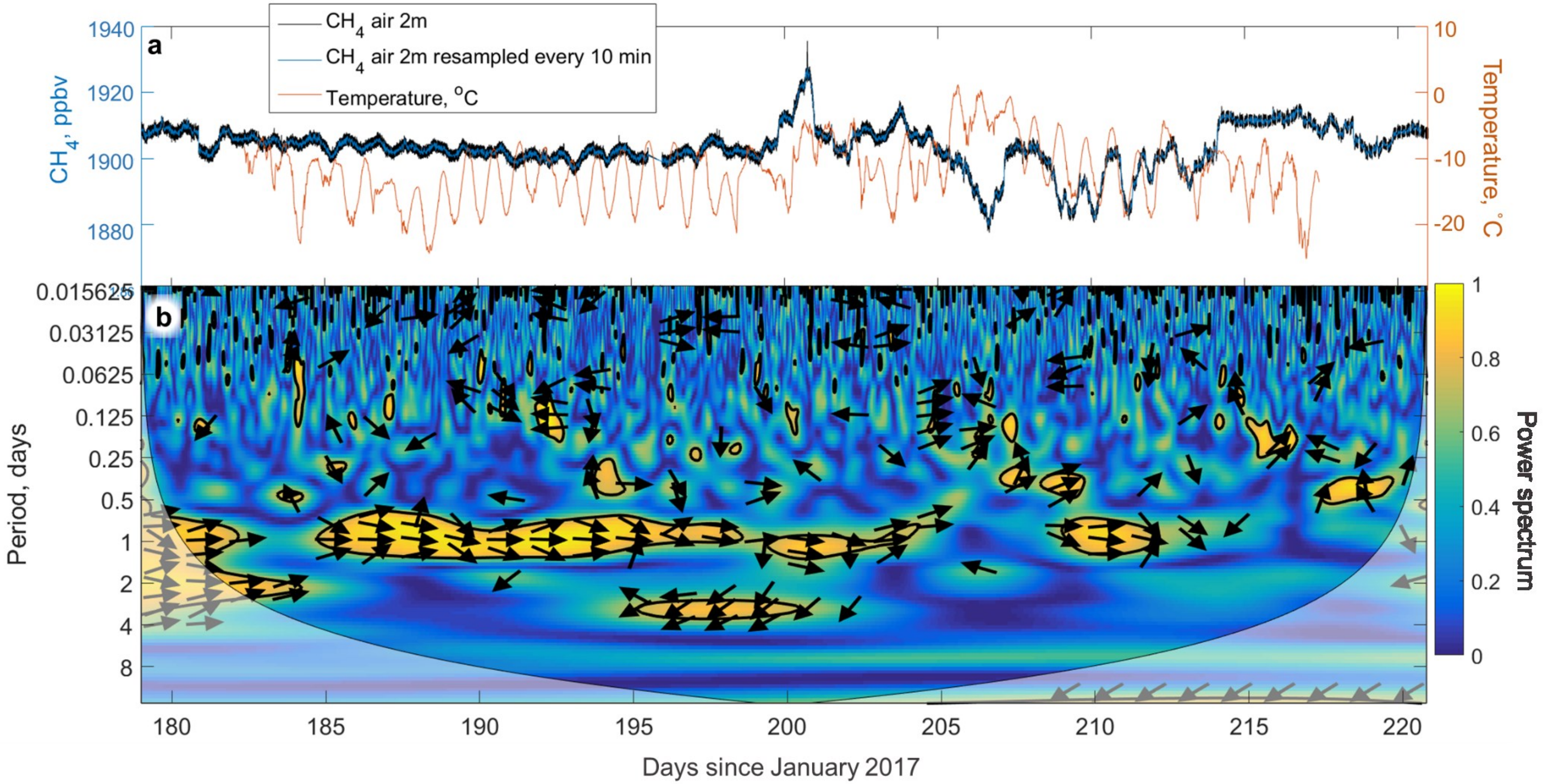

Figure 61: a – the CH₄ concentration measured in the air 2m above the surface at EGRIP and the surface air temperature. b – the results of the wavelet coherence analysis of the CH₄ and temperature series. The legend for the panel (a) as similar to the Fig. 60d.

The CH_4 variability reveals a significant covariation in phase with the surface air temperature (Fig. 61) persistent over calm days with no surface melting (180-200 since January 2017). The amplitude of the diurnal signal is in the order of 10 ppbv. A simultaneous variability of the temperature inside the instrument does not appear as a possible reason of the CH_4 drift as the operational Picarro mode maintains the constant temperature (+45˚C) inside the analytical cavity.

The diurnal variations in methane flux were identified earlier by measuring boreal fens emissions in Saskatchewan, Canada (Suyker et al. 1996). The diurnal variations were observed in the selected days in July and August, when the high temporal resolution measurements were conducted. The daytime flux exceeded the nighttime fluxes by 27-46%. Similar variations were observed in other place in arctic tundra (Fan et al. 1992) and Hudson Bay (Edwards et al. 1994). The origin of the diurnal cycle is debated in the aforementioned studies. One of the possible mechanisms is a change in the stomata activity. Dependence on the wind speed above the water surface is not clear. A relation of the methane flux diurnal cycle to the meteorological parameters was to be studied further in the details.

To our knowledge there is no monitoring datasets demonstrating the presence of the of the CH_4 diurnal cycle in the polar regions remote from the methane sources. The only monitoring data with an hourly resolution of the CH_4 atmospheric measurements from Barrow, Alaska (ftp://aftp.cmdl.noaa.gov/data/trace_gases/ch4/in-situ/surface/brw/ch4_brw_surface-insitu_1_ccgg_DailyData.txt) does not reveal a diurnal variability and shows episodic spikes (six spikes of 100-300 ppbv amplitude, one reaching 500 ppbv over 1.5 months selected observational period) of an unknown origin. We can only hypothesize that it was either a contamination or an in-situ production, i.e. wetlands or tundra emissions. The origin of the diurnal signal in CH_4 at EGRIP is a subject of the discussion. EGRIP is located 400 km remote from the nearest coast, i.e. marine, tundra or wetland CH_4 source.

Apparently, there is a low chance of any biological cycles being distinguished by the methane tracers measured at EGRIP. It is mostly due to the remoteness of the sources. Among the meteorological parameters only temperature variations are coherent with the CH_4 concertation change, the daily minimum of the CH_4 concentration coincides with the temperature minimum. A biologically related methane concentration change would have a lag to the temperature variability due to the activation time required to the methane trapping (Suyker et al. 1996), (Nisbeth, pers. communication, 2018).

However, recently it was shown that Greenland Ice Sheet represents a global CH_4 sink. (Dieser et al. 2014) demonstrated the presence of the methane cycle on the west margin of the Greenland Ice Sheet and proved the involvement of the methanotrophic bacteria. It remains unclear if the subglacial or glacier margins' consumption by the bacterial ecosystems can be traced from inland summit area.

Alternatively, the diurnal variations of the CH_4 concentration in the atmosphere might be caused by the sink influence rather than source. In this case, ≈10 ppbv daily amplitude would suggest a regional residence time of the CH_4 in the atmosphere being ≈200 days (0.5 yr) in contrast with global average residence time 9.1±0.9 yr.

The more efficient sink, i.e. the OH^- radicals produced at a higher rate, might potentially be induced by the lower ozone concentration in the polar regions. On the one hand, the tropospheric ozone is strongly influenced by the photochemical production (Crutzen and Gidel 1983), which at the EGRIP site is also closely related to the temperature variations (in the relatively dry atmosphere the angle of the solar irradiation reaching the ground modulates the surface air temperature variations with almost no lag in time).

(Ono and Oda 2003) based on the experiment conducted in the humid-air flow reactor, showed a decreasing amount of ozone and OH^- radical density as a response to the additional water vapor. The measurements of the surface air humidity using the laser spectroscopy (at the same sample that CH_4) demonstrated as expected a clear diurnal cycle in the absolute humidity, which decreases in the night hours in phase with the temperature. In other words, the lower the temperature and the absolute humidity become during the day, the higher is the ozone production and OH^- radical density increases correspondingly, the methane molecules oxidation enhances and the its concentration in the sampled air declines. The CH_4 oxidation rate by the OH^- radical occurs at a rate $3.92 \pm 0.16 \cdot 10^9$ cm^3 $(mol\cdot sec)^{-1}$ (Overend, Paraskevopoulos and Cvetanović 1975). Given the ideal gas law, average surface temperature -12°C and pressure 0.717 atm during the observational period, the reaction rate (r) can be translated in the amount of ppbv of CH_4, which can be oxidized over half a day:

$$\eta = \frac{V \cdot P}{R \cdot T} \Rightarrow \frac{1\, cm^3 \cdot 0.717\, atm}{82.06 \frac{cm^3 \cdot atm}{K \cdot mol} \cdot 261.15\, K} = 3.35 \cdot 10^{-5} mol$$

$$r = 3.92 \pm 0.16 \cdot 10^{9} \cdot \frac{3.35 \cdot 10^{-5} mol_{Tot}}{mol_{CH_4} \cdot sec} = 13.13 \pm 0.54 \cdot 10^{4} \frac{mol_{Tot}}{mol_{CH_4} \cdot sec}$$
$$= 13.13 \pm 0.54 \cdot 10^{-5} \frac{1}{ppb \cdot sec} = 5.7 \pm 0.23 \frac{1}{ppb \cdot {}^{1}/_{2}\, day}$$

Given the obtained reaction rate and the concentration of OH^- radical in the atmosphere at the elevation of EGRIP camp (2700 m) is equal to $4.6 \cdot 10^{-5}$ ppb (Seinfeld and Pandis 2012), the total amount of the CH_4, which can potentially be oxidized is:

$$[CH_4]_{oxidized} = r \cdot [CH_4] \cdot [OH^-]$$
$$[CH_4]_{oxidized} = \left(5.7 \pm 0.23 \frac{1}{ppb \cdot {}^{1}/_{2}\, day}\right) \cdot 1905\, ppb \cdot 4.6 \cdot 10^{-5}\, ppb = 0.5 \pm 0.02\, ppb$$

A rough estimation shows that 0.5 ppb CH_4 can be removed per ½ day only by the OH^- radical oxidation. It is less by one order of the magnitude than an average magnitude of the CH_4 diurnal cycle (≈10 ppbv). A hypothesis of the diurnal CH_4 cycle in Northeast Greenland induced by the sink variations remains thus arguable.

5.5. Summary

We measured the CH_4 concentration in the air 2 m above the ground and at 1 m and 2 m depth in the upper firn column on site of the EGRIP camp, Northeast Greenland. We identified no significant difference in the CH_4 concentration in the above- and subsurface measurements in the calm days with no significant daily mean temperatures change and in the absence of the surface melting. The subsurface CH_4 concertation signal revealed a lag in time from the one measured in the 2 m height after the surface melting occurred and a thin ice crust was formed. The diurnal variability of the CH_4 concentration was not propagated from the atmosphere to the upper firn column in the days with enhanced wind activity thus supporting a suggestion of the wind mixing in the convective firn zone. As a main result of this field study, we observed a diurnal cycle of the CH_4 concertation in the air above and subsurface of an average amplitude 10 ppbv. The diurnal cycle is persistent in the calm days with no significant daily mean temperatures change and in the absence of the surface melting. The diurnal cycle of CH_4 is significantly coherent and in phase with the temperature variability. To our knowledge there is no data obtained before showing similar diurnal CH_4 concentration variability. We hypothesize that the diurnal cycle in the atmospheric CH_4 measured at EGRIP site was caused by the sink variability, i.e. the enhanced OH^- radical production in the hours of low temperature. At this time, the absolute humidity decreases influencing the higher ozone and corresponding OH^- radical production, which oxides the CH_4 more active. A simple calculation based on the CH_4 oxidation rate by OH^- radical and the concentration of the two species in the atmosphere identified a possibility of 0.5 ± 0.02 ppbv CH_4 destructed by the OH- radical per half a day, which is lower by one order of magnitude than the observed diurnal cycle. The further atmospheric and upper firn air monitoring is needed along with at least hourly average CH_4 data from the other locations in Central Greenland to argue about the presence of the diurnal cycle all over the Greenland ice sheet and its origin.

Conclusions

We presented the high-resolution methane (CH_4) record of the REnland ice CAP (RECAP) ice core (Eastern Greenland). The core was obtained in the frame of the drilling project targeted to obtain the eastern Greenland climate record and to study the atmospheric gas content at the ice cap with assumingly no elevation change in the past. The RECAP gas record covered the last climatic cycle, i.e. Holocene (modern interglacial), the Last Glacial and the latest part of Eemian (penultimate interglacial). The CH_4 measurements were conducted using the continuous flow analysis (CFA) method providing ±10 ppbv analytical uncertainty. The effective resolution of the Holocene section was 3.5 data points 100 yr^{-1}, and 0.6 d.p. 100 yr^{-1} for the Last Glacial section.

The lower boundary of the Holocene section (532 m out of the 584 m of the total core length) was still above the brittle ice zone, which provided a unique opportunity of obtaining high-resolution continuous gas and chemistry records. The RECAP record represents the first Northern Hemisphere continuous high-resolution Holocene CH_4 record. A centennial-scale variability was traceable in the RECAP CH_4 record and its pattern turned out to be coherent with the earlier published Southern Hemisphere record based on the West Antarctic Ice Divide (WAIS) CH_4 record. The wavelet coherence analysis identified a high correlation on the long- and midterm variability (600-700, 200-500 yr periodicity); the late Holocene section revealed a common variability down to 70 yr. We argued that the centennial variability in the CH_4 is explained by the intertropical convergence zone global teleconnection and its influence on the monsoon activity and thus the CH_4 emissions by tropical wetlands.

The CH_4 concentration closely followed Greenland temperature variations during the dramatic climatic shifts from cold Greenland Stadials (GS) and relatively mild Greenland Interstadials (GI). However, the relative amplitudes of the variations in temperature and CH_4 concentration vary across different GI/GS transitions. Specifically, GI-19-20 (76.39-69.35 ka BP) were characterized by a pronounced stadial-interstadial temperature contrast, while the stadial-interstadial amplitude of CH_4 was relatively low (70 and 97±10 ppbv). In opposite, GI-21 (85.01-77.71 ka BP) was indicated by an unusually large amplitude in CH_4 (222±10 ppbv).

We combined the RECAP record with high-resolution Greenland data and published Antarctic data to calculate the relative CH_4 interpolar difference (rIPD) changes at a centennial scale across the time interval 65-87 kyr b2k.

We identified increased values of the CH_4 rIPD 78-83 ka BP, which pointed to an additional CH_4 source in the Northern Hemisphere being active at a time. We suggested that this source were boreal wetlands formed after the ice sheet retreat and the drainage of the ice-dammed lakes, which is corroborated by the paleoclimatic and deglaciation reconstructions as well as the peat studies.

As a side project, we conducted the on-site measurements of the CH_4 concentration at the Eastern GReenland Ice core Project (EGRIP) camp during the field season 2017. We identified presence of the diurnal variability of the CH_4 signal in the upper firn layer as well as in the surface air (2 m above the ground). This variability is persistent during the calm days; the upper firn signal matches the average value and the amplitude of the atmospheric signal. An increased wind activity mixes up the air in the pores and the diurnal variability cannot be traced. Surface melting episodes with the following formation of the ice crust caused a daylong lag between a change in the atmospheric CH_4 concentration and the signal propagation to the upper firn. The traced CH_4 concentration variability in the convective zone of the firn, which was considered as a zone with the well-mixed gas content, revealed a new feature and gave a hint on the further studies of the firn gas signal trapping and transformation.

Future improvements and refinements

This study as almost any PhD project opens up a wider perspective on the future studies. Once a side of the big research question is touched upon and one dives deeper into it, he realizes how infinite is the world of investigation beyond.

In the scope of this PhD project the three main lines were drawn: the technical side of the CFA gas method, the climatic interpretation of the high-resolution methane record and the monitoring of the diurnal-scale CH_4 variability.

Here we propose some further improvements and refinements based on the experience of conducting the current study:

- The CFA setup: the depth registration should be synchronized by installing the conductivity loggers at the inlets of every analytical line. On the gas extraction line side: the degassers should be replaced as soon as they begin to lose the gas extraction efficiency; the Nafion has to be cooled down in the lower gas stream rather than heated; the MiliQ water should be degassed over the night; the melthead should not be cleaned using the alcohol.
- Calibration of the CFA gas data: multi-regression calibration should be carried out defining the tracers of the gas-to-water ratio; if the Nafion works properly drying the gas sample to 0.02-0.03% v then the water correction is not needed; first the instrumental adjustment to the absolute values should be implemented and then the correction to the gas-to-water ratio; the calibration coefficients should be revised after the major changes and/or replacements in the setup; the system response time should be calibrated simulating different gas-to-water ratio conditions with at least two gas standards.
- Depth assignment system: the usage of the laser pointer is preferable to the usage of Encoder for the ultra-high resolution measurements.
- Gas signal deconvolution: an iterative protocol should be created in order to attempt deconvolution the actual atmospheric amplitude of the CH_4 variations during the climatic transitions. Similarly, the gas signal may be deconvoluted from the diffused CFA measurements in order to reveal the actual amplitude of the atmospheric CH_4 variability on the centennial scale.
- IPD based on the samples measured at one laboratory and the CH_4 flux modelling: conduct the parallel measurements of Greenland and Antarctica ice core samples during the same analytical campaign covering the same time interval. This would allow to exclude the

argument of the interlaboratory offsets when discussing the methane interpolar difference variations.

- Further monitoring of the CH_4 in the surface air (2m above the ground) and in the upper firn layer should be conducted at EGRIP. If there is a way to overcome the technical challenge penetrating deeper than 2 m below the snow surface without interrupting the firn thickness, then the attempt should be made. Possibly the experimental setup should be slightly modified in order to proof the presence of the diurnal cycle in calm days and that it is an atmospheric signal rather than a measurement artifact.

References

Ahn, J. & E. J. Brook (2008) Atmospheric CO<sub>2</sub> and Climate on Millennial Time Scales During the Last Glacial Period. *Science,* 322**,** 83.

--- (2014) Siple Dome ice reveals two modes of millennial CO2 change during the last ice age. *Nature Communications,* 5**,** 3723.

Allan, W., H. Struthers & D. C. Lowe (2007) Methane carbon isotope effects caused by atomic chlorine in the marine boundary layer: Global model results compared with Southern Hemisphere measurements. *Journal of Geophysical Research: Atmospheres,* 112.

Alley, R. (1987) Firn densification by grain-boundary sliding: a first model. *Le Journal de Physique Colloques,* 48**,** C1-249-C1-256.

Andersen, K. K., N. Azuma, J.-M. Barnola, M. Bigler, P. Biscaye, N. Caillon, J. Chappellaz, H. B. Clausen, D. Dahl-Jensen & H. Fischer (2004) High-resolution record of Northern Hemisphere climate extending into the last interglacial period. *Nature,* 431**,** 147.

Anderson, D. & C. Benson. 1993. The densification and diagenesis of snow: properties, processes and applications. Ice and snow: properties, processes, and applications/Ed WD Kingery. Cambridge, MA, MIT Press.

Ann, G. K. & P. L. C. (2014) A 0.6 million year record of millennial-scale climate variability in the tropics. *Geophysical Research Letters,* 41**,** 969-975.

Anthony, K. M. W., P. Anthony, G. Grosse & J. Chanton (2012) Geologic methane seeps along boundaries of Arctic permafrost thaw and melting glaciers. *Nature Geoscience,* 5**,** 419.

Arnaud, L., V. Lipenkov, J.-M. Barnola, M. Gay & P. Duval (1998) Modelling of the densification of polar firn: characterization of the snow–firn transition. *Annals of Glaciology,* 26**,** 39-44.

Arzt, E., M. F. Ashby & R. Verrall (1983) Interface controlled diffusional creep. *Acta metallurgica,* 31**,** 1977-1989.

Astakhov, V.I., Nazarov, D.V. (2010). Stratigraphy of the upper Neoplestocene of the north of Western Siberia and its geochronometric justification. *Regional geology and metallogeny, 43*, 36-47 (in Russian).

Baker, P. A. & S. C. Fritz (2015) Nature and causes of Quaternary climate variation of tropical South America. *Quaternary Science Reviews,* 124**,** 31-47.

Bakker, P., P. U. Clark, N. R. Golledge, A. Schmittner & M. E. Weber (2017) Centennial-scale Holocene climate variations amplified by Antarctic Ice Sheet discharge. *Nature,* 541**,** 72.

Barnola, J. M., D. Raynaud, A. Neftel & H. Oeschger (1983) Comparison of CO2 measurements by two laboratories on air from bubbles in polar ice. *Nature,* 303**,** 410.

Baumgartner, M., P. Kindler, O. Eicher, G. Floch, A. Schilt, J. Schwander, R. Spahni, E. Capron, J. Chappellaz, M. Leuenberger, H. Fischer & T. F. Stocker (2014) NGRIP CH4 concentration from 120 to 10 kyr before present and its relation to a δ15N temperature reconstruction from the same ice core. *Climate of the Past,* 10**,** 903-920.

Baumgartner, M., A. Schilt, O. Eicher, J. Schmitt, J. Schwander, R. Spahni, H. Fischer & T. Stocker (2012) High-resolution interpolar difference of atmospheric methane around the Last Glacial Maximum. *Biogeosciences,* 9**,** 3961-3977.

Bender, M., T. Sowers & E. Brook (1997) Gases in ice cores. *Proceedings of the National Academy of Sciences,* 94**,** 8343-8349.

Berger, A. & M. F. Loutre (2002) An Exceptionally Long Interglacial Ahead? *Science,* 297**,** 1287.

Bernal, J. P., F. W. Cruz, N. M. Stríkis, X. Wang, M. Deininger, M. C. A. Catunda, C. Ortega-Obregón, H. Cheng, R. L. Edwards & A. S. Auler (2016) High-resolution Holocene South American monsoon history recorded by a speleothem from Botuverá Cave, Brazil. *Earth and Planetary Science Letters,* 450**,** 186-196.

Bird, B. W., Y. Lei, M. Perello, P. J. Polissar, T. Yao, B. Finney, D. Bain, D. Pompeani & L. G. Thompson (2016) Late-Holocene Indian summer monsoon variability revealed from a 3300-year-long lake sediment record from Nir'pa Co, southeastern Tibet. *The Holocene,* 27**,** 541-552.

Blunier, T. & E. J. Brook (2001) Timing of Millennial-Scale Climate Change in Antarctica and Greenland During the Last Glacial Period. *Science,* 291**,** 109-112.

Blunier, T., J. Chappellaz, J. Schwander, A. Dällenbach, B. Stauffer, T. F. Stocker, D. Raynaud, J. Jouzel, H. B. Clausen, C. U. Hammer & S. J. Johnsen (1998) Asynchrony of Antarctic and Greenland climate change during the last glacial period. *Nature,* 394**,** 739.

Blunier, T., J. Chappellaz, J. Schwander, B. Stauffer & D. Raynaud (1995) Variations in atmospheric methane concentration during the Holocene epoch. *Nature,* 374**,** 46.

Blunier, T. & J. Schwander. 2000. Gas enclosure in ice: age difference and fractionation. In *Physics of Ice Core Records*, 307-326. Hokkaido University Press.

Boucher, O., P. Friedlingstein, B. Collins & K. P. Shine (2009) The indirect global warming potential and global temperature change potential due to methane oxidation. *Environmental Research Letters,* 4**,** 044007.

Bousquet, P., P. Ciais, J. Miller, E. Dlugokencky, D. Hauglustaine, C. Prigent, G. Van der Werf, P. Peylin, E.-G. Brunke & C. Carouge (2006) Contribution of anthropogenic and natural sources to atmospheric methane variability. *Nature,* 443**,** 439.

Bréant, C., P. Martinerie, A. Orsi, L. Arnaud & A. Landais (2017) Modelling firn thickness evolution during the last deglaciation: constraints on sensitivity to temperature and impurities. *Climate of the Past,* 13**,** 833-853.

Brook, E. J., S. Harder, J. Sevennghaus, E. J. Steig & C. M. Suche (2000) On the origin and timing of rapid changes in atmospheric methane during the last glacial period. *Global Biogeochemical Cycles,* 14**,** 559-572.

Brook, E. J., T. Sowers & J. Orchardo (1996a) Rapid Variations in Atmospheric Methane Concentration During the Past 110,000 Years. *Science,* 273**,** 1087-1091.

Buizert, C., K. Cuffey, J. Severinghaus, D. Baggenstos, T. Fudge, E. Steig, B. Markle, M. Winstrup, R. Rhodes & E. Brook (2015) The WAIS Divide deep ice core WD2014 chronology–Part 1: Methane synchronization (68–31 ka BP) and the gas age–ice age difference. *Climate of the Past,* 11**,** 153-173.

Buizert, C. & J. P. Severinghaus (2016) Dispersion in deep polar firn driven by synoptic-scale surface pressure variability. *The Cryosphere,* 10**,** 2099-2111.

Buizert, C. (2012) The influence of firn air transport processes and radiocarbon production on gas records from polar firn and ice. PhD Thesis, University of Copenhagen.

Capron, E., A. Landais, B. Lemieux-Dudon, A. Schilt, V. Masson-Delmotte, D. Buiron, J. Chappellaz, D. Dahl-Jensen, S. Johnsen, M. Leuenberger, L. Loulergue & H. Oerter (2010) Synchronising EDML and NorthGRIP ice cores using δ18O of atmospheric oxygen (δ18Oatm) and CH4 measurements over MIS5 (80–123 kyr). *Quaternary Science Reviews,* 29**,** 222-234.

Chappellaz, J., T. Blunier, S. Kints, A. Dällenbach, J. M. Barnola, J. Schwander, D. Raynaud & B. Stauffer (1997) Changes in the atmospheric CH4 gradient between Greenland and Antarctica during the Holocene. *Journal of Geophysical Research: Atmospheres,* 102**,** 15987-15997.

Chappellaz, J., T. Bluniert, D. Raynaud, J. M. Barnola, J. Schwander & B. Stauffert (1993) Synchronous changes in atmospheric CH4 and Greenland climate between 40 and 8 kyr BP. *Nature,* 366**,** 443.

Chappellaz, J., C. Stowasser, T. Blunier, D. Baslev-Clausen, E. J. Brook, R. Dallmayr, X. Faïn, J. E. Lee, L. E. Mitchell, O. Pascual, D. Romanini, J. Rosen & S. Schüpbach (2013) High-resolution glacial and deglacial record of atmospheric methane by continuous-flow and laser spectrometer analysis along the NEEM ice core. *Clim. Past,* 9**,** 2579-2593.

Charbit, S., C. Ritz, G. Philippon, V. Peyaud & M. Kageyama (2007) Numerical reconstructions of the Northern Hemisphere ice sheets through the last glacial-interglacial cycle. *Climate of the Past,* 3**,** 15-37.

Cohen, K., S. Finney, P. Gibbard & J.-X. Fan (2013) The ICS international chronostratigraphic chart. *Episodes,* 36**,** 199-204.

Collins, W., S. Sitch & O. Boucher (2010) How vegetation impacts affect climate metrics for ozone precursors. *Journal of Geophysical Research: Atmospheres,* 115.

Conroy, J. L., J. T. Overpeck, J. E. Cole, T. M. Shanahan & M. Steinitz-Kannan (2008) Holocene changes in eastern tropical Pacific climate inferred from a Galápagos lake sediment record. *Quaternary Science Reviews,* 27**,** 1166-1180.

Craig, H., Y. Horibe & T. Sowers (1988) Gravitational separation of gases and isotopes in polar ice caps. *Science,* 242**,** 1675-1678.

Crutzen, P. J. & L. T. Gidel (1983) A two-dimensional photochemical model of the atmosphere: 2. The tropospheric budgets of the anthropogenic chlorocarbons CO, CH4, CH3Cl and the effect of various NO x sources on tropospheric ozone. *Journal of Geophysical Research: Oceans,* 88**,** 6641-6661.

Cuffey, K. M., G. D. Clow, E. J. Steig, C. Buizert, T. Fudge, M. Koutnik, E. D. Waddington, R. B. Alley & J. P. Severinghaus (2016) Deglacial temperature history of West Antarctica. *Proceedings of the National Academy of Sciences,* 113**,** 14249-14254.

Cuffey, K. M. & W. S. B. Paterson. 2010. *The physics of glaciers*. Academic Press.

Curry, C. L. (2007) Modeling the soil consumption of atmospheric methane at the global scale. *Global Biogeochemical Cycles,* 21.

Dahl-Jensen, D., M. Albert, A. Aldahan, N. Azuma, D. Balslev-Clausen, M. Baumgartner, A.-M. Berggren, M. Bigler, T. Binder & T. Blunier (2013) Eemian interglacial reconstructed from a Greenland folded ice core. *Nature,* 493**,** 489.

Dällenbach, A., T. Blunier, J. Flückiger, B. Stauffer, J. Chappellaz & D. Raynaud (2000) Changes in the atmospheric CH4 gradient between Greenland and Antarctica during the Last Glacial and the transition to the Holocene. *Geophysical Research Letters,* 27**,** 1005-1008.

Dansgaard, W., S. J. Johnsen, H. B. Clausen, D. Dahl-Jensen, N. S. Gundestrup, C. U. Hammer, C. S. Hvidberg, J. P. Steffensen, A. E. Sveinbjörnsdottir, J. Jouzel & G. Bond (1993) Evidence for general instability of past climate from a 250-kyr ice-core record. *Nature,* 364**,** 218.

de Vernal, A., G. H. Miller & C. Hillaire-Marcel (1991) Paleoenvironments of the last interglacial in northwest north atlantic region and adjacent mainland Canada. *Quaternary International,* 10-12**,** 95-106.

Delmotte, M., J. Chappellaz, E. Brook, P. Yiou, J. M. Barnola, C. Goujon, D. Raynaud & V. I. Lipenkov (2004) Atmospheric methane during the last four glacial-interglacial cycles: Rapid changes and their link with Antarctic temperature. *Journal of Geophysical Research: Atmospheres,* 109.

Dieser, M., E. L. J. E. Broemsen, K. A. Cameron, G. M. King, A. Achberger, K. Choquette, B. Hagedorn, R. Sletten, K. Junge & B. C. Christner (2014) Molecular and biogeochemical evidence for methane cycling beneath the western margin of the Greenland Ice Sheet. *The Isme Journal,* 8**,** 2305.

Dlugokencky, E., L. Bruhwiler, J. White, L. Emmons, P. C. Novelli, S. A. Montzka, K. A. Masarie, P. M. Lang, A. Crotwell & J. B. Miller (2009) Observational constraints on recent increases in the atmospheric CH4 burden. *Geophysical Research Letters,* 36.

Dlugokencky, E.J., P.M. Lang, A.M. Crotwell, J.W. Mund, M.J. Crotwell, and K.W. Thoning (2018) Atmospheric Methane Dry Air Mole Fractions from the NOAA ESRL Carbon Cycle

Cooperative Global Air Sampling Network, 1983-2017, Version: 2018-08-01, Path: ftp://aftp.cmdl.noaa.gov/data/trace_gases/ch4/flask/surface/ .

Dlugokencky, E., R. Myers, P. Lang, K. Masarie, A. Crotwell, K. Thoning, B. Hall, J. Elkins & L. Steele (2005) Conversion of NOAA atmospheric dry air CH4 mole fractions to a gravimetrically prepared standard scale. *Journal of Geophysical Research: Atmospheres,* 110.

Dutaur, L. & L. V. Verchot (2007) A global inventory of the soil CH4 sink. *Global Biogeochemical Cycles,* 21.

Edwards, G. C., H. Neumann, G. Den Hartog, G. Thurtell & G. Kidd (1994) Eddy correlation measurements of methane fluxes using a tunable diode laser at the Kinosheo Lake tower site during the Northern Wetlands Study (NOWES). *Journal of Geophysical Research: Atmospheres,* 99**,** 1511-1517.

Eroglu, D., F. H. McRobie, I. Ozken, T. Stemler, K.-H. Wyrwoll, S. F. M. Breitenbach, N. Marwan & J. Kurths (2016) See–saw relationship of the Holocene East Asian–Australian summer monsoon. *Nature Communications,* 7**,** 12929.

Etheridge, D. M., L. P. Steele, R. Francey & R. Langenfelds (1998) Atmospheric methane between 1000 AD and present: Evidence of anthropogenic emissions and climatic variability. *Journal of Geophysical Research: Atmospheres,* 103**,** 15979-15993.

Fan, S., S. C. Wofsy, P. Bakwin, D. J. Jacob, S. Anderson, P. Kebabian, J. McManus, C. Kolb & D. Fitzjarrald (1992) Micrometeorological measurements of CH4 and CO2 exchange between the atmosphere and subarctic tundra. *Journal of Geophysical Research: Atmospheres,* 97**,** 16627-16643.

Feilberg, K. L., D. W. Griffith, M. S. Johnson & C. J. Nielsen (2005) The 13C and D kinetic isotope effects in the reaction of CH4 with Cl. *International journal of chemical kinetics,* 37**,** 110-118.

Fischer, H., M. Behrens, M. Bock, U. Richter, J. Schmitt, L. Loulergue, J. Chappellaz, R. Spahni, T. Blunier, M. Leuenberger & T. F. Stocker (2008) Changing boreal methane sources and constant biomass burning during the last termination. *Nature,* 452**,** 864.

Fleitmann, D., S. J. Burns, A. Mangini, M. Mudelsee, J. Kramers, I. Villa, U. Neff, A. A. Al-Subbary, A. Buettner, D. Hippler & A. Matter (2007) Holocene ITCZ and Indian monsoon dynamics recorded in stalagmites from Oman and Yemen (Socotra). *Quaternary Science Reviews,* 26**,** 170-188.

Flückiger, J., T. Blunier, B. Stauffer, J. Chappellaz, R. Spahni, K. Kawamura, J. Schwander, T. F. Stocker & D. Dahl-Jensen (2004) N_2O and CH_4 variations during the last glacial epoch: Insight into global processes. *Global Biogeochemical Cycles,* 18**,** 1-14.

Fourteau, K., X. Faïn, P. Martinerie, A. Landais, A. A. Ekaykin, V. Y. Lipenkov & J. Chappellaz (2017) Analytical constraints on layered gas trapping and smoothing of atmospheric variability in ice under low-accumulation conditions. *Clim. Past,* 13**,** 1815-1830.

Gasse, F. & E. Van Campo (2001) Late Quaternary environmental changes from a pollen and diatom record in the southern tropics (Lake Tritrivakely, Madagascar). *Palaeogeography, Palaeoclimatology, Palaeoecology,* 167**,** 287-308.

Gkinis, V., T. J. Popp, S. J. Johnsen & T. Blunier (2010) A continuous stream flash evaporator for the calibration of an IR cavity ring-down spectrometer for the isotopic analysis of water. *Isotopes in environmental and health studies,* 46**,** 463-475.

Grinsted, A., J. C. Moore & S. Jevrejeva (2004) Application of the cross wavelet transform and wavelet coherence to geophysical time series. *Nonlinear processes in geophysics,* 11**,** 561-566.

Hansen, J., M. Sato, G. Russell & P. Kharecha (2013) Climate sensitivity, sea level and atmospheric carbon dioxide. *Philosophical Transactions of the Royal Society A: Mathematical, Physical and Engineering Sciences,* 371.

Hansson, M. E. (1994) The Renland ice core. A Northern Hemisphere record of aerosol composition over 120,000 years. *Tellus B: Chemical and Physical Meteorology,* 46**,** 390-418.

Harder, S., D. Shindell, G. Schmidt & E. Brook (2007) A global climate model study of CH4 emissions during the Holocene and glacial-interglacial transitions constrained by ice core data. *Global Biogeochemical Cycles,* 21.

IPCC. 2013. *Climate Change 2013: The Physical Science Basis. Contribution of Working Group I to the Fifth Assessment Report of the Intergovernmental Panel on Climate Change*. Cambridge, United Kingdom and New York, NY, USA: Cambridge University Press.

Ito, A. & M. Inatomi (2012) Use of a process-based model for assessing the methane budgets of global terrestrial ecosystems and evaluation of uncertainty. *Biogeosciences,* 9**,** 759-773.

Joos, F. & R. Spahni (2008) Rates of change in natural and anthropogenic radiative forcing over the past 20,000 years. *Proceedings of the National Academy of Sciences,* 105**,** 1425-1430.

Jouzel, J., V. Masson-Delmotte, O. Cattani, G. Dreyfus, S. Falourd, G. Hoffmann, B. Minster, J. Nouet, J. Barnola & J. Chappellaz (2007) EPICA Dome C ice core 800KYr deuterium data and temperature estimates. *IGBP PAGES/World Data Center for Paleoclimatology data contribution series,* 91**,** 2007.

Kameda, T. & R. Naruse (1994) Characteristics of bubble volumes in firn-ice transition layers of ice cores from polar ice sheets. *Annals of Glaciology,* 20**,** 95-100.

Kaplan, J. O., G. Folberth & D. A. Hauglustaine (2006) Role of methane and biogenic volatile organic compound sources in late glacial and Holocene fluctuations of atmospheric methane concentrations. *Global Biogeochemical Cycles,* 20.

Kaufmann, P. R., U. Federer, M. A. Hutterli, M. Bigler, S. Schüpbach, U. Ruth, J. Schmitt & T. F. Stocker (2008) An improved continuous flow analysis system for high-resolution field measurements on ice cores. *Environmental science & technology,* 42**,** 8044-8050.

Khalil, M. A. K. 2000. Atmospheric methane: an introduction. In *Atmospheric Methane*, 1-8. Springer.

Kiehl, J. T. & K. E. Trenberth (1997) Earth's annual global mean energy budget. *Bulletin of the American Meteorological Society,* 78**,** 197-208.

Kindler, P., M. Guillevic, M. Baumgartner, J. Schwander, A. Landais & M. Leuenberger (2014) Temperature reconstruction from 10 to 120 kyr b2k from the NGRIP ice core. *Climate of the Past,* 10**,** 887–902.

Kobashi, T., J. P. Severinghaus, E. J. Brook, J.-M. Barnola & A. M. Grachev (2007) Precise timing and characterization of abrupt climate change 8200 years ago from air trapped in polar ice. *Quaternary Science Reviews,* 26**,** 1212-1222.

Köhler, P., G. Knorr, D. Buiron, A. Lourantou & J. Chappellaz (2011) Abrupt rise in atmospheric CO2 at the onset of the Bølling/Allerød: in-situ ice core data versus true atmospheric signal. *Climate of the Past,* 7**,** 473-486.

Köhler, P., C. Nehrbass-Ahles, J. Schmitt, T. F. Stocker & H. Fischer (2017) A 156 kyr smoothed history of the atmospheric greenhouse gases CO2, CH4, and N2O and their radiative forcing. *Earth Syst. Sci. Data,* 9**,** 363-387.

Krinner, G., J. Mangerud, M. Jakobsson, M. Crucifix, C. Ritz & J. I. Svendsen (2004) Enhanced ice sheet growth in Eurasia owing to adjacent ice-dammed lakes. *Nature,* 427**,** 429.

Lachniet, M. S., Y. Asmerom, S. J. Burns, W. P. Patterson, V. J. Polyak & G. O. Seltzer (2004) Tropical response to the 8200 yr BP cold event? Speleothem isotopes indicate a weakened early Holocene monsoon in Costa Rica. *Geology,* 32**,** 957-960.

Lee et al., Roosvelt ISland ice corE (RISE) continuous flow analysis results (in prep.)

Lee, J.E., Edwards, J.S., Schmitt, J., Brook, E. J., Bock, M., Fischer, H. (2018). The fidelity of ice core methane records: excess methane in Greenlandic ice cores associated with high dust concentrations. *SCAR/IASC Open Science Conference, 19-23 June 2018, Davos, Switzerland.*

Lee, J.E., J. S. Edwards, J. Schmitt, E. J. Brook, M. Bock, H. Fischer. Excess methane in Greenland ice cores associated with high dust concentrations (in prep.)

Levine, J., E. Wolff, P. Hopcroft & P. Valdes (2012) Controls on the tropospheric oxidizing capacity during an idealized Dansgaard-Oeschger event, and their implications for the rapid rises in atmospheric methane during the last glacial period. *Geophysical Research Letters,* 39.

Levine, J., E. Wolff, A. Jones, L. Sime, P. Valdes, A. Archibald, G. Carver, N. Warwick & J. Pyle (2011) Reconciling the changes in atmospheric methane sources and sinks between the Last Glacial Maximum and the pre-industrial era. *Geophysical Research Letters,* 38.

Lisiecki, L. E. & M. E. Raymo (2005) A Pliocene-Pleistocene stack of 57 globally distributed benthic δ18O records. *Paleoceanography,* 20.

Long, K. D., L. B. Flanagan & T. Cai (2010) Diurnal and seasonal variation in methane emissions in a northern Canadian peatland measured by eddy covariance. *Global change biology,* 16**,** 2420-2435.

Loulergue, L., A. Schilt, R. Spahni, V. Masson-Delmotte, T. Blunier, B. Lemieux, J.-M. Barnola, D. Raynaud, T. F. Stocker & J. Chappellaz (2008) Orbital and millennial-scale features of atmospheric CH4 over the past 800,000 years. *Nature,* 453**,** 383.

Lozhkin, A., P. Anderson, T. Matrosova & P. Minyuk (2007) The pollen record from El'gygytgyn Lake: implications for vegetation and climate histories of northern Chukotka since the late middle Pleistocene. *Journal of Paleolimnology,* 37**,** 135-153.

Lüthi, D., M. Le Floch, B. Bereiter, T. Blunier, J.-M. Barnola, U. Siegenthaler, D. Raynaud, J. Jouzel, H. Fischer, K. Kawamura & T. F. Stocker (2008) High-resolution carbon dioxide concentration record 650,000–800,000 years before present. *Nature,* 453**,** 379.

MacDonald, G. M., D. W. Beilman, K. V. Kremenetski, Y. Sheng, L. C. Smith & A. A. Velichko (2006) Rapid early development of circumarctic peatlands and atmospheric CH4 and CO2 variations. *Science,* 314**,** 285-288.

Maeno, N. & T. Ebinuma (1983) Pressure sintering of ice and its implication to the densification of snow at polar glaciers and ice sheets. *The Journal of Physical Chemistry,* 87**,** 4103-4110.

Marcott, S. A., J. D. Shakun, P. U. Clark & A. C. Mix (2013) A reconstruction of regional and global temperature for the past 11,300 years. *science,* 339**,** 1198-1201.

Marik, T. 1998. Atmospheric d13C and dD measurements to balance the global methane budget.

Meltzner, A. J., A. D. Switzer, B. P. Horton, E. Ashe, Q. Qiu, D. F. Hill, S. L. Bradley, R. E. Kopp, E. M. Hill, J. M. Majewski, D. H. Natawidjaja & B. W. Suwargadi (2017) Half-metre sea-level fluctuations on centennial timescales from mid-Holocene corals of Southeast Asia. *Nature Communications,* 8**,** 14387.

Members, W. D. P., T. J. Fudge, E. J. Steig, B. R. Markle, S. W. Schoenemann, Q. Ding, K. C. Taylor, J. R. McConnell, E. J. Brook, T. Sowers, J. W. C. White, R. B. Alley, H. Cheng, G. D. Clow, J. Cole-Dai, H. Conway, K. M. Cuffey, J. S. Edwards, R. Lawrence Edwards, R. Edwards, J. M. Fegyveresi, D. Ferris, J. J. Fitzpatrick, J. Johnson, G. Hargreaves, J. E. Lee, O. J. Maselli, W. Mason, K. C. McGwire, L. E. Mitchell, N. Mortensen, P. Neff, A. J. Orsi, T. J. Popp, A. J. Schauer, J. P. Severinghaus, M. Sigl, M. K. Spencer, B. H. Vaughn, D. E. Voigt, E. D. Waddington, X. Wang & G. J. Wong (2013) Onset of deglacial warming in West Antarctica driven by local orbital forcing. *Nature,* 500**,** 440.

Miller, G. H., W. N. Mode, A. P. Wolfe, P. E. Sauer, O. Bennike, S. L. Forman, S. K. Short & T. W. Stafford (1999) Stratified interglacial lacustrine sediments from Baffin Island, Arctic Canada: chronology and paleoenvironmental implications. *Quaternary Science Reviews,* 18, 789-810.

Mitchell, L., E. Brook, J. E. Lee, C. Buizert & T. Sowers (2013) Constraints on the Late Holocene Anthropogenic Contribution to the Atmospheric Methane Budget. *Science,* 342, 964-966.

Mitchell, L. E., E. J. Brook, T. Sowers, J. McConnell & K. Taylor (2011) Multidecadal variability of atmospheric methane, 1000–1800 CE. *Journal of Geophysical Research: Biogeosciences,* 116.

Mitchell, L. E., C. Buizert, E. J. Brook, D. J. Breton, J. Fegyveresi, D. Baggenstos, A. Orsi, J. Severinghaus, R. B. Alley, M. Albert, R. H. Rhodes, J. R. McConnell, M. Sigl, O. Maselli, S. Gregory & J. Ahn (2015) Observing and modeling the influence of layering on bubble trapping in polar firn. *Journal of Geophysical Research: Atmospheres,* 120, 2558–2574.

Monnin, E., A. Indermühle, A. Dällenbach, J. Flückiger, B. Stauffer, T. F. Stocker, D. Raynaud & J.-M. Barnola (2001) Atmospheric CO<sub>2</sub> Concentrations over the Last Glacial Termination. *Science,* 291, 112.

Monteil, G., S. Houweling, E. Dlugockenky, G. Maenhout, B. Vaughn, J. White & T. Rockmann (2011) Interpreting methane variations in the past two decades using measurements of CH 4 mixing ratio and isotopic composition. *Atmospheric Chemistry and Physics,* 11, 9141-9153.

Myhre, G., E. J. Highwood, K. P. Shine & F. Stordal (1998) New estimates of radiative forcing due to well mixed greenhouse gases. *Geophysical research letters,* 25, 2715-2718.

Neef, L., M. van Weele & P. van Velthoven (2010) Optimal estimation of the present-day global methane budget. *Global biogeochemical cycles,* 24.

Ono, R. & T. Oda (2003) Dynamics of ozone and OH radicals generated by pulsed corona discharge in humid-air flow reactor measured by laser spectroscopy. *Journal of applied physics,* 93, 5876-5882.

Overend, R., G. Paraskevopoulos & R. Cvetanović (1975) Rates of OH radical reactions. I. Reactions with H2, CH4, C2H6, and C3H8 at 295 K. *Canadian Journal of Chemistry,* 53, 3374-3382.

Parmentier, F. J. W., W. Zhang, Y. Mi, X. Zhu, J. Huissteden, D. J. Hayes, Q. Zhuang, T. R. Christensen & A. D. McGuire (2015) Rising methane emissions from northern wetlands associated with sea ice decline. *Geophysical research letters,* 42, 7214-7222.

Pearman, G., D. Etheridge, F. De Silva & P. Fraser (1986) Evidence of changing concentrations of atmospheric CO2, N2O and CH4 from air bubbles in Antarctic ice. *Nature,* 320, 248.

Petit, J. R., J. Jouzel, D. Raynaud, N. I. Barkov, J. M. Barnola, I. Basile, M. Bender, J. Chappellaz, M. Davis, G. Delaygue, M. Delmotte, V. M. Kotlyakov, M. Legrand, V. Y. Lipenkov, C. Lorius, L. PÉpin, C. Ritz, E. Saltzman & M. Stievenard (1999) Climate and atmospheric history of the past 420,000 years from the Vostok ice core, Antarctica. *Nature,* 399, 429.

Portnov, A., S. Vadakkepuliyambatta, J. Mienert & A. Hubbard (2016) Ice-sheet-driven methane storage and release in the Arctic. *Nature Communications,* 7, 10314.

Prather, M. J., C. D. Holmes & J. Hsu (2012) Reactive greenhouse gas scenarios: Systematic exploration of uncertainties and the role of atmospheric chemistry. *Geophysical Research Letters,* 39.

Rasmussen, S. O., M. Bigler, S. P. Blockley, T. Blunier, S. L. Buchardt, H. B. Clausen, I. Cvijanovic, D. Dahl-Jensen, S. J. Johnsen, H. Fischer, V. Gkinis, M. Guillevic, W. Z. Hoek, J. J. Lowe, J. B. Pedro, T. Popp, I. K. Seierstad, J. P. Steffensen, A. M. Svensson, P. Vallelonga, B. M. Vinther, M. J. C. Walker, J. J. Wheatley & M. Winstrup (2014) A stratigraphic framework for abrupt climatic changes during the Last Glacial period based on three synchronized Greenland ice-core records: refining and extending the INTIMATE event stratigraphy. *Quaternary Science Reviews,* 106**,** 14-28.

Rella, C. (2010) Accurate greenhouse gas measurements in humid gas streams using the Picarro G1301 carbon dioxide/methane/water vapor gas analyzer. *White paper, Picarro Inc, Sunnyvale, CA, USA*.

Revel, M., E. Ducassou, F. E. Grousset, S. M. Bernasconi, S. Migeon, S. Revillon, J. Mascle, A. Murat, S. Zaragosi & D. Bosch (2010) 100,000 Years of African monsoon variability recorded in sediments of the Nile margin. *Quaternary Science Reviews,* 29**,** 1342-1362.

Rhodes, R. H. 2015. WAIS Divide Ice Core 67.2-9.8 kaBP Continuous CH4 Data, original data file. Boulder: WDC Boulder and NOAA.

Rhodes, R. H., E. J. Brook, J. R. McConnell, T. Blunier, L. C. Sime, X. Faïn & R. Mulvaney (2017) Atmospheric methane variability: Centennial-scale signals in the Last Glacial Period. *Global Biogeochemical Cycles,* 31**,** 575-590.

Rhodes, R. H., X. Faïn, E. J. Brook, J. R. McConnell, O. J. Maselli, M. Sigl, J. Edwards, C. Buizert, T. Blunier & J. Chappellaz (2016) Local artifacts in ice core methane records caused by layered bubble trapping and in situ production: a multi-site investigation. *Climate of the Past,* 12**,** 1061-1077.

Rhodes, R. H., X. Faïn, C. Stowasser, T. Blunier, J. Chappellaz, J. R. McConnell, D. Romanini, L. E. Mitchell & E. J. Brook (2013) Continuous methane measurements from a late Holocene Greenland ice core: Atmospheric and in-situ signals. *Earth and Planetary Science Letters,* 368**,** 9-19.

Rosen, J. L., E. J. Brook, J. P. Severinghaus, T. Blunier, L. E. Mitchell, J. E. Lee, J. S. Edwards & V. Gkinis (2014) An ice core record of near-synchronous global climate changes at the Bølling transition. *Nature Geoscience,* 7**,** 459.

Royer, D. L., R. A. Berner, I. P. Montañez, N. J. Tabor & D. J. Beerling (2004) Co~ 2 as a primary driver of phanerozoic climate. *GSA today,* 14**,** 4-10.

Salamatin, A. N., V. Ya. Lipenkov, J. M. Barnola, A. Hori, P. Duval & T. Hondoh (2009) Snow/firn densification in polar ice sheets. *低温科学= Low Temperature Science,* 68**,** 195-222.

Salamatin A.N., V.Ya. Lipenkov, J.M. Barnola, A. Hori, P. Duval and T. Hondoh (2006) Basic approaches to dry snow-fim densification modeling. *Mater. Glyatsiol. Issled. (Data of Glaciological Studies)*, 101, 3-16.

Sánchez Goñi, M. F., E. Bard, A. Landais, L. Rossignol & F. d'Errico (2013) Air–sea temperature decoupling in western Europe during the last interglacial–glacial transition. *Nature Geoscience,* 6**,** 837.

Sánchez Goñi, M. F., A. Landais, W. J. Fletcher, F. Naughton, S. Desprat & J. Duprat (2008) Contrasting impacts of Dansgaard–Oeschger events over a western European latitudinal transect modulated by orbital parameters. *Quaternary Science Reviews,* 27**,** 1136-1151.

Sapart, C. J., G. Monteil, M. Prokopiou, R. S. W. van de Wal, J. O. Kaplan, P. Sperlich, K. M. Krumhardt, C. van der Veen, S. Houweling, M. C. Krol, T. Blunier, T. Sowers, P. Martinerie, E. Witrant, D. Dahl-Jensen & T. Röckmann (2012) Natural and anthropogenic variations in methane sources during the past two millennia. *Nature,* 490**,** 85.

Schilt, A., M. Baumgartner, T. Blunier, J. Schwander, R. Spahni, H. Fischer & T. F. Stocker (2010) Glacial–interglacial and millennial-scale variations in the atmospheric nitrous oxide concentration during the last 800,000 years. *Quaternary Science Reviews,* 29**,** 182-192.

Schmitt, J., R. Schneider & H. Fischer (2011) A sublimation technique for high-precision measurements of δ 13 CO 2 and mixing ratios of CO 2 and N 2 O from air trapped in ice cores. *Atmospheric Measurement Techniques,* 4**,** 1445-1461.

Schüpbach, S., U. Federer, P. R. Kaufmann, M. A. Hutterli, D. Buiron, T. Blunier, H. Fischer & T. F. Stocker (2009) A New Method for High-Resolution Methane Measurements on Polar Ice Cores Using Continuous Flow Analysis. *Environmental Science & Technology,* 43**,** 5371-5376.

Schwander, J. (1989) The transformation of snow to ice and the occlusion of gases. *The environmental record in glaciers and ice sheets***,** 53-67.

Sebacher, D. I., R. C. Harriss, K. B. Bartlett, S. M. Sebacher & S. S. Grice (1986) Atmospheric methane sources: Alaskan tundra bogs, an alpine fen, and a subarctic boreal marsh. *Tellus B,* 38**,** 1-10.

Seinfeld, J. H. & S. N. Pandis. 2012. *Atmospheric chemistry and physics: from air pollution to climate change*. John Wiley & Sons.

Serov, P., S. Vadakkepuliyambatta, J. Mienert, H. Patton, A. Portnov, A. Silyakova, G. Panieri, M. Carroll, J. Carroll, K. Andreassen & A. Hubbard (2017) The post-glacial response of Arctic Ocean gas hydrates to climatic amelioration. *PNAS,* 114**,** 6215-6220.

Severinghaus, J. P. 1995. Studies of the terrestrial O2 and carbon cycles in sand dune gases and in Biosphere 2. Oak Ridge Associated Universities, Inc., TN (United States).

Severinghaus, J. P., M. R. Albert, Z. R. Courville, M. A. Fahnestock, K. Kawamura, S. A. Montzka, J. Mühle, T. A. Scambos, E. Shields, C. A. Shuman, M. Suwa, P. Tans & R. F. Weiss (2010) Deep air convection in the firn at a zero-accumulation site, central Antarctica. *Earth and Planetary Science Letters,* 293**,** 359-367.

Severinghaus, J. P., M. L. Bender, R. F. Keeling & W. S. Broecker (1996) Fractionation of soil gases by diffusion of water vapor, gravitational settling, and thermal diffusion. *Geochimica et Cosmochimica Acta,* 60**,** 1005-1018.

Shallcross, D. E., M. A. K. Khalil & C. L. Butenhoff (2007) 11 The Atmospheric Methane Sink. *Greenhouse Gas Sinks***,** 171.

Shieh, S. Y. & J. Evans (1991) The stability of cylindrical voids and of cylinders subject to closure by viscous flow or evaporation/condensation. *Journal of applied physics,* 70**,** 2968-2972.

Shindell, D. T., G. Faluvegi, D. M. Koch, G. A. Schmidt, N. Unger & S. E. Bauer (2009) Improved attribution of climate forcing to emissions. *Science,* 326**,** 716-718.

Siegenthaler, U., T. F. Stocker, E. Monnin, D. Lüthi, J. Schwander, B. Stauffer, D. Raynaud, J.-M. Barnola, H. Fischer, V. Masson-Delmotte & J. Jouzel (2005) Stable Carbon Cycle&#150;Climate Relationship During the Late Pleistocene. *Science,* 310**,** 1313.

Sigg, A., K. Fuhrer, M. Anklin, T. Staffelbach & D. Zurmuehle (1994) A continuous analysis technique for trace species in ice cores. *Environmental science & technology,* 28**,** 204-209.

Sigl, M., A, T. Fudge, A, M. Winstrup, A, J. Cole-Dai, D. Ferris, A, J. Mcconnell, A, K. Taylor, A, K. Welten, A, T. Woodruff, A, F. Adolphi, A, M. Bisiaux, A, E. Brook, A, C. Buizert, A, M. Caffee, A, N. Dunbar, A, R. Edwards, A, L. Geng, A, N. Iverson, A, B. Koffman, A, L. Layman, A, O. Maselli, A, K. Mcgwire, A, R. Muscheler, R, K. Nishiizumi, A, D. Pasteris, A, R. Rhodes, A & T. Sowers, A (2016) The WAIS Divide deep ice core WD2014 chronology - Part 2: Annual-layer counting (0-31 ka BP). *Climate of the Past,* 12**,** 769 - 786.

Simonsen, M.F., Baccolo, G., Blunier, T., Borunda, A., Delmonte, B., Goldstein, S., Grinsted, A., Kjær, H.A., Sowers, T., Svensson, A., Vinther, B., Vladimirova, D., Winckler, G., Winstrup, M., Vallelonga, P. Local ice core dust reveals past glacier extent in East Greenland (in prep.)

Smith, L. C., G. M. MacDonald, A. A. Velichko, D. W. Beilman, O. K. Borisova, K. E. Frey, K. V. Kremenetski & Y. Sheng (2004) Siberian Peatlands a Net Carbon Sink and Global Methane Source Since the Early Holocene. *Science,* 303**,** 353-356.

Sowers, T. (2006) Late Quaternary Atmospheric CH₄ Isotope Record Suggests Marine Clathrates Are Stable. *Science,* 311**,** 838-840.

--- (2010) Atmospheric methane isotope records covering the Holocene period. *Quaternary Science Reviews,* 29**,** 213-221.

Sowers, T., M. Bender & D. Raynaud (1989) Elemental and isotopic composition of occluded O2 and N2 in polar ice. *Journal of Geophysical Research: Atmospheres,* 94**,** 5137-5150.

Spahni, R., J. Chappellaz, T. F. Stocker, L. Loulergue, G. Hausammann, K. Kawamura, J. Flückiger, J. Schwander, D. Raynaud, V. Masson-Delmotte & J. Jouzel (2005) Atmospheric Methane and Nitrous Oxide of the Late Pleistocene from Antarctic Ice Cores. *Science,* 310**,** 1317.

Spahni, R., J. Schwander, J. Flückiger, B. Stauffer, J. Chappellaz & D. Raynaud (2003) The attenuation of fast atmospheric CH4 variations recorded in polar ice cores. *Geophysical Research Letters,* 30.

Spahni, R., R. Wania, P. van Velthoven, L. Neef, M. van Wheele, I. Pison, P. Bousquet, C. Frankenberg, P. Foster & F. Joos (2011) Constraining global methane emissions and uptake by ecosystems.

Sperlich, P., H. Schaefer, S. E. Mikaloff-Fletcher, M. Guillevic, K. Lassey, C. J. Sapart, T. Röckmann & T. Blunier (2015) Carbon isotope ratios suggest no additional methane from boreal wetlands during the rapid Greenland Interstadial 21.2. *Global Biogeochemical Cycles,* 29**,** 1-15.

Stauffer, B., G. Fischer, A. Neftel & H. Oeschger (1985) Increase of Atmospheric Methane Recorded in Antarctic Ice Core. *Science,* 229**,** 1386.

Stibal, M., J. L. Wadham, G. P. Lis, J. Telling, R. D. Pancost, A. Dubnick, M. J. Sharp, E. C. Lawson, C. E. Butler & F. Hasan (2012) Methanogenic potential of Arctic and Antarctic subglacial environments with contrasting organic carbon sources. *Global Change Biology,* 18**,** 3332-3345.

Stowasser, C., C. Buizert, V. Gkinis, J. Chappellaz, S. Schüpbach, M. Bigler, X. Faïn, P. Sperlich, M. Baumgartner, A. Schilt & T. Blunier (2012) Continuous measurements of methane mixing ratios from ice cores. *Atmospheric Measurement Techniques,* 5**,** 999- 1013.

Stowasser, C., A. Farinas, J. Ware, D. Wistisen, C. Rella, E. Wahl, E. Crosson & T. Blunier (2014) A low-volume cavity ring-down spectrometer for sample-limited applications. *Applied Physics B,* 116**,** 255-270.

Stowasser, C. (2010) A novel laser-based technique for continuous measurements of methane concentrations from deep ice cores. MSc Thesis, University of Copenhagen.

Suyker, A. E., S. B. Verma, R. J. Clement & D. P. Billesbach (1996) Methane flux in a boreal fen: Season-long measurement by eddy correlation. *Journal of Geophysical Research: Atmospheres,* 101**,** 28637-28647.

Svendsen, J. I., L. C. Krüger, J. Mangerud, V. I. Astakhov, A. Paus, D. Nazarov & A. Murray (2014) Glacial and vegetation history of the Polar Ural Mountains in northern Russia during the last ice age, marine isotope stages 5–2. *Quaternary Science Reviews,* 92**,** 409-428.

Svensson, A., M. Bigler, T. Blunier, H. B. Clausen, D. Dahl-Jensen, H. Fischer, S. Fujita, K. Goto-Azuma, S. Johnsen & K. Kawamura (2013) Direct linking of Greenland and Antarctic ice cores at the Toba eruption (74 ka BP). *Climate of the Past,* 9**,** 749-766.

Tarnocai, C., J. Canadell, E. Schuur, P. Kuhry, G. Mazhitova & S. Zimov (2009) Soil organic carbon pools in the northern circumpolar permafrost region. *Global biogeochemical cycles,* 23.

Telling, J., E. Boyd, N. Bone, E. Jones, M. Tranter, J. MacFarlane, P. Martin, J. Wadham, G. Lamarche-Gagnon & M. Skidmore (2015) Rock comminution as a source of hydrogen for subglacial ecosystems. *Nature Geoscience,* 8**,** 851.

Thomas, E. R., E. W. Wolff, R. Mulvaney, J. P. Steffensen, S. J. Johnsen, C. Arrowsmith, J. W. C. White, B. Vaughn & T. Popp (2007) The 8.2ka event from Greenland ice cores. *Quaternary Science Reviews,* 26**,** 70-81.

Tierney, J. E., N. J. Abram, K. J. Anchukaitis, M. N. Evans, C. Giry, K. H. Kilbourne, C. P. Saenger, H. C. Wu & J. Zinke (2015) Tropical sea surface temperatures for the past four centuries reconstructed from coral archives. *Paleoceanography,* 30**,** 226-252.

Van Ommen, T. D., V. Morgan & M. A. Curran (2004) Deglacial and holocene changes in accumulation at Law Dome, East Antarctica. *Annals of Glaciology,* 39**,** 359-365.

Veizer, J., D. Ala, K. Azmy, P. Bruckschen, D. Buhl, F. Bruhn, G. A. F. Carden, A. Diener, S. Ebneth, Y. Godderis, T. Jasper, C. Korte, F. Pawellek, O. G. Podlaha & H. Strauss (1999) 87Sr/86Sr, δ13C and δ18O evolution of Phanerozoic seawater. *Chemical Geology,* 161**,** 59-88.

Voulgarakis, A., V. Naik, J.-F. Lamarque, D. T. Shindell, P. Young, M. J. Prather, O. Wild, R. Field, D. Bergmann & P. Cameron-Smith (2013) Analysis of present day and future OH and methane lifetime in the ACCMIP simulations. *Atmospheric Chemistry and Physics,* 13**,** 2563-2587.

Wen, X., B. Li, Y. Zheng, Q. Yang, D. Niu & P. Shu (2016) Early Holocene multi-centennial moisture change reconstructed from lithology, grain-size and chemical composition data in the eastern Mu Us desert and potential driving forces. *Palaeogeography, Palaeoclimatology, Palaeoecology,* 459**,** 440-452.

Whiticar, M. & H. Schaefer (2007) Constraining past global tropospheric methane budgets with carbon and hydrogen isotope ratios in ice. *Philosophical Transactions of the Royal Society A: Mathematical, Physical and Engineering Sciences,* 365**,** 1793-1828.

Wiersma, A. P. & H. Renssen (2006) Model–data comparison for the 8.2kaBP event: confirmation of a forcing mechanism by catastrophic drainage of Laurentide Lakes. *Quaternary Science Reviews,* 25**,** 63-88.

Yang, J.-W., J. Ahn, E. J. Brook & Y. Ryu (2017) Atmospheric methane control mechanisms during the early Holocene. *Climate of the Past,* 13**,** 1227-1242.

Young, P., A. Archibald, K. Bowman, J.-F. Lamarque, V. Naik, D. Stevenson, S. Tilmes, A. Voulgarakis, O. Wild & D. Bergmann (2013) Pre-industrial to end 21st century projections of tropospheric ozone from the Atmospheric Chemistry and Climate Model Intercomparison Project (ACCMIP). *Atmospheric Chemistry and Physics,* 13**,** 2063-2090.

Yu, Z., J. Loisel, P. Brosseau Daniel, W. Beilman David & J. Hunt Stephanie (2010) Global peatland dynamics since the Last Glacial Maximum. *Geophysical Research Letters,* 37.

Zachos, J., M. Pagani, L. Sloan, E. Thomas & K. Billups (2001) Trends, Rhythms, and Aberrations in Global Climate 65 Ma to Present. *Science,* 292**,** 686.

Zachos, J. C., G. R. Dickens & R. E. Zeebe (2008) An early Cenozoic perspective on greenhouse warming and carbon-cycle dynamics. *Nature,* 451**,** 279.

List of publications

Ekaykin A.A., Lipenkov V.YA., Kozachek A.V., Vladimirova D.O. Stable Water Isotope Content of the Antarctic Subglacial Lake Vostok: Implications for Understanding the Lake's Hydrology//*Isotopes in Environmental and Health Studies*, 2016; doi:10.1080/10256016.2015.1129327;

Ekaykin A.A., Vladimirova D.O., Lipenkov V. Ya., Masson-Delmotte V. Climatic variability in Princess Elizabeth Land (East Antarctica) over the last 350 years//*Clim. Past*, 2017, Vol. 13, p. 61-71; doi:10.5194/cp-13-61-2017;

PAGES2k Consortium A global multiproxy database for temperature reconstructions of the Common Era//*Nature Scientific data*, Vol. 4:170088. DOI:10.1038/sdata.2017.88;

Simonsen M.F., Baccolo G., Blunier T., Borunda A., Delmonte B., Goldstein S., Grinsted A., Kjær H.A., Sowers T., Svensson A., Vinther B., Vladimirova D., Winckler G., Winstrup M., Vallelonga P. Local ice core dust reveals past glacier extent in East Greenland (in prep.);

Madsen M. V., Steen-Larsen H. C., Hörhold M., Box J., Berben S., Capron E., Faber A.-K., Hubbard A., Jensen M., Jones T., Kipfstuhl S., Koldtoft I., Pillar H., Vaughn B., Vladimirova D., Dahl-Jensen D. Evidence of isotopic fractionation during vapor exchange between the atmosphere and the snow surface in Greenland (submitted);

Vladimirova D., Blunier T., Capron E., Dallmayr R., Ekaykin A., Gkinis V., Kjær H.A., Rasmussen S.O., Vallelonga P.T., Vinther B.M. An additional biogenic methane source 83-78 ka BP from the Northern Hemisphere (in prep.)

Special thanks

First and foremost I am deeply thankful to the Centre for Ice and Climate and all the friends and colleagues whom we had a pleasant chance to meet and collaborate, for the healthy scientific environment, for an inspirational experience. None of a great project is possible if the working environment is not pleasant. In this respect, the CIC is unique. It is the place where every day you can find a room for a quite and focused work as well as warm and social environment for a pleasant coffee or lunch break. The doors are open for the advice, one should only ask. Every PhD student is acknowledged as a grown up scientist and colleague, the ideas are considered and discussed, most of them find a lot of support to be moved forward. It is also important to conduct a research and to live a PhD life in the place full of young, responsible and energetic people and good vibes and a spirit of collaboration. This is what CIC is famous for. It could not be a better choice of place to conduct a PhD.

Especial thanks for the polar filed experience, for the long-waited opportunity to work in the field supporting the ice core drilling project. Two field seasons 2016 and 2017 at EGRIP are very memorable, they brought a lot of experience as well as field comrades and the feeling of being content with just the fact of getting in touch with the splendid world of Greenland.

This PhD project was conducted in the frame of double PhD agreement between the University of Copenhagen, Denmark, and St Petersburg State University, Russia. The host institution was the University of Copenhagen. The author is sincerely grateful to the Centre for Ice and Climate to the kind offer of support in making the agreement with no foreseen straightforward benefit for the project but with a perspective of the long-term scientific collaboration. The group of the Climate and Environment Research Laboratory at the Arctic and Antarctic Research Institute in turn supported the author generously in the moments of doubts professionally and personally wise, providing the mentoring on the way to conduct the research.

On behalf of the co-authors we are grateful to the CIC radar team for selecting a great drilling spot at the Renland ice cap in 2015, to the CIC drillers for obtaining a core of an excellent quality during the summer season 2015, RECAP (https://recap.nbi.ku.dk/about/) and Ice2Ice (https://ice2ice.w.uib.no/) collaborators for the help in the ice core processing and the CFA measurement campaign conduction in 2015-2016. The research leading to these results has received funding from the European Research Council under the European Community's Seventh Framework Programme (FP7/2007-2013) / ERC grant agreement 610055 as part of the ice2ice project.

I would like to acknowledge some of the collaborators personally: Rémi Dallmayr – for the great help in the CFA CH_4 setup construction and help in the RECAP measurement campaign preparations.

Todd Sowers – for the discrete CH_4 measurements of the RECAP ice core samples used for the calibration of the absolute CFA CH_4 values.

Christo Buizert – for an inspirational example of the PhD and many pieces of good advices on the further steps in various research processes, theoretical recap on gases in firn and discussions of the results in many details, which allowed seeing the stumbling blocks in the research.

Kumiko Goto-Azuma, Kenji Kawamura, Ikumi Oyabu and all the CFA and gas laboratories staff of the National Institute of Polar Research (NIPR), Tokyo, Japan, for the very fruitful opportunity having an internship at NIPR and learn about the their CFA setup and greenhouse gas measurements, to gain a lot of technical skills and measurement experience.

Euan Nisbeth – for a discussion of the CH_4 diurnal cycle origin.

Emilie Capron and Sune Olander Rasmussen – for their always pleasant and optimistic attitude, easygoing way of taking issues of different sorts on the way of conducting the research, and constructive criticisms of the texts and presentations, which always helped to improve the work greatly.

Many thanks to Manuel Figueiredo-Larsen for his kind help in the text editing and the Danish translation, for generating the good humor at the latest stages of writing and more importantly for his friendship and support in the moments of tiredness and doubts.

Appendices

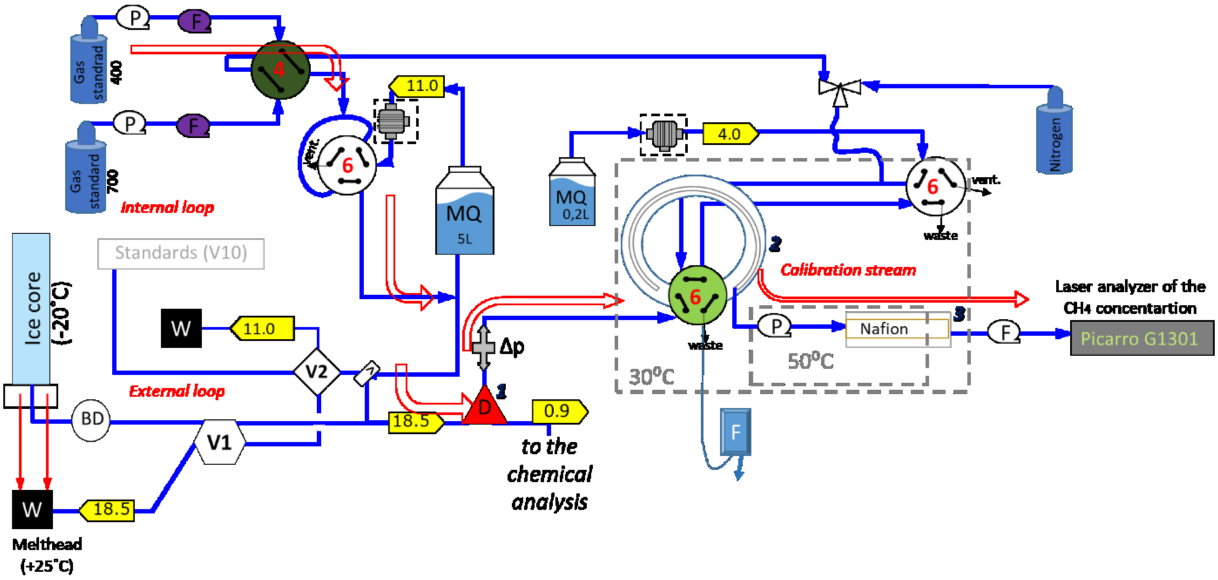

Figure A1: *Schematic of the CFA CH_4 setup. Arrows mark the flow direction during the calibration. See the text for the color notes*[2].

A1. A manual for the CFA CH_4 analysis

The CFA experimental setup for the methane concentration measurements is an insulated analytical line, connected to the outlet of the melthead. The setup is operated partially manually but predominantly using the customer-made script in LabVIEW 2015. This software allow monitoring of the system parameters variability during the measurements as well as switching the valves and controlling the mass flow of the standard gases. The script can be modified, some additional loggers can be added. The output data files is in .lvm format. A valve allowing to alternate between the internal (calibration and standby modes) and external (calibration and measurement modes) loops is operated manually as well as the peristaltic pumps. The tumbler leading to the inlet of the gas extraction line is marked as light green circle (6-way valve), see Fig. A1. The peristaltic pumps are marked as yellow arrays pointing toward the direction of

---

[2] All the object references such as “yellow arrow” or “purple valve” in the manual below will be referred to the Fig. A1.

pumping; numbers inside mean the set flowrate. These flowrate are subject of change depending on the particular ice core measurements or calibration needs.

A1.1. Calibration before the measurements start

- Launch the MiliQ water stream on the internal loop. In order to do that, set the tubes of the peristaltic pump into the clip holder, press ”Start” (*yellow arrow “4.0”*). Steadily increase the flowrate of the standard gas from 0.1 to 1.5 cc min^{-1} with increment 0.2 cc min^{-1} (*purple mass flow controllers “F”*, which are operated via LabVIEW).
- Wait until a pressure in the membrane gas outlet and the gas flowrate at the analyzer inlet (seen in LabVIEW) as well as the methane concentration (seen in the Picarro’s display) becomes stable and in ca. 10 min switch the line to the second standard gas (*dark green 4-way valve*, operated via the LabVIEW).
- Start the flow of the MiliQ water from the 5L bottle through the external line. Keep the pumping through the degassing micromodule (*squared in black dashed line*) under control by fixing the tube in the peristaltic pump’s clip (*yellow arrow “11.0”*), i.e. pulling the water through the degasser.
- When a debubbler (*red triangle “D”*) becomes full with water, launch the standard gas stream, the one that is not used at the moment in the internal loop: steadily increase the flowrate of the standard gas from 0.1 to 1.5 cc min^{-1} with increment 0.2 cc min^{-1} (*purple mass flow controllers “F”*, which are operated via LabVIEW); follow the air level inside the debubbler: it should look like a popping up and adsorbed air bubble. If the water level in the debubbler goes down, decrease the flowrate of the standard gas and then bring it back over 20-30 sec. It is important to keep the gas-to-water ratio 50:50 in the gas extraction line in order to reproduce the real ice core sample measuring conditions.
- Connect the gas extraction line to the external loop (by turning the *6-way green valve*), measure the standard gases: wait until the CH_4 concentration and the humidity of the sample become stable (ca. 10-20 min), continue measuring the CH4 concentration over 10-30 mi, follow the measurements stability. If any trend appears, troubleshoot the extraction line, check the leak tightness of the connections.
- Switch to the second standard gas (using the *4-way dark green valve*), repeat the procedure from the previous point. If it appears necessary to use more gas standards, repeat the procedure for every one of them.

- Make sure that the methane concentration of all the gas standards do not float in comparison with the previous measuring days (see the corresponding notes at the lab book and keep the daily spreadsheets of the average calibration values updated); if the values float, troubleshoot the system. The possible reasons are leaks in the connections, improperly degassed or flushed with helium MiliQ water, other reasons such as outdated Nafion.
- Switch the extraction line to the internal loop (turn the *6-way green valve*) and repeat the calibration. The direction of the gas and water stream is indicated as *red arrows*.
- Stand by mode is on the internal line, it is carried out by measuring the segmented flow of the standard gas in the MiliQ water stream. Choose the standard as the closest to the CH4 concentration of the ice core series measured. Preferably to choose the standard gas with a slightly lower CH4 concentration than expected in the ice core sample as the instrumental response time is shorter when transiting from the lower to the higher CH_4 concertation (see section 3.4, Fig. 27), and the transition is better marked in the data log, which makes the processing easier.

A1.2. Measurement protocol

- Right before the melting of the ice core sample begins, launch the stream of segmented standard gas flow in the MiliQ water through the external line in order to clean the line and the debubbler. Use the standard not involved in the standby mode in the internal loop and the 5L MiliQ bottle. Launch the clean-up procedure when the MiliQ ice, preceding the ice core sample is on melthead. It would also allow avoiding the ambient air penetration to the gas extraction line before the melting and causing the long memory effect.
- After 1 min 30 sec (or another time accounted on the length of the transporting line from the melthead to the gas extraction line) switch the tumbler to connect to the external line and connect to the measurements (6-way green valve). Keep the internal MiliQ running
- Follow the updating gas pressure and flow rate as well as the humidity of the sample. In any case of measurement troubles, such as ice core sample frozen to the frame or stuck, gas pressure decrease or plugging water drop in the gas extraction line, switch the line to the standby mode. If the humidity is high, flush the line with the standard gas only until it drops to 0.02-0.04%v. If possible, stop melting the ice core sample in order to avoid losing the gas data.

A1.3. Calibration after the measurements

- A calibration at the end of the measuring day is conducted the latest, i.e. after the chemistry lines' calibration. It is done due to the (1) risk of the standard gas bubble sneaking into the chemical compartments and affecting the baselines used throughout the day of measurements and (2) possible contamination of the gas line with the reagents. Between measurements and calibration, the gas extraction line should remain in standby mode measuring the standard gas stream segmented in the MiliQ water.
- Launch the standard gas, which is not currently in use in the internal loop, into the already being pumped MiliQ water on the external line (see the tumblers in section A1.1)
- Make sure that the segmented gas flow reaches the 6-way valve, which alternates the internal and external loops. Turn *6-way green valve* to connect the gas extraction line to the external loop.
- Repeat the protocol of the calibration before the measurement start.
- After this calibration is finished, switch the extraction line to the standby mode, terminate the standard gas flow rate by setting the mass flow controllers to 0.0, and close the valves on the standard gas bottles. Stop the peristaltic pumps and unlock the clips in order to preserve the tubes. Launch nitrogen into the gas line for the overnight standby.
- Back-up the data of the daily measurements to the hard drive.